STUDIES ON BEACH EROSION AND CHANNEL SEDIMENTATION(Dissertation_全文)

AUTHOR(S):

Ozasa, Hiroaki

STUDIES ON BEACH EROSION AND CHANNEL SEDIMENTATION

JULY 1983

HIROAKI OZASA

STUDIES ON BEACH EROSION AND CHANNEL SEDIMENTATION

JULY 1983

HIROAKI OZASA

CONTENTS

PREFACE

There are two engineering problems related to coastal sediment transport, i.e. beach erosion and channel sedimentation.

When breakwaters, jetties, or groins are constructed, alongshore sediment transport volume passing through the fixed beach cross-section changes and distribution of littoral drift volume will become varying in an alongshore direction. This causes beach erosion and accretion.

When sea bottoms are dredged for the preparation of channels at the areas where active sediment transportation exists, sediment transport volume or its direction at the fixed location changes and the channels suffer sedimentation (shoaling).

Beach erosion and channel sedimentation occur when a equilibrium state of sediment transport is broken. Only way of appearance of problems is different. Beach erosion is a more common phenomenon in Japan, but due to the above reason the author considers that study of channel sedimentation should have the same weight as that of beach erosion.

This report comprises fruits of the author's study about beach erosion and channel sedimentation.

PART I STUDIES ON BEACH EROSION

CHAPTER 1. INTRODUCTION

Beach erosion is a process that beach profile changes and shoreline retreats landward.

Main causes of beach erosion are as follows:

1) Beaches around river mouths erode, because sediment supply from rivers decreases due to construction works at the upstream rivers. For example, dams stop most sediment transport. This is one of the biggest causes of beach erosion in Japan.
2) Beaches erode in the vicinity of coastal structures such as breakwaters, jetties, and groins. Due to constructions of these structures, spatial distribution of mean level of water surface is changed. So, new pattern of nearshore current or circulating current is made and a coastal topography changes in accordance with new transport pattern of littoral sediment which is moved by those currents. Beaches erode in these processes of changes of coastal topographies. This type of beach erosion is seen at many beaches in Japan.
3) Bases of sea cliffs are scoured by waves, so the sea cliffs collapse and are washed away. Several sea cliffs in Japan erode seriously.

Land or houses are lost at eroded beaches. Port facilities or shore protection facilities suffer damages. When beaches in front of seawalls become narrower, wave overtopping volume increases and floods are induced at coastal areas.

Main portion of "Part I" is composed of three chapters. At Chapter 2, actual conditions of beach erosion in Japan are shown. Using aerial photographs selected from two series taken in 1946～1948 and in 1961～1974, the author measured positions of shorelines. Actual conditions of beach erosion were clarified by investigating changes of these positions of

shorelines. Several examples of beach erosion which are caused by different reasons are reported.

At Chapter 3, beach mathematical model which can be used for prediction of shoreline changes is shown. This model can be applied to the case where the width of a beach backed by a sea wall is narrow and this sea wall influences the advance of the shoreline change. The author also shows an alongshore sediment transport rate formula including the effect of varying breaker height along the beach.

At Chapter 4, the author shows results of mathematical simulation of shoreline changes which were calculated using the method shown at Chapter 3. Several difficulties which happen on applying the simulation method to the actual cases are examined. Based on the studies about reproduction of prototypical shoreline changes, the author proposes a method to calculate input data of beach mathematical model.

CHAPTER 2. STUDY OF INVESTIGATING ACTUAL CONDITIONS OF BEACH EROSION

2-1 Introduction

It is said that beach erosion is occurring along most sandy beaches in Japan. However, the changes of the shorelines have never previously been assessed to an objective standard. In the present chapter the author has tried to determine the changes of the shorelines by using aerial photographs taken by the U. S. Air Force between 1946 and 1948 and by the Geographical Survey Institute, Ministry of Construction after 1961. He has compared the positions of the shoreline appearing in those photographs and has analysed the changes.

There are two different approaches to the study of sand drift problems. One is a "microscopic" approach: studies of the dynamic mechanisms of sand transport are performed first, and beach changes are then viewed as an integrated form of the microscopic phenomena. The other is a "macroscopic" one: multiple examples of beach changes are first examined and then typical geomorphological patterns (for example, pattern of beach erosion at a delta) are obtained. The author has used the latter approach in this study.

Shoreline changes in the areas which include most of severely eroding beaches in Japan were first investigated: these areas are shown by bold solid lines in Fig. I-2-1. The results were reported in Technical Notes of the Port and Harbour Research Institute Nos. 163[1)], 192[2)], 266[3)]. This chapter summarizes these results illustrating some typical beach changes.

2-2 Method of analysis

2-2-1 Details of the methods

The method of analysis used is very simple and is described as follows:

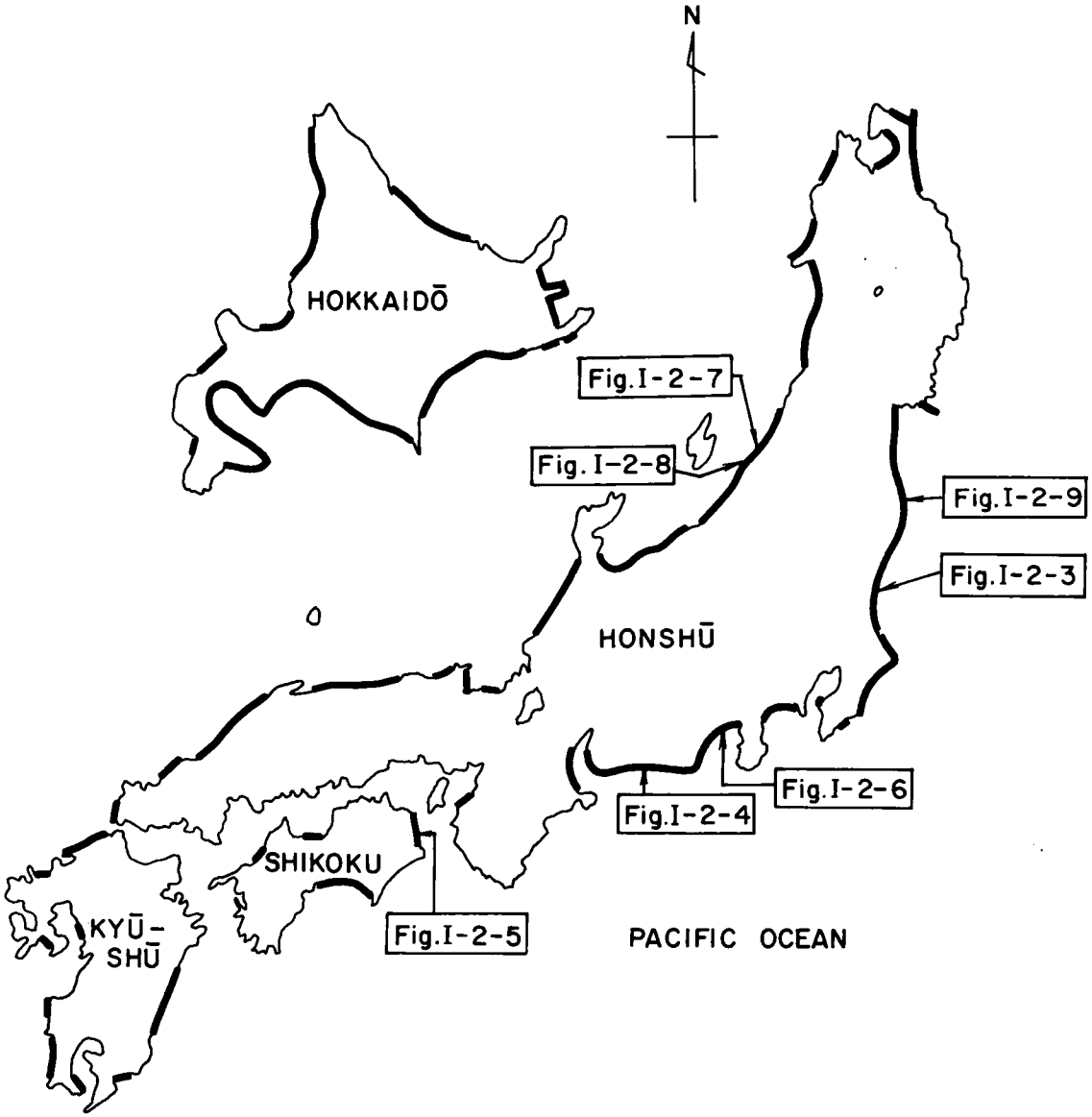

Fig. I-2-1 Areas investigated in study of beach changes

(1) Several aerial photographs of beaches that are to be studied are selected from two series taken in 1946-48 and in 1961-74.

(2) Basic points, common among the photographs, are marked on each photograph and basic lines are drawn on the photographs by using these basic points. During this operation, care must be taken in the following aspects:

(i) Basic points must be 'clear' points, for example, crossings of roads, ends of bridges, or houses.

(ii) Changes of level at the basic points must be small.

(iii) Ground distances between the basic lines and shorelines must be smaller than about 500 m.

(3) The quantitative ratio of the scale of each photograph is determined by comparing the length of the basic line on it. The scale of the newest of the selected photographs were determined as the ratio of the focal distance of the camera lens to the flight elevation. Scales of the other photographs were determined by using the scale of the newest photographs and the ratio of scales between photographs. The approximate scale of each photograph is 1/7000.

(4) The basic lines are divided every 167 m and marked. Perpendiculars to the basic lines are drawn through these marks. Only rarely did the positions shown by these marks have any discrepancy between photographs. In these cases, it is thought that the axis of the camera was not vertical. Photographs including such errors were discarded.

(5) Distances between the basic lines and shorelines are measured along the perpendiculars to the basic lines, and converted to actual distances according to the scales of the photographs.

2-2-2 Errors involved in the methods

The following errors are inherent in these methods:

(1) Errors due the the angle between the axis of a camera and a vertical line.

(2) Errors due to the changing positions of shorelines induced by the tide.

(3) Errors due to refraction of a ray through the air and the curvature of the earth.

(4) Errors due to the distortion of a camera lens and of light rays not behaving exactly according to accepted theory.

(5) Errors due to faults in a film.

(6) Errors due to undulations of the land.

(7) Errors due to the changing of shorelines caused by wave run-up.

It is thought that errors of types (1) and (2) are predominant while those of types (3), (4), and (5) are small due to the development of aerial photography techniques. Errors of type (6) are small because photographs of flat areas are used for this analysis. Finally, errors of type (7) are also small because most photographs were taken during calm weather.

Errors of type (1) are now considered. Any inclination of the axis of the camera causes changes of position both perpendicular and parallel to the shorelines. The changes of position parallel to the shoreline cause discrepancies in the perpendiculars to the basic lines. However, it was possible to decrease the number of these errors by eliminating such photographs. Therefore, it is thought that errors of positions perpendicular to the shorelines are the most predominant. These errors are considered as follows:

The following symbols are used in Fig. I-2-2.

o : center of lens

f : focal distance of lens

h : height of aeroplane

A, B, C, D, E : objects on the ground

a, b, c, d, e : pictures of A, B, C, D, E on the photograph

i : an angle between the axis of a camera and the vertical line (i is usually less than 3 degrees)

β, β' : $\tan\beta$ and $\tan\beta'$ are equal to the ratio of the distance between the measured point and the central point on the photograph (this distance is usually less than 12 cm) versus f

j : scale of the inclined photograph (cd) is equal to that of the horizontal photograph (ab) only on this point j

$\overline{a'e'}$: measured line on the inclined photograph

$\overline{ae}$: measured line on the horizontal photograph

The error of the length of the measured line is expressed, as follows, by using the above symbols:

$$\overline{ae}-\overline{a'e'}=f\cdot\sec\frac{i}{2}\left\{\sec\beta\cdot\sin\left(\beta-\frac{i}{2}\right)-\sec\beta'\cdot\sin\left(\beta'-\frac{i}{2}\right)\right.$$
$$\left.-\sec(\beta-i)\cdot\sin\left(\beta-\frac{i}{2}\right)+\sec(\beta'-i)\cdot\sin\left(\beta'-\frac{i}{2}\right)\right\}$$

As the lengths of measured lines on two different photographs are compared in this analysis, the errors in the shoreline positions are equal to difference between the values of ($\overline{ae}-\overline{a'e'}$) of the two photographs. Approximate values for the aerial photographs taken by the Geographical Survey Institute are f = 15 cm and h = 3000 m. If, for example, $\tan\beta$ = 6/15, $\tan\beta'$ = 3/15 (usual values in this analysis), and i = - 3° ~ + 3°, the errors are calculated as shown in Table I-2-1.

The maximum value of error of type (2) due to tides is approximately equal to the difference of level between H. W. and L. W. divided by the

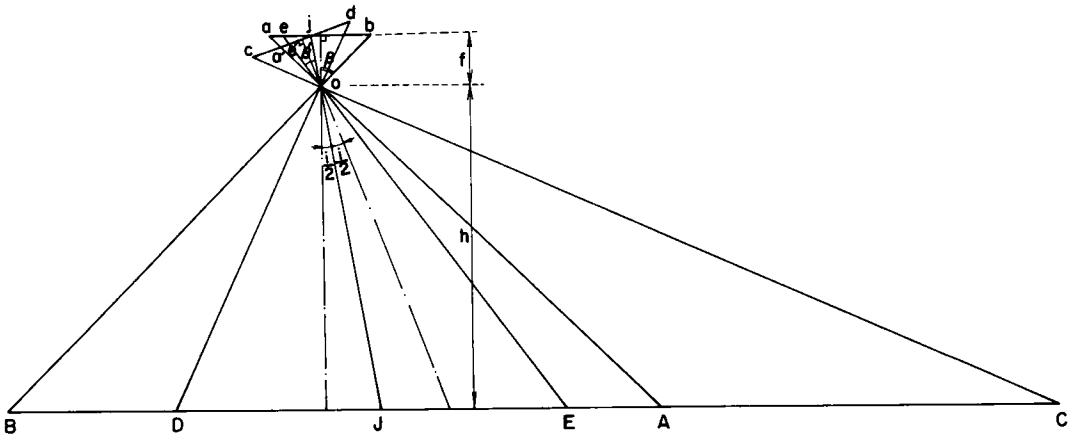

Fig. I-2-2 Error due to inclination between the axis of a camera and a vertical line

Table I-2-1 Calculated values of errors due to inclination between the axis of a camera and a vertical line.

Photographs of U. S. Air Force
tan = 6/15, tanβ = 3/15

(Unit: m)

Photographs of Geographical Survey Institute
tanβ = 6/15, tan = 3/15

i(°) \ i(°)	- 3	- 2	- 1	0	1	2	3
- 3	0	8	16	22	28	34	38
- 2	8	0	8	14	20	26	30
- 1	16	8	0	6	12	18	22
0	22	14	6	0	6	12	16
1	28	20	12	6	0	6	10
2	34	26	18	12	6	0	4
3	38	30	22	16	10	4	0

foreshore gradient.

The errors involved in this analysis are theoretically considered as above. The results of this analysis of errors in shoreline position were compared with the results of surveys of the actual shore, and it became clear that the maximum value of the errors is at most 20 ~ 30 m.

2-3 Some examples of shoreline changes

Typical examples of shoreline changes determined by this method are presented in this section. The location of the areas, shoreline changes of which are shown in Figs. I-2-3 ~ I-2-9, is indicated in Fig. I-2-1.

Shoreline changes on the sandy coast south of Hitachi Port are shown in Fig. I-2-3. The positions of the shoreline investigated by using the aerial photographs of the U. S. Air Force are indicated by thick solid lines (standard lines). The other lines indicate the positions of the shorelines appearing on aerial photographs of the Geographical Survey Institute. (Figs. I-2-4 ~ I-2-9 use the same conventions.) Shorelines in the area sheltered by the Hitachi Port breakwater have advanced offshore by about 100 m during 22 years. However, the shorelines extending over 2.8 km south of the area of accretion have retreated landwards. The maximum erosion is approximately 75 m during 17 years. It is considered that most sand from the erosion area has moved to the accretion area in the shelter of the breakwater.

Shoreline changes on the sandy coast around the mouth of the Hamana Lake are shown in Fig. I-2-4. After the construction of jetties at the mouth of the lake, the beaches around the jetties have advanced considerably. The maximum value of this advance is approximately 150 m during 24 years.

Shoreline changes on the Tokushima Coast are shown in Fig. I-2-5. Typhoon-generated waves and swell attack this coast from the south east.

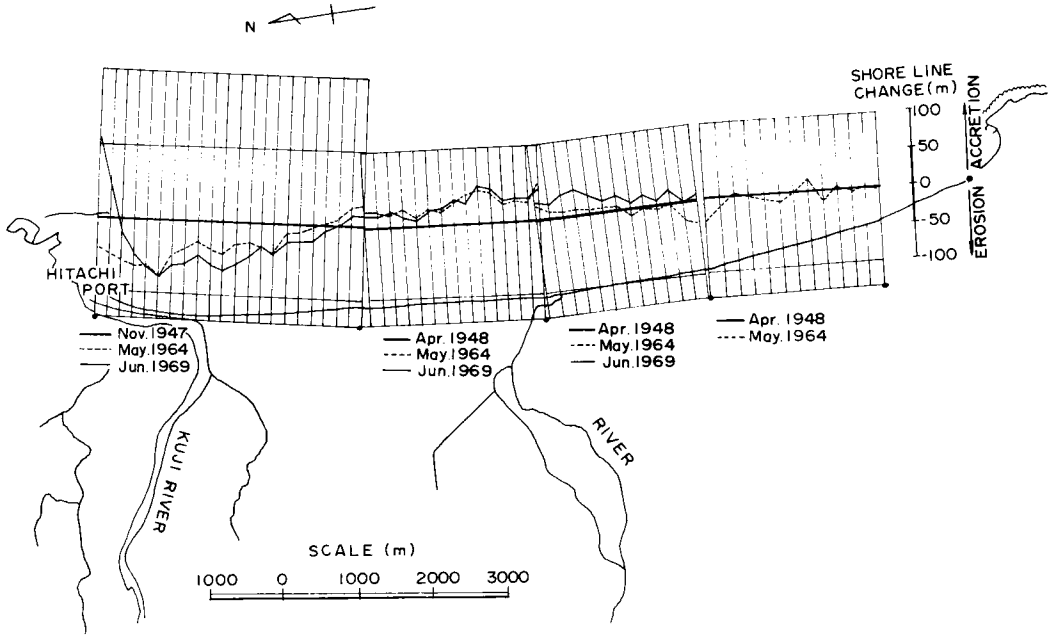

Fig. I-2-3 Shoreline changes at the coast south of Hitachi Port

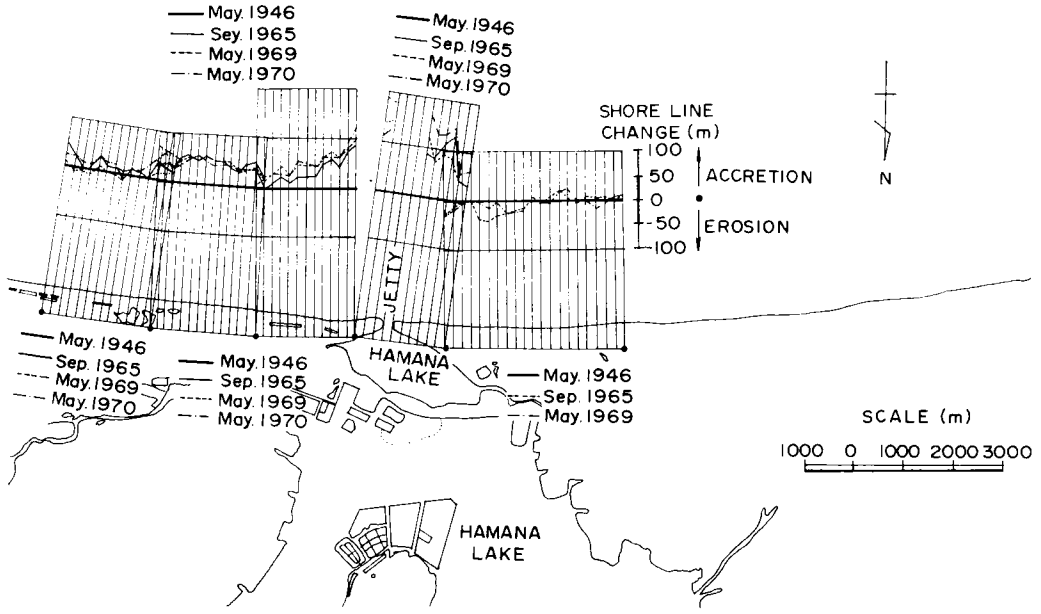

Fig. I-2-4 Shoreline changes at the coast around the mouth of the Hamana Lake

Therefore, the predominant littoral drift is from south to north. After construction of Awazu and Imagiri Ports, the beaches to the south of both ports advanced, whilst to the north the beaches retreated. The shoreline north of Awazu Port retreated very rapidly and the maximum value of the retreat was approximately 130 m during 17 years.

The Yoshino River is one of the largest rivers in Japan and the shoreline at the mouth of the river has retreated. Wadajima, located at the southern end of this coast, is a sand spit. It is thought to be formed by littoral drift from south to north. The tip of the sand spit has advanced by approximately 30 m during 20 years. Beaches at other parts of the sand spit have retreated by approximately 20 m and many groynes have been constructed there.

Shoreline changes at the coast around the mouth of the Fuji River are shown in Fig. I-2-6. The maximum value of shoreline retreat is approximately 250 m during 24 years. Offshore breakwaters have been constructed off the east coast of the left bank of the river. This shoreline retreat is thought to have been caused by a decrease of sand supply from the river due to the construction of dams and extraction of sand from the river.

Shoreline changes on the Niigata Coast are shown in Fig. I-2-7. There are two large rivers, called the Shinano River and the Agano River which meet this coast. The retreat of the shoreline here is thought to have been caused by the construction of the New Shinano River (a drainage canal, shown in Fig. I-2-8). The construction of this canal was intended to prevent the Shinano River from flooding and to reduce siltation at Niigata Port which is located at its mouth. The shoreline at this coast retreated because most of the discharge from the Shinano River now flows via the New Shinano River into the Sea of Japan and the sand supply from the Shinano River is thus decreased. Severe beach erosion has occurred along the coast south-west

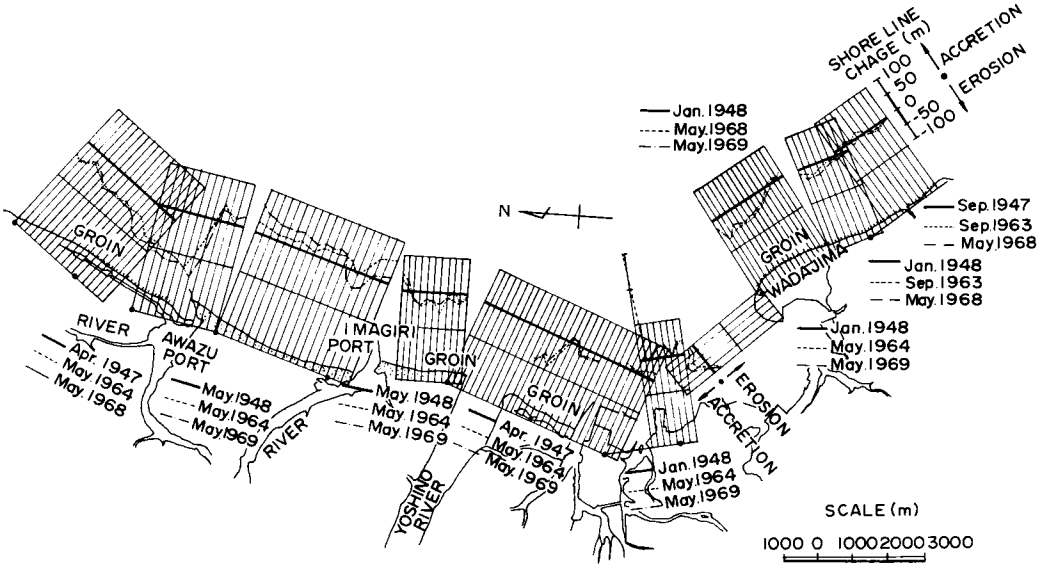

Fig. I-2-5 Shoreline changes at the Tokushima Coast

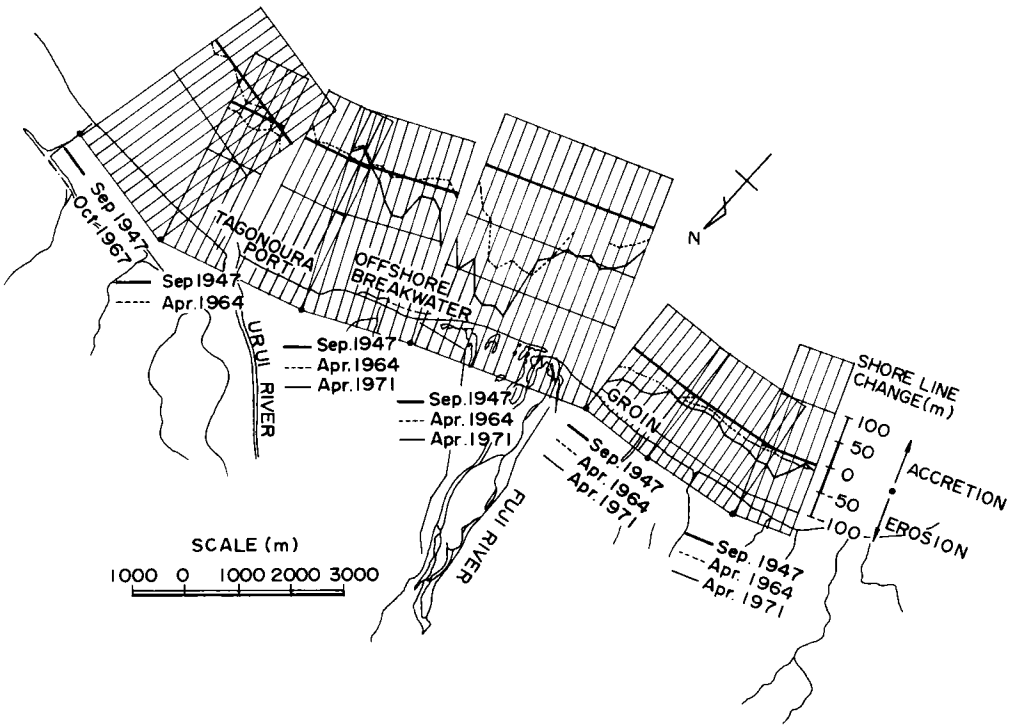

Fig. I-2-6 Shoreline changes at the coast around the mouth of the Fuji River

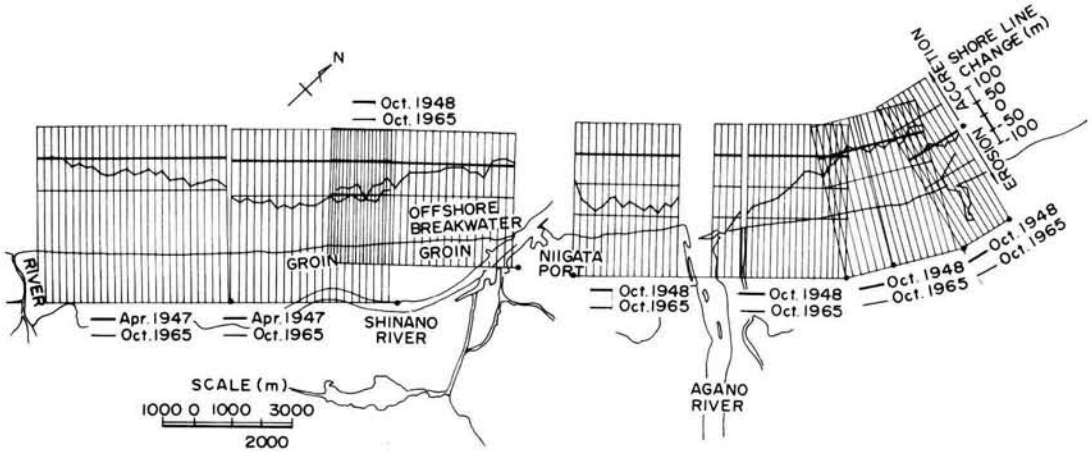

Fig. I-2-7 Shoreline changes at the Niigata Coast

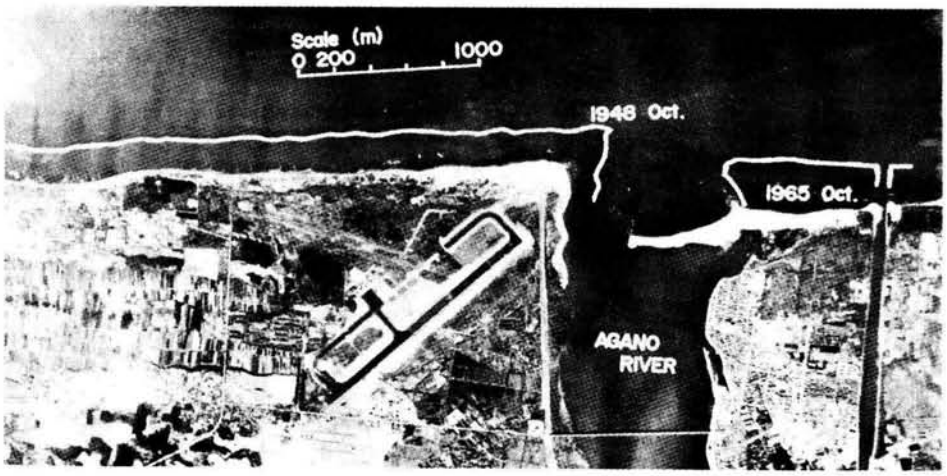

Photo I-2-1 Beach erosion at the coast around the mouth of the Agano River

of the mouth of the Shinano River and the average value of the retreat of the shoreline, extending over 13 km, is approximately 80 m during 18 years. The maximum shoreline retreat is approximately 130 m. It has also been noticed that the rate of beach erosion has decreased along the coast southwest of Niigata Port, because many offshore breakwaters, groynes, and seawalls were constructed and dredged sand was supplied to the coast. Beach erosion at the mouth of the Agano River has previously been thought not to be severe, because the amount of discharged sand was thought always to be small and so the effect of building dams was supposedly unimportant. However, it has become clear that severe beach erosion has occurred at the mouth of the Agano River (Photo I-2-1). Shoreline changes at the coast around the mouth of the New Shinano River are shown on Fig. I-2-8 and Photo I-2-2. The opposite phenomenon to the one at the mouth of the Shinano River (shown in Fig. I-2-7) has occurred here. The maximum value of shoreline advance is approximately 290 m during 18 years. Teradomari Port located on the coast south of the river has suffered from siltation due to this accretion.

Retreat of the cliffs on the Fukushima Coast is shown in Fig. I-2-9. The railway along this coast is threatened by this erosion. Beaches in front of the cliffs retreated by approximately 30 m (average value) and by 90 m (maximum value) during 13 years.

2-4 Some considerations about beach changes in Japan

2-4-1 Predominant directions of littoral drift

It is hardly necessary to say that littoral drift does not always move in one constant direction. If littoral drift always moved in one direction, a wide shallow sand bank would be formed on the downdrift side. However, there are some areas where accretion always occurs at the updrift side of coastal structures and erosion always occurs at the downdrift side. This

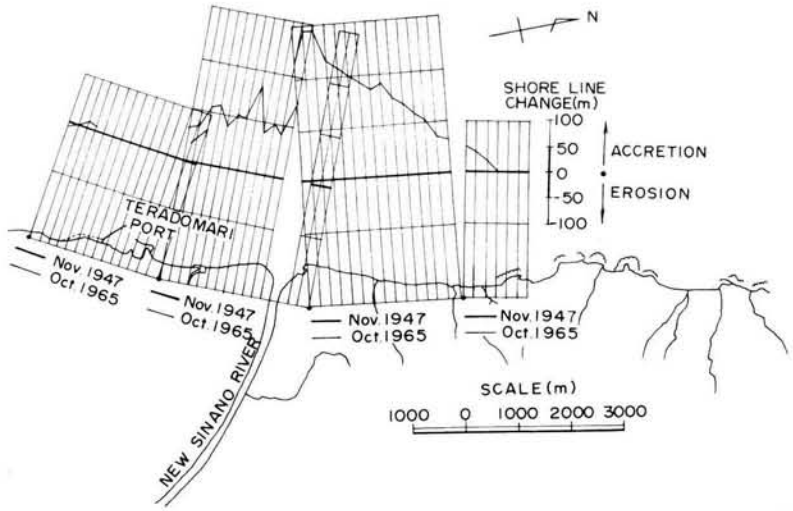

Fig. I-2-8 Shoreline changes at the coast around the mouth of the New-Shinano River

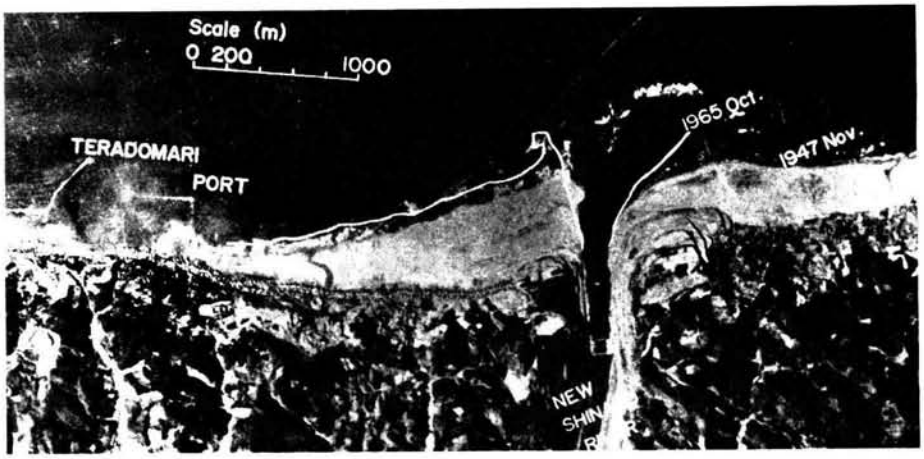

Photo I-2-2 Accretion at the coast around the mouth of the New-Shinano River

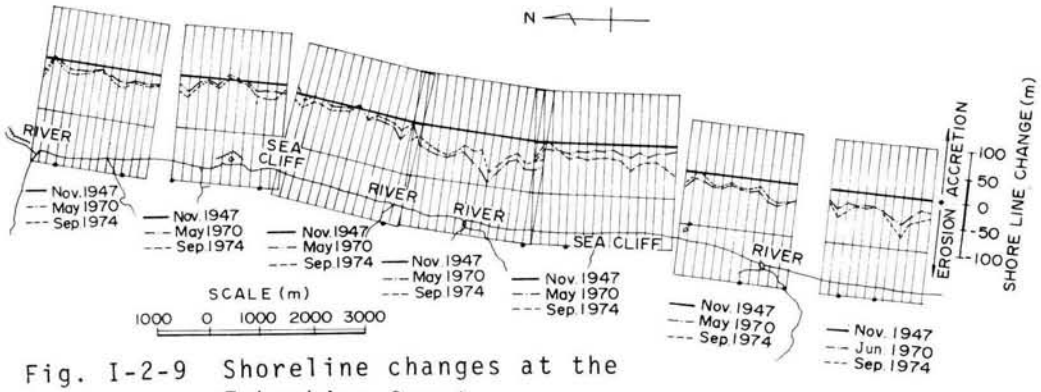

Fig. I-2-9 Shoreline changes at the Fukushima Coast

predominant transport direction is called the "predominant direction of littoral drift". For example, the Tokushima Coast shown in Fig. I-2-5 is an example of coasts where the predominant direction of littoral drift is very clear.

The author has determined the predominant directions of littoral drift on most coasts in Japan by using data about shoreline changes according to the above principles (Fig. I-2-10). These coastal areas where predominant directions are clear are classified into the following four categories:

(1) Sandy beaches which are located at the sides of bays and straits. Waves and swell which advance from the mouths of bays and straits to the interior attack the beaches from oblique directions. Therefore, the predominant direction of littoral drift at these beaches is from the mouth into the interior. The following sandy beaches (indicated by numbers shown in Fig. I-2-10) belong to this category: —
·②, ③, ⑤, ⑥, ⑦, ⑩, ⑮, ⑯, ⑰, ⑱, ⑲, ㉑, ㉔, ㉕, ㉙.

(2) Waves and swell caused by typhoons and low atmospheric pressures attack sandy beaches facing the Pacific Ocean from the south. If there are fairly large angles between perpendiculars to the shore and the south, waves and swell attack the beaches obliquely. Therefore, the predominant direction of littoral drift is obvious, see for example locations: —
④, ⑪, ㉘.

(3) At sandy beaches facing rectangular inland seas, the directions of long fetch are usually determined by the surrounding topography. Most of large waves attack the beaches from the long-axis directions and the predominant directions of littorial drift is obvious, see for

example locations: -

①, ⑩, ⑳, ㉒, ㉖, ㉗.

(4) At long concave sandy beaches, littoral drift transports sand from both sides to the central position, see for example locations: -

⑧, ⑨, ⑬, ⑭.

Only two small beaches, that is ⑫, ㉓ are not judged to belong to the above four categories.

2-4-2 Beach changes around river mouths

Rivers are, in general, the principal sources of sand supply to coasts. Therefore beach changes frequently occur at coasts around river mouths after construction of dams, river conservation works, or removal of sand from the river bed for construction material.

The Japanese Islands are divided into several zones by geological structure. Major tectonic lines are the Median Tectonic Line and the Itoigawa-Shizuoka Tectonic Line (Fig. I-2-11)[4]. The Islands are divided into Inner Zone and Outer Zone by the Median Tectonic Line. They are also divided into Southwest Japan and Northeast Japan by the Itoigawa-Shizuoka Tectonic Line. Hokkaido Island is divided into Central Zone and Peninsular Zone. Generally a river's characteristics depend upon those of the tectonic zone through which it passes[4]; in similar fashion the coastline, especially at river mouths, will also depend upon the characteristics of the tectonic zone.

The characteristics of coasts are also supposed to be affected by the properties of the sea into which the rivers flow. The major seas around Japan are the Pacific Ocean, the Sea of Japan, and the Sea of Okhotsk. On beaches facing the Pacific Ocean, waves and swell caused by typhoons are predominant, while waves caused by low atmospheric pressures in winter are predominant on beaches facing the Sea of Japan.

Beaches around mouths of 91 principal rivers were selected and coast

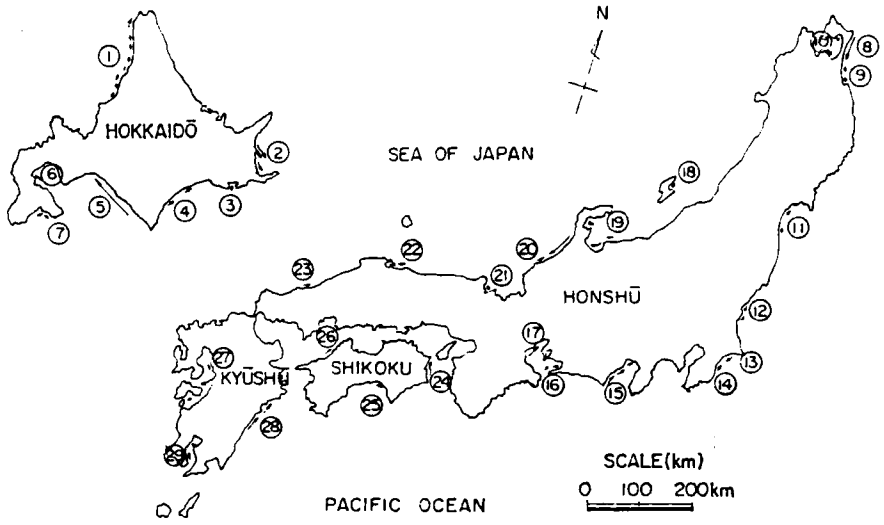

Fig. I-2-10 Predominant directions of littoral drift

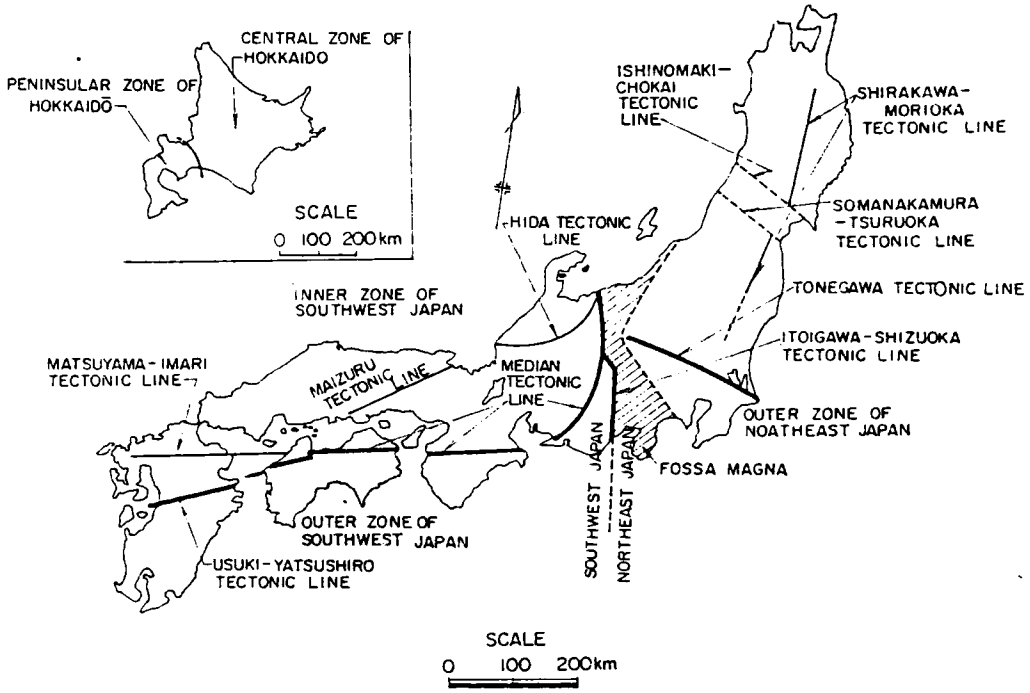

Fig. I-2-11 Tectonic structure of the Japanese Islands (after Koide)

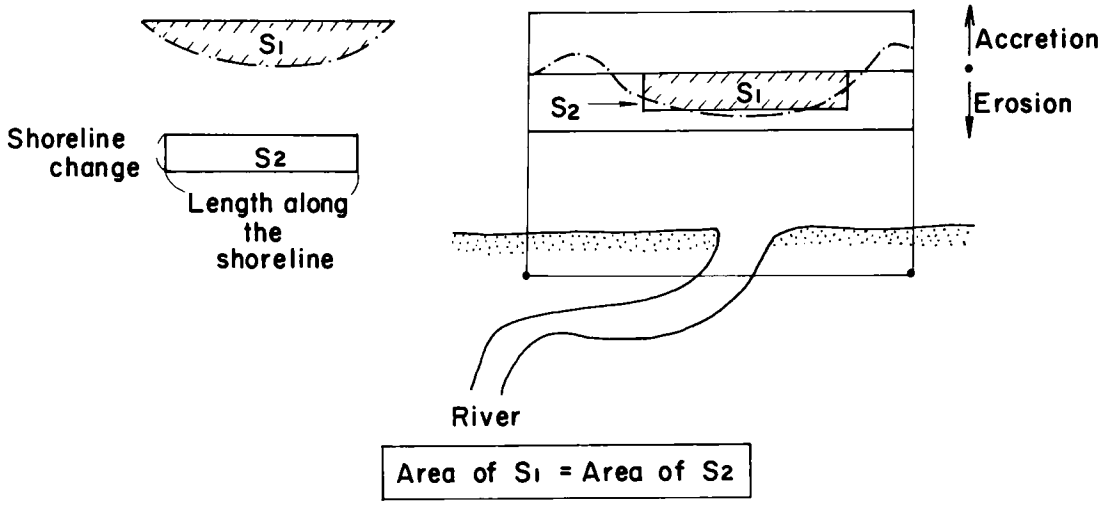

Fig. I-2-12 Calculations of changes in beach area at coasts around river mouths

alterations there have been arranged according to the above viewpoint. It is difficult to determine the extent to which adjacent areas are affected due to sediment discharges out of rivers. The author determined such areas by using data about shoreline changes (Fig. I-2-12).

Annual rates of shoreline changes of the beaches adjoining river mouths, and the lengths along the shoreline of these beaches were measured. By multiplying these two quantities, changes in beach area have been obtained. If the character of beach changes at a coast around one bank of a river differs from that of the other bank, changes of beach area were calculated on both sides separately. Calculated changes in beach areas are shown in Fig. I-2-13.

The following points are noted in referring to Fig. I-2-13.

(1) Changes of beach area (accretion and erosion) of the Central Zone of Hokkaido are larger than those of the Peninsular Zone of Hokkaido. One of the reasons for this phenomenon is that the scales of sandy beaches in the Peninsular Zone are smaller than those in the Central Zone of Hokkaido. Changes in beach areas facing the Pacific Ocean and the Sea of Japan in the Central Zone of Hokkaido are larger than those facing the Sea of Okhotsk.

(2) Changes in area (accretion and erosion) of beaches facing the Sea of Japan in the Northeast Japan are larger than those facing the Pacific Ocean in Northeast Japan.

(3) Beach erosion is very severe at Fossa Magna (the largest fracturing area in Japan) for beaches facing the Sea of Japan in Northeast Japan and facing the Pacific Ocean in the Outer Zone of Northeast Japan. Changes in beach area at the coast around the mouth of the New Shinano River (shown on Fig. I-2-8 and Photo I-2-2) show severe accretion. This accretion occurs at the mouth of the drainage canal and may be

Fig. I-2-13 Changes in beach area at coasts around river mouths in Japan

considered to be an exception.

(4) Changes in beach area (accretion and erosion) in Southwest Japan are smaller than those of Northeast Japan.

(5) Changes in beach area in the Outer Zone of Southwest Japan facing the Pacific Ocean are a little larger than those of the Inner Zone of Southwest Japan facing the Sea of Japan. Most changes in beach area in the Outer Zone of Southwest Japan facing the Pacific Ocean show erosion.

2-5 Conclusions

The main conclusions of this chapter are:

(1) Aerial photographs can be very useful means for investigating shoreline changes. In this chapter, the author has shown the way of studying shoreline changes using aerial photographs. Then, he has shown magnitudes of errors involved in the results of these shoreline change analyses.

(2) Beach erosion in Japan is very serious and it is caused by construction of coastal structures or decrease of sand supply from rivers, etc. According to causes of erosion, beach erosion can be classified into various types. In this chapter, typical examples of various cases of beach erosion have been shown.

(3) Predominant directions of littoral drift are clear at some coasts in Japan. The author has classified the reasons of existence of predominant directions into four categories.

(4) Characteristics of rivers in Japan are said to depend upon the characteristics of the tectonic zones through which they pass. In this chapter, some findings have been obtained by comparing situations of shoreline changes with those of geological structure.

REFERENCES

1) Tanaka, N., Ozasa, H., and A. Ogasawara: Note of the investigations on changes of shorelines in Japan, Part 1, Technical Note of the Port and Harbour Research Institute, No. 163, 1973 (in Japanese).

2) Tanaka, N. and H. Ozasa: Note of the investigations on changes of shorelines in Japan, Part 2, Technical Note of the Port and Harbour Research Institute, No. 192, 1974 (in Japanese).

3) Tanaka, N., Ozasa, H., Hachisuka, K., and E. Miyoshi: Note of the investigations on changes of shorelines in Japan, Part 3, Technical Note of the Port and Harbour Research Institute, No. 266, 1977 (in Japanese).

4) Koide, H.: Rivers in Japan, Tokyo University Press, 1970 (in Japanese).

CHAPTER 3. STUDY OF MATHEMATICAL CALCULATION OF SHORELINE CHANGE

3-1 Introduction

When various structures like breakwater, groyne, offshore breakwater etc. are built on coasts, topographies around these structures change in various ways. As dams are built in rivers, beaches at the mouths of these rivers suffer from erosion at most cases. It is desired that the technique for predicting these shoreline changes quantitatively be developed and various alternatives be evaluated from the viewpoint of beach erosion caused by the construction accompanied by the alternatives using this technique.

There are two techniques for predicting changes of coastal topography. They are physical model experiment and mathematical model calculation. However, the former has a big problem that the exact similitude between the prototype and the physical model has not been established yet. Therefore, the physical model experiment has to always rely upon the method of trial and error.

On the other hand, various mathematical model techniques have recently been developed in the field of hydraulics. Affected by this tendency, techniques for mathematically predicting shoreline changes are studied very keenly. There are two types of mathematical models. The one is a method of calculating accretion or erosion of the beach having constant slope (so called 'one line theory'). The other is a method where a beach is divided into several meshes of two dimensional plan and topographic changes on these meshes are calculated using both equation of sediment transport rate and continuity equation of sediment transport. However, the latter method still has some unsolved difficulties and is on the stage of basic

research. The former method has been developed in France, the Netherland, and U. K. and is often used for calculating shoreline changes caused by various constructions on coasts.

The first attempt to mathematically model the evolution of a beach using 'one-line' theory was described in 1956, by R Pelnard-Considere[1]. His very simple model dealt solely with changes in the plan shape of a beach, which was represented by a single contour. By considering the continuity of alongshore sediment flux, he equated changes in beach volume, ie accretion or erosion, with changes in the rate of sediment transport along the beach.

This idea has been taken up and improved by many coastal engineers, and the model of Price, Tomlinson, and Willis[2] is of this type. Clearly, a method which represents a beach by a single contour cannot give information on changing beach profiles, but despite this, when used with care, a 'one-line' theory can be very valuable in predicting the long term evolution of a beach.

In a situation where movement of beach material in an offshore or onshore direction is important, a more detailed approach is required. In 1968, W Bakker described a more sophisticated model[3] where the beach is represented by two contours which in general, are not parallel. This 'two-line' theory allows for onshore-offshore sediment transport and changes in beach slope. The model has the disadvantage that it is very difficult to quantify such effects and hence realise the full potential of the method. A recent review of the published mathematical beach models, of both the 'one-line' and 'two-line' types, can be found in papers by Le Mehaute and Soldate, 1977[4] and H. Nishimura, 1978[5].

One use of such models is to predict the effect of engineering works on a beach, and it is therefore surprising to find very little work on the effect of a sea wall on the plan shape of a beach in front of it. This chapter presents a simple 'one-line' theory, based on the work of Price, Tomlinson and Willis[2], which can deal with a beach in front of a sea wall, even if it erodes and reaches the wall.

The chapter includes the derivation of a new formula for the alongshore transport of sediment. This formula extends the Scripps equation, developed by Komar and Inman[6], to situations where the wave height along a beach varies.

The first part of the chapter describes the theory of the model and this is followed by a description of the numerical method used to solve the differential equations obtained.

3-2 The beach mathematical model

3-2-1 Theory on the beach mathematical model

As a first step in the description of the model the author introduces a rectangular co-ordinate system (x,y) and lists the most important assumptions. The orientation of the co-ordinate system is chosen so that the x-axis lies roughly parallel to the beach. If a coastline has a substantial curve, this requirement clearly cannot be met by a single co-ordinate system. In such cases it is necessary to divide the beach into more than one section to study the changes in plan shape.

The beach is assumed to be represented by a single line, $y(x,T)$, where T is time. It is also assumed to have everywhere a constant slope, $\tan\beta$, , between the swash limit, or the crest of the berm, and some underwater contour beyond which profile changes can be assumed negligible. Under this last assumption, the level on the beach profile which defines

the line y(x,T) can be chosen in a variety of ways. For our purposes it is convenient to choose Mean Sea Level (MSL) as both the datum to which depths are reduced and the contour to which y(x,T) is measured. The depth below which profile changes are negligible is called D and is usually assumed constant along the beach. The height of the swash limit, or the beach berm, above MSL is denoted by BH.

The model can now be conveniently handled into two stages. In the first, the beach above MSL is assumed sufficiently wide that any seawall behind it has no significant effect on the alongshore sediment transport. This situation is shown diagrammatically in Fig. I-3-1 and can be represented by the equation:

$$y \geqslant y_w + \frac{BH}{\tan\beta} \qquad \text{----- (1)}$$

where y_w is the distance of the sea wall from the baseline. In this situation the berm height is taken as a constant, although if the beach erodes it will become, in general, a function of both x and T. This point is taken up again later, but we first consider the equations governing the movement of sediment along the shore for the simple first stage of the model.

Considering sediment motion across two lines δx apart and perpendicular to the base line (y = 0), for a small time interval δT , we obtain for the change in beach volume in that strip:

$$\delta V = \delta T \left\{ Q - \left(Q + \frac{\partial Q}{\partial x} . \delta x \right) \right\} \qquad \text{----- (2)}$$

where Q is the volume rate of alongshore sediment transport. If we assume that as the beach either erodes or accretes, its profile retains the same slope, ie tan β , then we obtain:

$$\begin{aligned} \delta V &\doteq \{\text{Area of (ABCD)}\} . \delta x \\ &= (D + BH)\delta x . \delta y \end{aligned} \qquad \text{----- (3)}$$

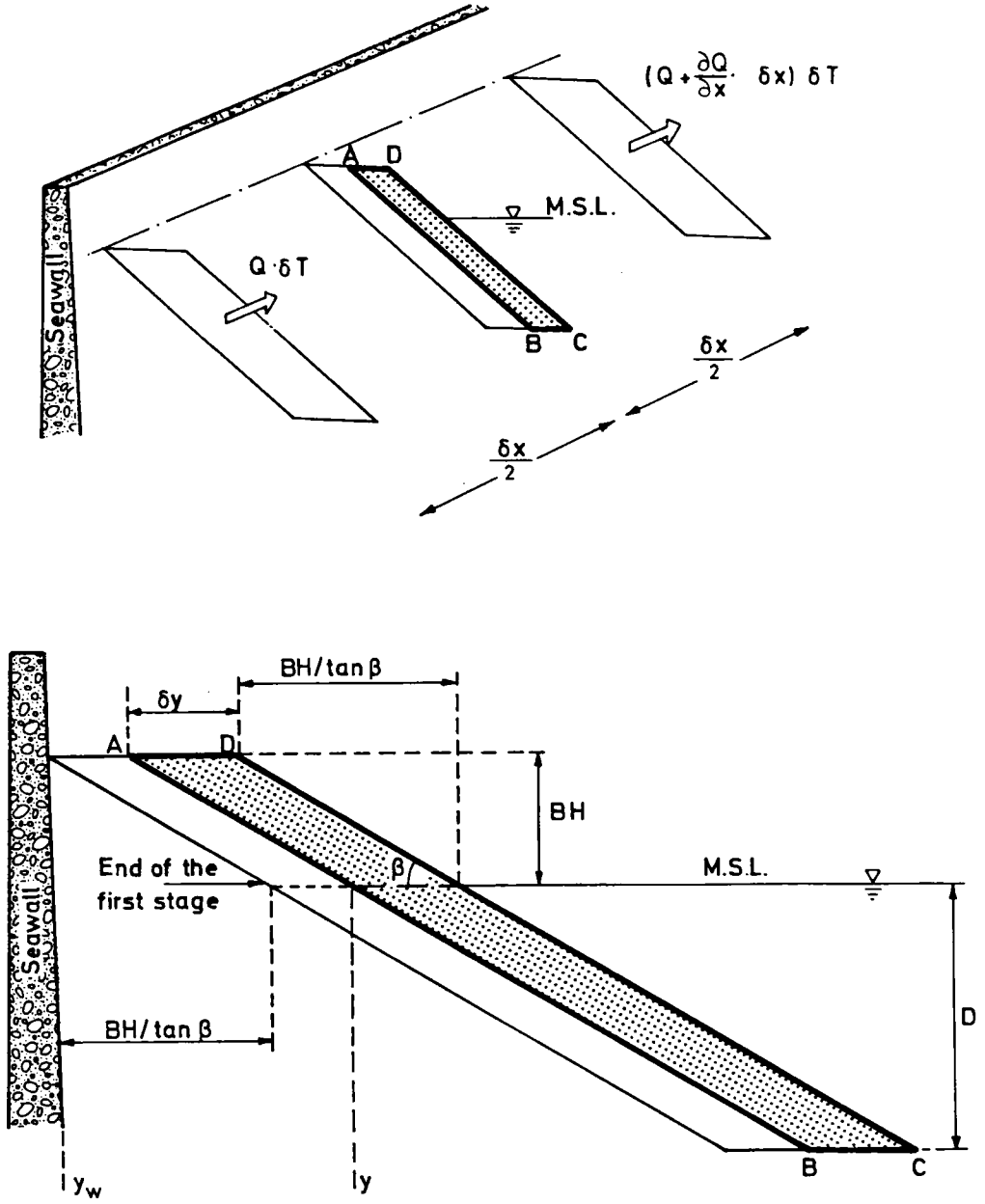

Fig. I-3-1 Continuity equation (first stage)

where δy is the mean translation of the profile in that strip (see Fig. I-3-1). Combining these two equations, and letting both δx and δT tend to zero, we obtain the continuity equation:

$$\frac{\partial Q}{\partial x} + (D + BH)\frac{\partial y}{\partial T} = 0 \qquad \text{----- (4)}$$

The term D + BH is, of course, the total depth over which the beach profile changes.

In normal situations, alongshore sediment transport on a beach is caused by the oblique breaking of waves, and this mechanism has been extensively studied. In some cases, however, alongshore wave height gradients must also be considered. Such situations often occur when waves diffract around a headland or a breakwater. The equation for the volume rate of alongshore sediment transport used in this report takes both these effects into account and is given by:

$$Q = \frac{0.385(EC_g)_b}{\gamma_s}\left(\sin 2\alpha_b - 3.24\frac{\partial H_b}{\partial x}\cot\beta\cos\alpha_b\right) \qquad \text{----- (5)}$$

where

E : the energy density of the waves = $1/8\ \rho g H^2$,

H : the wave height,

g : the acceleration due to gravity,

C_g : the group velocity of the waves,

α : the angle their crests make with the shoreline,

ρ : the density of the water,

γ_s : the density of beach material in place, and where subscript b refers to breaking wave conditions.

If the alongshore wave height gradient $\partial H_b/\partial x$ is zero, then this equation reduces to the Scripps Equation[6] (The Scripps Equation is described in Appendix A). The derivation of equation (5) is discussed in "3-4" below.

Turning to Fig. I-3-2, we relate the angle α_b to the angle between the breaking crests and the baseline α_x by :

$$\alpha_b = \alpha_x - \tan^{-1} \frac{\partial y}{\partial x} \qquad \text{----- (6)}$$

In most prototype situations, α_x will depend on x, and as the beach advances or retreats with time, so the wave refraction pattern will alter, also causing changes of α_x. To remain completely consistent, therefore, we should regard α_x as a function of both x and T. However, experience has shown that provided the model is run for only short periods before a wave refraction exercise is re-run to find the new value of α_x (x), then treating α_x as time-independent does not cause any significant error. The numerical solution of equations (4), (5) and (6) by a finite difference method is then very straight forward as explained in "3-3" below.

Before that, however, we need to consider the situation where the beach in front of a sea wall is so narrow that the alongshore sediment transport is affected by the wall's presence. This stage begins when, as shown in Fig. I-3-3, the beach profile lies along the line AD and, as explained later, ends when the profile lies along the line BC. In this situation (Fig. I-3-3):

$$y_w \leqslant y < y_w + \frac{BH}{\tan\beta} \qquad \text{----- (7)}$$

where BH is the value used in the first part of the model described above. Although the basic continuity relation (equation (2)) still holds, the subsequent equations (4) and (5) have to be adjusted.

In the absence of exact theory, the necessary changes were based on observations in the following manner. Experience has shown that a beach in front of a see wall will erode to a certain level and then reach a state of static equilibrium (providing that the sea wall has not collapsed in

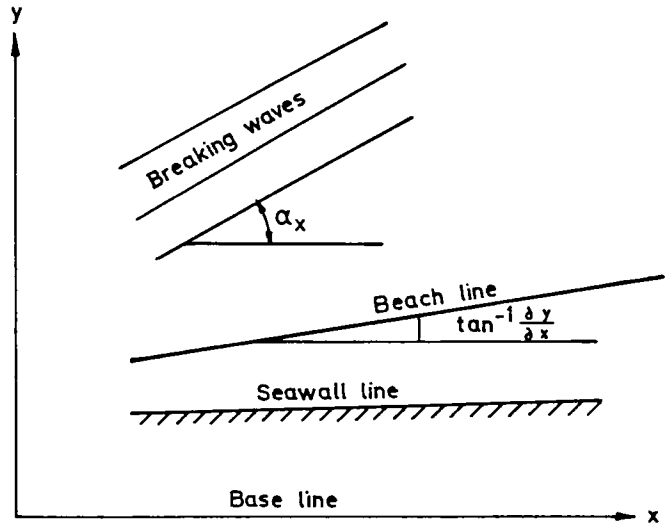

Fig. I-3-2 Breaker angle

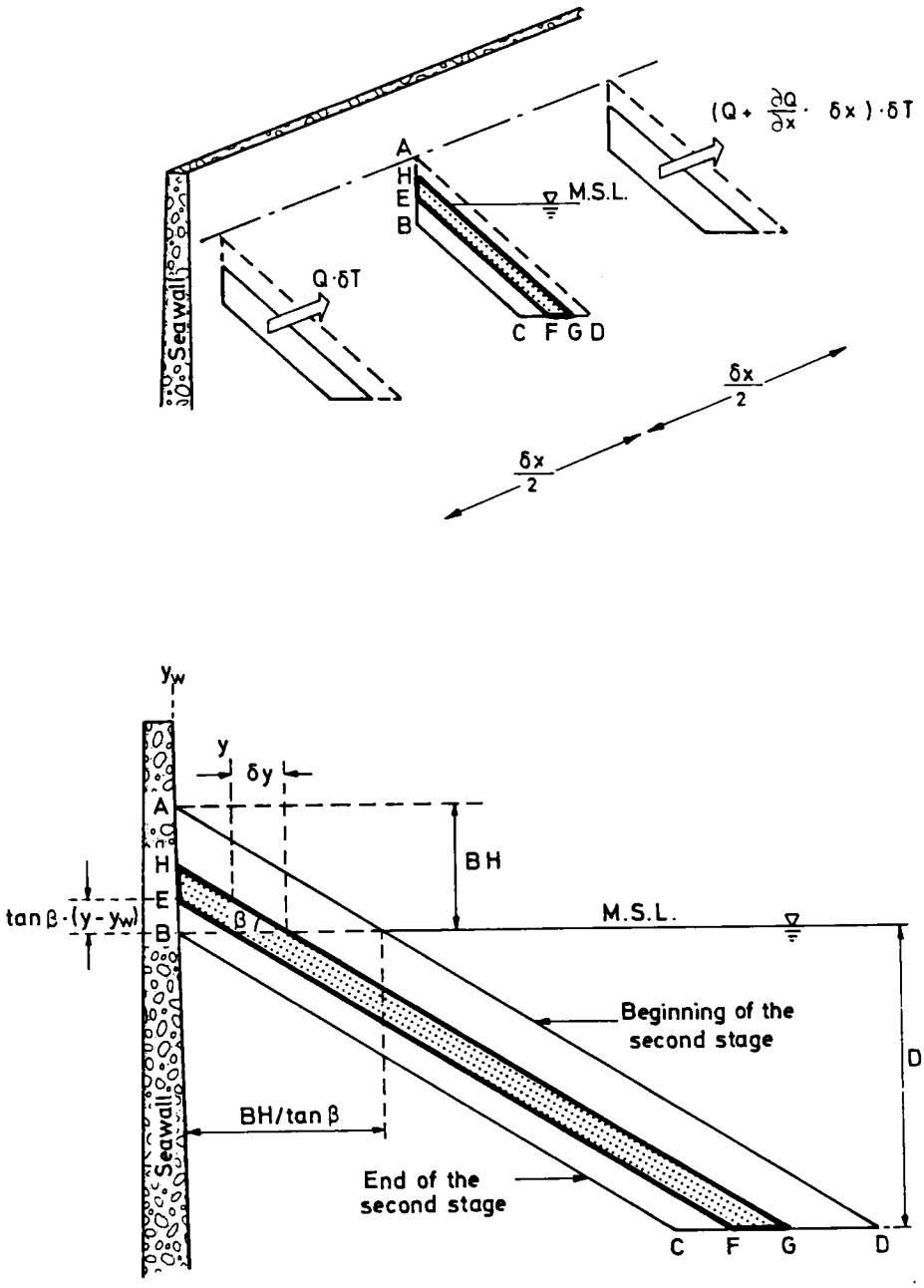

Fig. I-3-3 Continuity equation (second stage)

the meantime!). The level at which this occurs depends considerably on local conditions, but normally the highest part of the beach is at about MSL which is why this particular level was chosen as our depth datum. The prototype beach profile and our simplified approximation to it at this final equilibrium are sketched in Fig. I-3-4. In this situation, the alongshore sediment transport becomes negligible. Notice also that there is now no berm, ie BH has become zero.

The second stage of our model thus has to represent not only an alongshore transport rate which diminishes to zero, but also reduces the berm height in a similar way. The first step is to derive an equivalent to equation (4) above. Returning to Fig. I-3-3, we assume:

$$\left\{Q - \left(Q + \frac{\partial Q}{\partial x} \cdot \delta x\right)\right\}\delta T \triangleq \{\text{Area of (EFGH)}\}\delta x$$
$$\triangleq \{D + \tan\beta(y - y_w)\}\delta x \cdot \delta y \qquad \text{----- (8)}$$

so that in the limit:

$$\frac{\partial Q}{\partial x} + (D + B)\frac{\partial y}{\partial T} = 0 \qquad \text{----- (9)}$$

where $B = \tan\beta(y - y_w)$, the height of the beach above mean sea level. Notice here that the assumption of constant beach slope, $\tan\beta$, still remains.

The problem that now arises is how to diminish Q as the beach retreats. Two possible methods come to mind. Denoting Q in the first stage by Q_1 (equation (5)) and in the second stage by Q_2, we could either set:

$$Q_2 = \frac{B}{BH} Q_1 \qquad \text{----- (10)}$$

that diminishes Q by the ratio of the remaining height of beach above MSL to the original berm height on referring to Fig. I-3-3, or set:

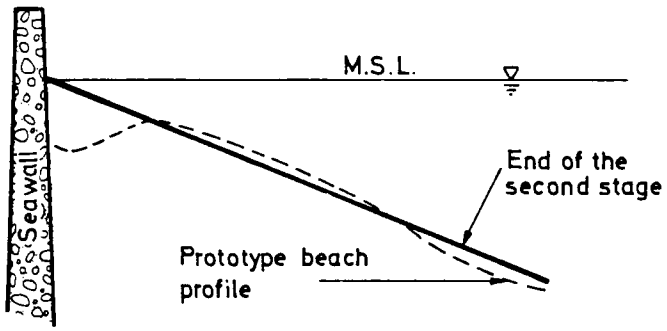

Fig. I-3-4 Equilibrium profile

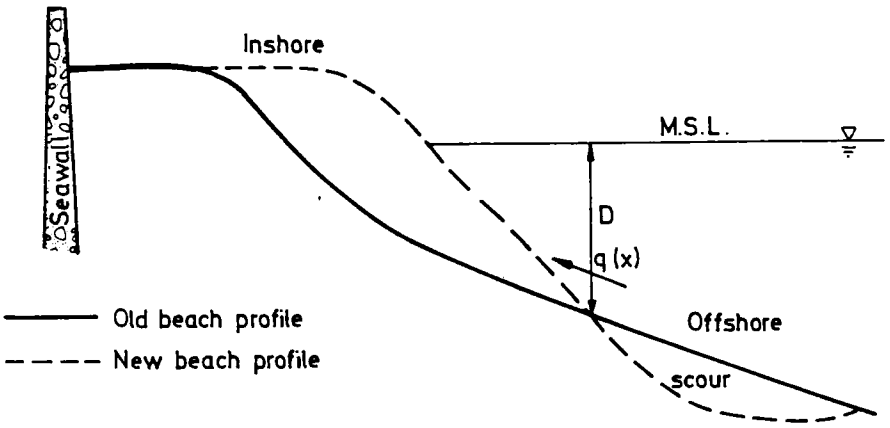

Fig. I-3-5 Onshore - offshore movement

$$Q_2 = \frac{\text{Area of (EBCF)}}{\text{Area of (ABCD)}} Q_1$$

$$= \frac{B}{BH} \frac{2D + B}{2D + BH} Q_1 \qquad \text{----- (11)}$$

Both possibilities satisfy $Q_2 = Q_1$, at the beginning of this second stage and $Q_2 = 0$ at the end of it.

The numerical method for this stage is based on equations (6), (9) and either (10) or (11).

3-2-2 Effect of onshore-offshore transport

So far, only alongshore sediment transport has been considered, but often the onshore-offshore transport of sediment can be important. An example of such a movement is the seasonal variation of beach profiles, but since the purpose of our model is to predict the evolution of a beach over a long period, we have not taken this sort of onshore-offshore transport into consideration.

Another example of onshore-offshore sediment movement occurs near breakwaters and jetties. These structures often cause sediment to be scoured from the sea-bed offshore and transported inshore, producing a steeper beach slope (Fig. I-3-5). Since this process will produce a permanent change of the beach profile, a proper evaluation of the transport is required.

In the case shown in Fig. I-3-5, we have defined D as the water depth at the inshore edge of the scoured area. Then defining $q(x)$ as the onshore sediment transport rate per unit length of beach, the sediment volume change, δV between two ordinates δx apart in time δT is given by:

$$\delta V = \left\{Q - \left(Q + \frac{\partial Q}{\partial x} \delta x\right) + q(x)\delta x\right\}\delta T \qquad \text{----- (12)}$$

where $q(x)$ is positive for onshore sediment transport. For the case where

the beach is wide enough that a sea wall has no effect, then we obtain, in the limit:

$$\frac{\partial Q}{\partial x} + (D + BH)\frac{\partial y}{\partial T} - q(x) = 0 \qquad \text{----- (13)}$$

This equation would then be used instead of equation (4) in the numerical method. In a similar way, for the second stage of the model, equation (9) would become:

$$\frac{\partial Q}{\partial x} + (D + B)\frac{\partial y}{\partial T} - q(x) = 0 \qquad \text{----- (14)}$$

3-3 Numerical solution of the beach mathematical model

In "3-3", a finite difference numerical method for solving the differential equation of "3-2" is presented. As a first step we divide the baseline ($y = 0$, $x \geqslant 0$) into small sections of length Δx . For the purpose of this chapter it is sufficient to consider the case Δx constant.

The ordinates separating these small sections are numbered sequentially from the origin. We use 'n' as a counter for these ordinates, so $x = 0$ is given by $n = 1$, $x = \Delta x$ by $n = 2$ and so forth.

The position of the shoreline is calculated at time intervals ΔT , also taken in this chapter as a constant. We use the counter 't' to denote these time steps, with $t = 0$ indicating the initial beach position, $t = 1$ its position after ΔT and so on.

The possibility of using both a variable Δx and a variable ΔT is discussed by Brampton and Motyka[7].

As seen in "3-2", there are three equations which, at either stage of the model, have to be solved. The first is a continuity equation of form

$$\frac{\partial Q}{\partial x} + L\frac{\partial y}{\partial T} - q(x) = 0$$

where in the first stage L = D + BH and in second stage L = D + B. The term q(x) is optional, depending on the likely importance of the onshore-offshore transport. In finite difference form, this becomes:

$$\frac{Q[n+2,t] - Q[n,t]}{2\Delta x} + L\,\frac{y[n+1,t+1] - y[n+1,t]}{\Delta T} - \tfrac{1}{2}\{q(n+2) + q(n)\} = 0 \qquad \text{---- (15)}$$

or more usefully:

$$y[n+1,t+1] = y[n+1,t] - \frac{\Delta T}{2L}\left\{\frac{Q[n+2,t] - Q[n,t]}{\Delta x} - q(n+2) - q(n)\right\} \qquad \text{---- (16)}$$

where [n,t] refer to the number of Δx and ΔT steps respectively as mentioned above. For computational simplicity, we only allow n to take odd values in this equation and those that follow.

The second equation is of the form:

$$Q(x,T) = \frac{0.385(EC_g)_b}{\gamma_s}\left\{\sin(2\alpha_b) - 3.24\,\frac{\partial H_b}{\partial x}\,\cot\beta\cos\alpha_b\right\}R$$

where in the first stage R = 1 and in the second stage we can choose between

$$R = \frac{B}{BH} \text{ or } R = \frac{B}{BH}\,\frac{2D + B}{2D + BH}.$$

In finite difference form, then we have:

$$Q[n,t] = \frac{0.385}{\gamma_s}\{E[n]C_g[n]\}_b \cdot \{\sin(2\alpha_b[n,t] - 3.24\,\frac{H_b[n+2] - H_b[n-2]}{4\Delta x} \cdot \cot\beta\cos\alpha_b[n,t]\} \cdot R \qquad \text{----- (17)}$$

Finally, we have equation (6), which in finite difference form reads:

$$\alpha_b[n,t] = \alpha_x[n] - \tan^{-1}\left\{\frac{y[n+1,t] - y[n-1,t]}{2\Delta x}\right\} \qquad \text{----- (18)}$$

Notice here that the breaking wave height H_b (and hence wave energy and group velocity at breaking) as well as α_x are assumed to depend only on alongshore distance, x. As mentioned above, if the beach changes sufficiently

during the period being considered, these quantities will have to be recalculated using a wave refraction model.

The supplementary variables, L and R, in equations (16) and (17) above are calculated by considering the distance of the shoreline from the sea wall, as follows:

if $y[n+1,t] \geqslant y_w[n+1] + BH \cdot \cot\beta$

then $R = 1$ and $L = D + BH$, whilst if $y[n+1,t] < y_w[n+1] + BH \cdot \cot\beta$

then $L = D + \tan\beta(y[n+1,t] - y_w[n+1]) = D + B$

and either $R = \frac{B}{BH}$ or $R = \frac{B}{BH} \cdot \frac{2D + B}{2D + BH}$

where in this case $B = \frac{\tan\beta}{2}(y[n+1,t] + y[n-1,t] - y_w[n+1] - y_w[n-1])$

The numerical method is thus given by equations (16), (17) and (18) together with the conditions for setting the variables R and L. The method presented is explicit, because using equation (16) we can deduce $y[n+1,t+1]$ from the values of H, C_g, α_b β, D and BH or B (which give Q) together with q and the position of the shoreline at time t.

A flow chart showing the order of calculations is shown in Fig. I-3-6. The working arrays yy, QQ, $\alpha\alpha_b$ and BB are used for temporary storage of y Q, α_b and B respectively. Appendix B shows a condition under which the numerical calculation mentioned above is stable.

In the next section we discuss the derivation of the formula for alongshore sediment transport used in this method (equation (5)).

3-4 Alongshore sediment volume transport rate--In the case of alongshore variation of wave height--

3-4-1 Bakker's alongshore current velocity formula

W Bakker[8] calculated the alongshore current velocity due to oblique wave attack and alongshore variation of wave height. He assumed the following

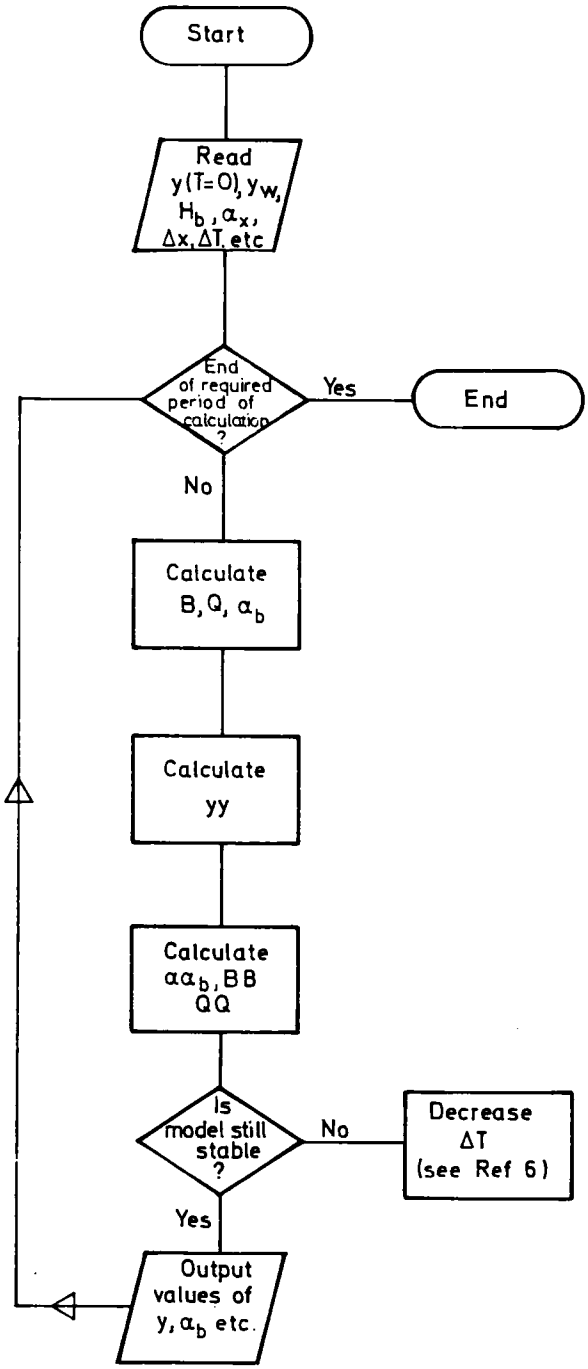

Fig. I-3-6 Skeletal flowchart of the mathematical model

about the beach profile (Fig. I-3-7 and I-3-8).

a) All beach contours below depth h_1 are straight and parallel.

b) All beach contours above depth h_1 are parallel to the shoreline, y_0 where y_0 is a function of alongshore distance x.

c) There is a horizontal shoal at depth h_1 .

d) h_1 is slightly greater than the maximum breaker depth, h_b.

e) The cross-section of the 'beach', ie water depth less than h_1, taken parallel to the y-axis is a straight line sloping at an angle β.

He also assumed the following about the waves.

f) In water depths greater than h_1 all wave rays are parallel although wave heights may vary along the shore.

g) At depth h_1 the wave rays are parallel to the y-axis, ie this defines the y-direction. The 'coastline' $y_0(x)$ is assumed to always make a small angle to the x-axis, ie dy_0/dx is small.

h) The curvature of the coastline, and hence d^2y_0/dx^2 is assumed to be so small that:
the effect of refraction is not enough to reduce wave heights to less than γh where γ is constant (usually taken as 0.8) and
that parallel depth contours can be assumed for refraction calculations

i) The wave velocity for depths $h < h_1$ is assumed to be $\sqrt{gh}$.

Bakker then used two dynamic equations for motion parallel to and perpendicular to the coast. The alongshore equation is:

$$-\rho g h \frac{\partial \bar{\eta}}{\partial x} - C_f \cdot u - \frac{\partial S_{xx}}{\partial x} - \frac{\partial S_{xy}}{\partial y} = 0 \qquad \text{----- (19)}$$

where

h : the water depth,

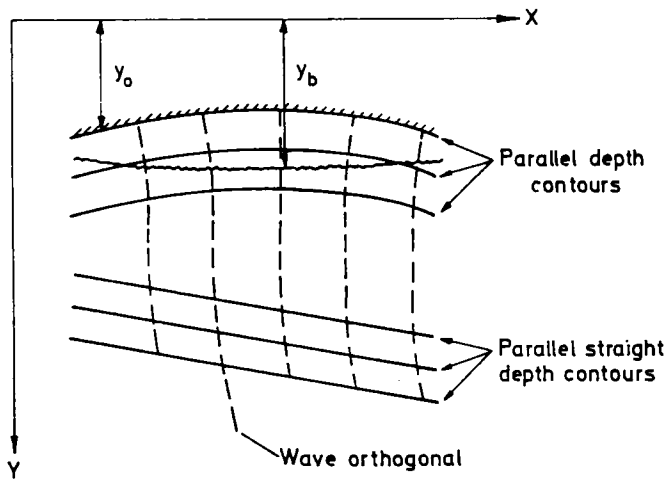

Fig. I-3-7 Definition sketch for Bakker's model

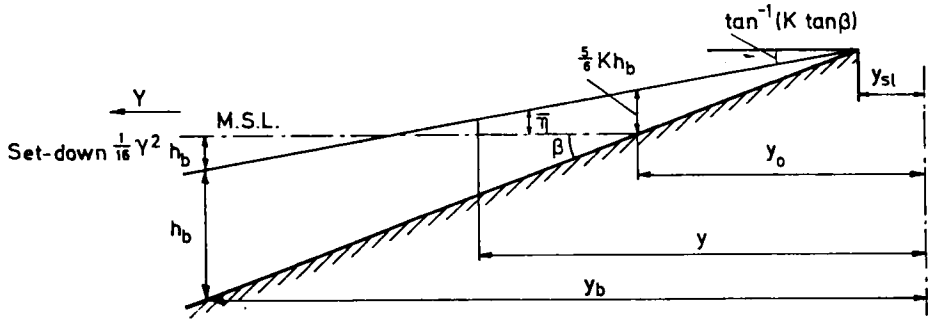

Fig. I-3-8 Beach profile (after Bakker)

$\bar{\eta}$: the mean water level,

S_{xx} : the normal radiation stress in the x-direction, given by

$\frac{1}{16}\rho g H^2(2-\cos 2\delta)$

which for small angles δ becomes $\frac{1}{16}\rho g H^2$

$= \frac{1}{16}\rho g \gamma^2 h^2$

where the wave height $H = \gamma h$.

S_{xy} : the radiation stress in the x-direction across a plane y = constant and is given by $-\frac{1}{16}\rho g H^2 \sin 2\delta$ which reduces to $-\frac{1}{8}\rho g \gamma^2 h^2 \delta$ for small angles, δ, between the wave direction and the y-axis so

$$\delta = \frac{dy_0}{dx}\left(1 - \sqrt{h/h_1}\right) \quad \text{and finally}$$

C_f : a friction factor = $\frac{1}{\pi\sqrt{8}}\, p\kappa\gamma\rho\sqrt{fgh}$

where

κ : the von Karman constant (=0.4),

f : the Darcy-Weisbach friction coefficient, and

p : Bijker's 'constant'. According to Bijker[9] $p \triangleq 0.45$, but Swart[10] showed that p is given more accurately by $\sqrt{f_w/2}\,.\,1/\kappa$ where f_w is the wave friction factor derived by Jonsson[11].

If equation (19) is compared with the equation which Longuet - Higgins[12] used to obtain alongshore current velocity in the codition of alongshore constant wave height, $\rho g h \partial\bar{\eta}/\partial x$ and $\partial S_{xx}/\partial x$ are added due to alongshore variation of wave height, but $\partial(N\,\partial u/\partial y)/\partial y$ showing the effect of horizontal mixing is eliminated.

The equation used by Bakker for motion perpendicular to the coast is:

$$\frac{\partial S_{yy}}{\partial y} + \rho g h \frac{\partial \eta}{\partial y} = 0 \qquad \text{----- (20)}$$

where S_{yy}, the normal radiation stress in the y-direction is given by $\frac{1}{16}\rho gH^2(2 + \cos 2\delta)$ which for small angles δ reduces to $\frac{3}{16}\rho g\gamma^2 h^2$. Equation (20) is the equation which Longuest-Higgins and Stewart[13] used for the study of wave set-up.

By substituting for $\frac{\partial \bar{\eta}}{\partial x}$ $(= \frac{\partial h}{\partial x} + \frac{dy_0}{dx}\tan\beta)$, S_{xy} and S_{xx} into equation (19) Bakker obtained for the longshore current, u,

$$u = -\frac{5\pi\gamma\sqrt{8g}\, m}{16p\kappa\sqrt{f}}\left\{\frac{h}{\sqrt{h_1}}\frac{dy_0}{dx} + (1 + \frac{\gamma^2}{8})\frac{dh_b}{dx}\frac{\sqrt{h}}{\tan\beta}\right\} \qquad \text{----- (21)}$$

where $m = \frac{\partial h}{\partial y} = \tan\beta/(1 + \frac{3}{8}\gamma^2) = (1 - K)\tan\beta$

where $K = (1 + 8/3\gamma^2)^{-1}$ which, assuming $\gamma = 0.8$

$= 0.194.$

Bakker did not take horizontal mixing into account so equation (21) is not correct locally. However, the effect of such mixing is to eliminate the discontinuity of velocity at the breaker line and produce a smoother velocity profile down the beach, see Longuet-Higgins[12]. Therefore equation (21) can still be integrated to give the total alongshore current.

3-4-2 Average alongshore current velocity

We start from equation (21) using the same method of calculation as in Motyka and Willis[14]. By integrating that equation across the surfzone, we find the average alongshore velocity (Fig. I-3-8):

$$\bar{V} = \frac{2}{h_b(y_b - y_{sl})}\int_{y_{sl}}^{y_b} u \cdot h\, dy$$

where y_b is the breaker line and y_{sl} the shoreline,

$$= \frac{2C_1}{h_b(y_b - y_{sl})}\left(\frac{C_2}{3}h_b^3 + \frac{2}{5}C_3 h_b^{5/2}\right)$$

where

$$C_1 = -\frac{5\pi\gamma}{16p\kappa}\sqrt{8g/f} = -4.36\sqrt{8g/f}$$

$$C_2 = \frac{1}{\sqrt{h_1}}\frac{dy_0}{dx} \quad \text{and}$$

$$C_3 = (1 + \frac{\gamma^2}{8})\frac{dh_b}{dx}\cot\beta = 1.08\frac{dh_b}{dx}\cot\beta$$

----- (22)

By substituting $\frac{h_b}{y_b - y_{sl}} = \tan\beta(1-K)$, we obtain:

$$\bar{V} = (\tfrac{2}{3} C_2 h_b + \tfrac{4}{5} C_3 h_b^{1/2}) C_1 \tan\beta(1-K) \qquad \text{----- (23)}$$

3-4-3 Alongshore sediment transport

Having obtained an average alongshore current velocity, we now have to find a sediment volume transport rate. For this we turn to the work of Komar and Inman[6] who considered long-crested waves of uniform height incident on an infinitely long, straight and parallel contoured beach. They found that the total immersed weight of sediment transport in unit time past a section of beach, I_ℓ , is given by

$$I_\ell = 0.28(EC_g)_b \cos\alpha_b \cdot \frac{\bar{V}}{U_m} \qquad \text{----- (24)}$$

where U_m is the maximum orbital velocity under the breaking waves

$$= \sqrt{g}\, H_b / (2\sqrt{h_b})$$

and where α_b is the angle between the breaking wave crests and the shoreline.

By substituting equation (23) into this equation we find:

$$I_\ell = \frac{0.56(EC_g)_b}{\sqrt{g}\, H_b} C_1 h_b (\tfrac{2}{3} C_2 h_b^{1/2} + \tfrac{4}{5} C_3) \tan\beta(1-K)\cos\alpha_b \qquad \text{----- (25)}$$

Now we assume $\tan\beta = A \cdot f$ (according to Komar[15], A = constant. see Appendix C) and since

$$h_1 \doteq h_b, \quad -\frac{dy_0}{dx} \doteq \tan\alpha_b \doteq \sin\alpha_b \quad \text{and} \quad \frac{dh_b}{dx} = \frac{1}{0.8}\frac{dH_b}{dx}$$

from equations (22) and (25) we obtain:

$$I_{\ell} = -6.97(EC_g)_b \cos\alpha_b \, A\sqrt{f} \left(-\tfrac{2}{3}\sin\alpha_b + 1.08 \frac{dH_b}{dx}\cot\beta\right) \quad \text{----- (26)}$$

When $\frac{dH_b}{dx} = 0$, this should reduce to the Scripps equation, so

$$4.65(EC_g)_b \cos\alpha_b \sin\alpha_b \cdot A\sqrt{f} = 0.77(EC_g)_b \sin\alpha_b \cos\alpha_b$$

and hence

$$A\sqrt{f} = 0.166 \quad \text{----- (27)}$$

Since the value of $\sqrt{f}$ varies only slightly, the approximate equality of equation (27) is thought reasonable. Hence we obtain:

$$I_{\ell} = 0.385(EC_g)_b(\sin 2\alpha_b - 3.24 \frac{dH_b}{dx}\cot\beta\cos\alpha_b) \quad \text{----- (28)}$$

which converted to a volume rate of transport is:

$$Q = \frac{0.385}{\gamma_s}(EC_g)_b(\sin 2\alpha_b - 3.24 \frac{dH_b}{dx}\cot\beta\cos\alpha_b) \quad \text{----- (29)}$$

If H_b is a function of time as well as distance x, then the term dH_b/dx will be replaced by $\partial H_b/\partial x$ which is equation (5) above.

If we are to study beaches in the laboratory, then the coefficient in the Scripps equation of 0.77 for prototype beaches should be altered to 0.36; (see Fig. I-3-9 from Komar and Inman[6]). The corresponding volume rate of alongshore transport is given by:

$$Q = \frac{0.18(EC_g)_b}{\gamma_s}(\sin 2\alpha_b - 3.24 \frac{\partial H_b}{\partial x}\cot\beta\cos\alpha_b) \quad \text{----- (30)}$$

3-5 Conclusions

(1) "One line theory" first described by Pelnard-Considere is based on the assumption that a beach is wide enough. Therefore, this theory can not be applied to the case where the width of a beach backed by a sea wall is narrow and this sea wall influences the advance of the shoreline

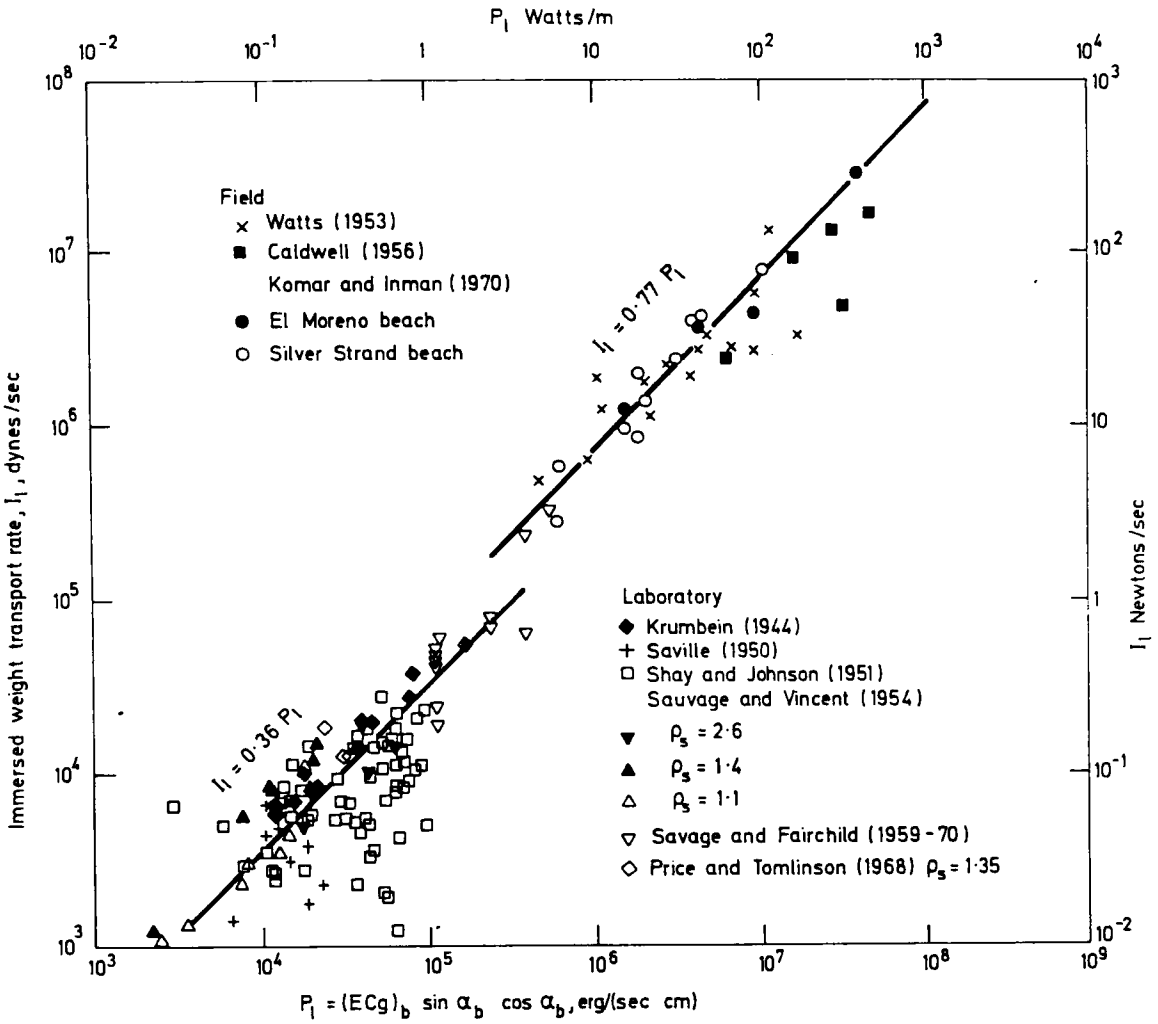

Fig. I-3-9 Alongshore sediment transport rate
(after Komar and Inman)

change. The author proposes a mathematical model for predicting the evolution of a beach backed by a sea wall. The model is in two stages. In the first, the beach in front of the sea wall has a berm and is sufficiently wide that the sea wall does not influence the alongshore sediment transport. If the beach erodes so that the berm disappears, then the second stage is entered. The sea wall causes a reduction in the alongshore transport rate, and if the beach continues to retreat, this rate will become almost zero. At such a time, the beach profile will reach a state of equilibrium and the second stage ends.

(2) The usual equation for the continuity of sediment motion alongshore has been extended to include onshore-offshore sediment movement.

(3) An alongshore sediment transport rate formula including the effect of varying breaker height along the beach has been derived using the work of both Bakker[8] and Komar and Inman[6].

(4) A finite difference scheme for numerical solution of the model's differential equations has been outlined.

Appendix A Scripps Equation

Scripps Equation is a following equation for the volume rate of alongshore sediment transport and has first been proposed by Komar and Inman[6].

$$Q = \frac{0.385(EC_g)_b}{\gamma_s} \cdot \sin(2\alpha_b) \qquad \text{----- (A1)}$$

For deriving the Scripps Equation, they used data of alongshore sediment transport rate measured using fluorescent tracers at EL Moreno Beach* and Silver Strand Beach** as well as many previous data. It is known that alongshore sediment transport rates calculated by the Scripps Equation agree with sediment transport rates measured both in prototypes and at physical models.

One of the features of the Scripps Equation is that a dimension of the left hand side of (A1) is same as that of the right hand side. For example, taking SI unit, dimensions of E, H, g, Cg, ρ, and γ_s are (kg/s^2), (m), (m/s^2), (m/s), (kg/m^3), and $(Newton/m^3)$ respectively. So, dimensions of both the left and right hand sides of (A1) are (m^3/s).

Appendix B Time step of numerical solution

When width of a beach backed by a seawall is wide enough and gradients of alongshore wave heights and wave directions are zero, stability

---

* EL Moreno Beach is a beach sheltered by Baja California and facing the Golf de California. Spring tidal range is about 8.6 m. Median diameter of beach sand is 0.6 mm. Gradient of the steep foreshore ($\tan\beta$) is 0.138.

** Silver Strand Beach near San Diego is facing the Pacific Ocean. Median diameter of beach sand is 0.175 mm and gradient of the foreshore ($\tan\beta$) is 0.034. Swell is predominant.

conditions of the numerical solution are easily derived.

Under the above situations equations (4), (5), and (6) of Chapter 3 are

$$\frac{\partial Q}{\partial x} + (D + BH)\frac{\partial y}{\partial T} = 0 \qquad \text{----- (B1)}$$

$$Q = \frac{0.385(EC_g)_b}{\gamma_s} \cdot \sin 2\alpha_b \qquad \text{----- (B2)}$$

$$\alpha_b = \alpha_x - \tan^{-1}\frac{\partial y}{\partial x} \qquad \text{----- (B3)}$$

Since $\partial H_b/\partial x = \partial \alpha_x / \partial x = 0$

these equations reduce to:

$$\frac{\partial y}{\partial T} = \left\{ \frac{0.77(EC_g)_b}{D + BH} \cdot \frac{\cos 2\alpha_b}{\gamma_s} \cdot \frac{1}{1 + \left(\frac{\partial y}{\partial x}\right)^2} \right\} \cdot \frac{\partial^2 y}{\partial x^2} \qquad \text{--- (B4)}$$

(B4) is a non-linear parabolic equation (diffusion equation). When (B4) is solved by an explicit finite-difference method, a stability condition[16] required for time step ΔT is:

$$\Delta T \leq \frac{1}{2}(\Delta x)^2 \Big/ \left\{ \frac{1}{D + BH} \cdot \frac{0.77(EC_g)_b}{\gamma_s} \cdot \cos 2\alpha_b \cdot \frac{1}{1 + \left(\frac{\partial y}{\partial x}\right)^2} \right\} \text{--- (B5)}$$

In the case of a physical model study described in 4-2 (Chapter 4)

D = 0.12 m

BH = 0.05 m

Δx = 0.5 m

H = 0.05 m

ρ = 1,000 kg/m^3

g = 9.8 m/s^2

E = $\frac{1}{8}\rho g H^2$ = 3.1 kg/s^2

h (water depth) = 0.06 m

Tw (wave period) = 1.41 s

C (wave celerity) = 0.75 m/s

Lw (wave length) = 0.96 m

n_w (ratio between wave group velocity and wave celerity)

$$= \frac{1}{2}\left\{1 + (4\pi h / Lw) / \sin h\,(4\pi h / Lw)\right\}$$

$$= 0.95$$

Cg (wave group velocity) = 0.71 m/s

σ (density of sand) = 2,650 kg/m^3

λ (porosity of sand) = 0.32

$$\gamma_s = (\sigma - \rho)(1 - \lambda)g$$

$$= 11{,}000\ N/m^3$$

$\alpha_b = -15°$

$\cos 2\alpha_b = 0.87$

$\partial y / \partial x = 0.15$

By substituting the above into (B5),

$$\Delta T \leq 162 \text{ seconds}$$

If $\cos 2\alpha_b < 0$ in (B4), oscillations involved in calculated shoreline do not decay and solutions are not stable[17].

When alongshore gradient of a shoreline $\partial y / \partial x$ and α_x (angle between the breaking crests and the baseline) are small, (B3) reduces to:

$$\sin 2\alpha_b = 2\tan\alpha_x - 2\frac{\partial y}{\partial x} \qquad \text{----- (B6)}$$

Hashimoto[18] used (B6) for his numerical calculation of shoreline changes. In this case, the following equation is obtained instead of (B4):

$$\frac{\partial y}{\partial T} = \frac{1}{D + BH} \cdot \frac{0.77\,(EC_g)_b}{\gamma_s} \cdot \frac{\partial^2 y}{\partial x^2} \qquad \text{----- (B7)}$$

$\left\{ 0.77(EC_g)_b \right\} / \left\{ \gamma_s \ (D + BH) \right\}$ of (B7) is always positive.

So, instability due to the negative coefficient of the diffusion equation does not happen.

Appendix C Komar's method of calculating $\tan\beta / f$

Longuet-Higgins[12] gave the following longshore current velocity equation:

$$\left.\begin{aligned} <u> &= \left(\frac{h}{h_b}\right) \times \begin{cases} v_0 & h < h_b \\ 0 & h > h_b \end{cases} \\ v_0 &= \frac{5}{16}\pi \frac{\gamma}{C_f} (gh_b)^{1/2} \tan\beta \sin\alpha_b \end{aligned}\right\} \quad \text{----- (C1)}$$

where C_f is a friction coefficient. Therefore, the average alongshore current velocity is:

$$\begin{aligned} \bar{V} &= \frac{\int_{h=h_b}^{h=0} h<u>\, dy}{\int_{h=h_b}^{h=0} h\, dy} \\ &= \frac{2}{3} v_0 \\ &= \frac{5\pi}{24} \cdot \frac{\gamma}{C_f} \sqrt{gh_b} \tan\beta \sin\alpha_b \\ &\propto U_m \frac{\tan\beta}{C_f} \sin\alpha_b \end{aligned} \quad \text{----- (C2)}$$

Komar and Inman[6] derived the average alongshore current velocity using equation (24) and the Scripps Equation:

$$\bar{V} = 2.7\ U_m \sin\alpha_b \quad \text{----- (C3)}$$

As equations (C2) and (C3) are equivalent, hence $\frac{\tan\beta}{C_f}$ should be constant[15]. C_f and f are comparative. So,

$$\frac{\tan\beta}{f} = \text{constant}$$

$$= A \qquad \text{----- (C4)}$$

REFERENCES

1) Pelnard-Considere, R: Essai de Theorie de l'Evolution des Formes de Rivage en Plages de Sable et de Galets. 4th Journees de l'Hydraulique, Les Energies de la Mer, Question III, Rapport No 1, 1956.

2) Price, W A, Tomlinson, K W and Willis, D H: Predicting changes in the plan shape of beaches. Proceedings of the 13th Coastal Engineering Conference, 1972.

3) Bakker, W T: The dynamics of a coast with a groyne system. Proceedings of the 11th Conference on Coastal Engineering, Chapter 31, 1968.

4) Mehaute, B L and Soldate M: Mathematical modelling of shoreline evolution. CERC Misc Report No 77-10, 1977.

5) Nishimura, H: Mathematical Simulation of beach evolution, Lecture Notes of the 14th Summer Seminar on Hydraulics, 1978, Course B (in Japanese).

6) Komar, P D and Inman D L: Longshore sand transport on beaches. Journal of Geophysical Research, 75, No 30, 1970.

7) Brampton, A H and Motyka, J M: Report in preparation.

8) Bakker, W T: The influence of longshore variation of the wave height on the littoral current. Study Report WWK 71-19, Ministry of Public Works (Rijkswaterstaat), The Hague, The Netherlands, 1971.

9) Bijker, E W: Some considerations about scales for coastal models with movable bed. Delft Hydraulics Laboratory, Publication No 50, 1967.

10) Swart, D H: Offshore sediment transport and equilibrium beach profiles. Delft Hydraulics Laboratory, Publication No 131, p 211, 1974.

11) Jonsson, I G: Wave boundary layers and friction factors. Proceedings of the 10th Conference on Coastal Engineering, 1966.

12) Longuet-Higgins, M S: Longshore currents generated by oblique incident sea waves. 1, Journal of Geophysical Research, 75, No 33, 1970.

13) Longuet-Higgins, M S and Stewart, R W: Radiation stresses in water waves; a physical discussion, with applications, Deep Sea Research, Vol. 11, pp. 529-562, 1964.

14) Motyka, J M and Willis D H: Alongshore sediment transport due to variations in wave height. Hydraulics Research Station Notes 17, 1975.

15) Komar, P D: Beach processes and sedimentation. Prentice-Hall, Inc. p 211.

16) For example, Richtmyer, R D and Morton, K W: Difference methods for initial-value problems, Second Edition, pp.12, Interscience, 1967.

17) Heath, R F W and Wood, W L: Evolution of beach plan due to wave action, Proceedings of international conference on numerical methods in fluid dynamics, Southampton University, 1973.

18) Hashimoto H: Models for predicting the shoreline evolution caused by the offshore breakwater, Proc. of 21st Japanese Coastal Engineeering Conference, 1974, (in Japanese).

CHAPTER 4. STUDY OF APPLICATION OF BEACH MATHEMATICAL MODEL

4-1 Introduction

Theory of beach mathematical model has been shown on Chapter 3. Several difficulties will happen on applying this theory to the actual cases. The author has tried to reproduce both the shoreline changes in the physical model experiment and those in the prototype in order to find the best way for dealing with these difficulties. In this chapter, some applications of the beach mathematical model are presented, both as a demonstration of its use and as an attempt to verify the assumptions made.

A physical model study about a reclamation projected into the sea was done by Sato, Ozasa, and Nagai[1]. Shoreline changes were measured during this model study.

Prototype shoreline changes which were reproduced were observed at Tokushima Coast and at Nigerian Coast near Lagos.

4-2 Application of the beach mathematical model to the shoreline changes measured in the physical model experiment

4-2-1 The physical model experiments

The purpose of the experiments was to predict the shoreline changes which would result from the extension of a runway at Tokushima Airport into the sea. The proposed land reclamation for the runway cuts the bay between the ports of Imagiri and Awazu into two sections as shown in Fig. I-4-1. The model was built to a horizontal scale of 1/200 and a vertical scale of 1/50. Waves approach this stretch of coast mainly from the south-east, and this was the direction used in the physical model.

There is, therefore, a steady drift of beach material towards Awazu Port. The beach crest near Imagiri Port has already dropped to about

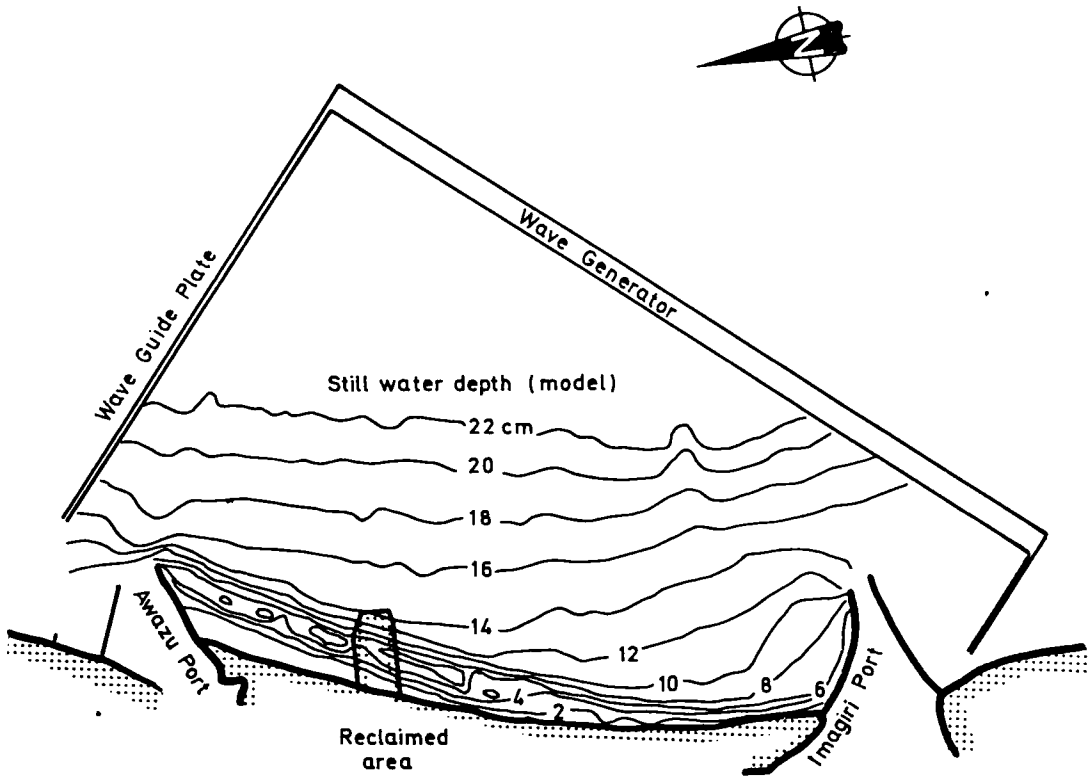

Fig. I-4-1 Contour map of the physical model experiment (after Sato et al.)

Mean Sea Level, and at the start of the experiments the beach at this end of the model was at that level for the first 8 metres. From that point it gradually increased in width until, at Awazu Port, it was about 50 cm across. The median diameter of the sand used was 0.29 mm and throughout the tests the waves offshore had a period of 1.41 seconds and a height of 8.5 cm. The resulting beach profile was on the border between a 'storm beach' and a 'normal beach', as proposed by Johnson[2] and Iwagaki and Noda[3]. Any reduction of the wave heights due to, for example, diffraction can be expected to cause a change of beach type. Once waves reached the model sea walls, small stones were put in front of them to decrease the wave reflection.

The beach mathematical model was used to try to reproduce beach changes which occurred during two 360 minute runs of the physical model. In the first run, the development of the beach without the reclamation was studied, and used as a basis of comparison for the second run, which included the reclamation. Because the reclamation cuts the beach into two parts, this second run is studied using two mathematical models, one on each side of the reclaimed area. Fig. I-4-2 shows the beach positions at both the beginning and the end of the two runs, which are called, for convenience, Case 1 and Case 2. These are now dealt with separately.

4-2-2 Shoreline evolution of the coast without the reclamation - Case 1

In this section, a mathematical model for the whole bay from Imagiri to Awazu, is used to predict changes of the coastline in the absence of the reclamation. Fig. I-4-3 (a) shows the refraction diagram used to calculate the wave directions in this case.

The baseline for the mathematical model is shown on Fig. I-4-2. Section number 1 is at the Awazu Port breakwater and section number 39 at the Imagiri Port breakwater. The distance between consecutive section lines

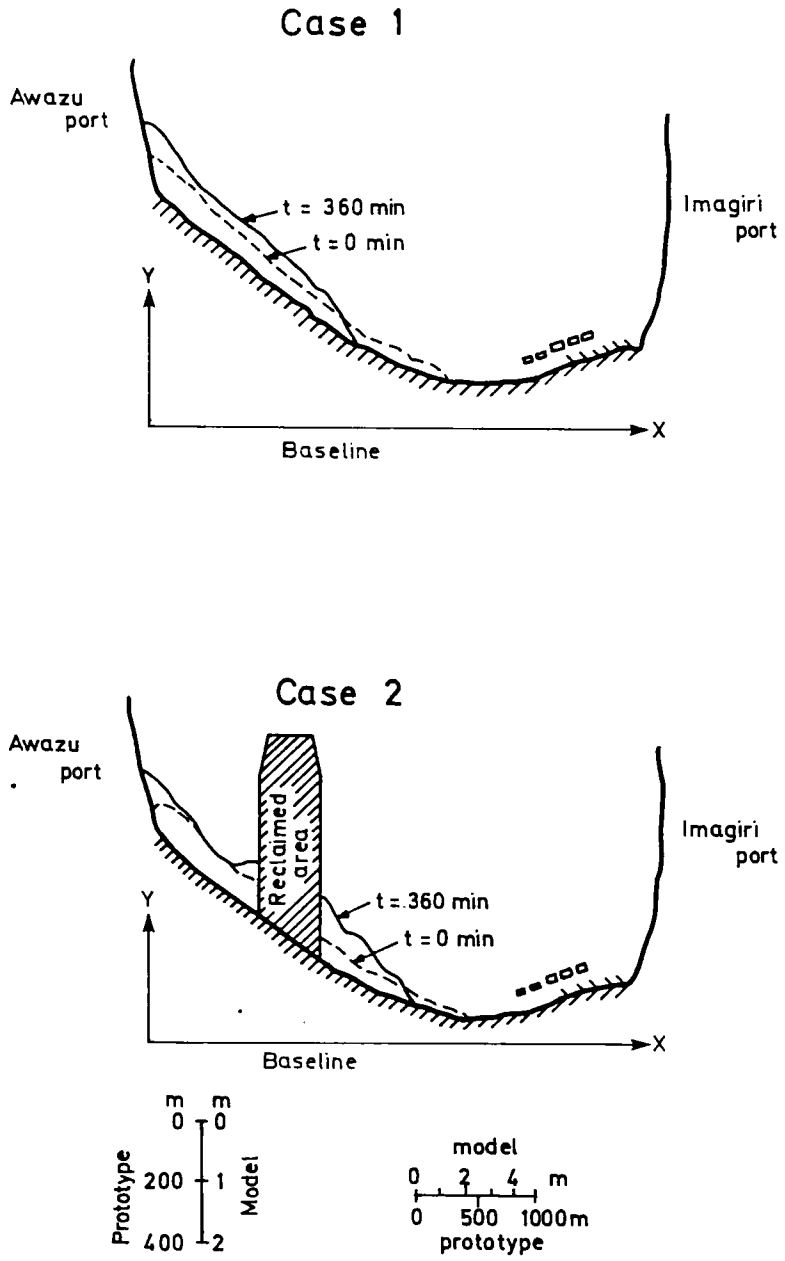

Fig. I-4-2 Changes of the position of mean water line (after Sato et al.)

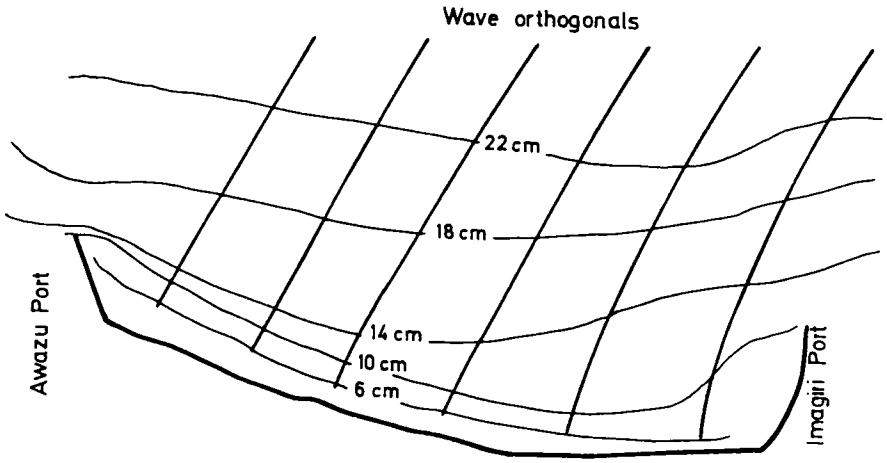

(a) Refraction diagram (case 1)

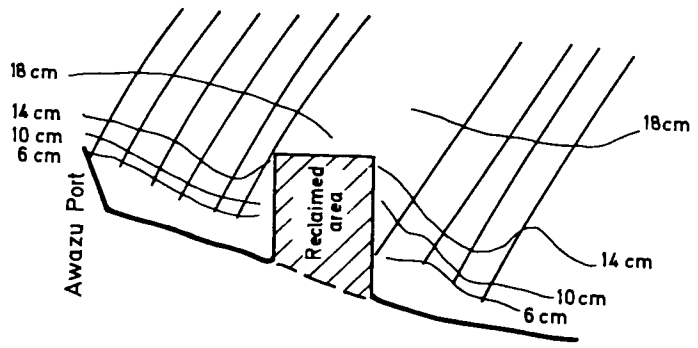

(b) Refraction diagram (case 2)

Fig. I-4-3 Refraction diagram

is 0.5 m. Both breakwaters stop the sediment movement almost completely, so the author sets the sediment transport rate to zero at these boundaries in the numerical calculations. Wave heights, H_b, were measured on the physical model and are shown as the open circles on Fig. I-4-4. The solid line on that figure represents the simplified wave height distribution used by the mathematical model.

In a similar way, Fig. I-4-5 shows with open circles the wave directions, α_x, obtained from the refraction diagram, whilst the solid line gives the directions used in the mathematical model. In this case, onshore-offshore sediment transport was neglected, and the values used in the calculations for BH, D and $\tan\beta$, taken from the physical model, were 0.05 m, 0.12 m and 0.125 respectively.

The results of the physical model are compared with the predictions of the mathematical model in Fig. I-4-6.

Both forms of the alongshore sediment transport formula were tried (ie equations (10) and (11) of chapter 3) and the results obtained from each are shown, although the difference between the two was always less than 1 cm. As a result only the second of these formulae (equation (11)) was used for later calculations.

The predicted shorelines agree fairly well with the physical model results, although they fail to show the observed curve between sections 4 to 16. This may well be explained by long period oscillations in the model basin and some onshore sediment movement.

The subsidiary graph in Fig. I-4-6 shows the berm height, B (I) as calculated by the mathematical model, at the end of the run. Notice that up to section 11 the beach is sufficiently wide that this height is equal to its maximum value, namely BH = 0.05 m. Between sections 11 and 20 this berm height decreases, so that the model is in the second stage in this

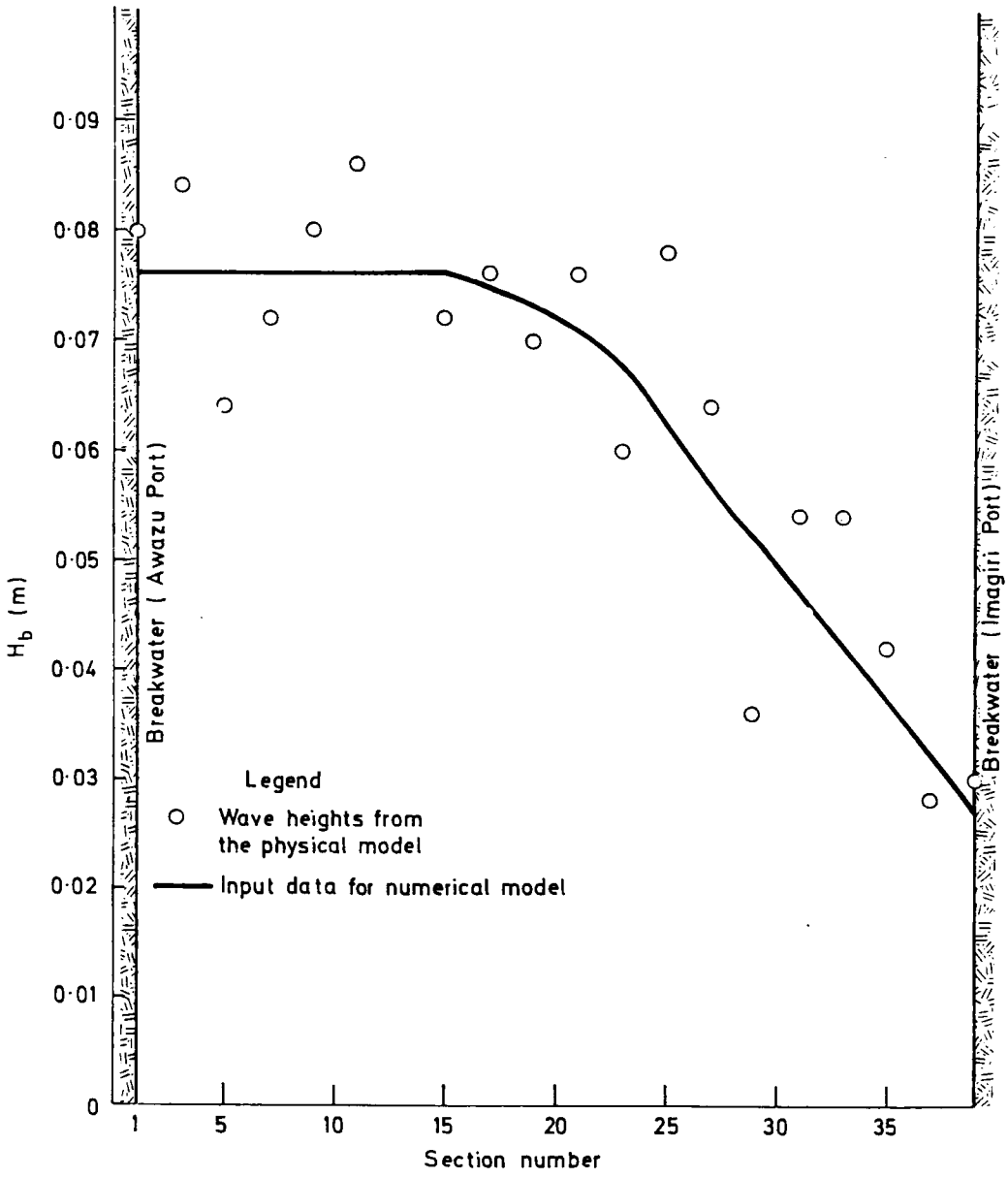

Fig. I-4-4 Wave heights between Imagiri and Awazu Ports (case 1)

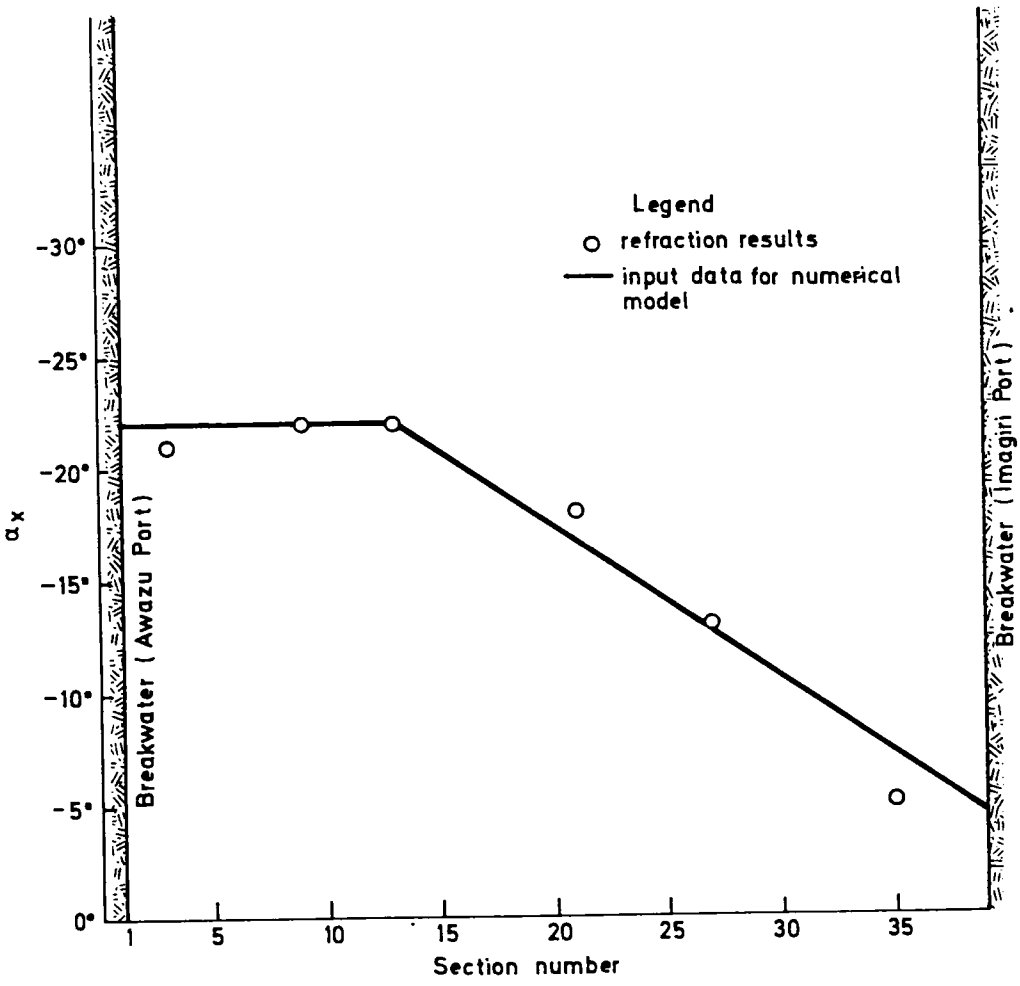

Fig. I-4-5 Wave directions between Imagiri and Awazu Ports (case 1)

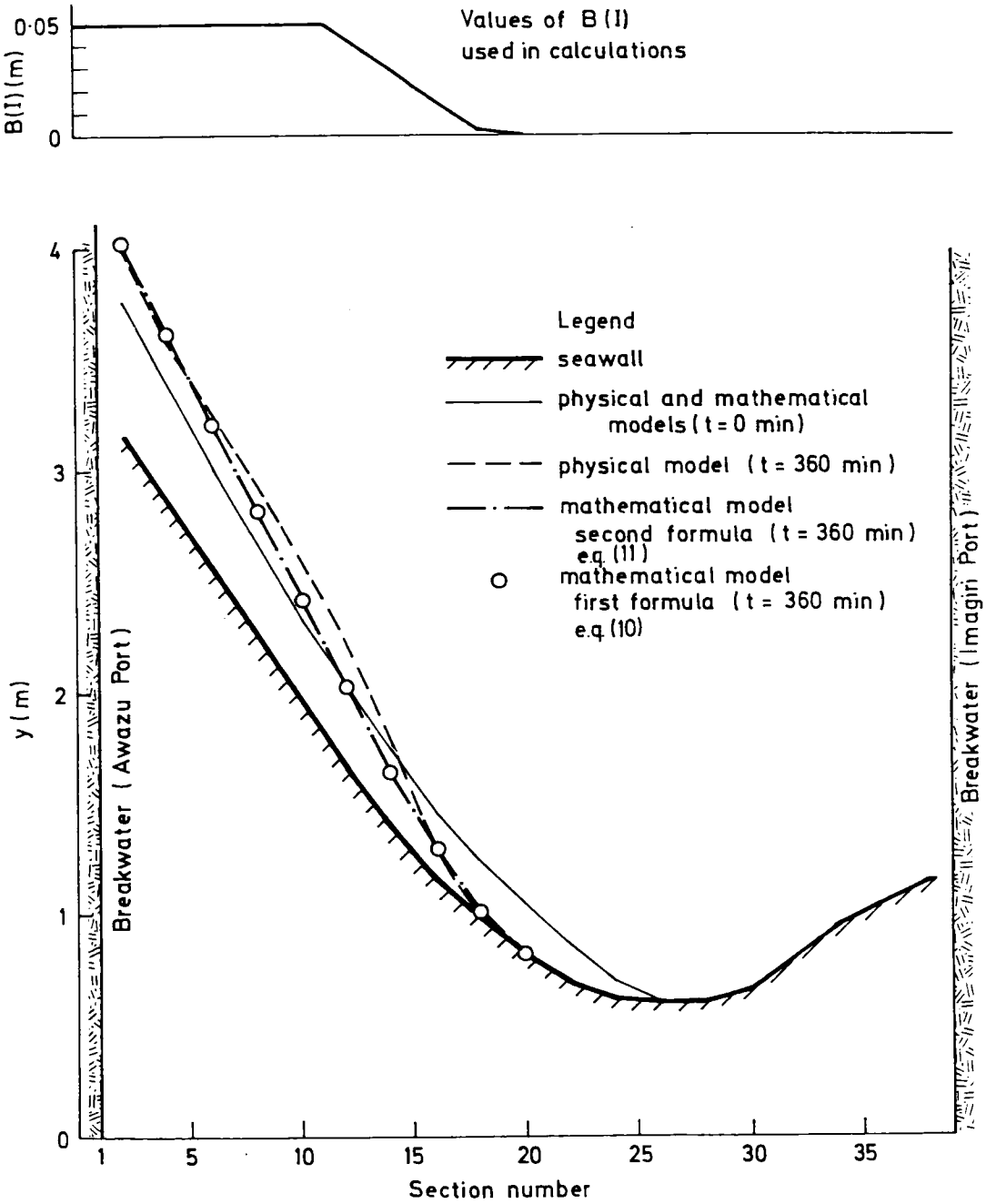

Fig. I-4-6 Shoreline evolution between Imagiri and Awazu Ports (case 1)

region. Beyond section 20 the beach has reached its equilibrium profile.

As a further check on the accuracy of the mathematical model, the predicted sediment transport rate at section 13 was compared to a rate measured on the model. Between minutes 120 and 130 of the run, the predicted value of the transport was 4.4×10^{-4} m^3/min towards Awazu Port, whilst the measured rate was 6.7×10^{-4} m^3/min. In view of the inaccuracies involved in measuring alongshore transport rate, this comparison is not too discouraging.

4-2-3 Shoreline evolution - Case 2 (between the reclamation and Imagiri Port)

In this, and the following section, comparisons are made between the mathematical model and the second run of the physical model, ie with the reclamation present (Case 2 - Fig. I-4-2). Because the reclamation projects so far into the bay, it reduces the alongshore drift to virtually zero on each flank. As a result, it is possible to model the bay mathematically by considering its two portions separately. This section considers the portion between the reclaimed area and Imagiri Port, whilst the next section deals with the part between the reclamation and Awazu Port.

The mathematical model for both these portions has to include the effects of onshore-offshore transport, because one of the effects of the reclamation in the physical model was to induce scouring of the offshore bed. The areas of scour are shown in Fig. I-4-7, and it is believed that they were principally the result of circulating currents set up by breaking waves of varying height.

The effect of such changes in the sea bed is two-fold. Firstly much of the material eroded travels onshore producing a wider beach and secondly, as the depths offshore change, the wave refraction patterns in the area are also altered. This latter point is demonstrated by the wave refraction diagram, Fig. I-4-3 (b), which shows the new situation after 120 minutes of the run.

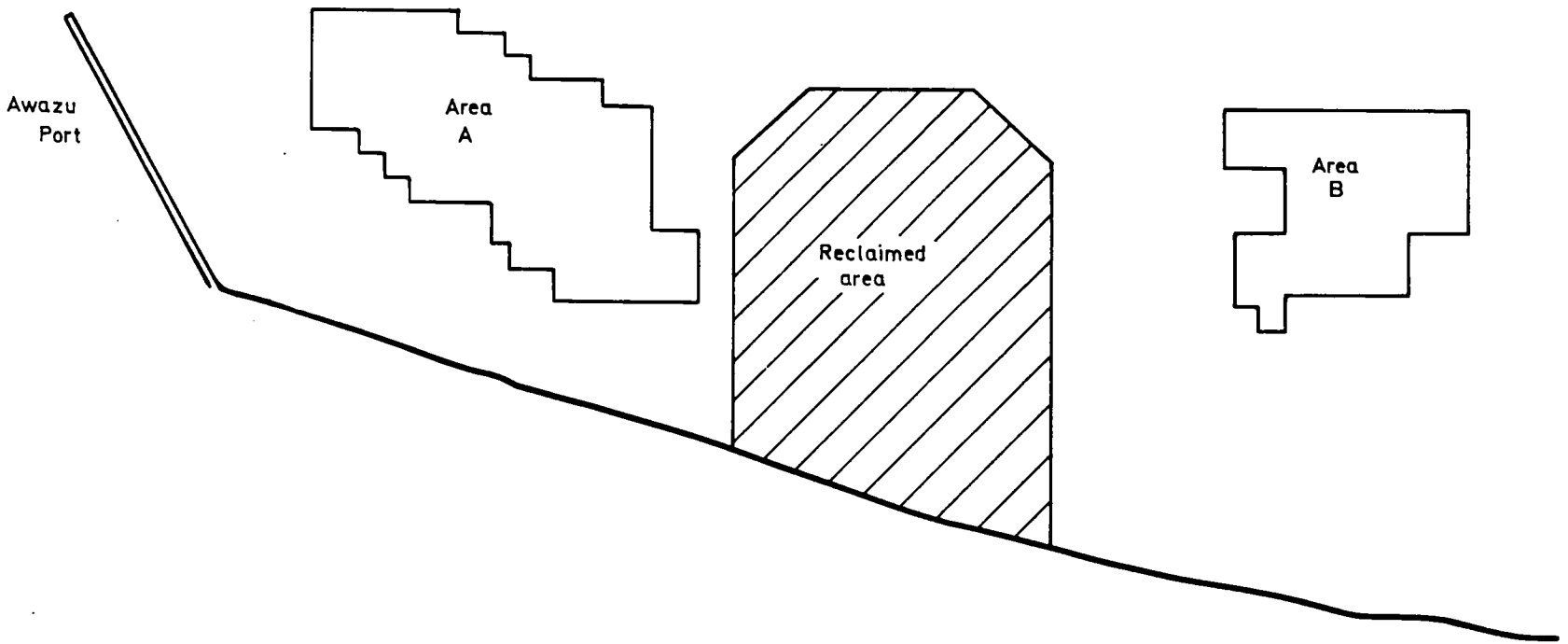

Fig. I-4-7 Scoured areas in the offshore zone

It is not possible, at present, to formulate the amount of onshore transport likely to occur in such a situation and for this purpose the author had to rely on measurements from the physical model.

Turning now to the specific case of the stretch of beach between the reclamation and Imagiri Port, a model was set up using part of the baseline used for the whole bay (Case 1) as described above. The alongshore drift was taken as zero at both ends of the model, that is at section 1, on the flank of the reclamation and at section 27 at the Imagiri Port breakwater. The distance between sections was again taken as 0.5 m.

Wave heights along this frontage were measured on the physical model and are shown by open circles on Fig. I-4-8. The solid line shows the simplified data used by the mathematical model.

The wave directions, α_x , needed for the mathematical model were deduced from the refraction diagram, Fig. I-4-3 (b). The actual values obtained are shown by the open circles, together with the smoothed data for the mathematical model indicated by the solid line on Fig. I-4-9. The dashed line shows the results which would have been obtained if the change in refraction pattern over the scoured area had been ignored.

To obtain the onshore-offshore transport, q (see equations (13) and (14) of Chapter 3) it was necessary not only to take measurements from the model, but also to make certain simplifying assumptions. Fig. I-4-10 shows the measured volume of sediment eroded from the scoured area B of Fig. I-4-7, as a function of time. This sediment erosion rate was simplified, as shown by the solid line, to 2.90×10^{-6} m^3/s, and it was then assumed that all the sediment scoured travelled onshore. Because it was not possible to find out where this material came ashore, it was assumed that it travelled along the wave direction and was uniformly distributed between sections 1 and 7.

The values used for BH, D and $\tan\beta$ were the same as in the previous

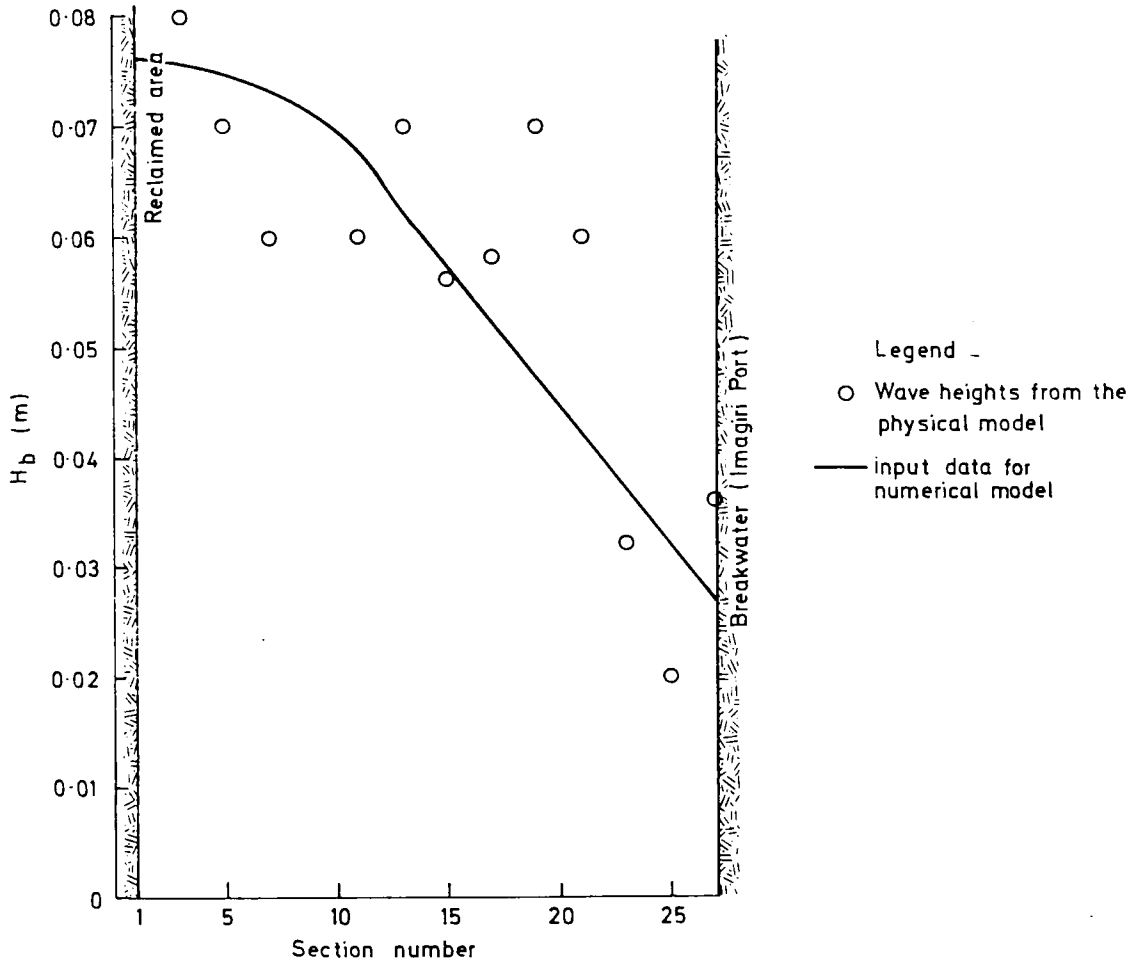

Fig. I-4-8 Wave heights between the reclaimed area and Imagiri Port (case 2)

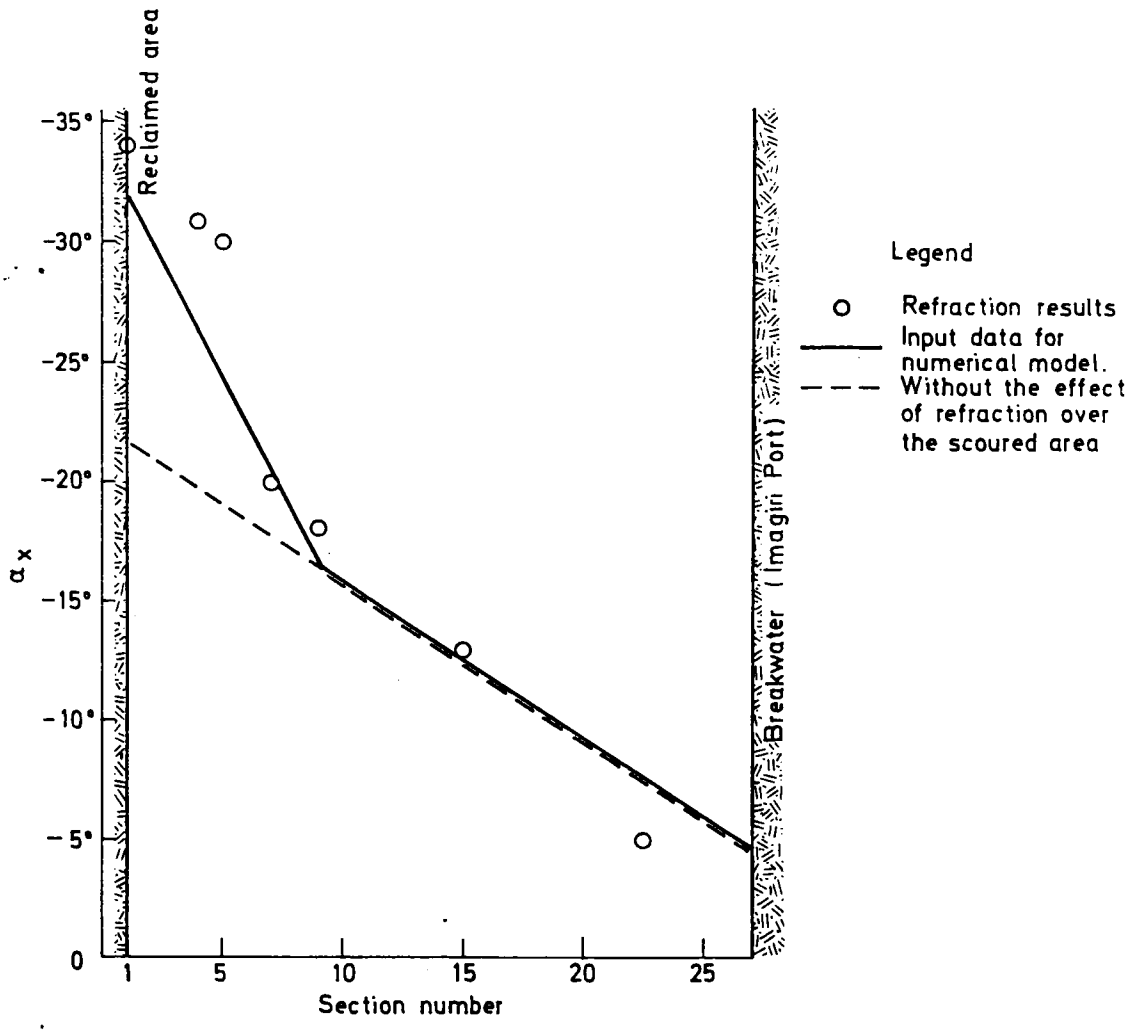

Fig. I-4-9 Wave directions between the reclaimed area and Imagiri Port (case 2)

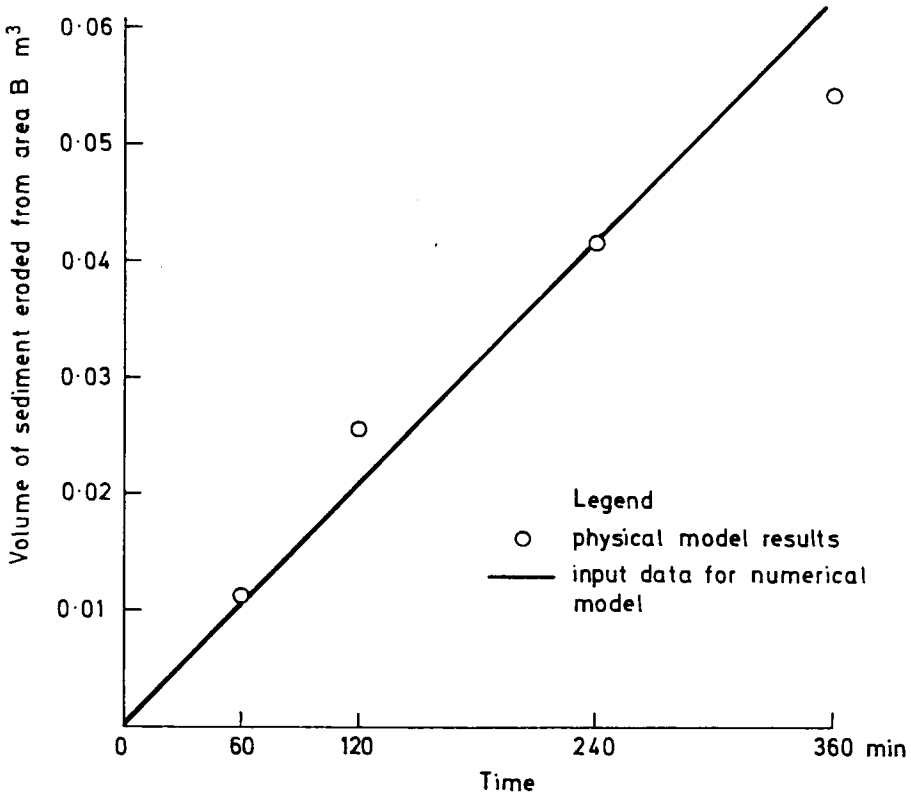

Fig. I-4-10 Onshore sediment transport between the reclaimed area and Imagiri Port (case 2)

model, namely 0.05 m, 0.12 m and 0.125 respectively.

Figs. I-4-11 and I-4-12 both show the comparison between the physical model (light dashed line) and the mathematical model (heavy solid line), which for most of the beach is quite satisfactory. Each of these figures also shows however, the result of neglecting one effect of the scoured area in the mathematical model. In Fig. I-4-11 the chain-dot line shows the result of ignoring the onshore transport of material, but using the correct refraction diagram. Although the beach alignment is still correct, its area, above mean sea level, is much too small.

In Fig. I-4-12, the chain-dot line shows the result of not taking into account the changes in wave refraction caused by the scoured area. In this case, the predicted beach alignment is incorrect.

The subsidiary graph on Fig. I-4-11 shows the values of B (I), the berm height, at the end of the run. Between sections 1 to 5, the berm height is at its maximum value but from section 5 to 10 it decreases to zero. In this area the mathematical model is in its second stage. The point at which the beach drops to its equilibrium profile in front of the sea wall is well reproduced by the model.

4-2-4 Shoreline evolution - Case 2 (between Awazu Port and the reclamation)

As in the previous section, the mathematical model of this part of the beach had to include the effects of a scouring of the offshore sea bed (area A, Fig. I-4-7). However, because of the shelter provided by the reclamation, the wave heights decreased very considerably towards the southern end of the model. The measured heights are shown by open circles on Fig. I-4-13, and the smoothed input data used by the mathematical model by the solid line.

The baseline used for the mathematical model was the same as that used in Case 1, but only extending from section 1, Awazu Port, to the reclamation, section 23. The distance between sections was taken as 0.25 m from sections 1 to 16 and as 0.125 m from sections 16 to 23.

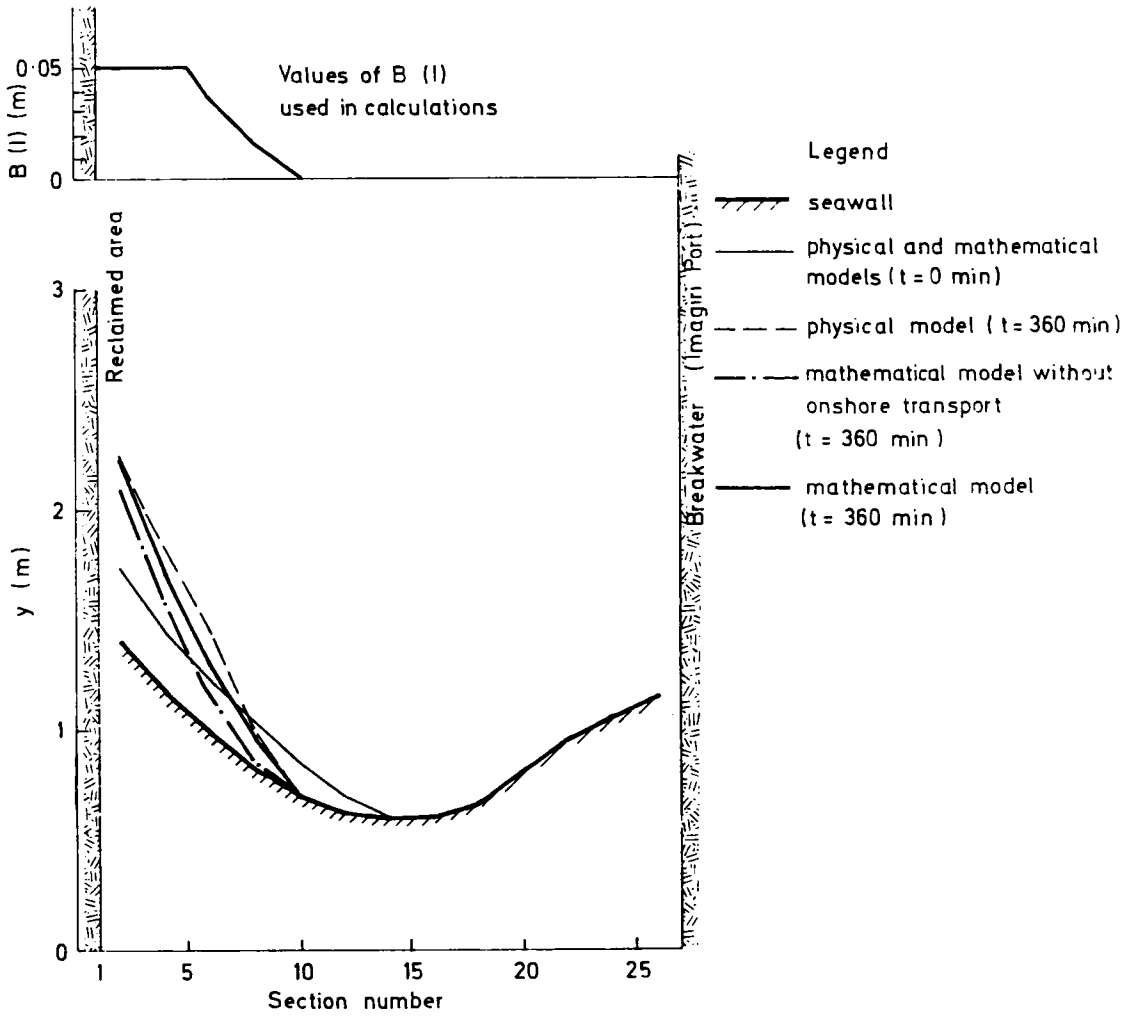

Fig. I-4-11 Shoreline evolution between the reclaimed area and Imagiri Port (case 2)

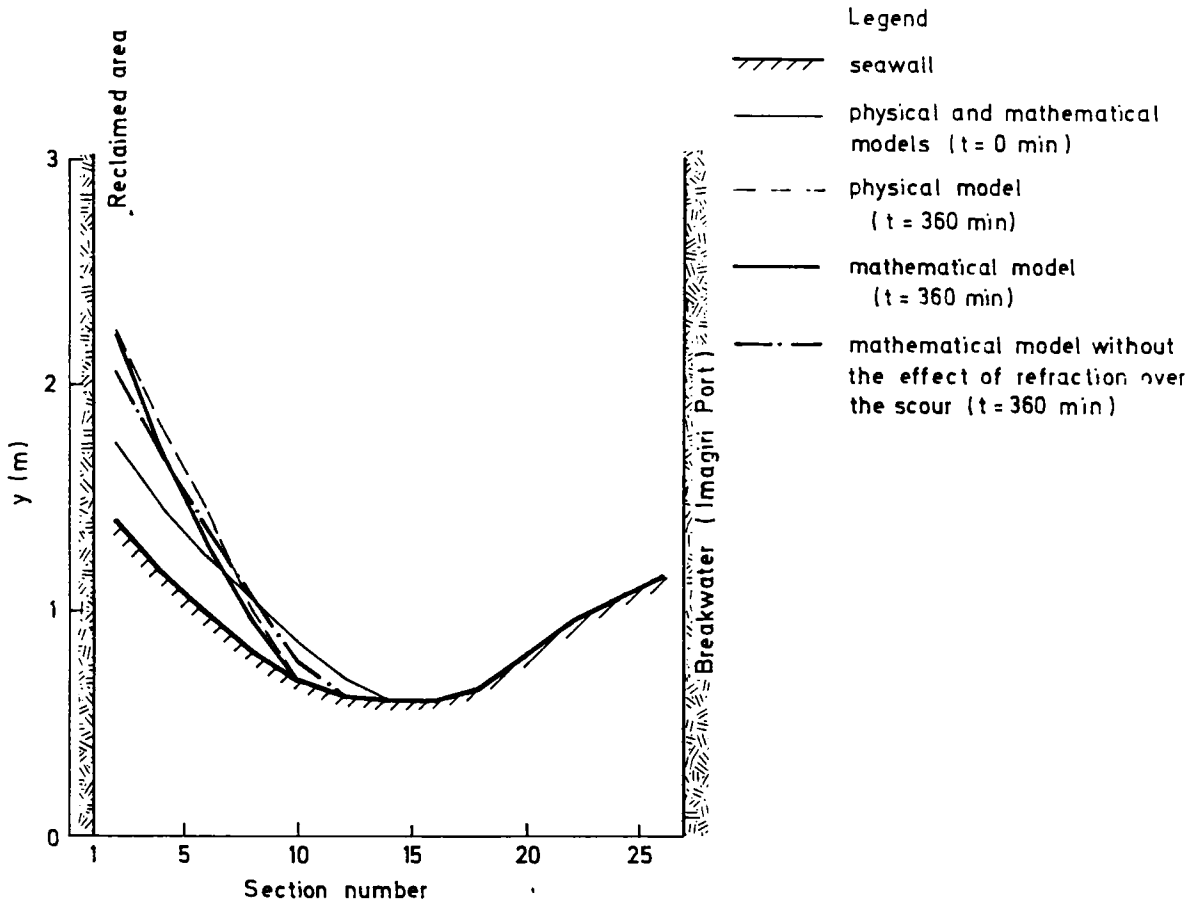

Fig. I-4-12 Shoreline evolution between the reclaimed area and Imagiri Port (case 2)

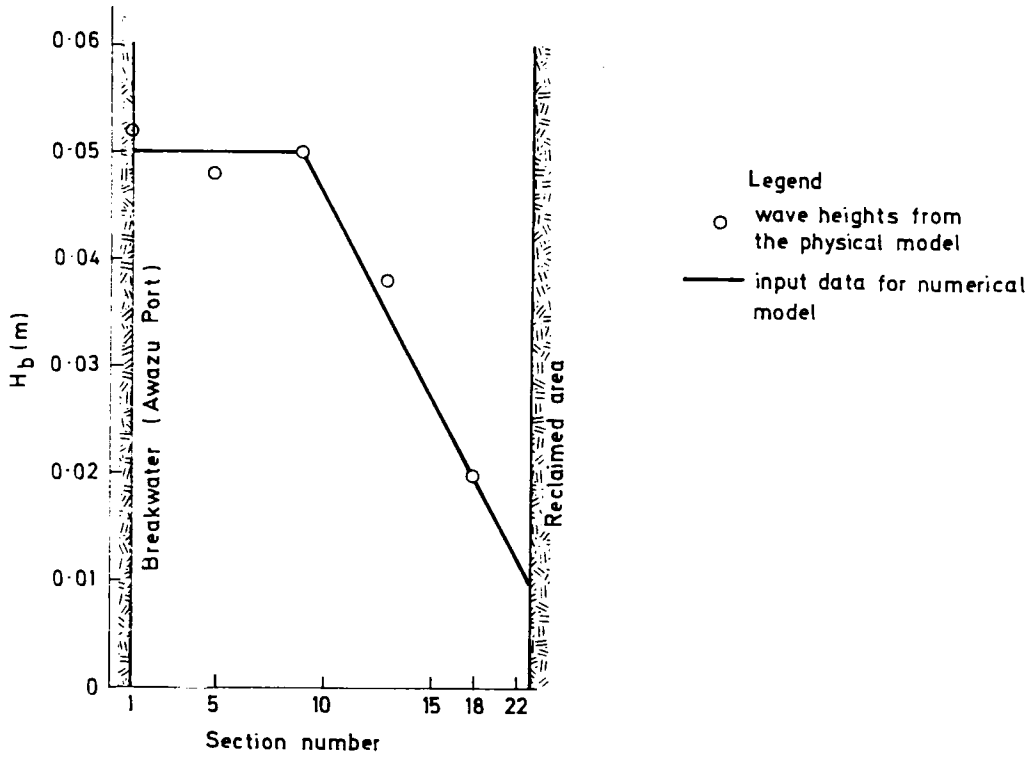

Fig. I-4-13 Wave heights between Awazu Port and the reclaimed area (case 2)

The open circles in Fig. I-4-14 show the values of α_x obtained from Fig. I-4-3 which includes the effects of refraction over the scoured area. It was assumed, that waves diffracted around the tip of the reclamation travelled radially. The solid line shows, as usual, the values used for the mathematical model. The dashed line shows the value of α_x when we ignore the effect of refraction.

Fig. I-4-15 shows, as a function of time, the volume of sediment eroded from the area A of Fig. I-4-7. This scouring was thought to be caused by a combination of circulating currents, produced by breaker heights which varied along the beach, and by a reduction in wave steepness caused by the shelter of the reclamation. Unlike the previous case, however, the eroded sediment did not all come ashore. By comparing measured beach volumes with the amount eroded, it was found that only about 75 % of the material removed from area A found its way on to the beach.

As previously it was not possible to determine where this material came ashore, and two alternative assumptions have been made. Firstly, it can be assumed that the material is uniformly distributed along the coast, that is that the onshore transport rate is the same everywhere.

The second assumption is that the sediment travels with the waves, and the onshore transport is greatest where the scouring is deepest. These two alternatives are shown diagrammatically in Fig. I-4-16 by a dashed and a solid line respectively.

For this section of the beach, because of the general reduction in wave heights, the values measured for BH, D and $\tan\beta$ were different to their previous values, at 0.07 m, 0.07 m and 0.154 respectively.

Fig. I-4-17 shows the results of the calculations. The heavy solid line shows the shoreline predicted assuming uniform onshore sediment transport whilst the open circles show the prediction assuming the non-uniform

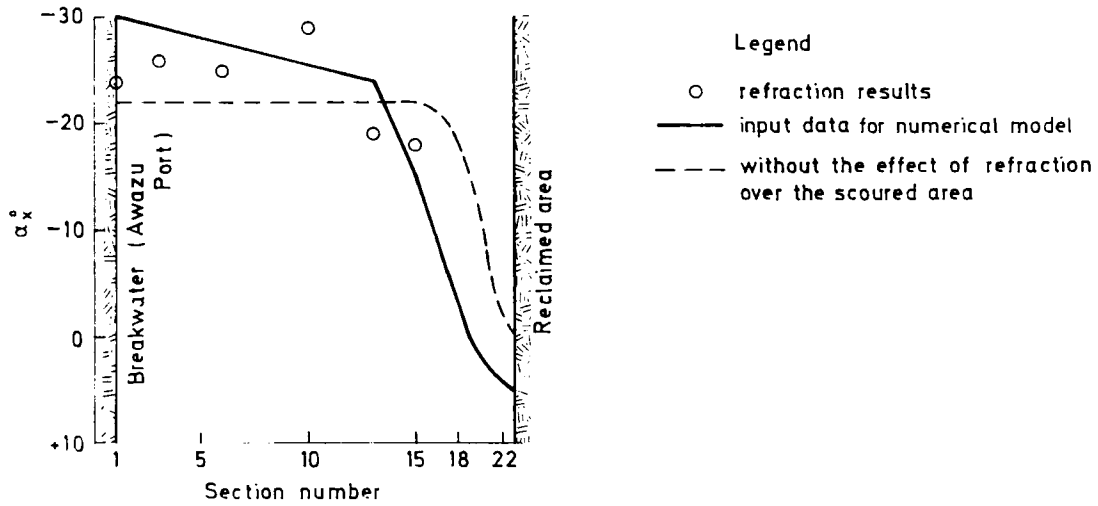

Fig. I-4-14 Wave directions between Awazu Port and the reclaimed area (case 2)

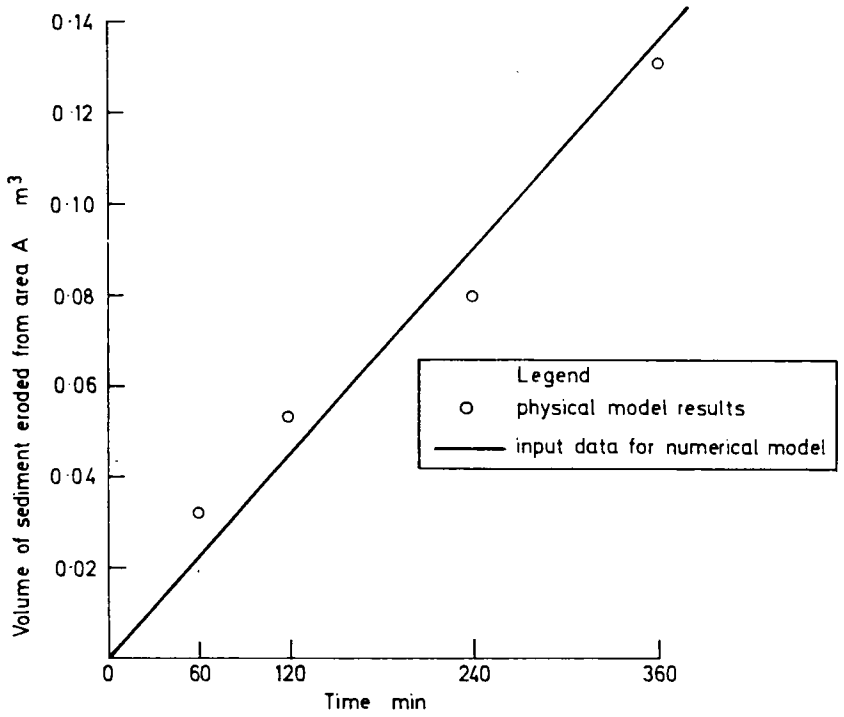

Fig. I-4-15 Onshore sediment transport between Awazu Port and the reclaimed area. (case 2)

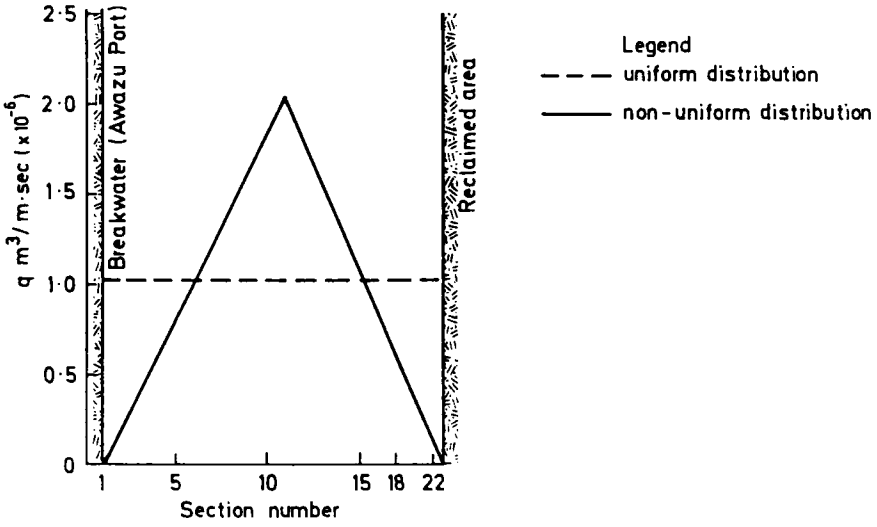

Fig. I-4-16 Distribution of onshore sediment transport

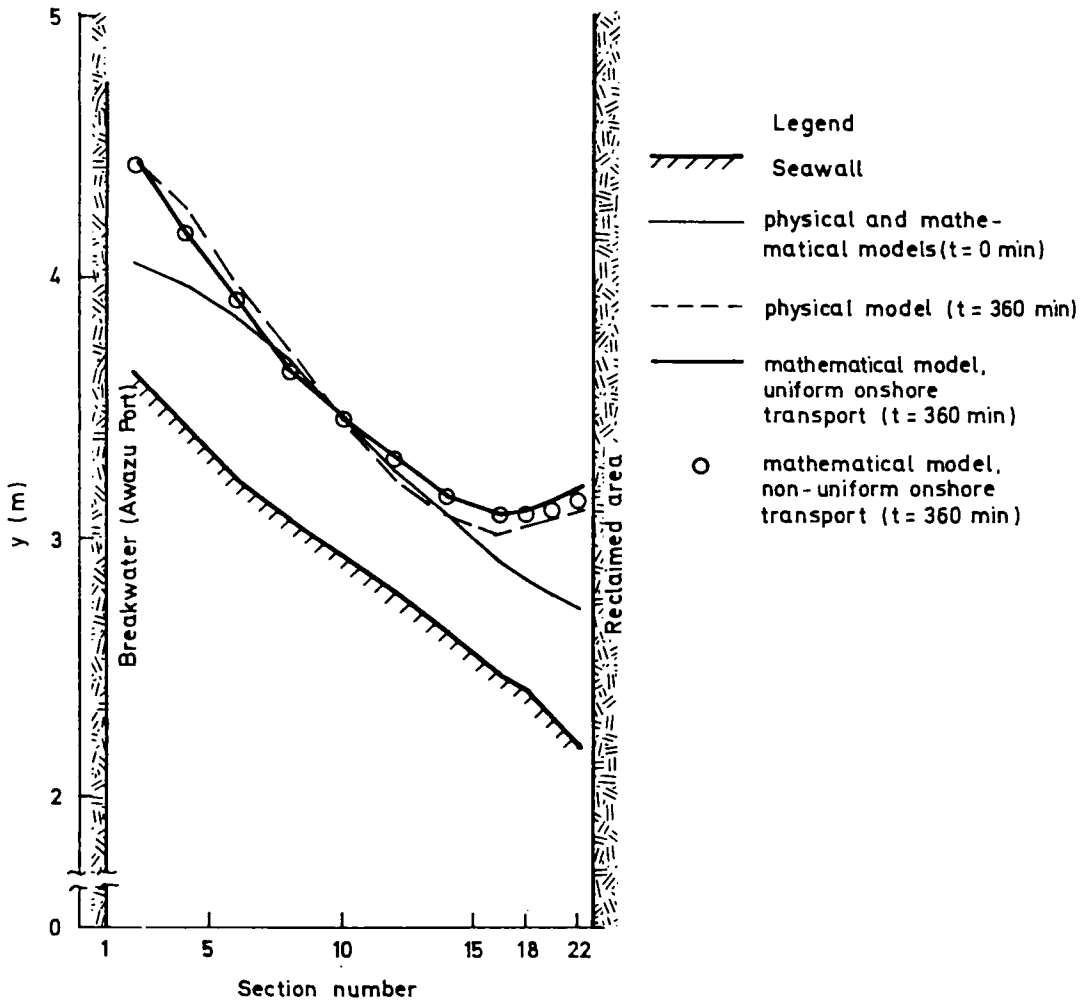

Fig. I-4-17 Shoreline evolution between Awazu Port and the reclaimed area (case 2)

distribution. Differences between these two methods are greatest near the reclamation, but are never greater than 5 cm. For the remainder of the section, therefore, the author only considers the case of non-uniform onshore transport (Fig. I-4-16). B (I) was equal to BH for most of the calculation and the sea wall rarely influenced sediment transport.

Fig. I-4-18 shows, as a function of time, the changes in the position of the shoreline at three sections, namely 2, 12 and 22. At sections 2 and 22 there is, initially, rapid accretion which reduces in rate after about 90 minutes. At section 12, there is some erosion at first, but after 90 minutes this trend reverses and the beach there slowly accretes. This all suggests that alongshore movement predominates for the first 90 minutes but onshore movement becomes increasingly important thereafter.

To investigate this further it is interesting to start from the equation for alongshore transport rate (equation (30) of chapter 3):

$$Q = \frac{0.18}{\gamma_s} (EC_g)_b \left(\sin 2\alpha_b - 3.24 \frac{\partial H_b}{\partial x} \cot\beta \cos\alpha_b\right)$$

and separate it into two parts:

$$= Q(\alpha) + Q\left(\frac{\partial H}{\partial x}\right)$$

where

$$Q(\alpha) = \frac{0.18}{\gamma_s} (EC_g)_b \sin 2\alpha_b$$

and

$$Q\left(\frac{\partial H}{\partial x}\right) = -\frac{0.58}{\gamma_s} (EC_g)_b \frac{\partial H_b}{\partial x} \cot\beta \cos\alpha_b.$$

The net alongshore transport rate is given by the difference between $Q(\partial H/\partial x)$ and $-Q(\alpha)$, and for a beach in equilibrium, they must become equal

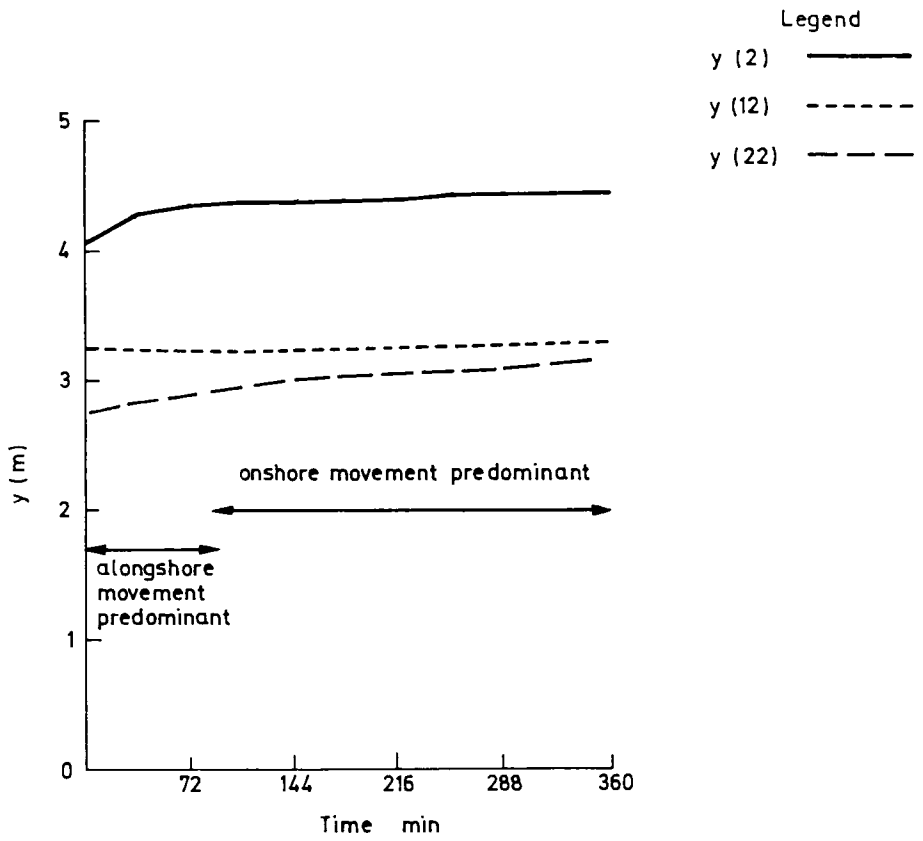

Fig. I-4-18 Shoreline changes at sections 2, 12, and 22 (non - uniform onshore sediment transport)

(but not necessarily zero). Figs. I-4-19 (a) and (b) shows, at each section, the values of $-Q(\alpha)$ and $Q(\partial H/\partial x)$ averaged over the periods 0-36 minutes and 324-360 minutes respectively. It will be noticed that the term $Q(\partial H/\partial x)$ has a significant effect in the area close to, and sheltered by, the reclamation. The differences between the two terms are much smaller in Fig. I-4-19 (b) when the beach is nearly in equilibrium. In both figures, the net alongshore transport is towards Awazu Port for sections 1-9 and towards the reclamation for sections 11-23.

It is interesting to look at the results from the model if the contribution to the alongshore sediment movement due to varying breaker height, ie $Q(\partial H/\partial x)$ is omitted. Fig. I-4-20 shows the results of such omission as a heavy dashed line. It is clear that the agreement between this line and the physical model results is much poorer than that obtained using the full model (heavy solid line) especially in the sheltered area between sections 14 to 22.

Heavy dashed line of Fig. I-4-21 shows the shorelines calculated by eliminating onshore sediment transport. $Q(\partial H/\partial x)$ of the alongshore sediment transport rate is taken into consideration. So, the shorelines obtained are almost parallel to those calculated by taking onshore transport into consideration (heavy solid lines). Differences between the heavy solid line and the heavy dashed line are almost same over the whole beach.

Heavy dashed line of Fig. I-4-22 demonstrates the effect of ignoring refraction over the area A of Fig. I-4-7. In this case, wave directions are shown by the dashed line of Fig. I-4-14. Though $Q(\partial H/\partial x)$ is included, the direction of the calculated shorelines is different from that of the physical model experiment and shape of the shorelines near the reclamation is not concave enough.

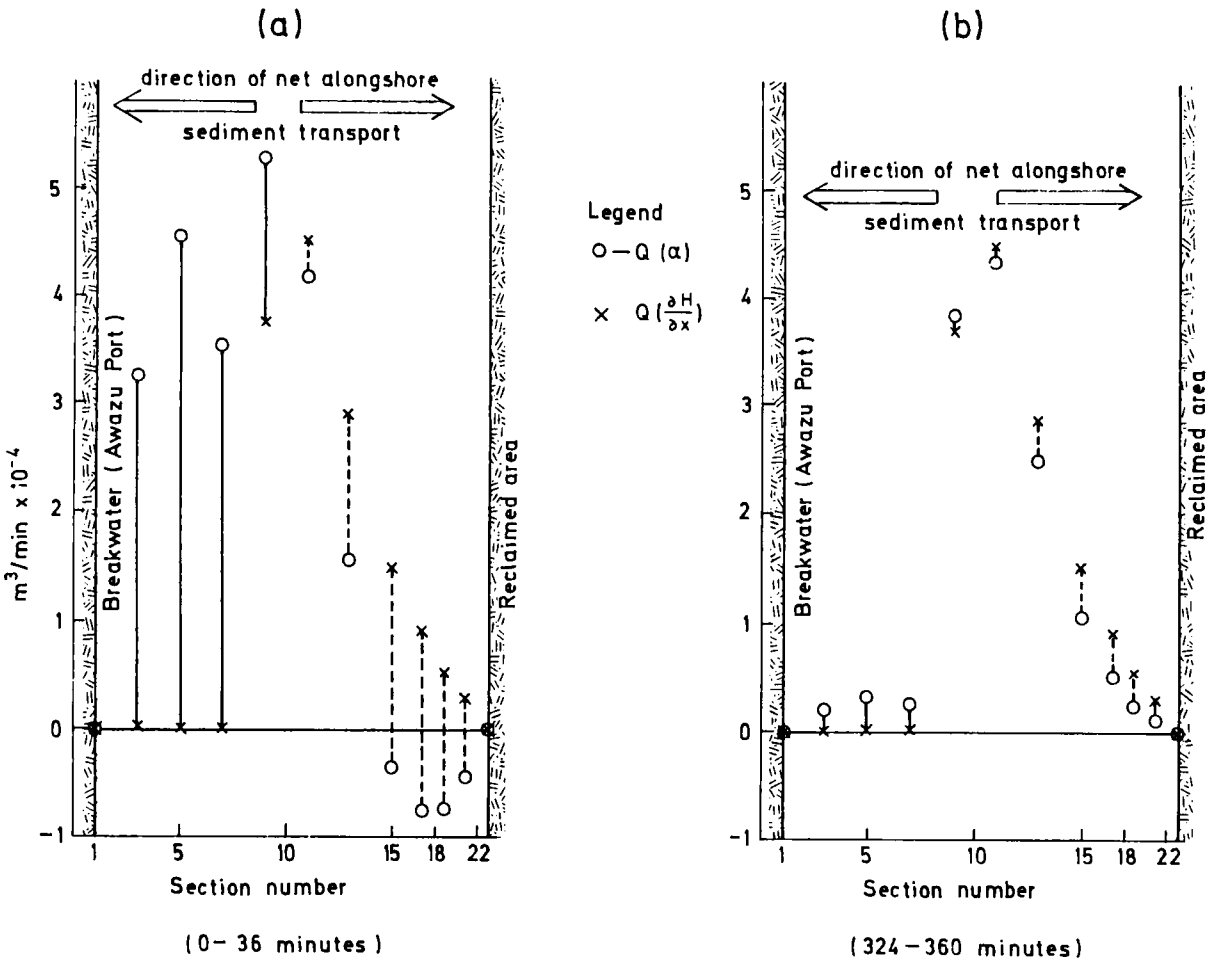

Fig. I-4-19 Alongshore sediment transport

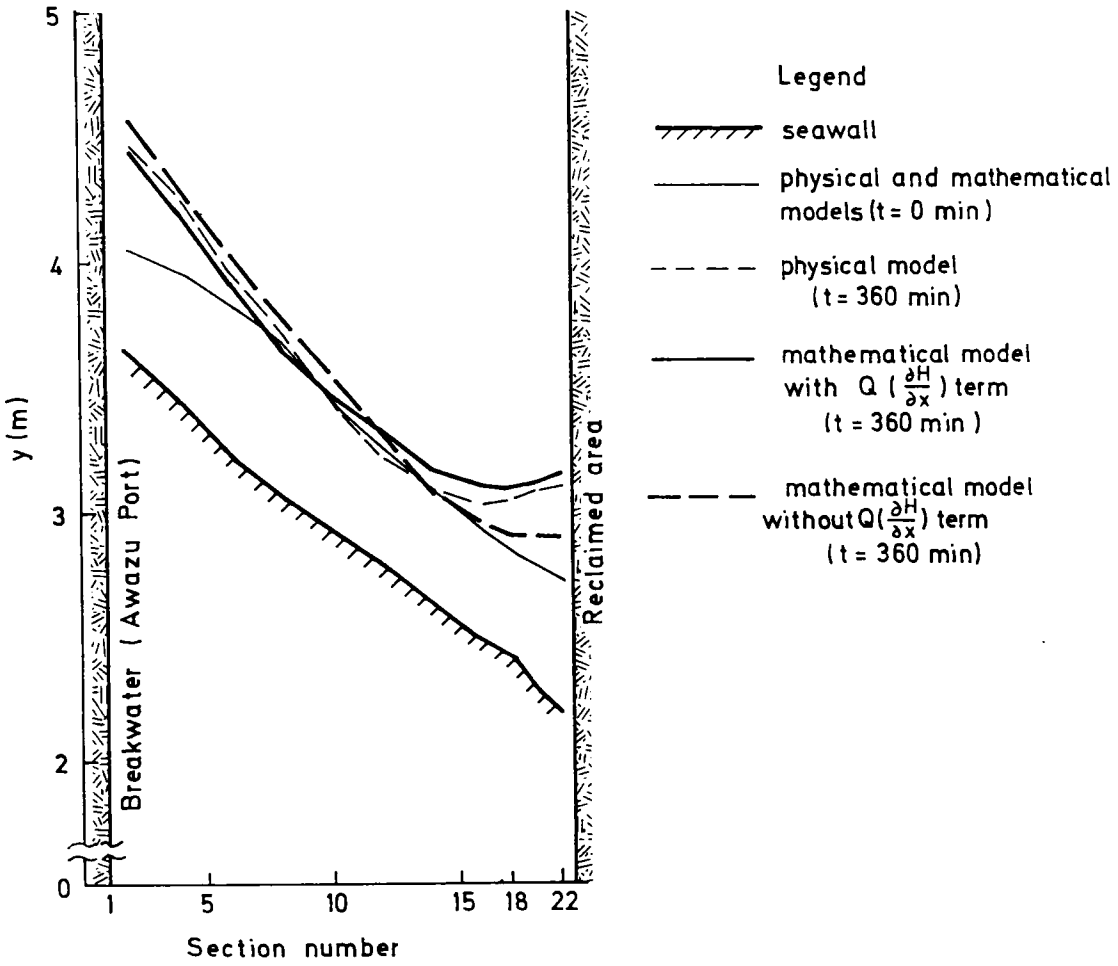

Fig. I-4-20 Shoreline evolution between Awazu Port and the reclaimed area (case 2)

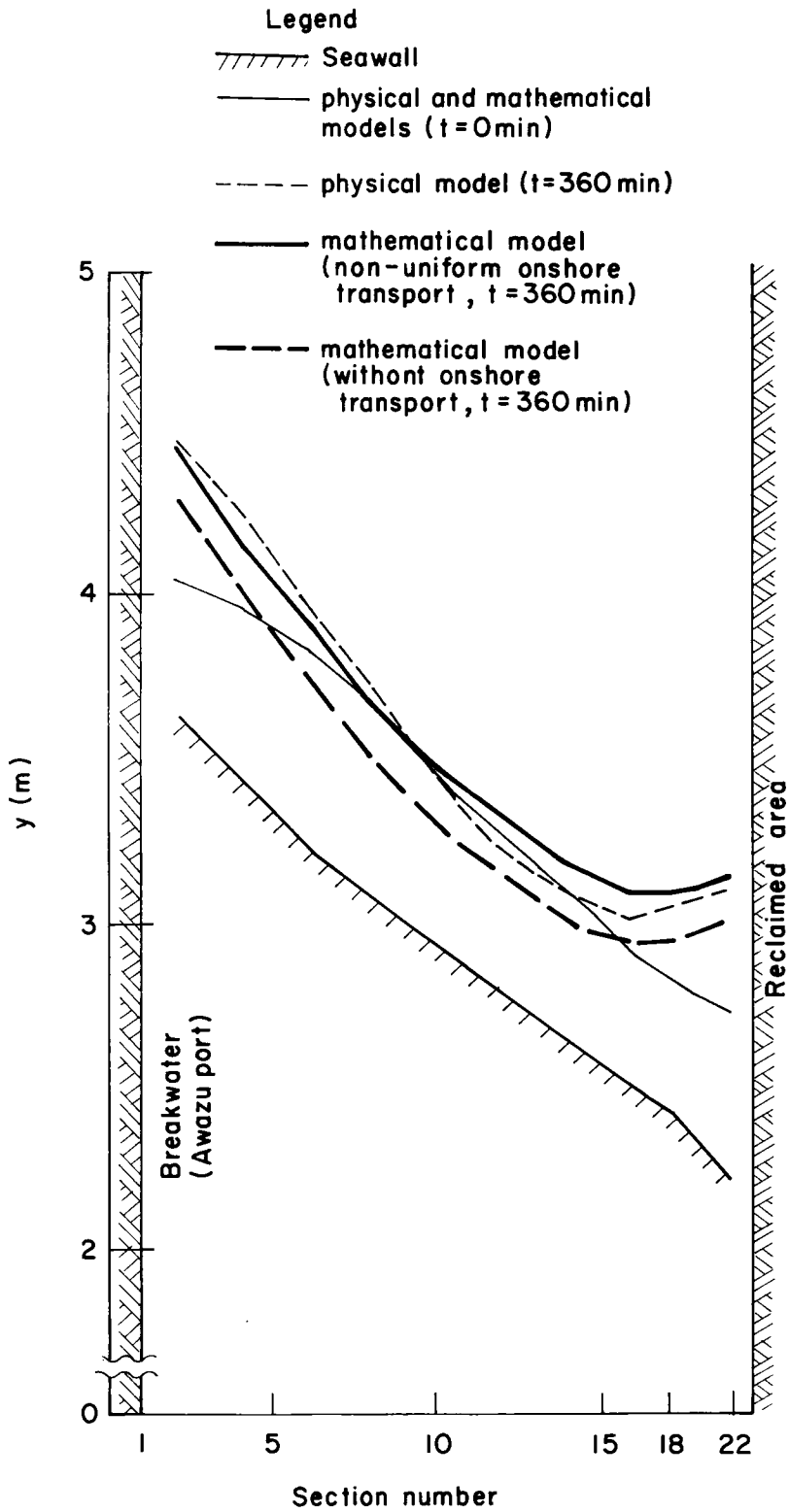

Fig. I-4-21 Shoreline evolution between Awazu Port and the reclaimed area (case 2)

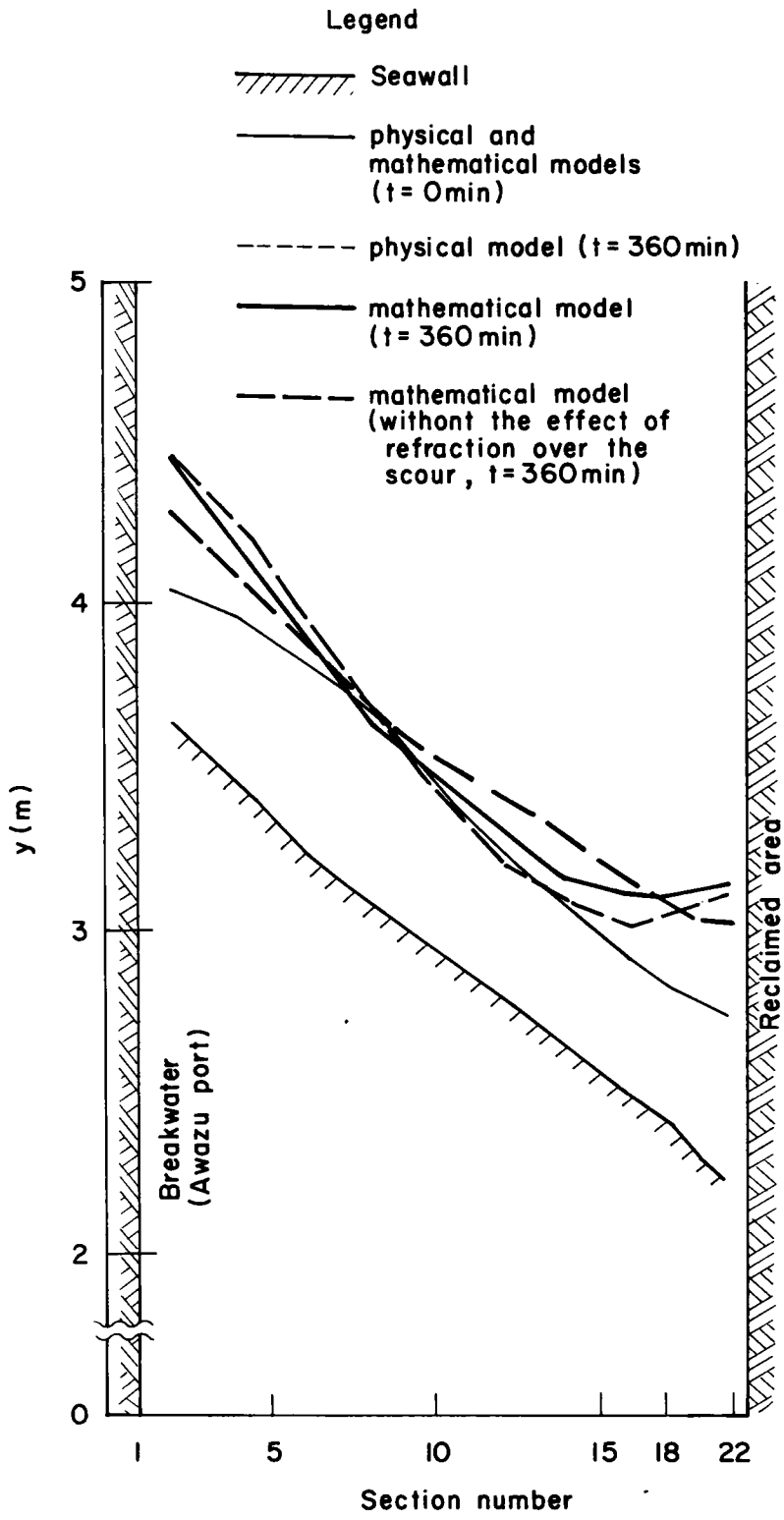

Fig. I-4-22 Shoreline evolution between Awazu Port and the reclaimed area (case 2)

4-3 Application of the beach mathematical model to field problems

4-3-1 Intension of carrying out the study

When the beach mathematical model is applied to field problems, the essential procedure for determining input data such as wave height, period, and direction is,

> first to look for input data which can be used for the mathematical reproduction of previous shoreline changes, secondly to calculate future shoreline changes using these input data.

However, coastal engineers are often asked to estimate future shoreline changes of beaches, the previous shoreline changes of which have not been known. On the other hand, tables of frequency distribution of significant wave height and period can be obtained at many beaches, so these tables might successfully be utilized for determining the input data. The primary intension of the study is to examine this possibility.

There are two types of alongshore sediment transport equations, i.e. gross littoral drift equation and net littoral drift equation. Taking up a simple example, northward littoral drift volume is 300 thousand m^3/year and southward littoral drift volume is 200 thousand m^3/year. The gross littoral drift is sum of these volumes, i.e. 500 thousand m^3/year. the net littoral drift is their difference, i.e. 100 thousand m^3/year northward.

Equation (5) of Chapter 3 expresses relation between littoral drift volume and wave energy flux at the definite instant. The input data for this equation must be time series data of wave height, period, and direction. Needless to say, it is almost impossible to calculate shoreline changes using this time series data changing all the time. More simple method is to use typical (hypothetical) wave height, period, and direction which can simulate shoreline changes. Another point is to calculate net littoral

drift volume using equation (5). The second intension of carrying out this study is to examine the method for determining the typical wave height, period, and direction using tables of frequency distribution of significant wave height and period.

4-3-2 Application of the beach mathematical model to shoreline changes at Tokushima Coast

Fig. I-4-23 shows shoreline changes observed at the beach between Imagiri Port and Awazu Port in Tokushima Coast. Beach near Imagiri Port eroded whilst beach near Awazu Port accreted.

Table I-4-1 represents frequency distribution of significant wave height and period off the beach. Water depth of this wave observation point was -10 meters. Observation was done every two hours during a whole year, and they managed to obtain wave data for 67 % of the total period. (67 % is called "success rate of wave observation.") Symbol of "calm" in Table I-4-1 represents that observed wave heights are smaller than 80 cm.

Table I-4-2 shows distribution of wave energy "e" calculated using Table I-4-1 and the following equation.

$$e = \frac{1}{8} \rho g H_m^2 \cdot n \cdot C \cdot N \cdot \alpha \cdot \Delta t \qquad \text{----- (31)}$$

where

e : wave energy reaching the beach,

H_m : median of wave heights at each column of Table I-4-1,

n : ratio between wave group velocity and wave celerity,

C : wave celerity calculated using median wave period,

N : frequency shown in Table I-4-1,

α : inverse of success rate of wave observation,

Δt : interval of wave observations

(7,200 seconds, i.e. 2 hours)

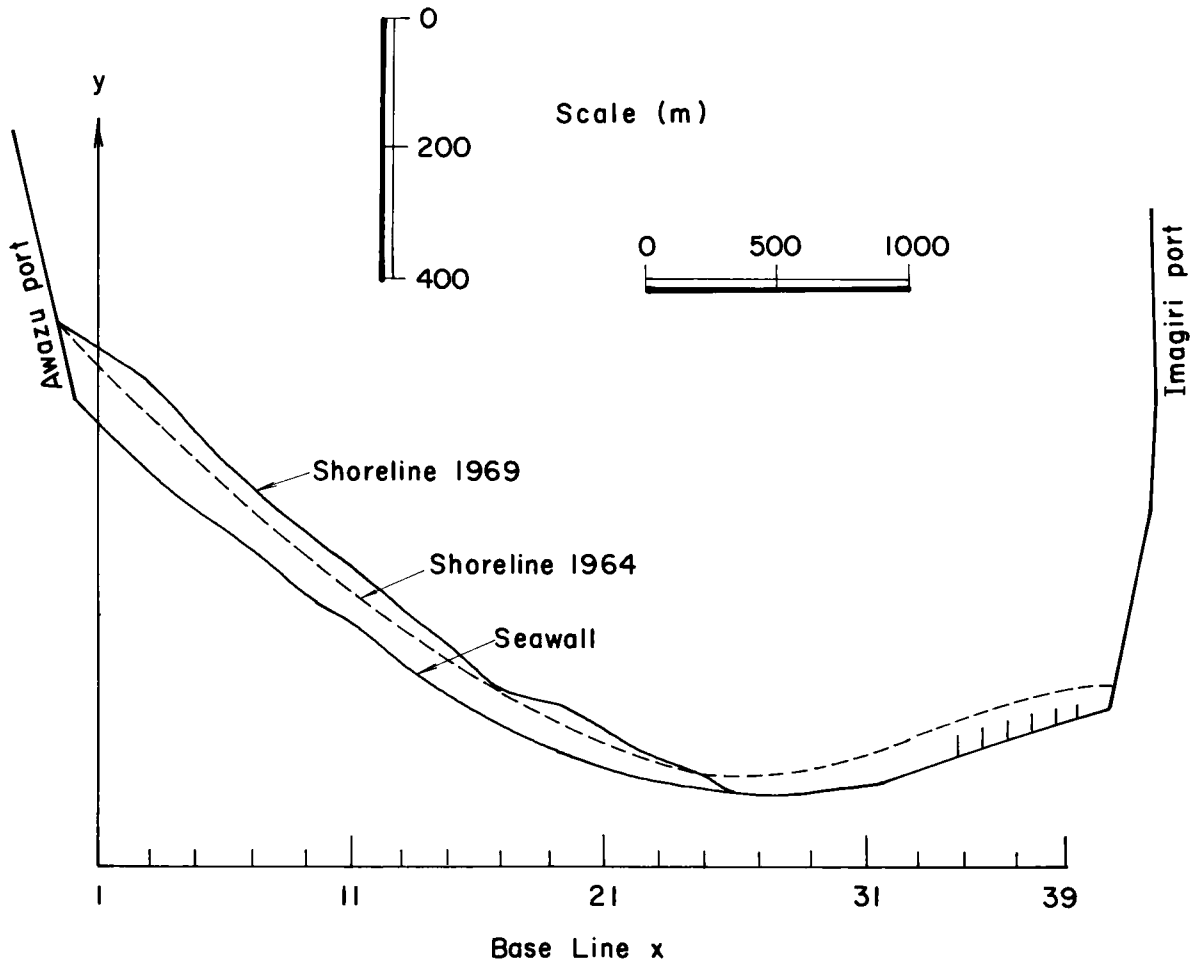

Fig. I-4-23 Shoreline changes at Tokushima Coast

Table I-4-1 Frequency distribution of significant wave height and period

Wave Height (m) / Wave Period (sec)	Calm	0.25 ∫ 0.49	0.50 ∫ 0.74	0.75 ∫ 0.99	1.00 ∫ 1.24	1.25 ∫ 1.49
Calm	2,713					
5.0～ 5.9		7	2			
6.0～ 6.9		8	17	7	1	
7.0～ 7.9		8	15	3	2	2
8.0～ 8.9		3	12	1		
9.0～ 9.9		1	19			2
10.0～10.9		1	8	1	1	1
11.0～11.9		2	19	6		
12.0～12.9			8	6		
13.0～13.9			5	7	2	
14.0～14.9			4	10	3	
15.0～15.9			4	7	6	1
16.0～16.9			2	4	2	

Table I-4-2 Distribution of wave energy

Unit (10^7 Newton)

H_m(m) / T_m(sec)	0.375	0.625	0.875	1.125	1.375	Total	Probability p	pT_m
5.5	6.7	5.3				12.0	0.0090	0.05
6.5	9.3	54.8	44.2	10.4		118.7	0.0893	0.58
7.5	10.5	54.7	21.5	23.6	35.3	145.6	0.1095	0.82
8.5	4.3	47.4	7.7			59.4	0.0447	0.38
9.5	1.5	79.3			40.4	121.2	0.0912	0.87
10.5	1.6	34.7	8.5	14.0	21.0	79.8	0.0600	0.63
11.5	3.2	85.1	52.6			140.9	0.1060	1.22
12.5		36.9	54.3			91.2	0.0686	0.86
13.5		23.5	64.5	30.5		118.5	0.0892	1.20
14.5		19.1	93.6	46.4		159.1	0.1197	1.74
15.5		19.4	66.5	94.2	23.4	203.5	0.1531	2.37
16.5		9.7	38.1	31.5		79.3	0.0597	0.99
Total	37.1	469.9	451.5	250.6	120.1	1329.2		
Probability p	0.0279	0.3535	0.3397	0.1885	0.0904			
pH_m	0.01	0.22	0.30	0.21	0.12			

$\Sigma p = 1.0$, $\overline{T} = \Sigma pT_m = 11.7$ sec

$\overline{H} = \Sigma pH_m = 0.86$ m

ρ : water density,

g : acceleration due to gravity.

When the probability of energy flux, p, is obtained for each period and each wave height from Table I-4-2, the representative significant wave heitht $\overline{H}_{1/3}$, and the representative wave period, $\overline{T}$, where energy flux is most concentrated, can be obtained by $\Sigma p \cdot H$ and $\Sigma p \cdot T$. $\overline{H}_{1/3}$ is 0.86 m and $\overline{T}$ is 11.7 sec. Since H_b of the Scripps Equation (equation (5) of Chapter 3) is root mean square value of wave heights, $\overline{H}_{1/3}$ has to be converted into $\overline{H}_{rms}$. So,

$$\overline{H}_{rms} = \overline{H}_{1/3} / 1.42 = 0.61 \text{ m}$$

Wave direction to be used in the beach mathematical model was determined by refraction calculation, using SE as the predominant wave direction at Tokushima Coast. Fig. I-4-24 shows alongshore distribution of wave direction, i.e. α_x, angle between the breaking crests and the baseline. Wave height H_b at Awazu Port where refraction coefficient K_r is nearly 1.0 was set as 0.46 m in the beach mathematical model. Fig I-4-25 represents alongshore distribution of wave heights. Wave period, T, was set as 10 seconds in the beach mathematical model. Alongshore sediment transport rate was set as 0 at the locations of breakwaters of Imagiri and Awazu Ports, i.e. section numbers 1 and 39. Onshore-offshore sediment transport was also set as 0. The sea bottom slope is $\tan\beta = 1/32$; the water depth below which profile changes are negligible is -6.0 m; and the height of the beach berm is 2.5 m.

Fig. I-4-26 shows result of the simulation. Calculated shoreline in 1969 well agrees with the shoreline observed at the field. Calculating ratio between H_b, wave height used in the beach mathematical model at the point where effect of wave refraction is almost negligible,

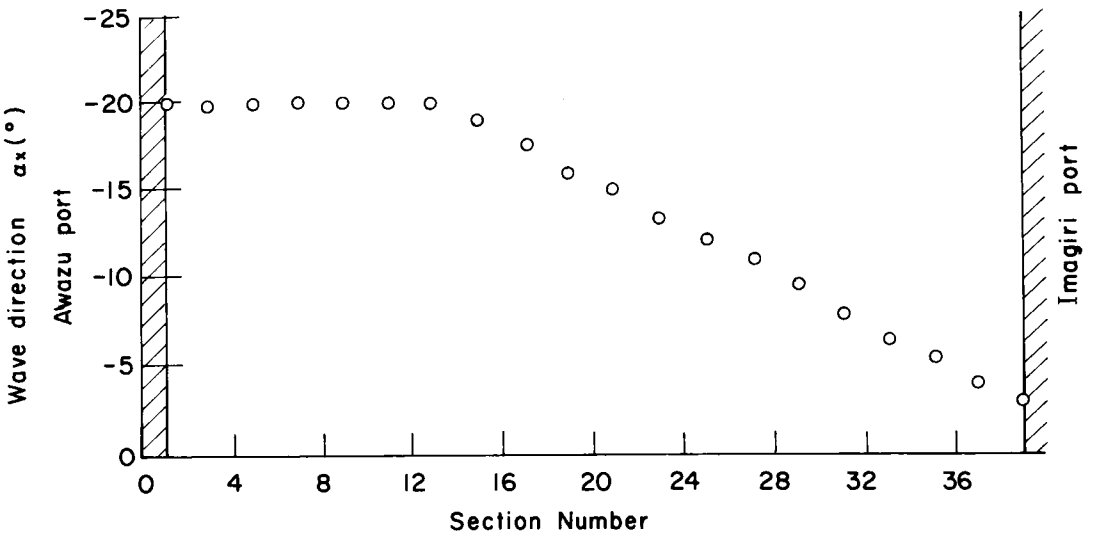

Fig. I-4-24 Alongshore distribution of wave direction

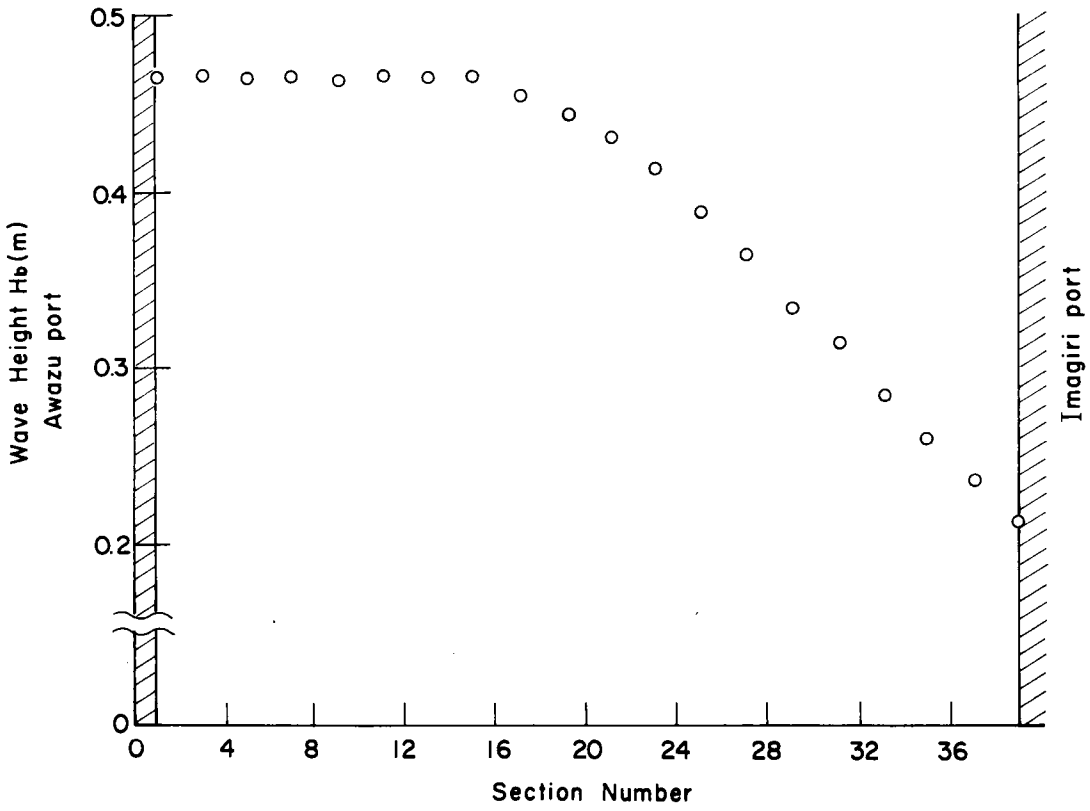

Fig. I-4-25 Alongshore distribution of wave heights

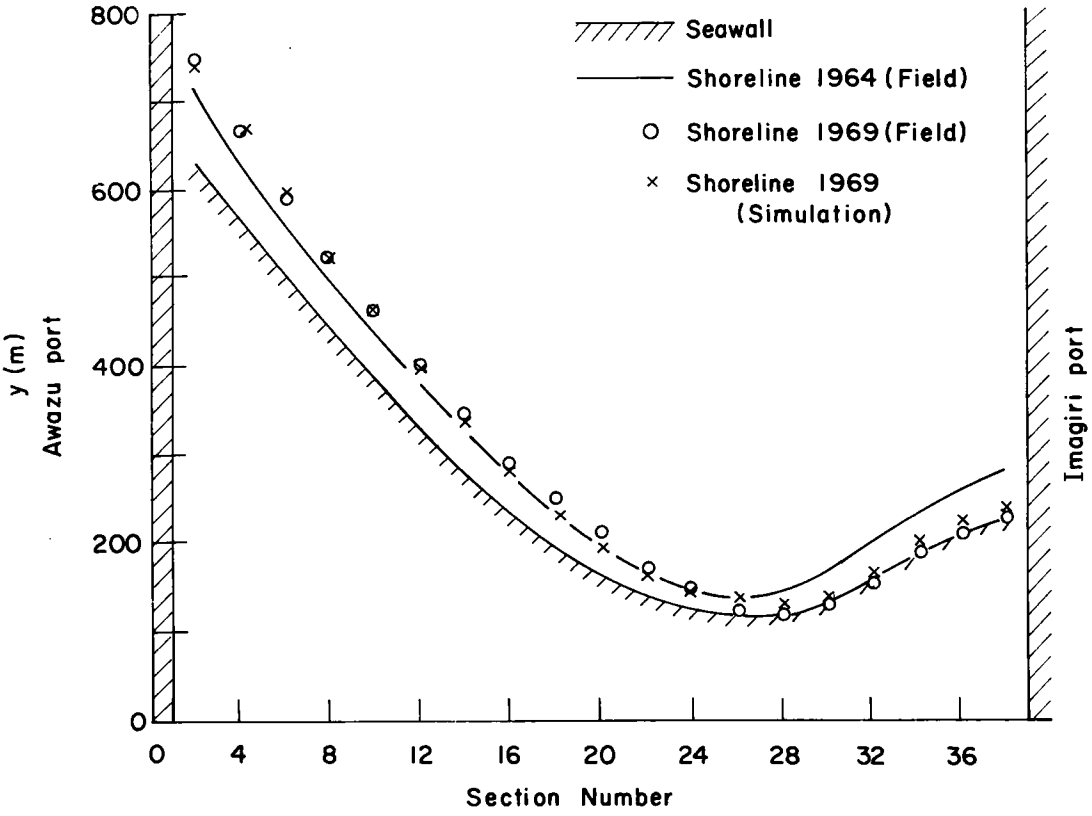

Fig. I-4-26 Shoreline evolution
(Field and simulation result)

and $K_r \cdot \overline{H}_{rms}$, we obtain

$$H_b / (K_r \cdot \overline{H}_{rms}) = 0.46 \text{ m} / 0.61 \text{ m} = 0.75$$

In the similar way, ratio between T, wave period used in the beach mathematical model, and $\overline{T}$, representative wave period, is

$$T / \overline{T} = 10.0 \text{ sec} / 11.7 \text{ sec} = 0.85$$

4-3-3 Application to shoreline change at Nigerian Coast near Lagos

On the West African Coast facing the Bight of Biafra, littoral drift is carried from west to east because swell from the southwest direction prevails throughout the year. So, when a breakwater is constructed, accretion occurs on the west side (updrift side of the sediment transport) while erosion occurs on the east side (downdrift side). In the case of Lagos Port, for example, accretion is observed on the shore west of the West Mole (Lighthouse Beach) and erosion is observed on the east side of the East Mole (Victoria Beach). Fig. I-4-27 shows the positions of the shorelines around Lagos Port in 1900, 1945 and 1959[4]. The moles of Lagos Port were constructed in 1908 ~ 1913.

The author has attempted to reproduce shoreline changes around Lagos Port shown in Fig. I-4-27 using beach mathematical model.

Table I-4-3 shows the annual frequency distribution of significant wave height and period at 5°23' N and 5°00' E off Forcados (water depth -50 m). Table I-4-4 shows the annual occurrence frequency of significant wave heights and directions at the same point. These tables can be used for the beach mathematical model around Lagos Port, because wave characteristics off Forcados is almost same as that at Lagos. Table I-4-5 shows the distribution of energy flux ($1/8 \cdot \rho g H_m^2 \cdot n \cdot c \cdot N$) calculated using Table I-4-3, where ρ is the density of water, g is the acceleration due to gravity, H_m is the wave height in Table I-4-3, nc is the group velocity of waves and N is the probability in Table I-4-3. When the probability of energy flux, p, is obtained for each period and each wave height from Table I-4-5, the representative significant wave height $\overline{H}_{1/3}$, and the representative period, $\overline{T}$, where energy flux is most concentrated on can be obtained by $\Sigma p \cdot H$ and $\Sigma p \cdot T$. $\overline{H}_{1/3}$ is 1.67 m and $\overline{T}$ is 12.5 sec. If $\overline{H}_{1/3}$ is converted into $\overline{H}_{rms}$, $\overline{H}_{rms} = \overline{H}_{1/3} / 1.42 = 1.18$ m.

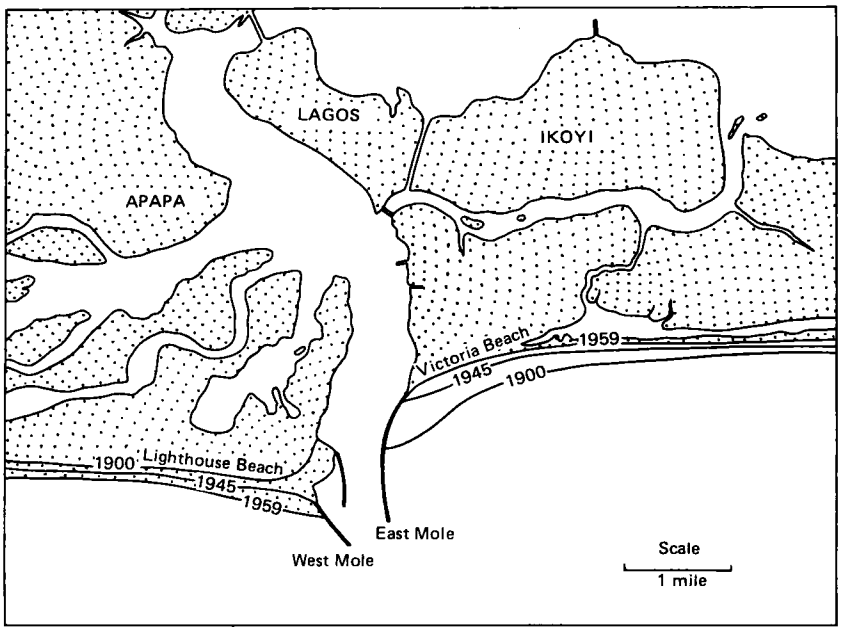

Fig. I-4-27 Shoreline changes around Lagos Port (after Webb)

Table I-4-3 Average annual frequency distribution of significant wave height and period (at 5°23' North, 5°00' East at approximately -50 m depth)

Period (sec)	Significant Wave Height ($H_{1/3}$) (m)							Total
	0–0.6	0.6–1.2	1.2–1.8	1.8–2.4	2.4–3.0	3.0–3.6	3.6 plus	
0–3	0.2	0.0	0.0	0.0	0.0	0.0	0.0	0.2
3–5	0.8	0.5	0.0	0.0	0.0	0.0	0.0	1.3
5–7	1.8	2.3	0.2	0.0	0.0	0.0	0.0	4.3
7–9	3.2	4.5	1.4	0.3	0.0	0.0	0.0	9.4
9–11	7.2	12.2	4.9	1.5	0.3	0.1	0.0	26.2
11–13	6.2	11.8	7.0	3.0	0.8	0.3	0.1	29.2
13–15	3.9	7.7	3.9	1.9	0.4	0.1	0.0	17.9
15–17	1.8	5.0	1.6	0.5	0.0	0.0	0.0	8.9
17–19	0.5	1.4	0.6	0.1	0.0	0.0	0.0	2.6
Total	25.8	45.3	19.4	7.3	1.6	0.5	0.1	100.00

Source: A.H. Glenn and Associate: Meteorological-Oceanographic factors affecting design and planning of petroleum operations in Nigerian oil company offshore leases.

Table I-4-4 Average frequency of occurrence of wave height-direction groups (at 5°23' North, 5°00' East at approximately -50 m depth)

Direction	Significant Wave Height (m)							Total
	0–0.6	0.6–1.2	1.2–1.8	1.8–2.4	2.4–3.0	3.0–3.6	3.6 plus	
N	1.1	0.8	0.2	0.0	0.0	0.0	0.0	2.1
NE	1.3	0.7	0.0	0.1	0.0	0.0	0.0	2.1
E	1.9	0.6	0.1	0.0	0.0	0.0	0.0	2.6
SE	2.5	2.4	0.7	0.2	0.1	0.0	0.0	5.9
S	6.3	9.9	3.6	1.1	0.3	0.1	0.0	21.3
SW	7.9	22.6	11.2	4.6	0.9	0.3	0.1	47.6
W	3.0	7.2	3.2	1.2	0.3	0.1	0.0	15.0
NW	1.8	1.1	0.4	0.1	0.0	0.0	0.0	3.4
Total	25.8	45.3	19.4	7.3	1.6	0.5	0.1	100.00

Table I-4-5 Distribution of energy flux

H(m) / T (sec.)	0.3	0.9	1.5	2.1	2.7	3.3	3.6	Total	p	pT
1.5	34	0	0	0	0	0	0	34	0.0000	0
4	275	1,548	0	0	0	0	0	1,823	0.0010	0.004
6	927	10,678	2,580	0	0	0	0	14,185	0.0081	0.049
8	2,232	28,302	24,462	10,275	0	0	0	65,271	0.0372	0.298
10	6,827	104,323	116,408	69,848	23,093	11,499	0	331,998	0.1891	1.891
12	7,434	127,591	210,283	176,645	77,870	43,622	17,305	660,750	0.3763	4.516
14	5,577	99,299	139,729	133,429	46,436	17,342	0	441,812	0.2516	3.522
16	2,930	73,408	65,262	39,975	0	0	0	181,575	0.1034	1.654
18	886	22,360	26,623	8,697	0	0	0	58,566	0.0334	0.601
Total	27,122	467,509	585,347	438,869	147,399	72,463	17,305	1,756,014		
p	0.0154	0.2662	0.3333	0.2499	0.0839	0.0413	0.0099			
pH	0.005	0.240	0.500	0.525	0.227	0.136	0.036			

$\bar{H} = \Sigma pH = 1.67$

$\bar{T} = \Sigma pH = 12.5$

The wave direction to be inputted for the beach mathematical model was determined by refraction calculation, using SW (referring to Table I-4-4, SW is clearly predominant wave direction.) as the direction of deepwater waves. Table I-4-6 shows the results of refraction calculation using assumed parallel contour lines. From the above calculation, the author has decided to use the refraction coefficient and the wave direction for the vicinity of the breaker zone, that is, at a water depth of -4 m.

Since K_d on the Lighthouse Beach (West side beach of the West Mole) is 1.0, the author has used H_b = 0.56 m, so that 382 ~459 thousand m^3/year, the longshore sediment transport rate reported by the Delft Hydraulic Laboratory, could be obtained. The sea bottom slope is tan β = 1/40, the water depth below which profile changes are negligible is 5.0 m and the height of the beach berm is 3.6 m.

Fig. I-4-28 shows the shoreline changes at Lighthouse Beach in the field as well as in the mathematical model. The positions of the shorelines in 1910 are assumed to be the same as in 1900, because the construction of the moles was completed in 1913. The axis of abscissas, x, shows the base line that is approximately parallel to the shoreline. According to Fig. I-4-28 the direction of the shoreline in the field is more inclined to the SE-NW direction than the direction of the shoreline calculated by the mathematical model on the west side of the West Mole (Station Nos. 2-6). This is probably because the refraction pattern has changed on the west side of the West Mole and the direction of the shoreline has been in accordance with this change. With this exception, the reproduction of the shoreline change on the Lighthouse Beach is considered to be generally satisfactory. The longshore sediment transport rate at a point sufficiently distant from the West Mole is about 395,000 m^3/year in the west to east direction.

Table I-4-6 Refraction calculation at Lagos Coast

h (m)	h/Lo	Kr	α
20	0.0889	0.88	25°
18	0.08	0.87	24°
16	0.0711	0.86	22°
14	0.0622	0.85	21°
12	0.0533	0.85	19°
10	0.0444	0.84	17°
8	0.0356	0.83	15°
6	0.0267	0.83	13°
4	0.0178	0.82	10°
2	0.0089	0.80	5°

h = Sea depth
Lo = Wave length in deep sea
Kr = Refraction coefficient
α = Predominant wave angle from south

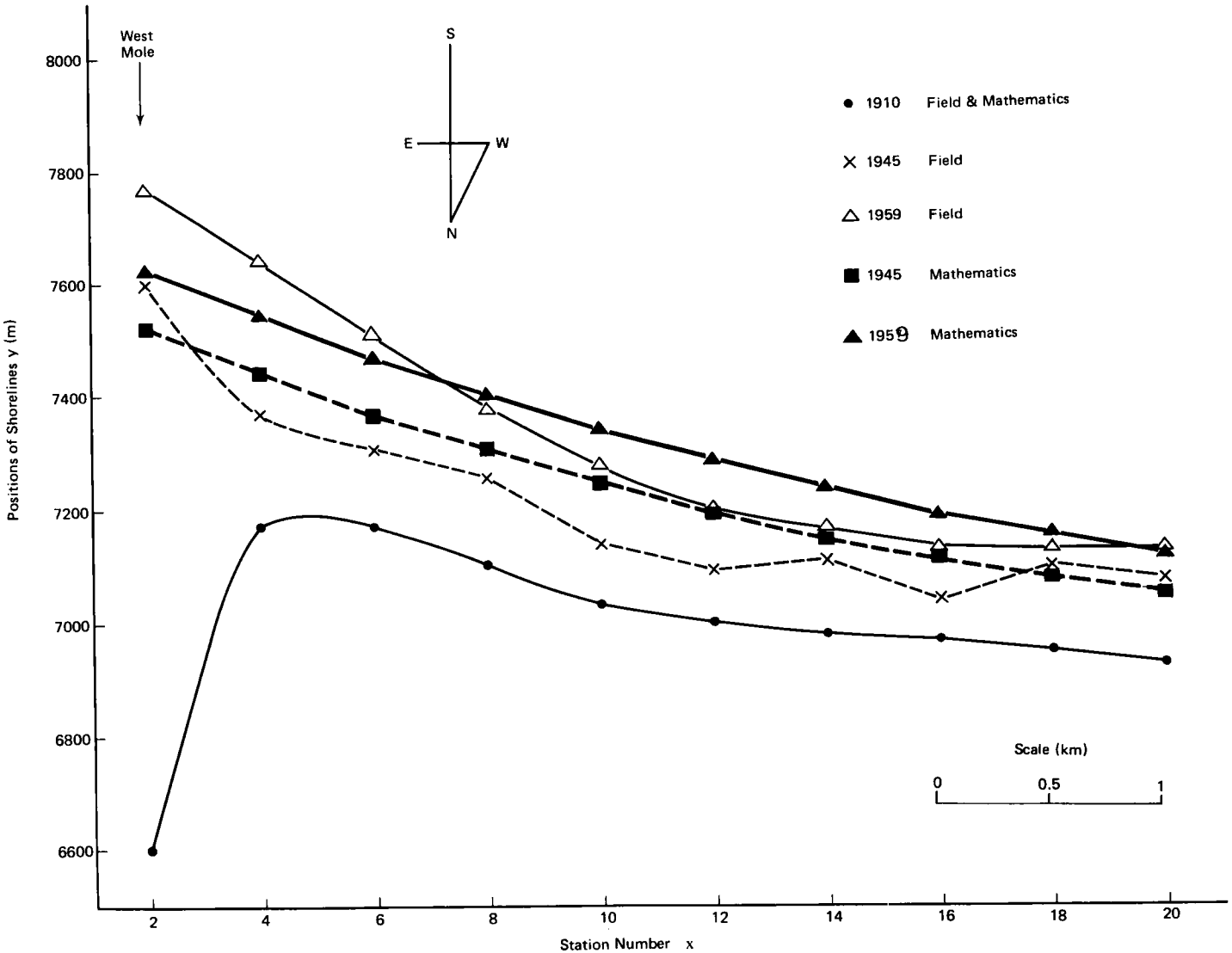

Fig. I-4-28 Shoreline changes at Lighthouse Beach

Fig. I-4-29 shows the shorelines on the Victoria Beach (east side beach of the east mole) in the field and the shorelines calculated by the mathematical model. Victoria Beach has eroded very seriously since the construction of the mole. Sandy beach used to completely disappear in the vicinity of the east mole. But now the sandy beach is being maintained there by dumping sands dredged in Lagos Port. The author has calculated the shoreline changes on the assumption that sea walls exist on the position of the shoreline in 1959 at the area of Station Nos. 50-58. The calculation is also based on the assumption that the wave height is somewhat smaller at Station Nos. 53-59 than elsewhere because of the effects of diffraction by the West Mole. According to Fig. I-4-29, the author has managed to reproduce the general trend of beach erosion, but the shoreline change in the field and the calculated shoreline change do not agree very well.

Refraction coefficient at the point of water depth -4m is 0.82 (see Table I-4-6). So, ratio between H_b and $K_r \cdot \overline{H}_{rms}$ is

$$H_b / K_r \cdot \overline{H}_{rms} = 0.56 / (0.82 \times 1.18) = 0.58$$

Ratio between T and $\overline{T}$ is

$$T / \overline{T} = 12 / 12.5 = 0.96$$

4-3-4 Proposal for a method to determine input data of the beach mathematical model

Based on the above mentioned studies, the author proposes a procedure to calculate input data using a table of frequency distribution of significant wave height and period as follows:

1) Calculation of the representative significant wave height $\overline{H}_{1/3}$ and the representative wave period $\overline{T}$ using a table of frequency distribution of significant wave height and period. $\overline{H}_{1/3}$ is converted into root mean square value of wave height $\overline{H}_{rms}$.

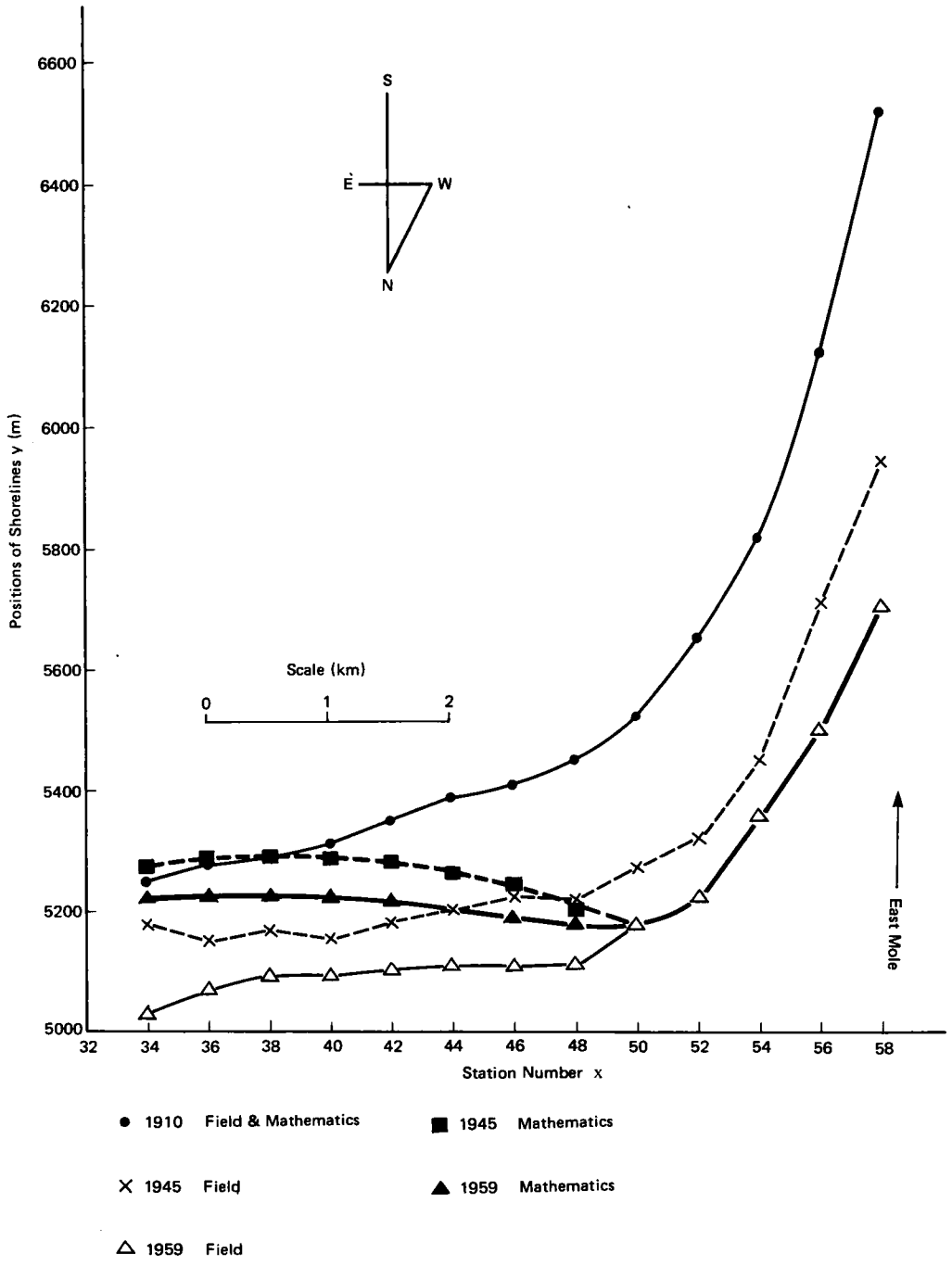

Fig. I-4-29 Shoreline changes at Victoria Beach

2) Execution of refraction calculation for the wave period of $\overline{T}$. After this calculation, refraction coefficient K_r is obtained.

3) Wave height H_b, input data for the beach mathematical model, is calculated according to the following equation.

$$H_b = \gamma \cdot K_r \cdot K_d \cdot \overline{H}_{rms}$$

where

K_d : diffraction coefficient,

γ : constant concerning overall characteristics of beaches.

γ is about 0.65 on the beaches having a well - defined sediment transport direction. (Hereinafter these beaches are referred to A - type beach. Locations of A - type beaches in Japan are shown in Fig. I-2-10. The value of 0.65 is a mean of H_b / $K_r \cdot \overline{H}_{rms}$ obtained at "4-3-2" and "4-3-3".). γ will be less than 0.65 on the beaches having an indistinct sediment transport direction. (Hereinafter these beaches are referred to B - type beach.). The value of γ of B - type beach should be examined by carrying out simulation calculations of shoreline changes further.

4) Wave period, input data for the beach mathematical model, is assumed to be equal to $\overline{T}$.

5) When a table of frequency distribution of significant wave height and period by wave direction is available, wave energy flux by wave direction is calculated first, then $\bar{\alpha}$ is calculated as $\Sigma p\alpha$. $\bar{\alpha}$ determines offshore wave direction, so α_x , wave direction at breaker zone, can be obtained after refraction calculation. When a table of frequency distribution of significant wave height and period by wave direction is not available, refraction calculation is executed for the most predominant wave direction at A - type beach. At B - type beach, two methods might be promising. The first method is to assume the intermediate

of several wave directions as main offshore wave direction. The second method is to perform refraction calculation for each offshore wave direction and make a series of data of α_x. Using this series of data, simulation calculation of shoreline change where value of α_x is alternately changed is performed.

4-4 Conclusions

One of the problems which have not yet been solved is how to calculate onshore - offshore sediment transport rate. Especially, onshore - offshore sediment transport rate arising from nearshore current, circulating current and mass transport near coastal structures has to be predicted more precisely. It also is important to predict changes of wave refraction pattern caused by the construction works.

Before the beach mathematical model is put to real practical use, reproduction of more prototypical shoreline changes has to be tried. Onshore-offshore sediment transport rate and change of refraction pattern might be predicted experimentally by comparing the calculated shoreline changes with the prototypical data and looking for values which give the best reproduction. These quantities of prototype beaches might have different features from those of physical models due to scale effect. So, this study should be done using prototypical data.

The author modelled coastal processes, which have not yet been clarified satisfactorily, at Chapter 3. Appropriateness of the author's assumptions has to be examined. The author's assumptions which have to be checked are

first that the constant slope is maintained during the whole process of beach evolution,

secondly that alongshore sediment transport rate diminishes to zero when the height of beach coincides with Mean Sea Level,

thirdly that Mean Sea Level is taken as a base water level for beach evolution,

fourthly that alongshore sediment transport rate affected by the seawall's presence is equated as equation (10) or equation (11).

It is the best that the above points are studied through field observations, but this can be done through physical model experiments as a first step.

Major points which have been made clear in this chapter are as follows:

(1) The mathematical model which has been proposed at Chapter 3 was used to predict beach changes observed both in a physical model and in prototype, and in general, good agreement was obtained. The model looks promising.

(2) In a situation where a major coastal structure was proposed, the importance of correctly estimating both the onshore - offshore sediment movement and the resulting changes in the wave refraction pattern was demonstrated.

(3) Based on the studies about reproduction of prototypical shoreline changes, the author has proposed a method to calculate input data of beach mathematical model using a table of frequency distribution of significant wave height and period.

REFERENCES

1) Sato, S., Ozasa, H. and Nagai, T.: Model experiments on beach profile change due to the runway extension of Tokushima Airport. Report of the Port and Harbour Research Institute, Vol. 17, No.1, 1978. (in Japanese)
or
Sato, S. and Ozasa, H.: Estimation using a movable bed model of shoreline changes caused by a reclamation projected into the sea. Proceedings of the 16th Coastal Engineering Conference, 1978.

2) Johnson, J.W.: Scale effects in hydraulic model involving wave motion. Transactions, American Geophysical Union, 30, No. 4, 1949.

3) Iwagaki, Y. and Noda, H.: Laboratory study of scale effects in two dimensional beach processes. Proceedings of the 8th Conference on Coastal Engineering, 1963.

4) Webb, J. E.: The erosion of Victoria beach, its cause and cure, Ibadan University Press, 1960.

CHAPTER 5. CONCLUSIONS

Littoral drift has been studied since the start of coastal engineering research, but it is often pointed out that littoral drift is a theme of coastal engineering which includes a lot of unsolved problems. Some people say that very little progress has been made in the investigation method for the last scores of years.

One of the reasons is that littoral drift is a complicated phenomenon which is related to interaction between water and sediments. It is very difficult to make a dynamic model of sediment transport and induced beach processes.

The author has been engaged in research of sediment transport while dealing with actual problems. The author's way of research was first to recognize field problems exactly, then to look for solutions of these problems. The author considers that a practical mathematical model of littoral drift should not be so complicated, because the present level of sedimentation engineering is primitive. A model which is as simple as possible will be more useful.

Part I is composed of the fruits of the author's researches which have been done according to the above mentioned considerations.

Main conclusions in Part I are listed as follows.

In Chapter 2, it is pointed out that beach erosion is caused by construction of coastal structures or decrease of sand supply from rivers. According to causes of erosion beach erosion can be classified into various types. Predominant directions of littoral drift are clear at some coasts in Japan. The reasons of existence of predominant directions can be classified into four categories.

In Chapter 3, the author proposed a model which can be applied to the case where the width of a beach backed by a sea wall is narrow and this sea wall influences the advance of the shoreline change. The model's differential equations can be solved using a finite difference method. The author also proposed an alongshore sediment transport rate formula including the effect of varying breaker height along the beach.

In Chapter 4, it is shown that the model which was proposed at Chapter 3 can be used for prediction of shoreline changes observed in a physical model and in prototype. However, it is necessary to correctly estimate both the onshore - offshore sediment movement and the resulting changes in the wave refraction pattern. Moreover, the author proposed a method to calculate input data of beach mathematical model using a table of frequency distribution of significant wave height and period.

PART II STUDIES ON CHANNEL SEDIMENTATION

CHAPTER 6. INTRODUCTION

Channel sedimentation is a phenomenon that sediments which are carried into the channel form shoals and block ships' navigation.

Some channels, dredged for increases in vessel size or the construction of new ports, are suffering serious sedimentation problems and consequently, much money is spent on maintenance dredging. In Japan, channel siltation was studied in Niigata Port situated at the mouth of the Shinano River[1]. But, most ports are recently constructed as sea ports facing the ocean and in these cases channel sedimentation volumes are not much.

Channel sedimentation which obstructs port activities is not directly endangering human lives whilst beach erosion directly destroys private houses and exposes people to danger.

Due to the above reasons, channel sedimentation has mever been paid enough attention by Japanese hydraulic engineers, especially by university scientists.

As an exceptional case, channel sedimentation has recently become a serious problem at Bisan Seto Seaway in Seto Inland Sea, Japan. Many shallow spots appeared after capital dredging, because large submarine sand waves, the crests of which were once taken off by dredging, were formed again. In order to deal with this sort of problem, characteristics of sand waves should first be studied and investigation results have to be applied for establishing proper countermeasures.

In the case of overseas ports, berthing facilities are often situated at estuaries or along rivers. Some long approach channels are not sheltered by training walls. So, enormous volume of sediments has to be dredged every year to maintain these channels. For example, maintenance dredging volume at Belawan Port, Indonesia is 6 million m^3. At Calcutta Port, it is 9 million

m^3. In these cases, hydraulic mechanism of sedimentation has to be made clear in order to estimate future sedimentation volume more exactly and find proper engineering methods for improving these situations.

Small fishing ports are sometimes silted up totally. Old Nobiru Port, Japan, suffered very serious shoaling and construction of Nobiru Port were given up. This sort of phenomenon that whole port facilities are filled up is called "Port Sedimentation". However, in the case of modern ports, port sedimentation occurs very rarely, because sedimentation environment is usually studied carefully before commencement of port construction, and money can be spent on the maintenance of the ports, if necessary.

The author considers that study of channel sedimentation should have the same weight as that of beach erosion, because both of them are phenomenon related to coastal sediment transport and only way of appearance of problems is different. According to this idea, channel sedimentation was taken up in Part II, separate from Part I about beach erosion.

Main portion of "Part II" is composed of two chapters. At Chapter 7, the author shows examples of channel sedimentation overseas as well as in Japan. Channel sedimentation at Qasim Port, Pakistan, is a case which the author investigated. Taking difference of topographical, geological, and hydraulic conditions into consideration, the author classifies examples of channel sedimentation and introduces their actual conditions. At Chapter 8, channel sedimentation due to large submarine sand waves at Bisan Seto Seaway in Japan is reported.

REFERENCES

1) Technical Committee on Niigata Port: Technical Report No. 1, 1948 (in Japanese)

CHAPTER 7. STUDY OF INVESTIGATING ACTUAL CONDITIONS OF CHANNEL SEDIMENTATION

7-1 Introduction

Channel sedimentation has become a problem at many overseas ports, but there is not serious channel sedimentation in Japan. Therefore, most Japanese hydraulic engineers are not familiar with this problem. One of the author's objects at this chapter is to introduce examples of channel sedimentation.

The author first explains factors influencing channel sedimentation. Based on these factors, channel sedimentation and their actual conditions are reported.

7-2 Factors influencing channel sedimentation

Channel sedimentation can be classified by where it happens, what sort of forces cause it, and what sort of sediments are deposited.

The topography of shoaling areas can be divided into estuary, river, and beach. "Estuary" has several definitions. The most popular, by Pritchard[1], reads: "An estuary is a semi - enclosed coastal body of water which has a free connection with the open sea and within which sea water is measurably diluted with fresh water derived from land drainage".

Rivers are defined in this chapter as the areas which are upstream from tidal limits and are occupied by discharged river water. Beaches are defined as areas, other than river mouths facing oceans and occupied by sea water.

The kinds of forces that cause sedimentation are closely related to topography. The forces, tidal and river currents and waves, occasionally act simultaneously; the combined force of waves and tidal currents, for example.

Tidal current is a cyclically changing force caused by tidal changes (for example, semi - diurnal and diurnal). Current velocity changes sinusoidally and is of high magnitude during spring tide, but low during neap tide. Current direction during flood tide is reversed during ebb tide.

River current always flows in the same direction, but current velocity and water discharge volume vary widely; velocity and volume are significantly greater in the rainy season than in the dry season.

Significant wave dimensions are height, direction and period. Typhoons or low atmospheric pressure bring about large wave height. Wave direction usually varies widely, but narrows especially at low latitudes. The period of a wind wave is short, typically several seconds, but that of a swell is usually longer than 10 seconds.

One of the most significant factors influencing sedimentation is sediment, classified into sand, silt, and clay (needless to say, there is more detailed classification in soil mechanics). According to the Japanese Industrial Standard (JIS A 1204 - 1970), the diameter of sand is larger than 0.074 mm, silt ranges 0.074$\sim$0.005 mm (74$\sim$5μ), and clay is smaller than 0.005 mm (5μ).

The British Standard (B. S.) defines sediments a little differently; the diameter of sand is larger than 0.06 mm; silt diameter is 0.06$\sim$0.002 mm (60$\sim$2μ); and clay diameter is smaller than 0.002 mm (2μ).

The word "mud" is often used, generally including both silt and clay. The most significant characteristic of mud is a cohesive force among mud particles[2]. This force causes mud to move in a different way than sand. The primary particles of clay and silt are so small that Brownian motion alone is enough to keep them suspended. However, under certain conditions, individual particles of cohesive materials join together in flocs (flocculation) and have a settling velocity large enough to overcome Brownian

motion.

The formation of flocs depends on two independent factors: collision and cohesion[2]. Cohesion is determined by the relative strengths and fields of influence of the attractive and repulsive forces between clay particles. The attractive forces are caused by the electrical interaction of atoms in each particle (Van der Waals forces). Repulsive forces are due to negative charge found on the surface of clay particles. This charge attracts a cloud of cations around the particles, and when two particles meet the clouds repel each other.

In distilled water, where cation concentration is low, the clouds are large, repulsive forces prevail, and the clay particles do not flocculate. In solutions having a high cation concentration, such as sea water, the clouds are depressed, attractive forces prevail, and the clay particles flocculate.

7-3 Channel sedimentation at Japanese ports

7-3-1 Features of Japanese ports

Japanese ports are usually located on beaches facing the ocean and well protected by breakwaters from waves and currents. Ports are constructed either on steep coasts or on coasts where contour lines come near to shores. So, lengths of the channels are not long, at most several kilometers. Water depths at the tips of the main breakwaters are deep and almost same as the channel water depths. Bottom sediments at the port areas are sand usually and ooze sometimes. They are natural mud rarely. Due to the above reasons, maintenance dredging volume at Japanese ports are not more than scores of thousands cubic meters per year.

7-3-2 Sedimentation caused by littoral sediment having a well-defined transport direction

Fig. Ⅱ-7-1[3] shows shoreline changes observed around Irako Port. Along this beach, littoral sand is transported from south to north. Accretion was observed at the updrift side (west of the west breakwater) and sediment transported along the west breakwater reached the port entrance channel, causing sedimentation there. In order to turn the sediment away, a new breakwater stretching offshore was added. To the north of the east breakwater (downdrift side), however, the beach experienced erosion.

Fig. Ⅱ-7-2[3] shows shoreline changes observed around Oharai Port. Littoral drift was transported from north to south on the NE coast of Oharai Port, then was carried along the main breakwater, and eventually formed a shoal around the tip of the breakwater, causing channel sedimentation .

The above examples show channel sedimentation observed at beaches having a well-defined sediment transport direction. The predominant direction of littoral drift is clearly defined in the following situations as explained at "2-4-1 Predominant directions of littoral drift". :

1) On sandy beaches which are located at the sides of bays and straits,
2) On sandy beaches facing the Pacific Ocean which waves and swell caused by typhoons and low atmospheric pressures attack from the south,
3) Along sandy beaches facing rectangular inland seas,
4) At long concave sandy beaches.

7-3-3 Sedimentation on beaches having an "indistinct" sediment transport direction

On beaches having an indistinct sediment transport direction, sediments

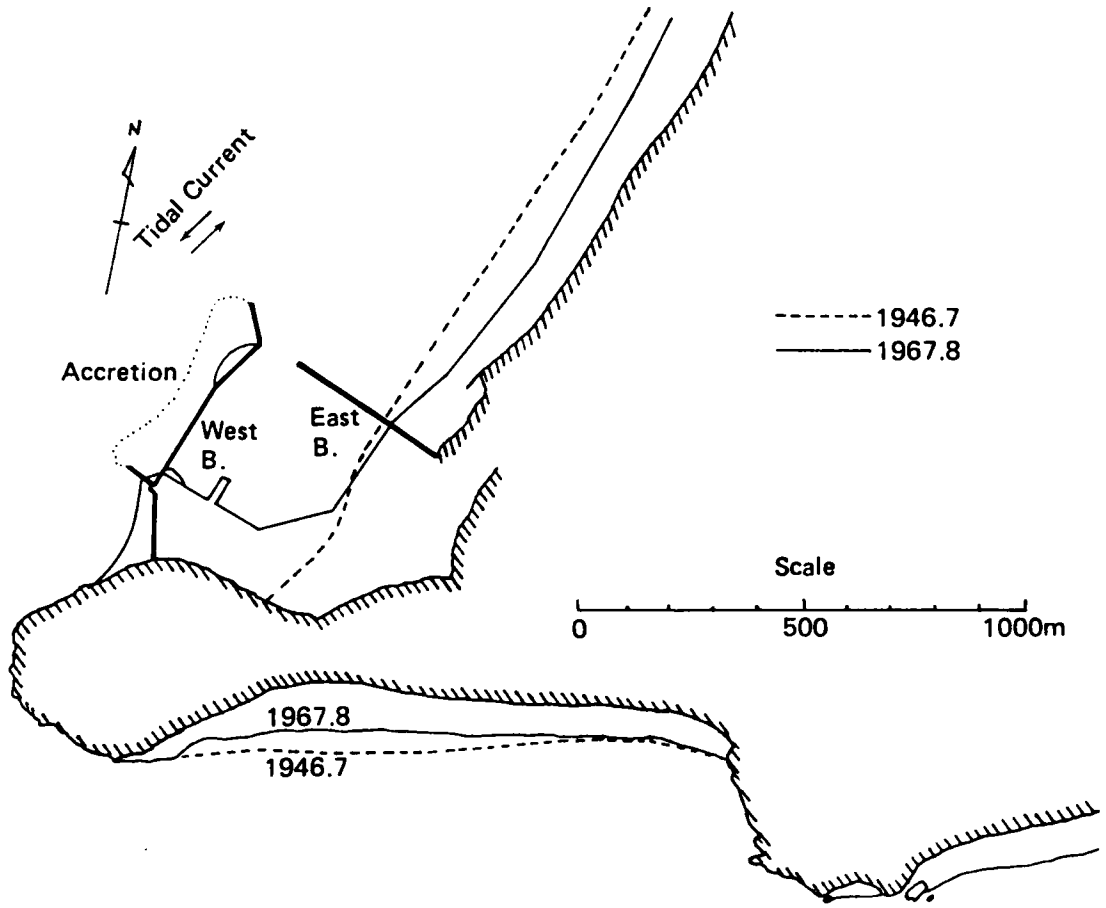

Fig. II -7-1 Shoreline changes around Irako Port
(after Tanaka & Sawamoto)

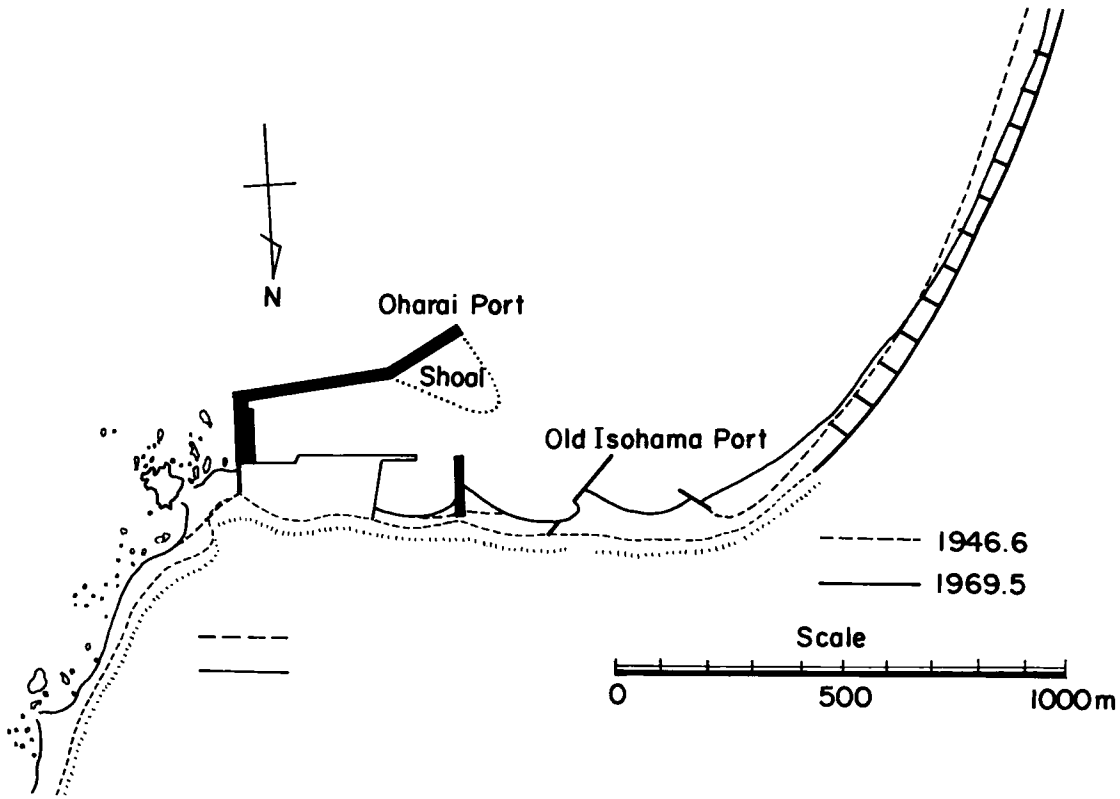

Fig. II -7-2 Shoreline changes around Oharai Port
(after Tanaka & Sawamoto)

are often transported from exposed areas to areas sheltered by breakwaters as shown in Fig. Ⅱ-7-3. On the way of this transport, sediments fill channels.

Fig. Ⅱ-7-4 shows a contour map of Fukui Port. Sedimentation of the entrance channel occurs due to sediment movement from Kuzuryu River mouth and the offshore region to Fukui Port.

On the beach, stretching in a north-south direction, waves approach the shore mainly from WNW and NW directions. The predominant littoral transport direction is likely to be south to north, but is not well defined.

To the north of the beach, lies the Kuzuryu River (Designed flood discharge: 5,500 m^3/s, annual average discharge: 83 m^3/s).

The design water depth of the entrance channel is -10 m and the shoal, surrounded by a contour line of -10 m, extends from NW of the North Breakwater to the South Breakwater. This means the sediment crosses over the entrance channel and, consequently, sedimentation occurs.

Fig. Ⅱ-7-5 shows a plan of Sakata-kita Port[4]. Fig. Ⅱ-7-6 shows differences of water depths between Oct. 11, 1974 and Nov. 28, 1974. In Fig. Ⅱ-7-6, dotted parts show accreting areas and parts which are covered with obbique lines are scoured areas. The channel shoaled by more than 3 meters. According to Irie, this channel sedimentation occurred due to deposition of sediments which are transported from south (an exposed area) to north (a sheltered area) as littoral drift.

7-3-4 Characteristic of channel sedimentation at Japanese ports

Channel sedimentation at Japanese ports is classified into the above mentioned two types. Both types occur due to the series of sediment transport mechanisms which are causing shoreline changes. When transported sediments reach channels, sedimentation occurs.

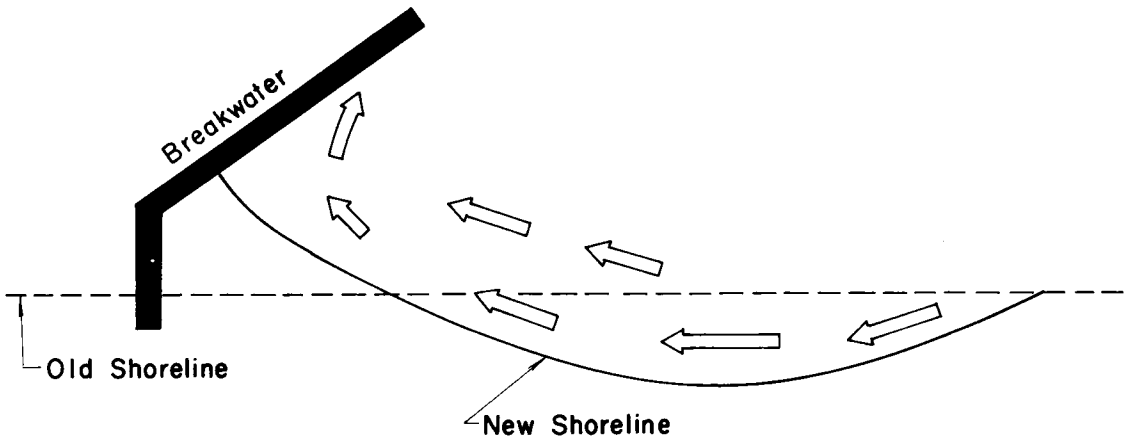

Fig. II -7-3 Sediment transport from exposed areas to sheltered areas

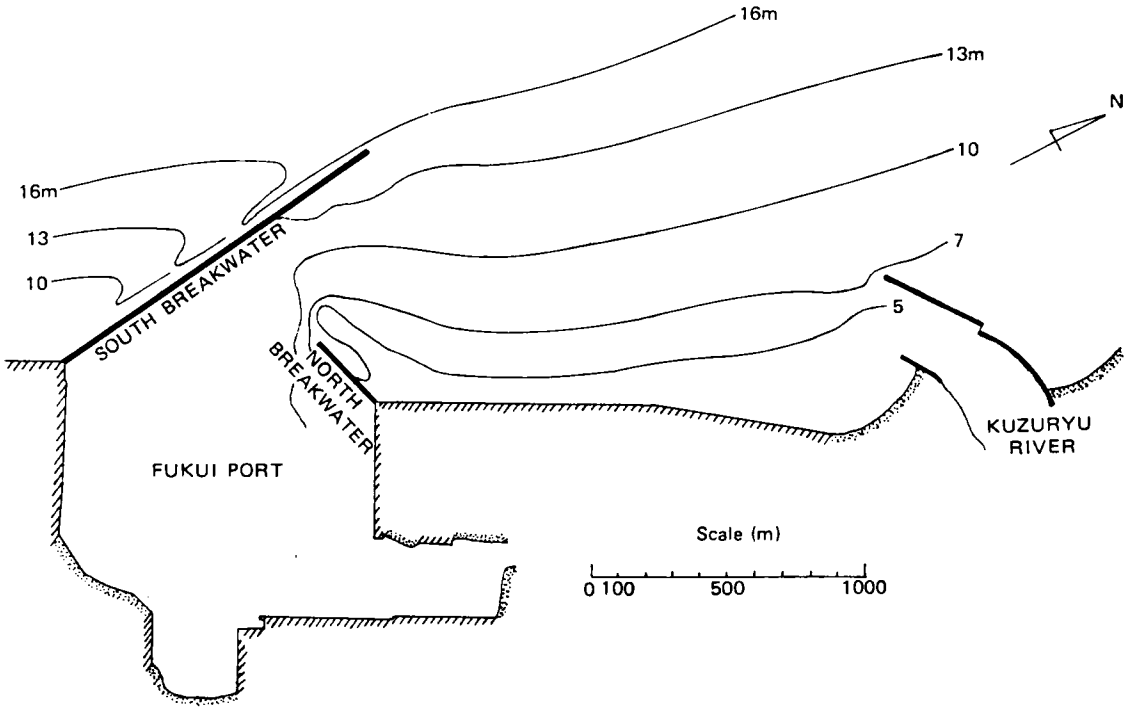

Fig. II -7-4 Fukui Port

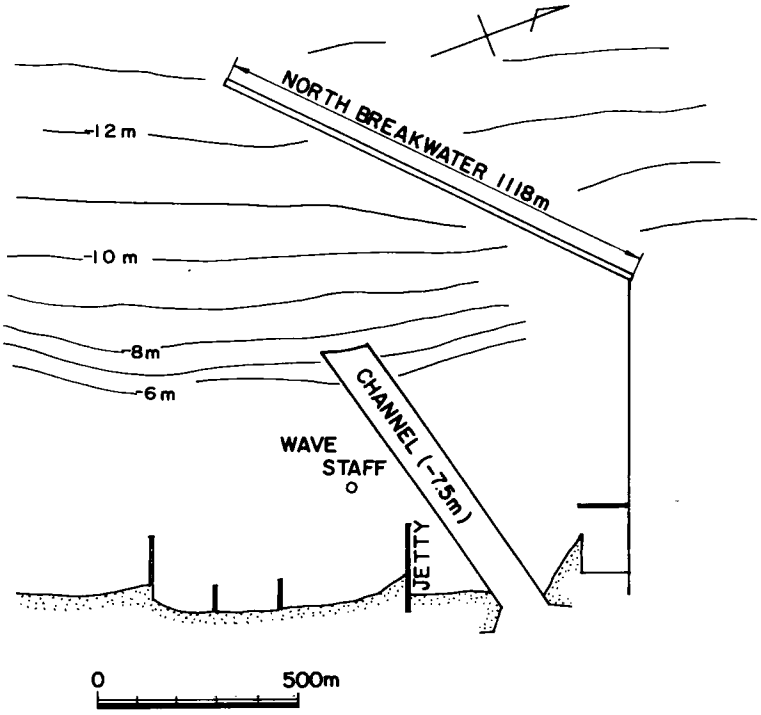

Fig. II -7-5 Sakata - Kita Port (after Irie)

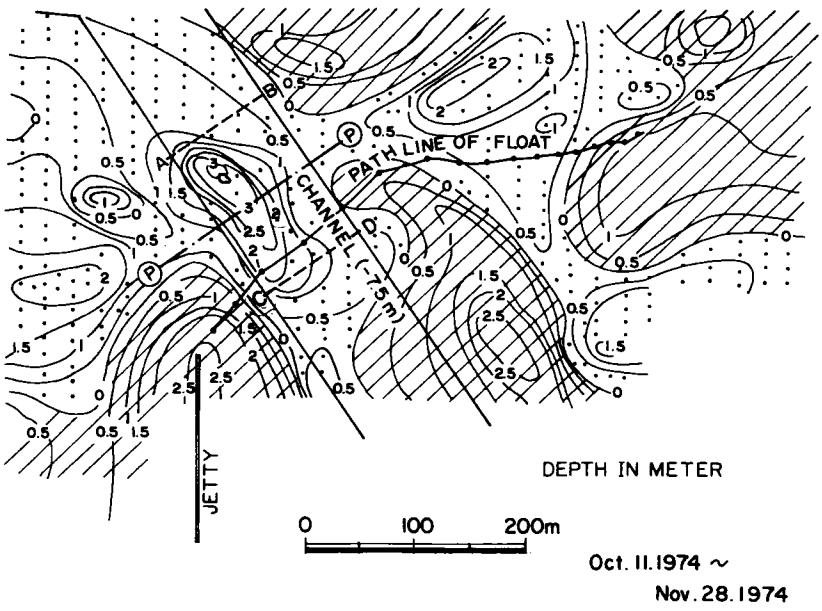

Fig. II -7-6 Differences of water depths (after Irie)

7-4 Channel sedimentation at overseas ports

7-4-1 Features of overseas ports

Many overseas ports are situated on estuaries or along river channels. Some approach channels are long, sometimes several kilometers to scores of kilometers, and are not sheltered by training walls or breakwaters. So, sediments suspended by waves and currents are transported and deposited onto the channels, causing channel sedimentation. Sedimentation volume occasionally reaches several million cubic meters.

Investigation methods of those channel sedimentation differ depending on factors influencing sedimentation, i. e. topographies of shoaling areas, forces causing sedimentation, and sediments types.

7-4-2 Sedimentation caused by littoral sediment

7-4-2-1 Sedimentation on beaches

At overseas beaches, especially in low latitude regions, the predominant waves are not wind waves (generated locally), but swell generated from afar (in some cases more than several thousand km away). Almost constantly throughout the year the swell reaches beaches from oblique directions and causes littoral drift in a constant direction.

So, channel sedimentation, caused by littoral sediment having a well-defined transport direction and similar to sedimentations at Irako and Oharai Ports, can be observed at ports the world over --- Madras Port (India), Santa Barbara Port (U. S. A.), Lagos Port (Nigeria), Salaverry Port (Peru), and Karachi Port (Pakistan) for example.

7-4-2-2 Sedimentation in an offshore sand bank (Qasim Port)

Fig. Ⅱ-7-7 shows layout of the approach channels of Qasim Port. Qasim Port is situated in the remains of the Indus River.

The whole channel is divided into outer and inner channels. The one

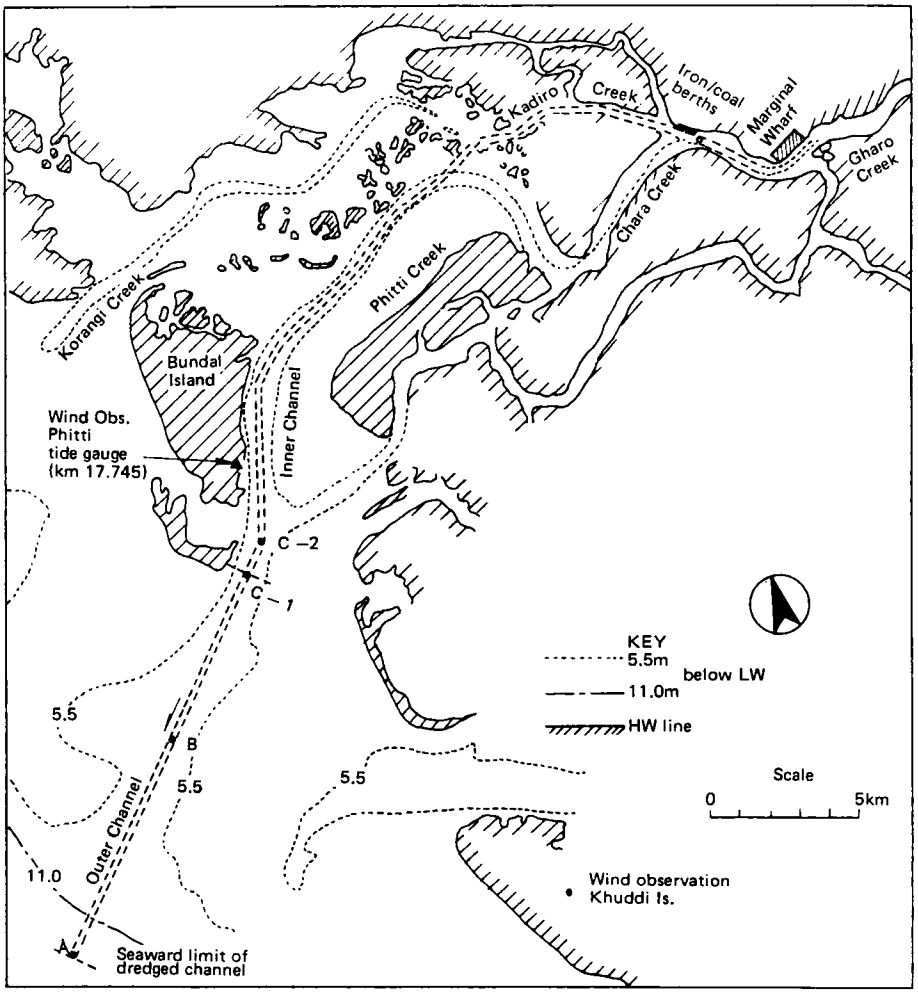

Fig. II-7-7 Qasim Port

is open to the waves approaching from South West during monsoon season whilst the other is in the protected creek. Lengths of the outer and inner channels are 14.1 km and 29.5 km, respectively. Therefore, length of the whole channel is 43.6 km. Width of the outer channel is 185∼280 m at the bottom. Design gradient of the slope is 1:20 and design water depth is -12.4 m. Width of the inner channel is 180 m and design gradient of the slope is 1:6. Design water depth is -11.3 m between C-1 and N points of Fig. Ⅱ-7-7 and -10.0 m between N and R. To the east and west sides of the outer channel are areas shallower than -5.5 m. Especially, sand bar at the north west is close to the channel between A and B points of Fig. Ⅱ-7-7.

Forces contributing to outer channel sedimentation are tides, currents and waves.

Difference between mean higher high water level and mean lower low water level is 2.38 m at Bundal Island near outer channel.

Fig. Ⅱ-7-8 shows the maximum velocity and direction of the currents during spring tide at the outer channel. The main features are:

1) Direction of the ebb current is almost parallel to that of the channel whilst the flood current is obliquely crossing the channel. The angle between the direction of the flood current and that of the channel is 20∼40°.

The velocity of the ebb current is higher than that of the flood current.

2) Current velocity at the location "2" is 0.65∼1.05 m/s and higher than the velocity at the location "1" where the velocity is 0.1∼0.55 m/s.

Wave observation was done near the Fair Way Buoy (water depth -18 m) in 1979 and 1980 using a wave rider buoy and OSPOS (Offshore Pressure Operated Suspended). Waves during the period between November and February

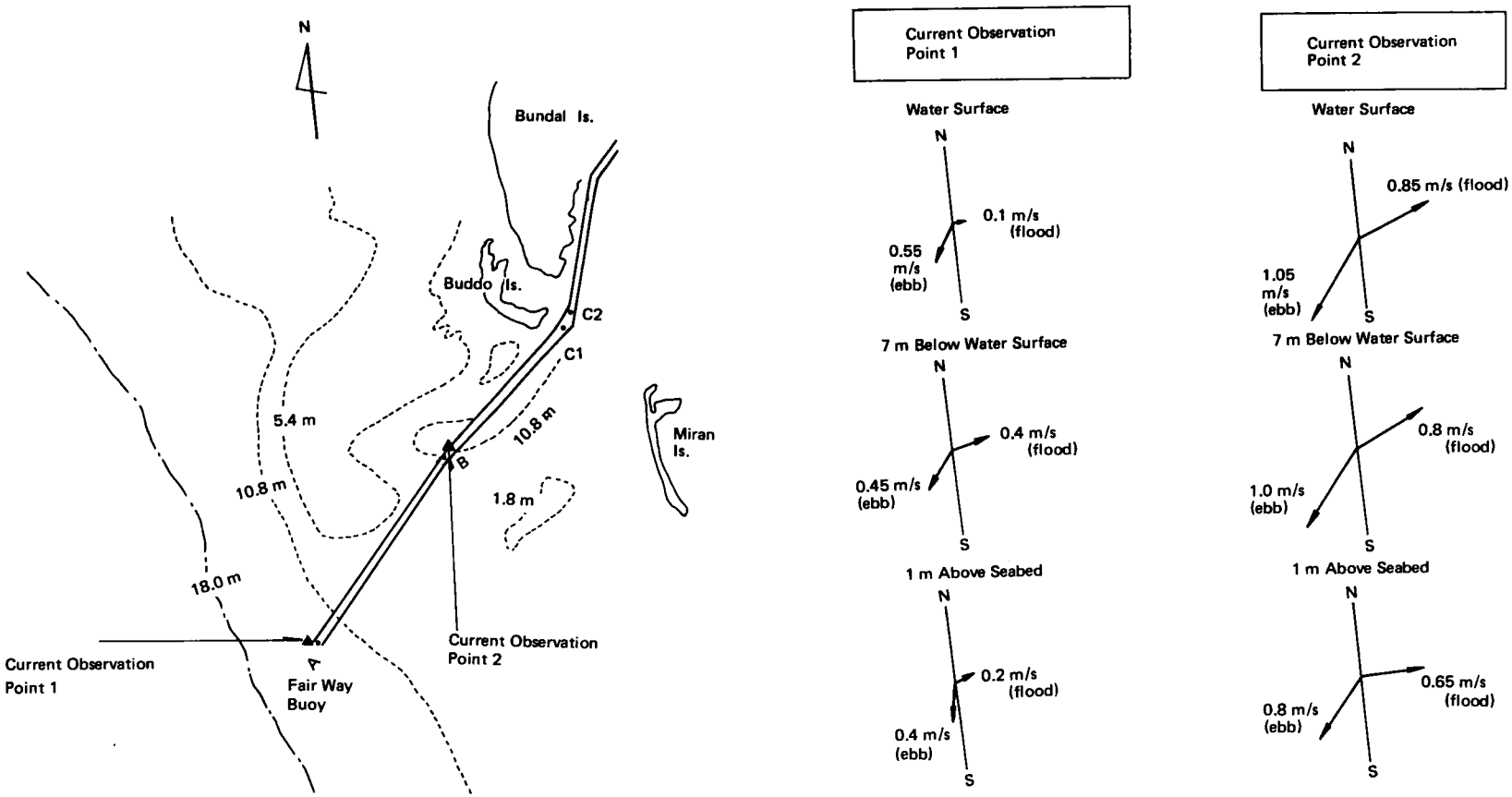

Fig. II -7-8 Maximum velocity and direction of currents

are small whilst large swell coming from South West is predominant during the time between April and September.

Fig. II-7-9 shows exceedance curve of significant wave heights ($H_{1/3}$, records of the wave rider buoy) and wave periods. Median significant wave heights during South West monsoon is approximately 2.2 m and median wave period is 9.5 seconds.

Figs. II-7-10-(a)~(c) show the distributions of median diameter d_{50}, sieve analysis coefficient S_0 ($\sqrt{d_{75}/d_{25}}$), and percentage of silt (smaller than 0.075 mm). The followings can be pointed out:

1) Median diameter of bottom sediments outside the channel is about 0.1 mm whilst d_{50} in the channel is approximately 0.05 mm.
2) Sediments have a little bit bigger S_0 in the channel than outside the channel.
3) Percentage of silt is 10~30 % outside the channel whilst it is more than 50 % in the channel.

Bottom Sediments which were taken on November 13th, 1980 have the same properties mentioned in the above.

According to the Institute of Marine Biology, Karachi University, bottom sediments sampled during monsoon season are fine sand at both outside and inside of the channel. Therefore, hydraulic mechanism will be as follows:

During monsoon season fine sand ($d_{50} \fallingdotseq 0.1$ mm) is deposited at the channel bottom, but after monsoon season suspended silt is transported to the relatively calm channel areas having bigger water depth and is deposited there.

The first stage dredging of the outer channel started in October 1978 and was completed in April 1980. Total dredged volume during the first

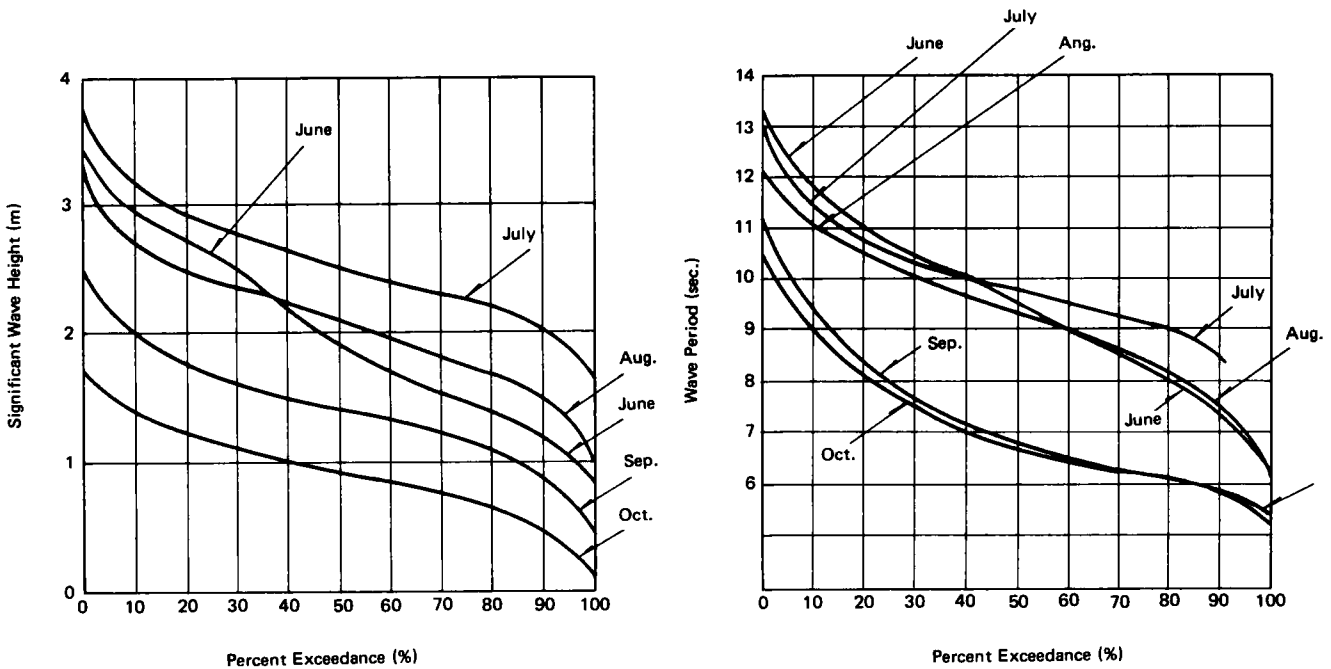

Fig. II -7-9 Wave exceedance curve at fairway buoy (1979, 1980)

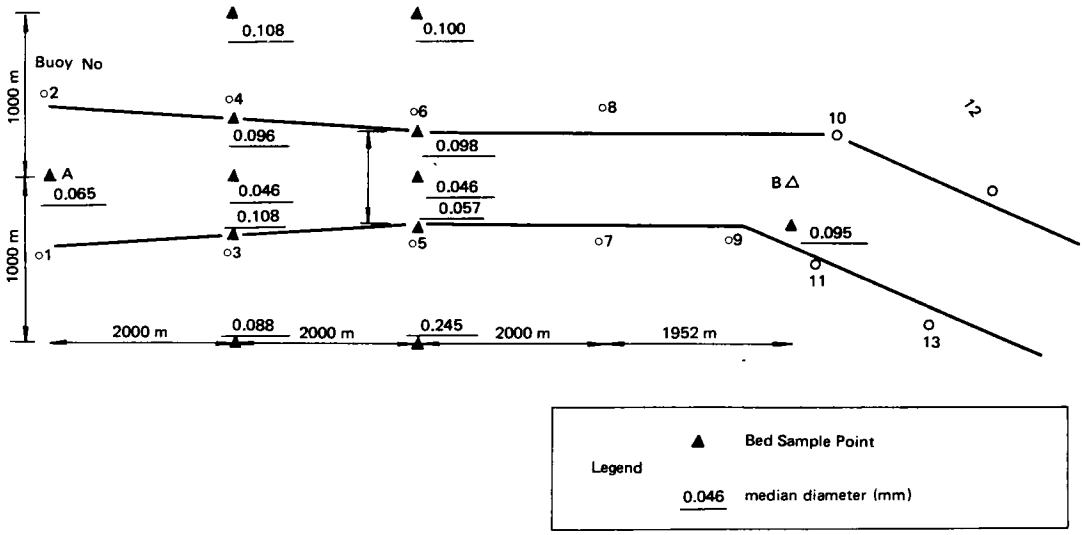

Fig. II -7-10-(a) Destribution of median diameter (d_{50}) of bottom sediments
(Reporting date, 22 Nov. '80) Unit (mm)

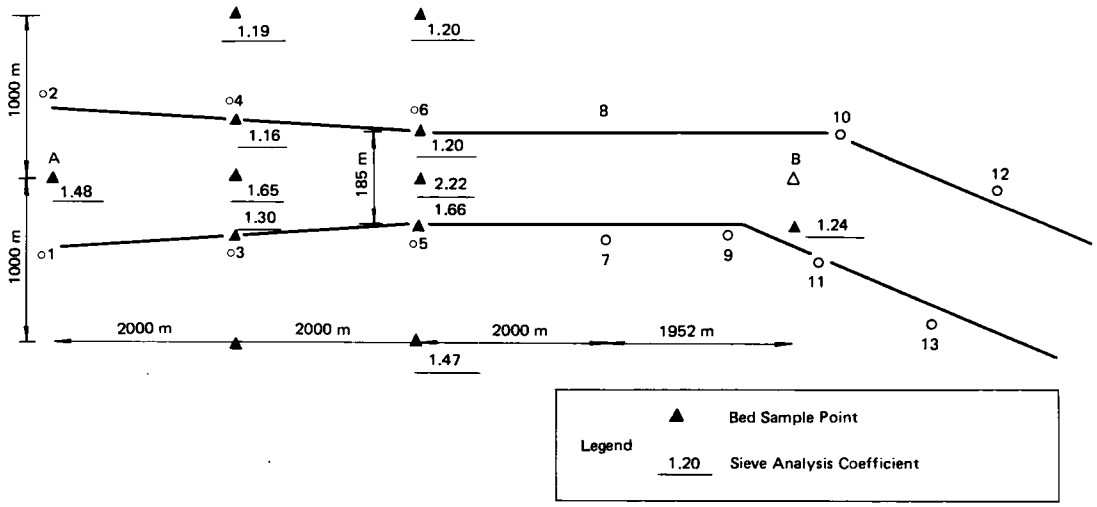

Fig. II -7-10-(b) Distribution of sieve analysis coefficient (So) of bottom sediment
(Reporting date, 22 Nov. '80)

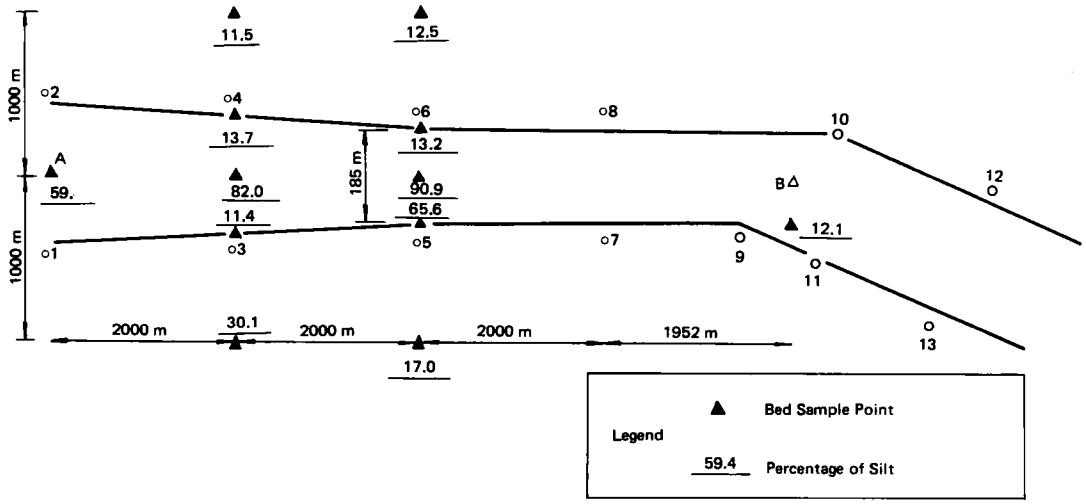

Fig. II -7-10-(c) Percentage of silt
(Reporting date, 22 Nov. '80)

stage was about 18 million cubic meters. The second stage dredging was initiated in October 1980 and is being carried on at present (March, 1981). Total volume of the second stage dredging will be approximately 8 million cubic meters.

Since the commencement of the first stage dredging, monsoons were experienced in 1979 and 1980 and sedimentation volumes during these monsoon seasons were calculated.

Fig. II-7-11 shows examples of cross sections of the channel before and after 1979 monsoon. Inside the channel shoaled by 2 m and to the west of the channel deepened by 1 m.

Fig. II-7-12[5] shows the distribution of the differences of the cross section areas between before and after the 1979 monsoon (+ means accretion and - means scour). The values on the abscissa are landward length measured from point A (see Fig. II-7-7) along the channel. In this figure the line shown as "central portion (HRS)" means differences of the cross section areas within 160 m of the channel center line. The area under this line is differences of the volume within the central portion and it was +1.01 million cubic meters. Dredging operation continued during the monsoon season in 1979, so it is not possible to know spatial distribution of the infill volumes. Dredged volume by this operation is 5.31 million cubic meters in case of dredging coefficient (ratio between dredged quantities and hopper volumes) of 1.2255 and 4.35 million cubic meters in case of the coefficient of 1.0.

The line shown as "North Western Bank (HRS)" means differences of the cross section areas on the North Western zone from 160 m to 1,360 m west of the center line. An area between point A and 1.4 km accreted and an area between 1.4 ~ 7 km was scoured. Differences of the cross section areas

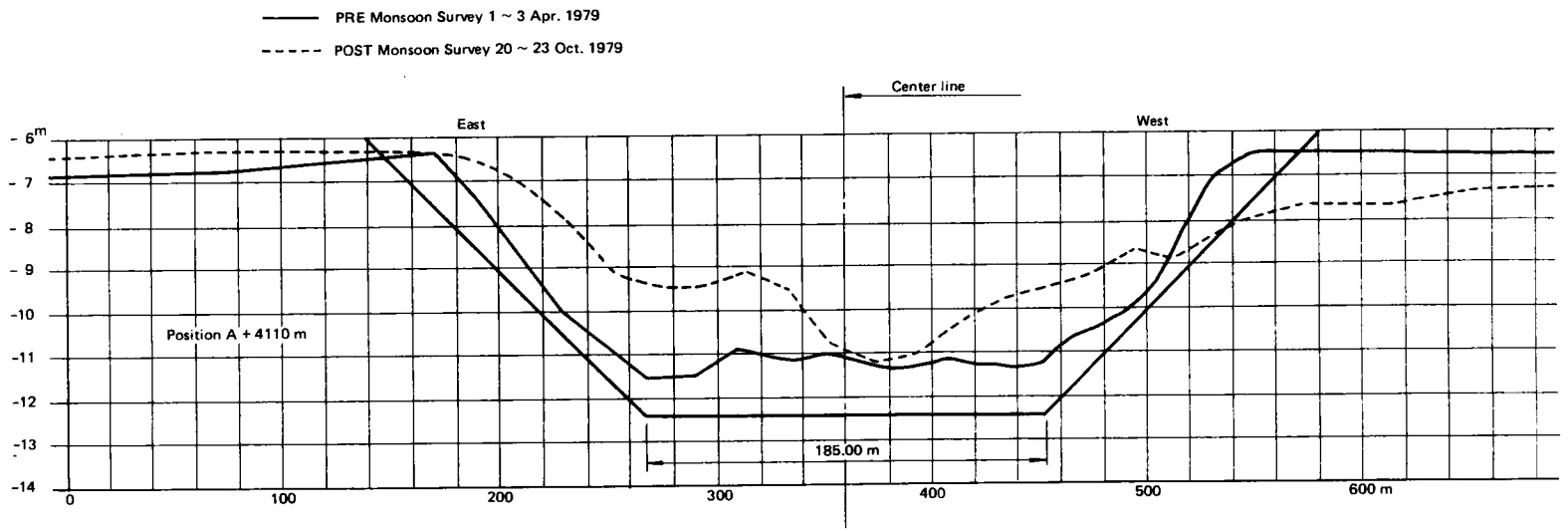

Fig. Ⅱ-7-11 Examples of the cross sections before and after the monsoon, 1979

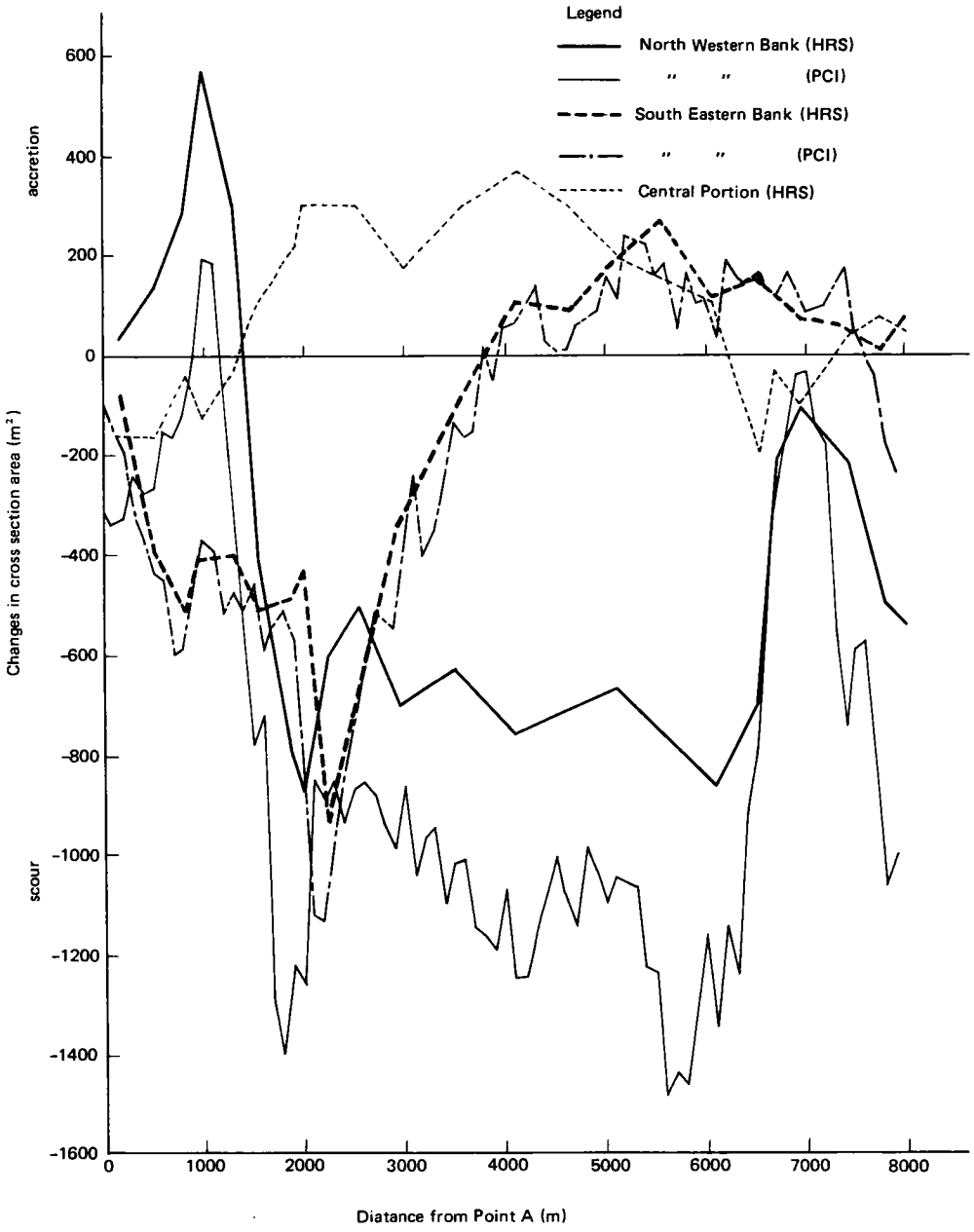

Fig. II -7-12 Distributions of the differences of the cross section areas in 1979

in the scoured area are approximately 500~800 m^2. Total difference of the volume on the North Western zone is 3.82 million cubic meters scour.

The line shown as "North Western Bank (Author)" means differences of the cross section areas on the North Western zone from 240 m to 1,590 m west of the center line. The area difference shows about 350 m^2 larger scour than that of "North Western Bank (HRS)". Total volume difference is 6.58 million cubic meters scour.

The line shown as "South Eastern Bank (HRS)" means area differences on the South Eastern zone from 160 m to 1,360 m east of the center line. The area between point A and 3.8 km is scoured and the area between 3.8 km and 8 km accretes a little bit. Quantity of the accretion at the latter area is 0.33 million cubic meters.

The line shown as "South Eastern Bank (Author)" shows differences of the cross section areas on the zone from 240 m to 1,590 m east of the center line. This line shows almost same tendency as the line shown as "South Eastern Bank (HRS)".

According to the line shown as "South Eastern Bank (HRS)", total quantity of the volume difference on the South Eastern zone is 0.70 million cubic meters scour.

Two different causes contributing to the sedimentation have to be separated in order to estimate the future infill volumes. Those are slumping, which will carry on only for short periods after a capital dredging (short term effect), and sediment transport by waves and currents, which will continue for long periods (long term effect).

HRS[5] has proposed a method to calculate sediment budget on a reasonable assumption that bottom sediments are transported from North West to South East. The North Western zone is on the upstream side in terms of sediment transport and will not suffer scour due to spatial non-uniformity

of the sediment transport rate. Therefore, scour on the North Western zone is due to slumping of the slope only. The area near Point B on the South Eastern zone is a relatively calm area, so sediment transport rate there is negligible. It was assumed that ten percent of the bottom sediments transported by waves and currents from the North Western zone to the South Eastern zone near Point A can cross the channel. Fig. II-7-13 shows sediment budget on the above assumptions. Sediment transport volume due to long term effect will be 3.13 million cubic meters from NW to SE.

Fig. II-7-14 shows differences of water depths between pre-monsoon (April 1980) and post-monsoon (October 1980). Any dredging operation was not done during monsoon season in 1980. Generally speaking, the North Western zone was scoured and both the shipping channel and the South Eastern zone accreted. Remarkable sedimentation occured at the locations near A + 2,000, A + 4,000, and A + 7,000. Especially, near A + 4,000 inside the channel accreted by 5 meters.

Fig. II-7-15 shows differences of the cross section areas between pre- and post-monsoons. Central portion is an area within 240 m of the channel center line and accreted by 4.05 million cubic meters. North Western Bank is an area from 240 m to 1,590 m west of the center line and the area between A + 3,000 and A + 8,000 is scoured. Total volume of scour is 1.72 million cubic meters. The Bank was scoured almost uniformly in 1979 (See Fig. II-7-12) whilst an area near Point B was scoured very severely in 1980. South Eastern Bank is an area from 240 m to 1,590 m east of the center line and shows nearly uniform accretion, although the Bank was scoured near Point A in 1979 (See Fig. II-7-12). Especially, the area between A + 5,000 and A + 8,000 shows about 400 square meters accretion. Total volume difference (accretion) on the South Eastern Bank is 1.88 million cubic meters.

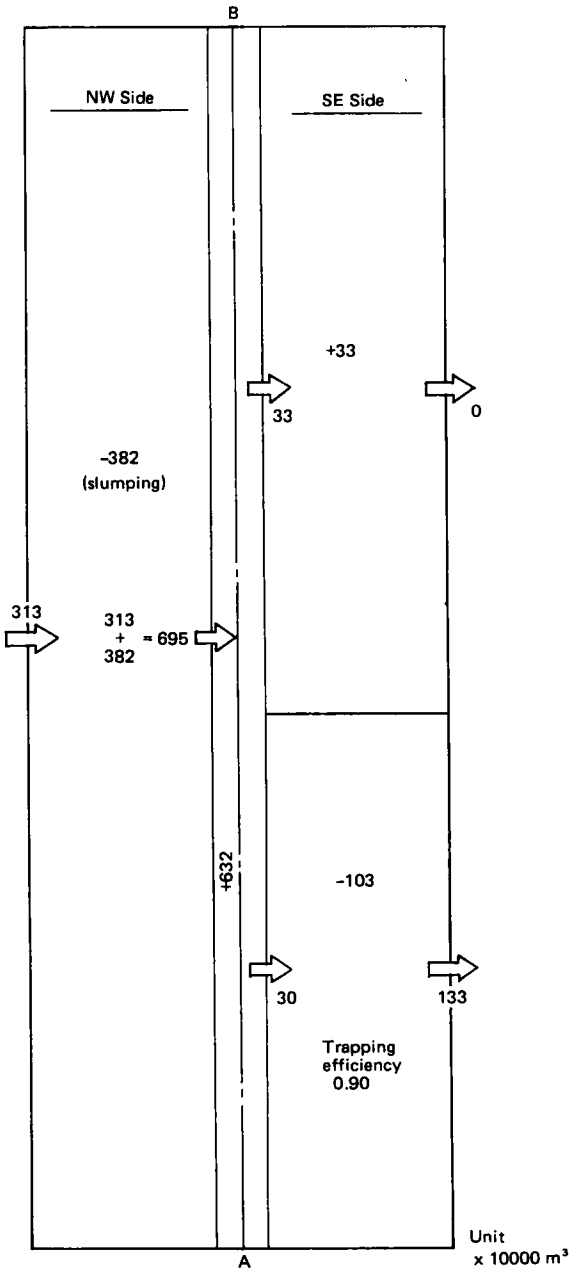

Fig. II -7-13 Sediment budget in 1979

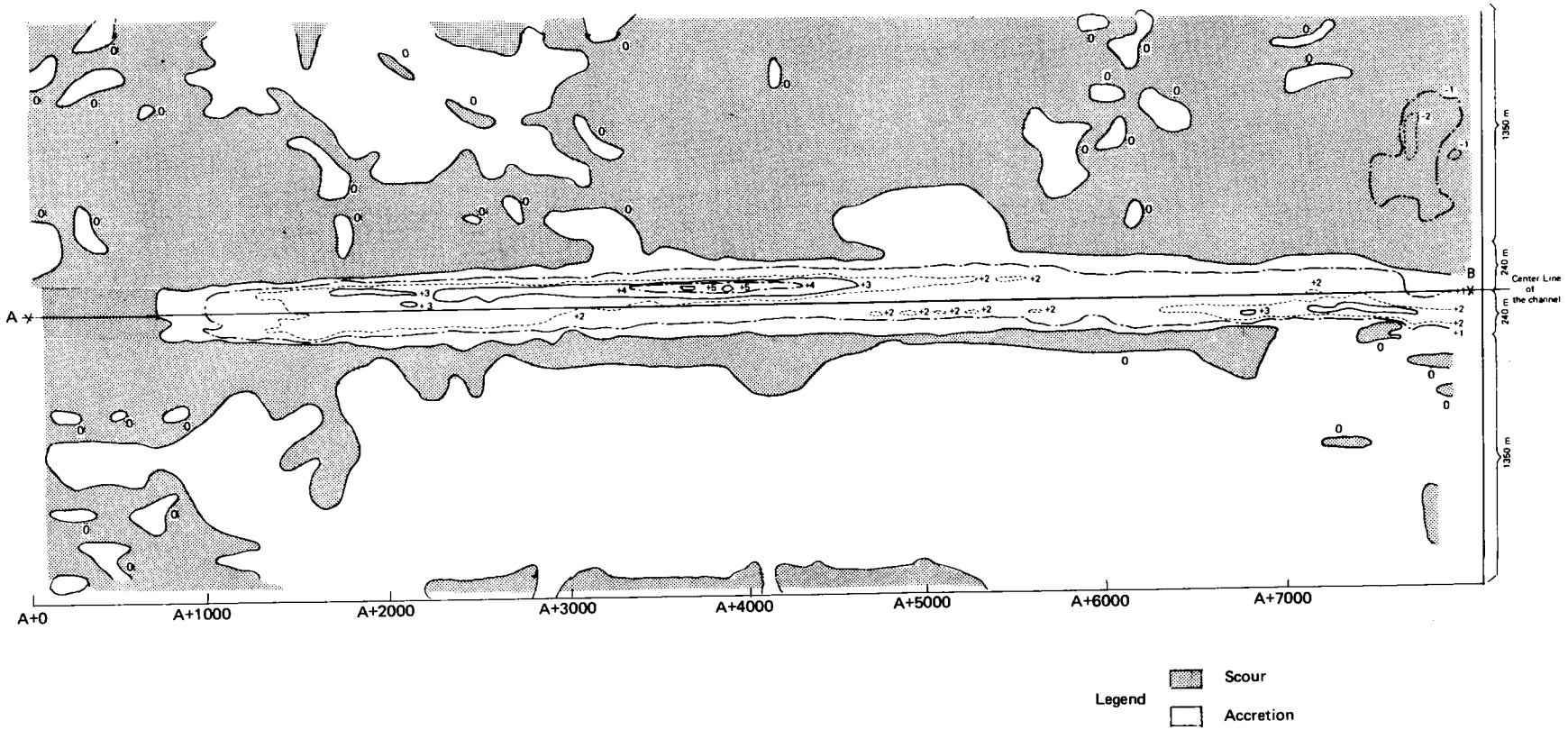

Fig. II -7-14 Differences of water depths

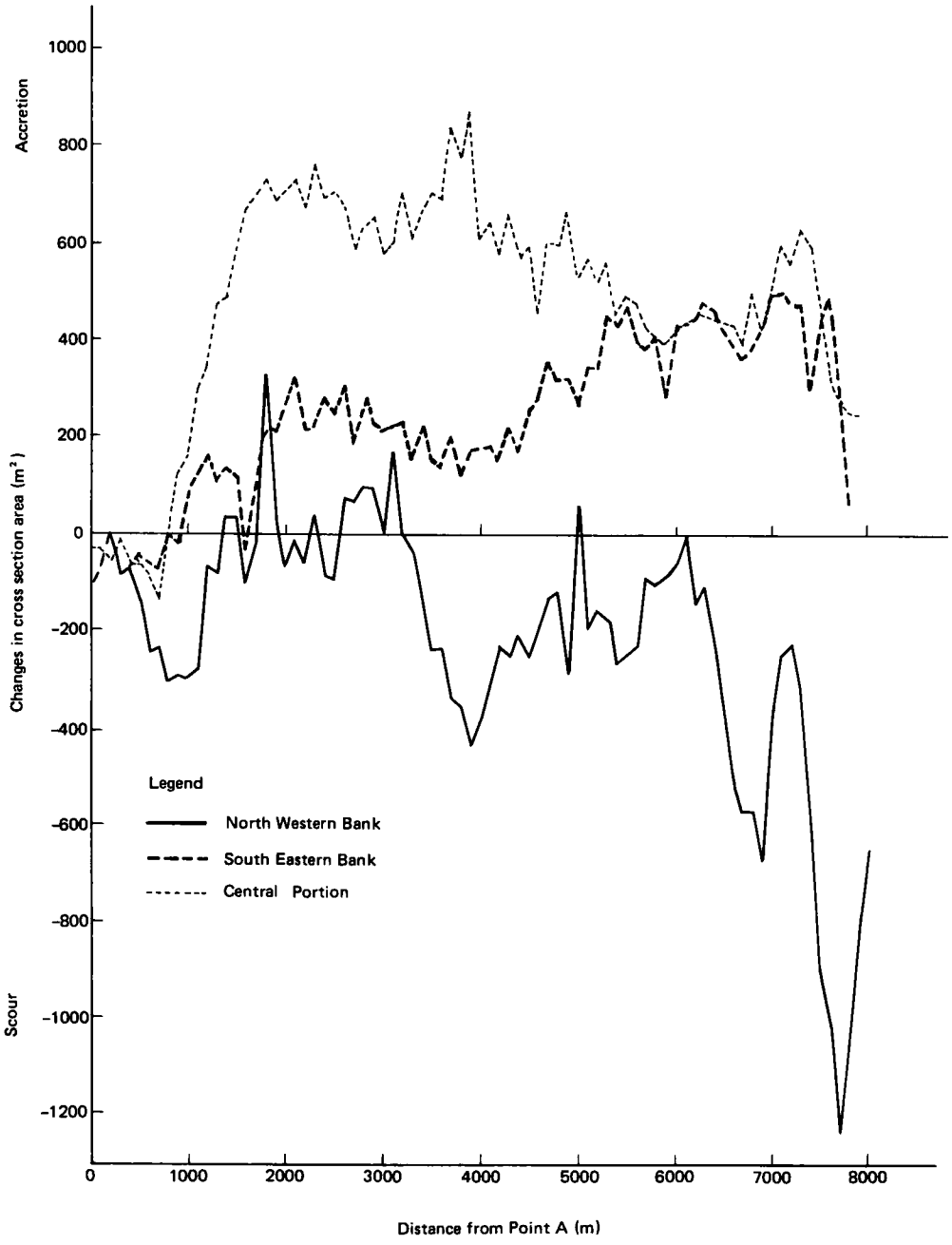

Fig. II -7-15 Distributions of the differences of the cross section areas in 1980

Fig. II-7-16 shows sediment budget in 1980 on the following assumptions:

Firstly, sediments are transported from North West to South East,

Secondly, slumping produces scour on the North Western zone, and

Thirdly, trapping efficiency of the channel is 90 percent. Calculated sediment transport volume due to the long term effect is 2.59 million cubic meters from NW to SE.

Volume of the accretion on the South Eastern zone is 1.88 million cubic meters. Volume of the sediments transported across the channel is 0.26 million cubic meters. Therefore, sediments of 1.62 million cubic meters should have been transported from either the offshore or inshore side of the South Eastern zone. Inshore part of the South Eastern zone is relatively calm area, so suspended sidements would have been transported from the surrounding areas and deposited there.

7-4-3 Sedimentation in estuaries

In estuaries, sediments often are mud and prominent hydraulic forces are tidal and river currents. From the viewpoint of a plan shape of an estuary, there are estuaries of uniform width and of varying width.

Analytical methods for solving sedimentation problems at estuaries was reviewed by the author in 1980[6].

7-4-3-1 Channel sedimentation in estuaries of uniform width (Thames Estuary[7])

Fig. II-7-17 shows the Thames Estuary. Port facilities exist along the river between London Bridge and Gallions Reach, and at Tilbury. The maintenance dredging volume for both channels and inside docks is about 2 million cubic meters per year. Siltation is serious at Mud Reaches (extending from mile 10 to mile 15 in the upper portion of Fig. II-7-17)

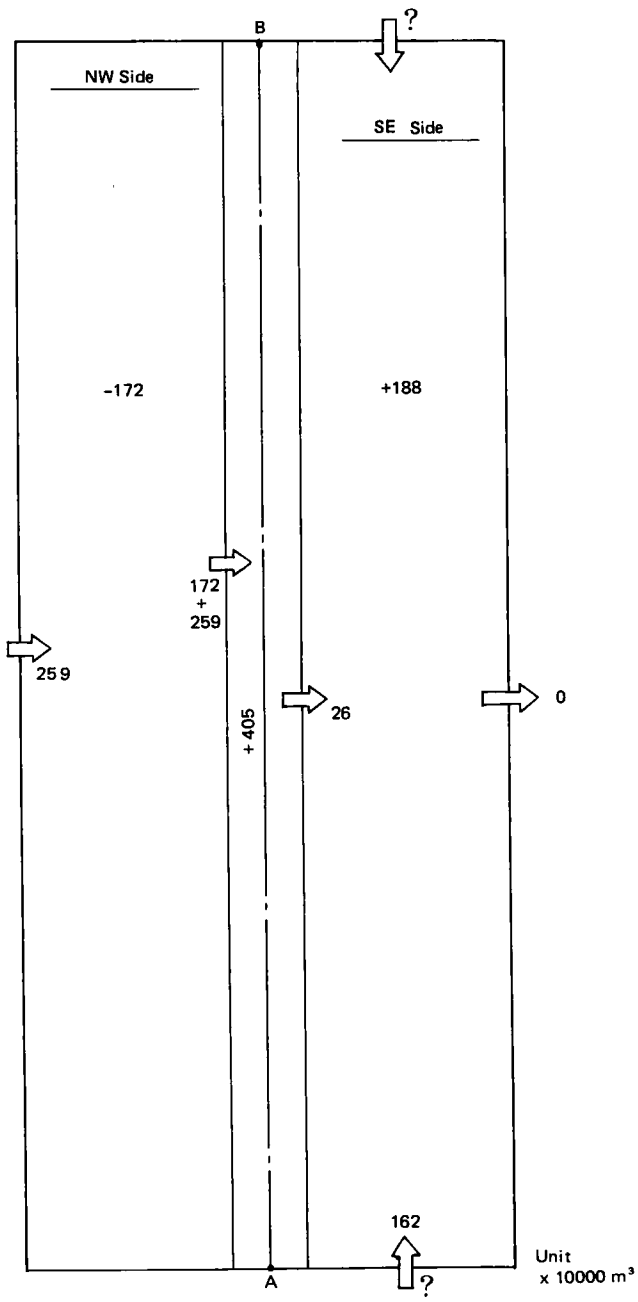

Fig. II -7-16 Sediment budget in 1980

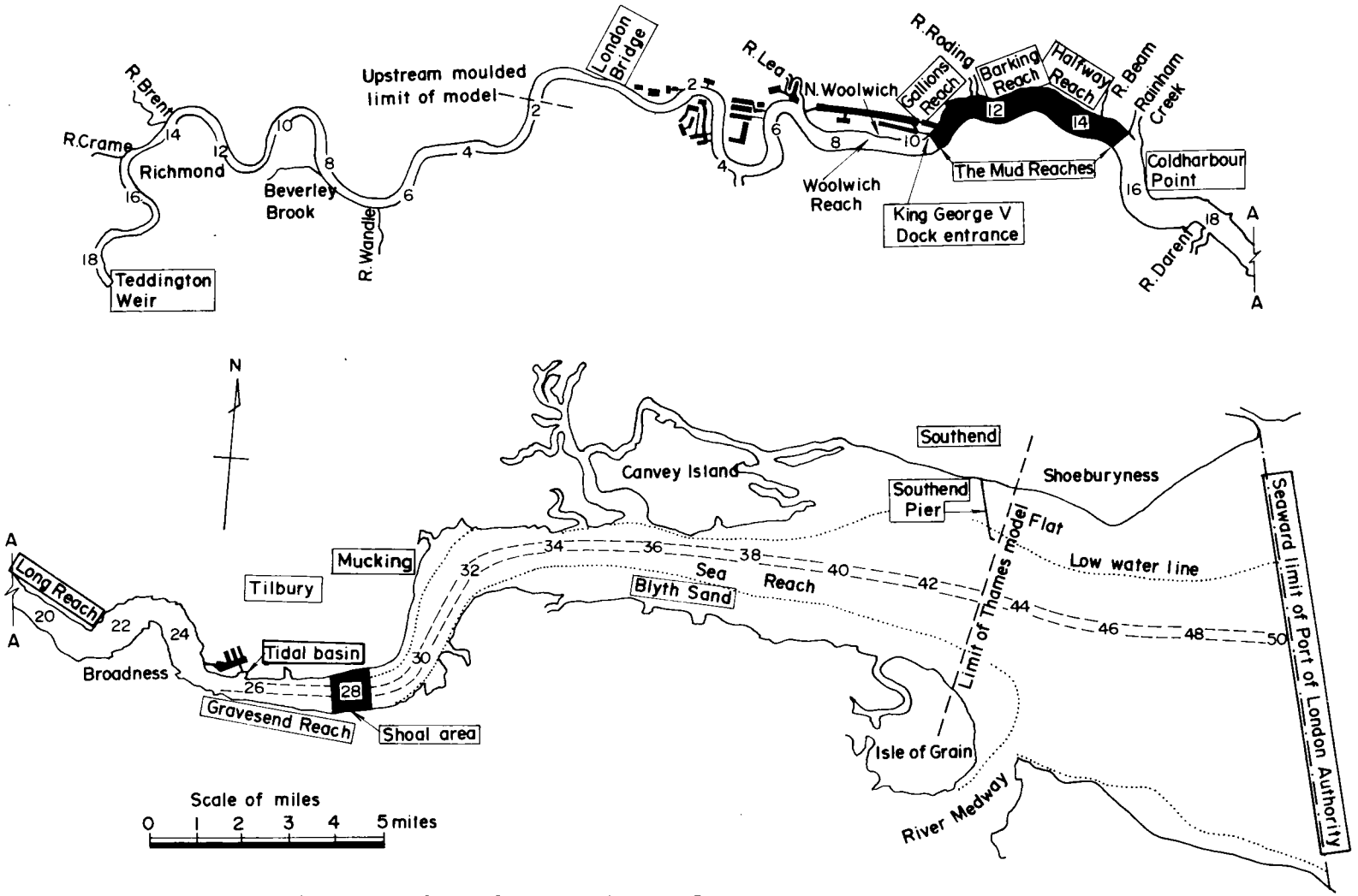

Fig. II -7-17 Plan of Thames Estuary

and at Gravesend Reach (at mile 28 in the lower portion of Fig. II-7-17).

The hydraulic conditions of the Thames Estuary are described as follows. Teddington Weir is at the tidal limit upstream. The distance from Teddington Weir to Southend (seaward limit) is approximately 99 km. In 1957, the channel was 300 meters wide from the seaward limit to Coldharbour Point and 9 meters deep below low water datum. From Coldharbour Point to the King George V Dock entrance, the width was 180 meters and the depth -8.1 meters. The tide is semi-diurnal and ranges can be seen at the five points shown in Table II-7-1. Tidal range increases from Southend to London Bridge and then decreases in the upstream direction. High waters at Tilbury, London Bridge, and Richmond, occur about 26, 77, and 138 minutes respectively after high water at Southend. The Thames discharge, which enters the estuary at Teddington Weir is, by average, 70 cubic meters per second.

The bed materials found at Southend Flats and Blythend (Sea Reach) consist largely of fine sand (of a mean diameter of approx. 0.15 mm) intermixed with black mud. With two major exceptions, the remainder of the river from Teddington to Mucking has a hard bed of gravel, stones, clay, or chalk. The two exceptions are areas where severe siltation occurs as a result of dredging, and the beds consist of fine black mud. One of these areas is at the seaward end of Gravesend Reach and the other includes the three consecutive reaches of Gallions Reach, Barking Reach and Halfway Reach (referred to collectively as the Mud Reaches). By weight, 20 to 35 % of the mud deposited in the Mud Reaches and Lower Gravesend Reach consists of humified organic matter. The inorganic fraction ranges in size from fine sand to clay particles of the order of 0.001 mm. The samples, naturally, vary considerably, but a typical value for the mean particle size is 0.035 mm. About 5 % of a sample may exceed 0.20 mm and an equal amount may be

Table II -7-1 Average tidal ranges in the Thames

	Tidal range (m)				
	Southend	Tilbury	North Woolwich	London Bridge	Richmond
Mean Springs	5.1	5.8	6.4	6.5	4.6
Mean	4.2	4.8	5.4	5.5	4.0
Mean Neaps	3.3	3.8	4.4	4.5	3.3

finer than 0.005 mm.

Siltation in the Mud Reaches is caused by attempts to maintain greater water depths than those dictated by regime for an area where concentration of suspended solids is high. The problem at Lower Gravesend Reach is one of local and rapid expansion in width which, for the same discharge, entails a reduced depth. The mean current velocity is greatly reduced at the critical section where the deposition of mud is occuring.

Fig. II-7-18 depicts the sample concentration of suspended solids measured at 60 % of the depth between London Bridge and Southend. Concentration is plotted against distance along the estuary. The concentration of suspended mud rises from Southend to the Mud Reaches. It peaks near the upper end of the Mud Reaches, and diminishes rapidly upstream.

7-4-3-2 Channel sedimentation in estuaries of varying width (Mersey Estuary[8])

Fig. II-7-19 is a schematic diagram of Liverpool Bay. The area at the right hand side of Fig. II-7-19 is known as "The Narrows". Beyond the Narrows lies the large tidal basin of the Mersey known as the upper estuary. The upper estuary stretches from Dingle Point to Howley Weir as shown in Fig. II-7-20. Liverpool Port is situated along the right bank of the Mersey Estuary.

Liverpool Bay is comprised of sand banks, large areas of which are exposed at low water. Training walls constructed of stone and measuring 14.4 km in length are set in the sand banks. The navigational channel runs between the training walls. Construction of the training walls began in 1909 and ended in 1936. The Narrows, the entrance to the inner estuary, consists of a deep-water channel, approximately 9.6 km long and 914 meters wide at its narrowest part. The Narrows and the main shipping lane through Liverpool Bay are maintained by the large tidal volume flowing in and out

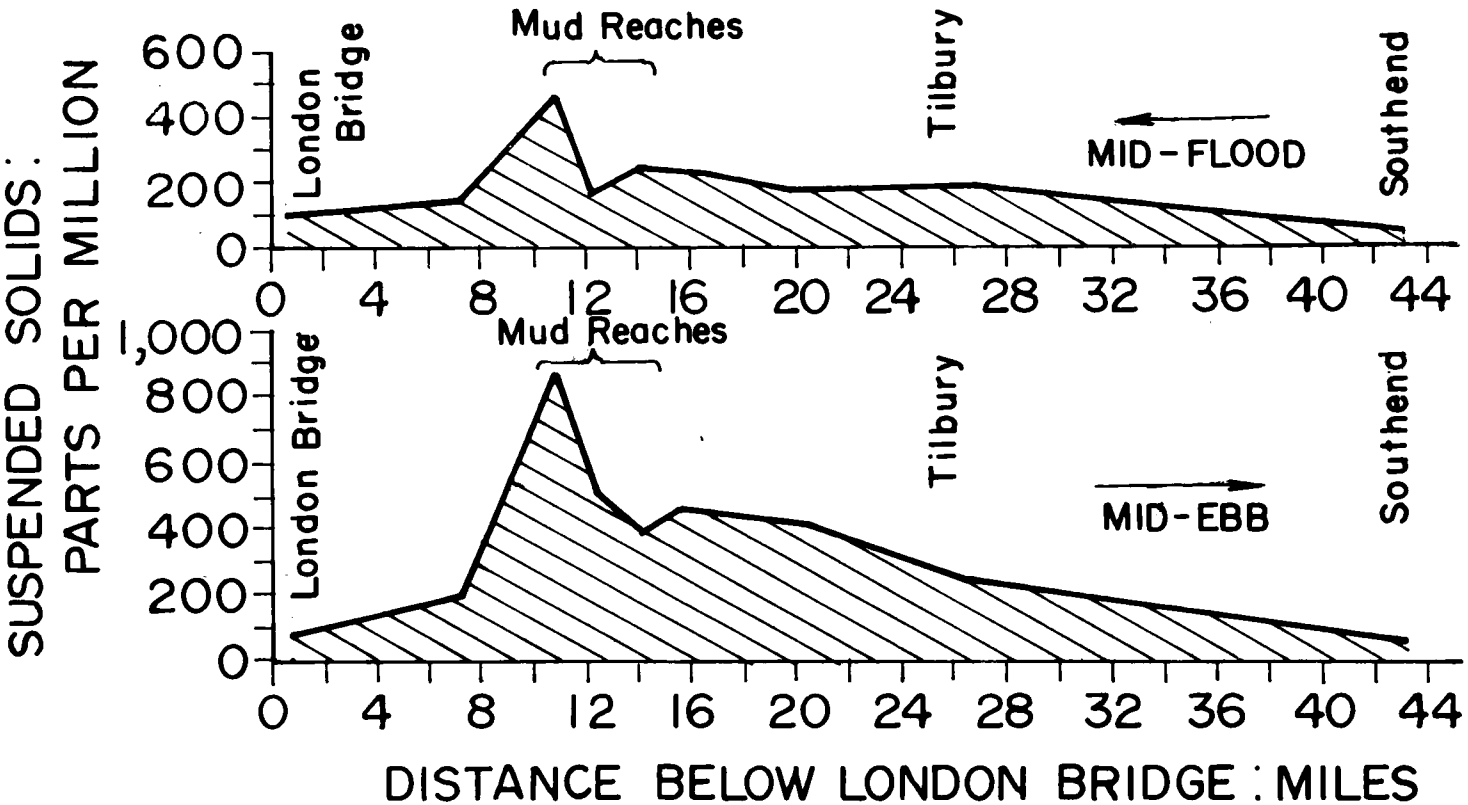

Fig. II -7-18 Typical longitudinal distributions of suspended solids at mid-flood and mid-ebb at 0.6 x depth

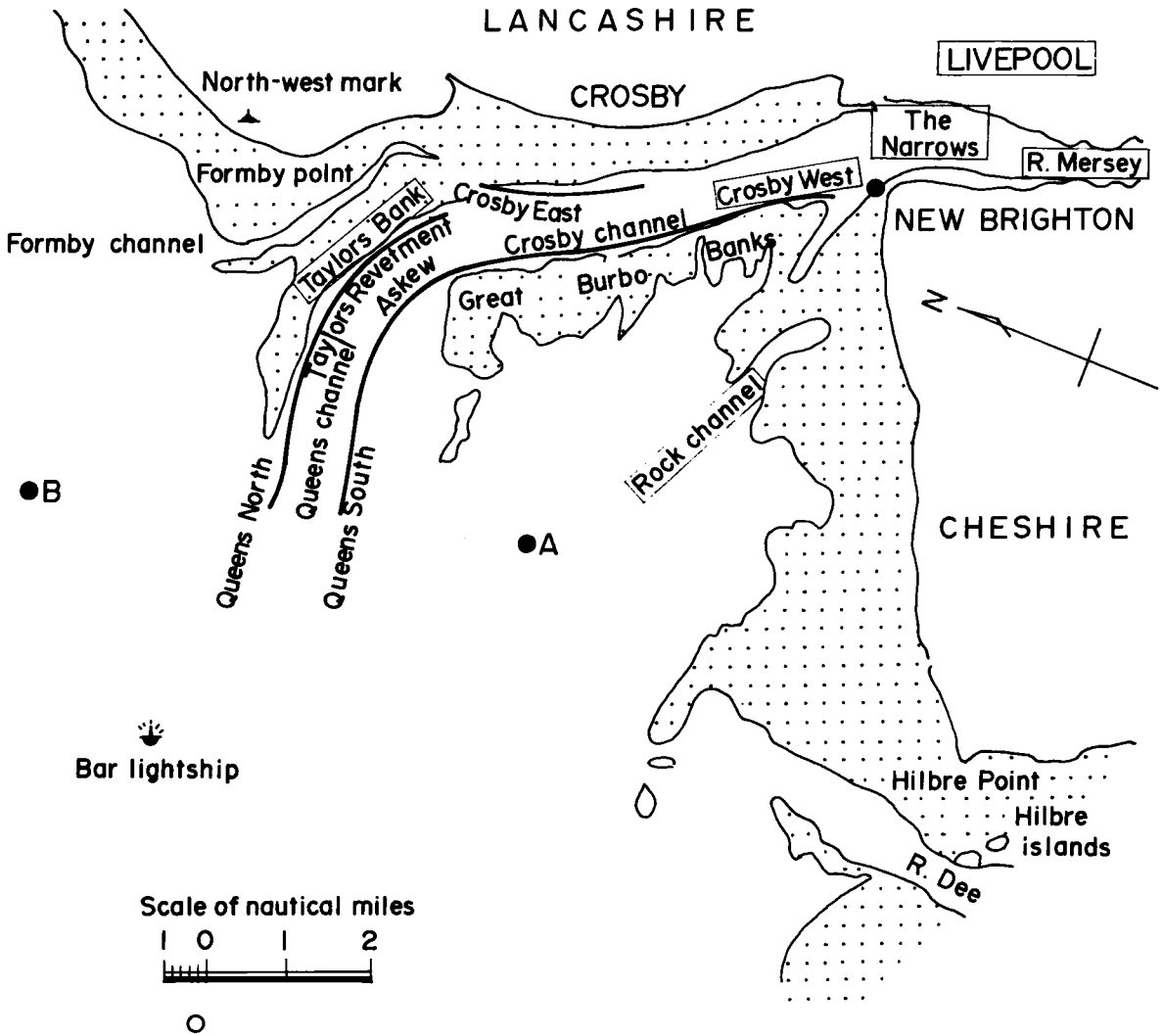

Fig. II -7-19 Plan of Liverpool Bay

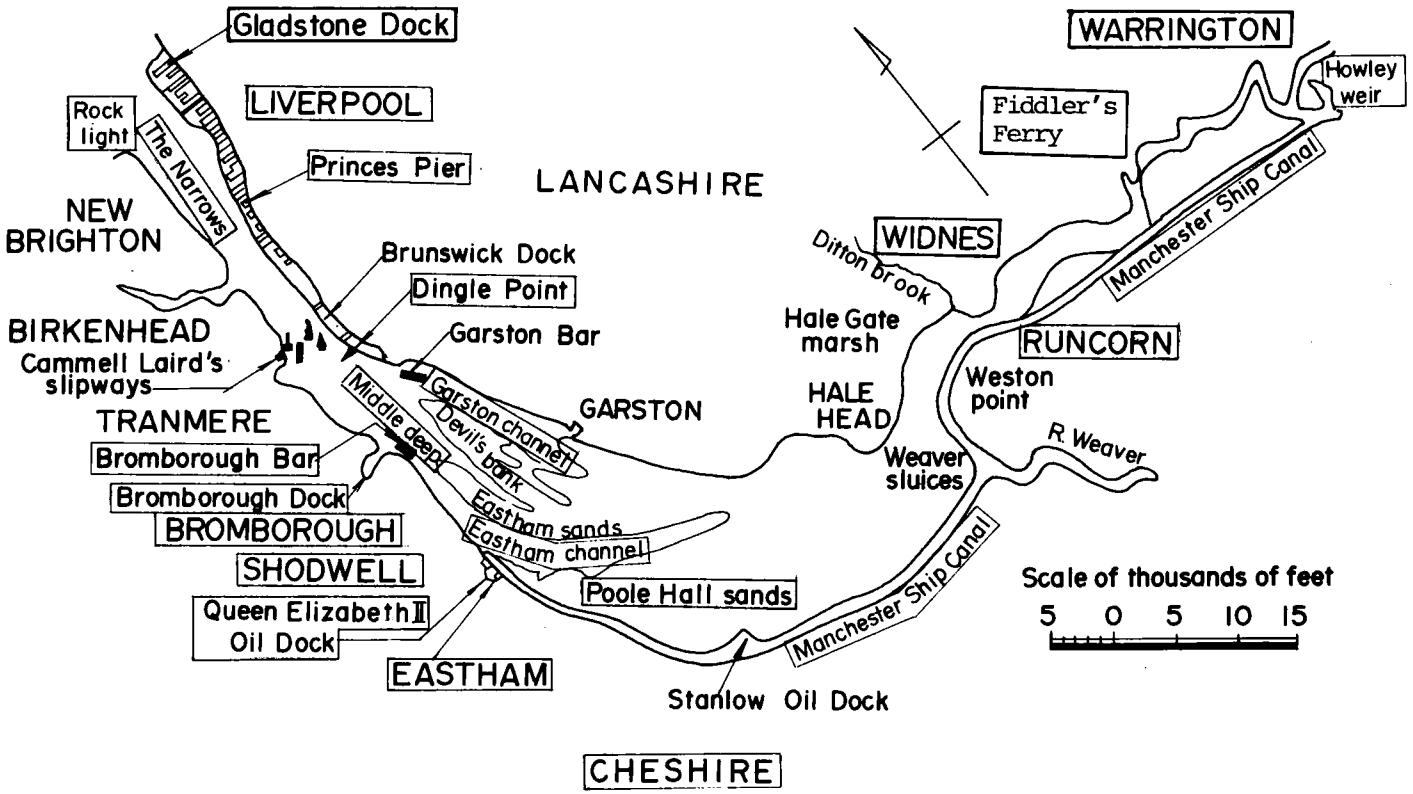

Fig. II -7-20 Plan of the Upper Estuary of the Mersey

of the estuary. The upper estuary's maximum width is 5,486 meters and extends a distance of about 41.6 km. At low tide almost the entire basin is drained. The downstream section between Dingle and Eastham characterized by the three channels of Garston, Middle Deep, and Eastham. Further upstream the low-water channel meanders through large areas of sand and mud, constantly changing its course.

Table Ⅱ-7-2 shows the range of tidal levels in the estuary. The volume of fresh water entering the Mersey Estuary is on an average 52.8 m^3/s.

Fig.Ⅱ-7-21 shows the water volume between Rock Light and Runcorn which approximates the upper estuary. Between 1861 and 1960 siltation caused a reduction in volume of about 100 million cubic yards (76.5 million cubic meters). Thus this severe siltation problem necessitates a maintenance dreging volume of 765,000 cubic meters per year. This silt accumulated in spite of the fact that between 1897 and 1955, approximately 300 million cubic meters of material were dredged from the area.

Figs. Ⅱ-7-22-(a) and (b) respectively represent the extent of the sand bank in Liverpool Bay in 1833 and 1955. In comparing these figures, the following topographical changes are noticed:

1) Formerly Rock Channel was the main approach to Liverpool Port. It deteriorated from a wide channel in 1833 with a depth of up to -9.1 meters at low tide, to a narrow one in 1955 with a depth of only -0.61～-0.91 meters at low tide.
2) Rapid shoaling along the banks also occurred in the Great Burbo Bank area during the period 1912～1936.
3) Shoaling accumulations calculated from the water volumes of Liverpool Bay, are 142 million cubic meters in 1833～1912 (about 1.8 million m^3 a year) and 66 million m^3 in 1912～1955 (about 1.53 million m^3 a year)

Table II -7-2 Tidal range in the Mersey

	Tidal range					
	Gladstone Dock	Princes Pier	Eastham	Widnes	Fiddler's Ferry	Warrington
Mean springs	8.2	8.4	8.9	4.5	2.9	2.1
Mean	6.4	6.5	6.9	3.6	1.8	1.2
Mean neaps	4.6	4.7	5.0	2.7	0.8	0.2

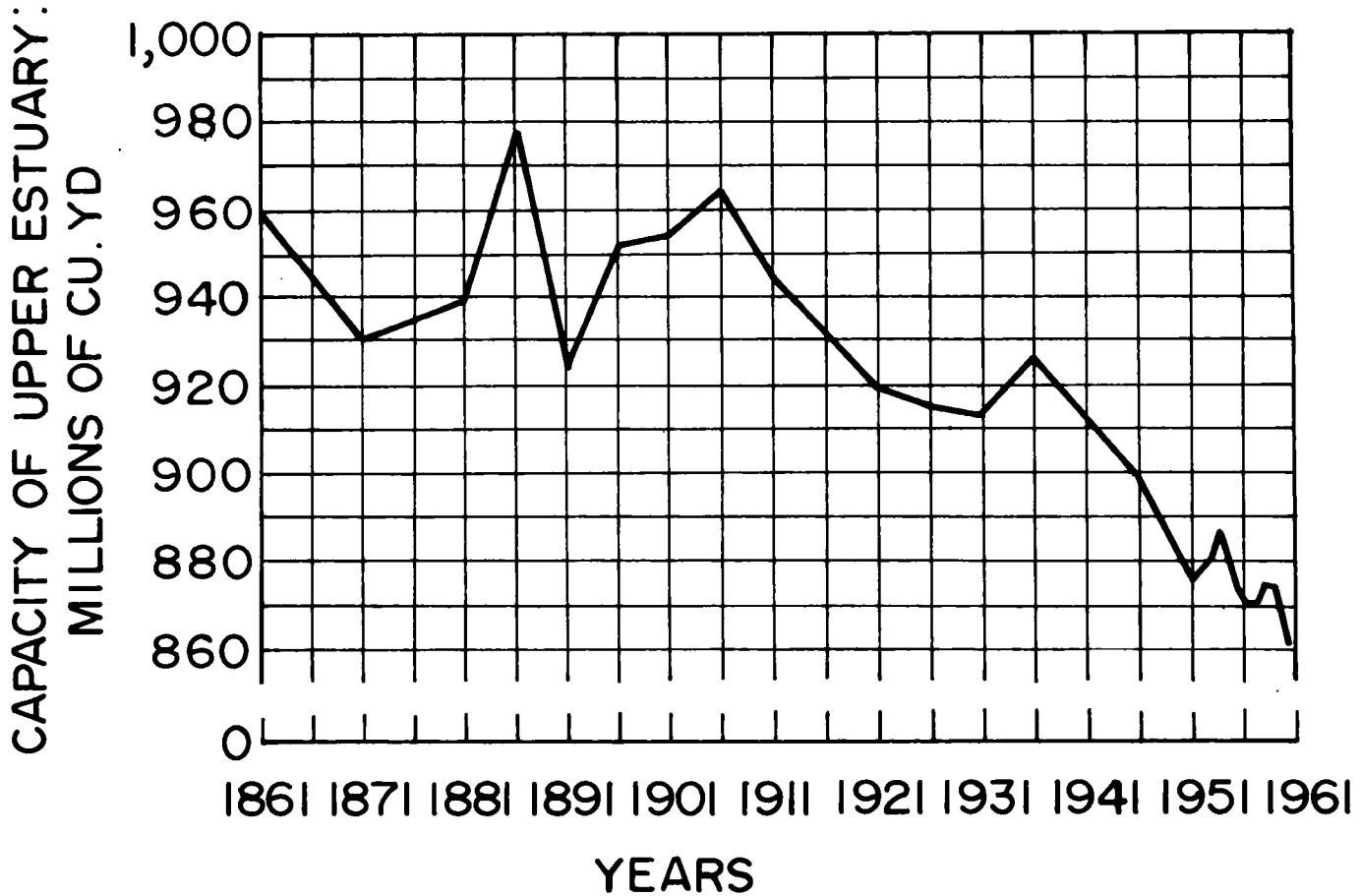

Fig. II -7-21 Variation in the capacity of Upper Estuary of the Mersey between Rock Light and Runcorn

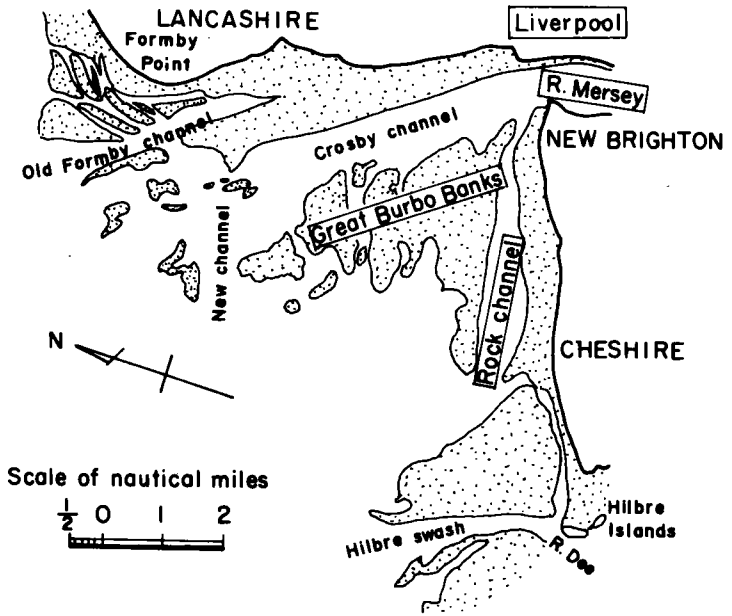

Fig. II -7-22-(a) Liverpool Bay in 1833

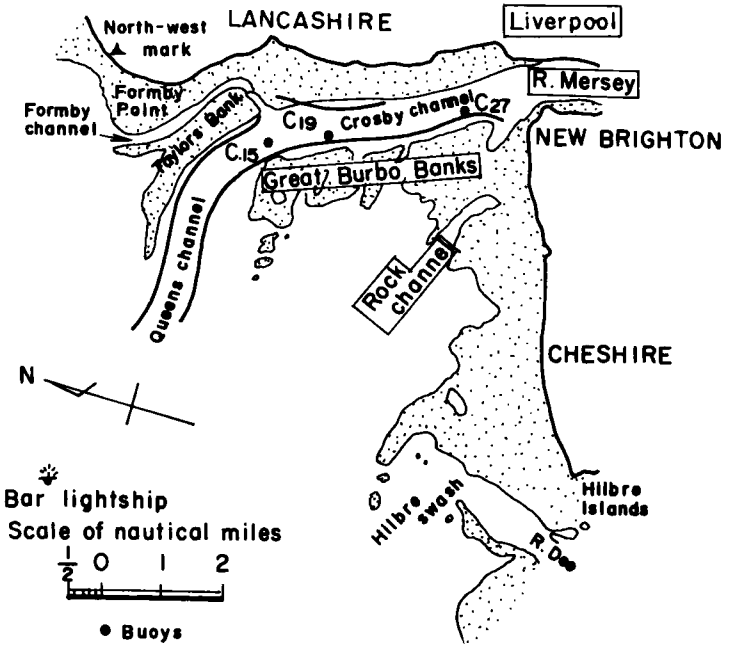

Fig. II -7-22-(b) Liverpool Bay in 1955

Figs. Ⅱ-7-23-(a) and (b) respectively represent net movement per tide of water near the bed in 1911 and 1957. Movement was measured in a rigid-bed model on a horizontal scale of 1/3,200 and a vertical scale of 1/120. In 1911, the training walls were only partially constructed. By 1957, the training walls had been completed. By comparing these two figures, the following observations are noticed:

1) Construction of the training walls concentrated the flow into the main channel between the training walls and extended the areas of ebb drift further seaward.
2) In 1957, the net drift behind the banks was predominantly in the flood direction. Consequently, more material was carried up to the wall by the flood tide than could be taken by the ebb, and as a result shoaling took place behind the revetment.

As a result of these studies, it was concluded that material crossing the training walls near the Mersey River mouth would be carried upstream and thus contribute siltation to the upper estuary. Material would be transported upstream by the action of density current, a mechanism operating similar to that found in the Thames Estuary.

7-5 Conclusions

Several examples of channel sedimentation at Japanese and overseas ports were introduced.

The main conclusions of this chapter are:

(1) Factors influencing sedimentation are topographies of shoaling areas, forces causing sedimentation, and sediments types. Investigation methods of channel sedimentation differ depending on these factors.
(2) Japanese ports are usually located on beaches facing the ocean. Channel sedimentation at Japanese ports is classified into the two types,

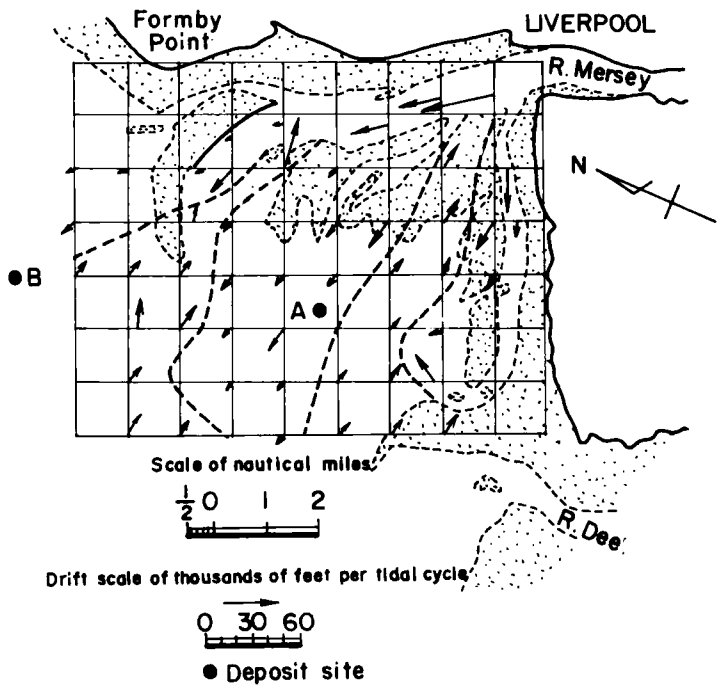

Fig. II -7-23-(a) Net movement per tide of water near the bed in 1911

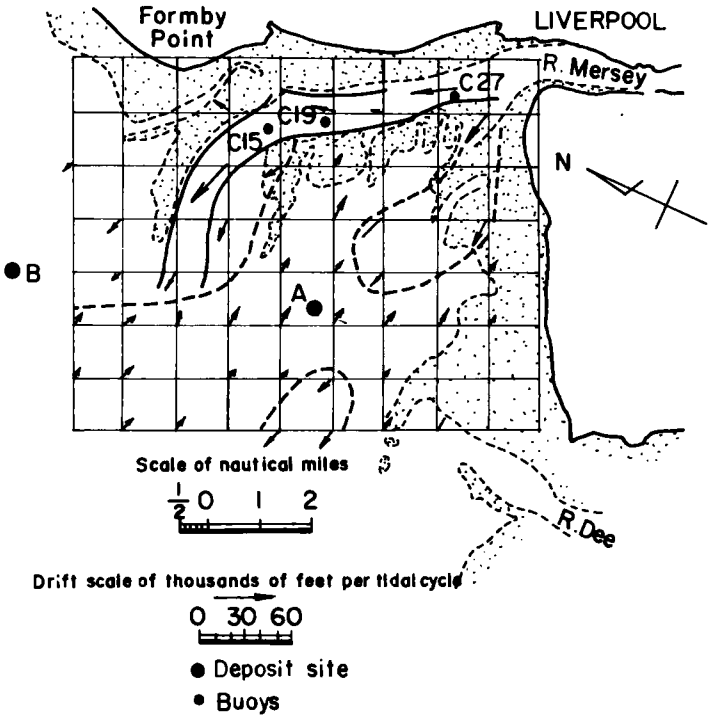

Fig. II -7-23-(b) Net movement per tide of water near the bed in 1957

i.e. "sedimentation caused by littoral sediment having a well - defined transport direction" and "sedimentation on beaches having an indistinct sediment transport direction". Both types occur due to the series of sediment transport mechanism which are causing shoreline changes.

(3) There are various types of channel sedimentation at overseas ports. Sedimentation volume sometimes reach several millions m^3. Sedimentation at Qasim Port approach channel was caused by littoral sediment which is prominent in an offshore sand bank. Two different causes contributed this sedimentation, i.e. slumping of channel slopes and sediment transport by waves and currents. Two examples of channel sedimentation in estuaries were introduced. In estuaries of uniform width, siltation was caused by attempts to maintain greater water depths than those dictated by regime for an area where concentration of suspended solids was high. In estuaries of varying width, channel sedimentation was caused by landward net drift after the construction of training walls.

REFERENCES

1) Pritchard D. W. : What is an estuary: Physical viewpoint, Estuaries, ed. Lauff, American Association for the Advancement of Science, 1967.

2) Owen M. W. : A study of the properties and behaviour of muds, Literature review, H. R. S. Report INT 61 , 1966.

3) Tanaka N. and Sawamoto M.: On shoreline change near harbours at sandy beaches —— Understanding of the present state on the basis of aerial photographs and an attempt of classification ——, Technical Note of the Port and Harbour Research Institute, No. 180, 1974. (in Japanese)

4) Irie I. : Mathematical simulation of channel sedimentation, Proc. of the 23rd Coastal Engineering Conference in Japan, 1976. (in Japanese)

5) Port Muhammad Bin Qasim, Pakistan, Infill of Phitti Creek Entrance Channel during the 1979 Monsoon, HRS Report EX 949 , 1980 October.

6) Ozasa H. : Review of the estuarine researches done at the Hydraulics Research Station, England, Technical Note of the Port and Harbour Research Institute No. 354, 1980. (in Japanese)

7) Sir Inglis, C. C. and Allen, F. H.: The regimen of the Thames Estuary as affected by currents, salinities, and river flow, Proc. Institution of Civil Engineers, 1957.

8) Price, W. A. and Kendrick, M. P. : Field and model investigation into the reasons for siltation in the Mersey Estuary, Proc. Institution of Civil Engineers, 1963.

CHAPTER 8. STUDY OF CHARACTERISTICS OF SAND WAVES AND CHANNEL SEDIMENTATION

8-1 Introduction

8-1-1 Background for execution of the study

There are many industrial areas located at coastal areas facing Seto Inland Sea. These industrial areas have berthing facilities and ships approach ports through shipping channels. The shipping channels have been deepened, accompanied by rapid increase of vessel size.

Bisan Seto Seaway is one of the major seaways in the region for large-sized ships. Fig. II-8-1 shows plan of seaways and areas dredged until 1972. The North Seaway was dredged to -17 meters deep* in March, 1968 and to -19 meters deep in March, 1972. The dredging of the South Seaway to -13 meters was completed in 1967. Approximately 38 million m^3 of soil in total has been dredged in the areas shown in Fig. II-8-1. The area shown by "G" in Fig. II-8-1 is a meeting place of the North Seaway, the Mizushima Branch Seaway, and the Connecting Seaway. There is a sand bank called Inosakinotsugai at the sea bottom of this place. Inosakinotsugai was dredged to -19 meters in 1972, but points shallower than -19 meters appeared in a stripe pattern a few months after the completion of dredging. Water depth of the shallowest point was -16.2 meters. The area shown by "H" in Fig. II-8-1 was dredged to -13 meters, but also shoaled. Water depth of the shallowest point was -8.7 meters.

This sedimentation (shoaling) was caused by sand waves which exist on Inosakinotsugai. Wave lengths of the sand waves are usually longer than 10 meters and their wave heights are several meters. Even though the sand

---

* This means that water depth of the shallowest part in the seaway is -17 meters, and so forth.

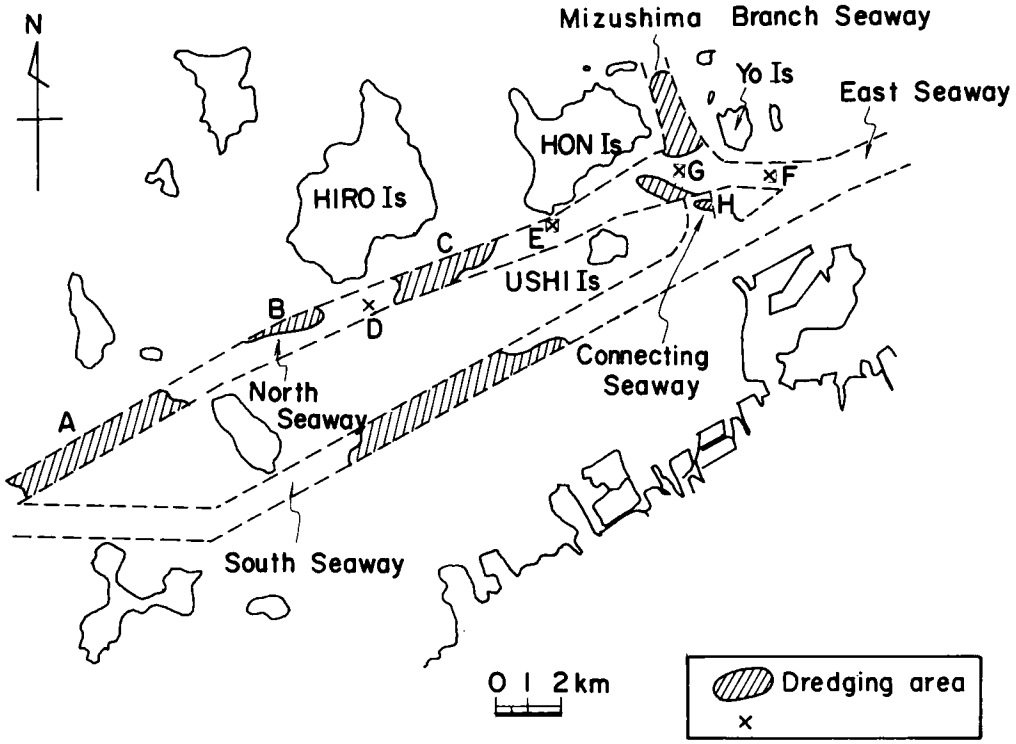

Fig. II -8-1 Bisan Seto Seaway and dredging areas

waves had once disappeared after dredging, they were formed again and many shallow spots appeared.

For safety navigation of large - sized ships, planned water depth must be maintained at all areas of the seaways. In order to study the phenomena of the sedimentation and find a proper method for maintaining enough water depth, topographical, geological, and hydraulic surveys were carried out.

8-1-2 Previous studies about sand waves and the intension of carrying out this study

When tidal currents flow fast over a submarine sand bed, large undulatory topography (submarine sand waves) appears. These phenomena have been observed in the North Sea, Georges Bank and many other places in the world. Similar sand waves exist at the Seto Inland Sea in Japan. By the tide, sea water flows into and out of this area. Velocity of tidal currents is fast. Especially at the Bisan Strait in the Sea, there are many sand waves on the bottom of the sea way. (See Fig. II-8-2)

Geologists have investigated submarine sand waves up to this time.[1)~4)] Mogi[5)] has summarized the results of the investigations as follows:

1) Sand waves do not exist on the sea bottom where tidal currents flow too fast, for example in the center of straits. They frequently appear on submarine sand banks (sand ridges) at the entrances of straits. Particularly they are easily formed on the tip of sand banks in the shade of islands.
2) Scales of sand waves are closely related with water depths. Their wave heights and the water depths at the trough of sand waves incline to increase with increase of wave lengths.
3) Referring to the geomorphological study on the relation between mean current velocity near sea bottom and diameters of bottom sediments, the submarine sand waves agree with the transitional region from ripples to antidunes and flat bed.
4) On the crest of sand wave, bottom sediments are small and well sorted. On the slope, generally, they are coarse and poorly sorted. On the trough, they are intermediate.
5) Sand waves move to and fro with tidal currents, but after long term, they gradually move to the direction of permanent current.

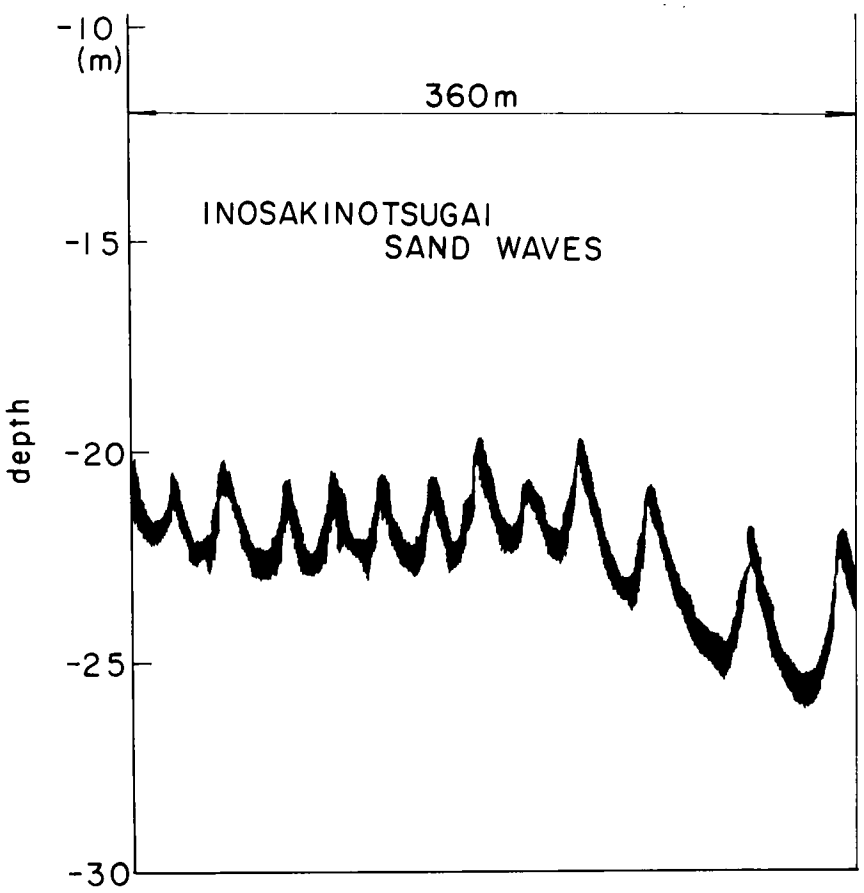

Fig. II -8-2 Sand waves at Inosakinotsugai

6) Sand waves which were destroyed by dredging are reformed after short period.

On the other hand, according to foreign reports, in the North Sea[6], Irish Sea[7], east coast of U. S. A. [8), 9)], and Fundy Bay in Canada[10] etc. sand waves exist on sand banks, and the bed material is sand.

In respect of the cause of sand waves formation, since they exist mostly in deep inland seas, they are not formed by the action of waves, but by that of tidal currents. Many geologists suppose that existence of sand bank is closely related to occurrence of sand waves. On the other hand, theoretical analysis and hydraulic experiments have been performed in order to make clear the causes. Including sand waves due to unidirectional flow, the obtained theories are classified as follows:

1) Theory by Cartwright[11]; He has proved that in the lee of a permanent obstacle, velocity perturbations grow under vertical variation in density and shear, so sand waves are generated.
2) Theories by Kennedy[12] and Hayashi[13]; These theories are concerned with mechanism of sand wave formation due to unidirectional flow. The cause of the formation is based on instability of the boundary between water and sand bed. This instability induces increasing of small perturbations on alluvial bed.
3) Theories by Raudkivi[14] etc. ; Sand waves are formed by the interaction between turbulence in the flow and sediments. Their studies have been conducted mainly by experiments of sand waves formation due to unidirectional flow.

The author considers that studies of sand waves by geologists go into details at the point of their configurations, but are insufficient in the investigations of hydraulic quantities, that is, those of tidal currents.

On the other hand, since studies from hydraulic side have been carried out through physical experiments mainly, large scale topographies such as sand banks or caldrons have not been taken care sufficiently. Hydraulic effects due to these large scale topographies have not been clarified. The primary interest of this study was limited to sand waves, when it started. However, the author has noticed the important role of the large scale topographies.

There are three topographies mentioned in this chapter. Scales of these topographies are ranked as large, medium, and small. The largest topographies are sand bank and caldron. The medium scale topographies are sand waves which cover the sand banks. The smallest topographies are ripples which cover the sand waves. Difference among scales of these topographies must be recognized exactly and hydraulic investigations suiting for each topography have to be done.

The present study deals with (1) configurations of sand banks and caldrons (2) sand wave configurations from the point of morphology (3) relations between characteristics of sand waves and hydraulic quantities from the point of alluvial hydraulics, and (4) statistical structures of submarine topography which have seldom been studied hitherto. The author thinks as follows: "While tidal currents flow from the area of no sand wave to the area of sand wave and vice versa, structures of tidal currents will certainly be changed as a result of the interaction between tidal currents and topography (sand bank and sand waves)". Therefore, the author has put stress on researches concerning both internal macro structure of tidal currents and the change of the structure. The following investigative methods are adopted:

1) A lot of floats were put into tidal currents and aerial photographs were taken. Using the photographs, tidal currents have been researched.

2) A current meter was set at the place of 50 cm above the sea bottom. Turbulence of tidal currents at the bottom layer has been observed.

8-2 General view of sand waves at the Bisan Strait

At the Bisan Strait, vast sand banks are formed in shades of scattered islands. Numerous sand waves appear on both crests and slopes of the sand banks. Mogi and Kato[3] introduced these sand waves formerly, but now let's look over their configurations paying attention to submarine topographies (sand banks and caldrons). Records of 8-2-1 ~ 8-2-3 were sounded by staffs belonging to Maritime Safety Agency (Mogi et al.). Records of 8-2-4 are ones of the author's investigation. Approximate submarine topography and areas of sand waves at the Bisan Strait are shown in Figs. II-8-3-a and b. Tidal currents flow from east to west at flood current, and from west to east at ebb current.

8-2-1 Sand waves around Kashiwa Is., Ogi Is., and Megi Is. (Fig. II-8-4)

There are numerous sand waves around Kashiwa Is. The outline of submarine topography is as follows: a narrow sand bank -- called Osono Shoal -- is formed from Ozuchi Is. to Kashiwa Is. (Fig. II-8-3-a). There is a caldron among Osono Shoal, Kashiwa Is. and Nao Is. — water depth of the deepest place in the caldron h_{max} is -50 m and plane scale of the caldron L x B (L: length of the caldron, B: width of the caldron) is 0.8 x 0.2 km. Moreover, there is a flat place — water depth is about -40 m — between Kashiwa Is. and Naka Shoal. On the other hand, maximum velocity of tidal currents at the southern part of Kashiwa Is. is 3 knots according to charts of tidal currents. Generally, there are two theories regarding the cause of caldron's formation[15]. One is the theory that caldrons were made by strong erosive force of tidal currents. The other is the theory that old river valleys which were not reclaimed by tidal currents became caldrons.

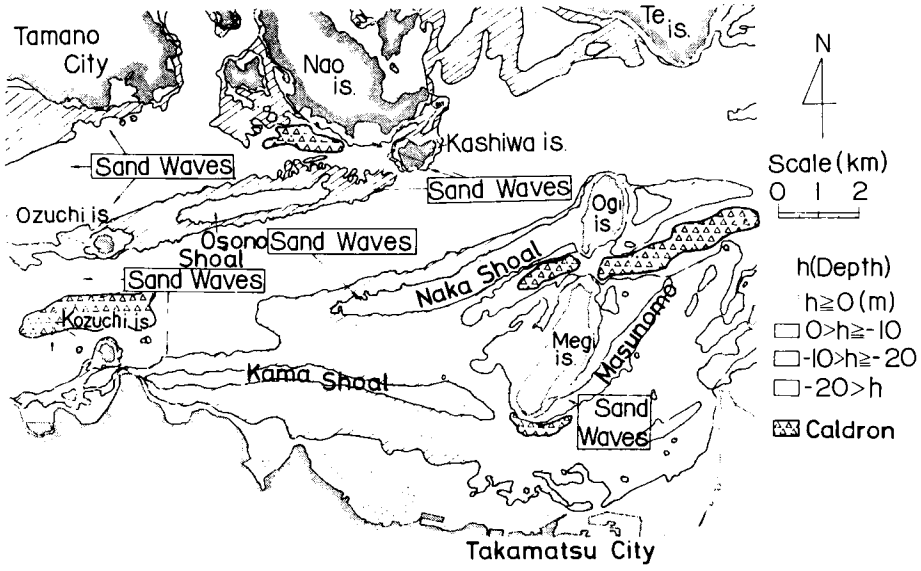

Fig. II -8-3-(a) Submarine topography at East Bisan Strait

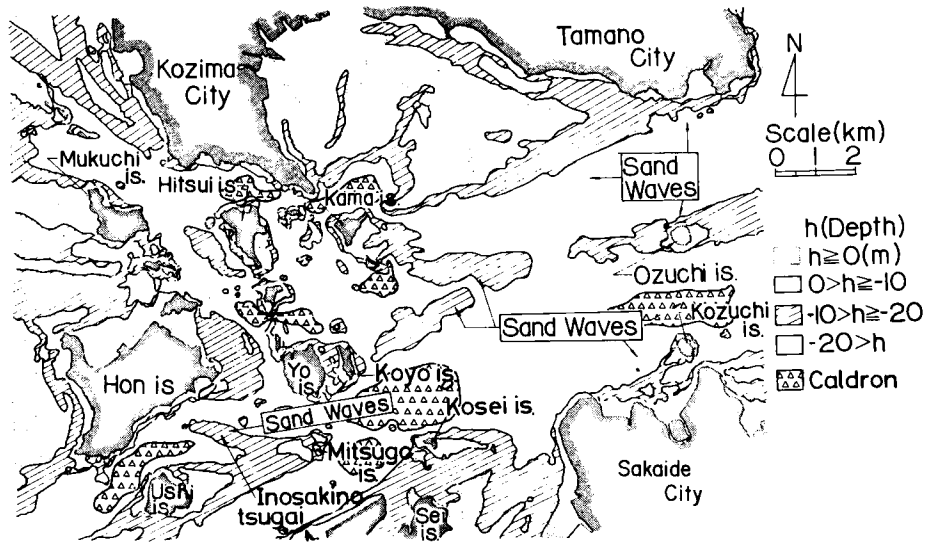

Fig. II -8-3-(b) Submarine topography at West Bisan Strait

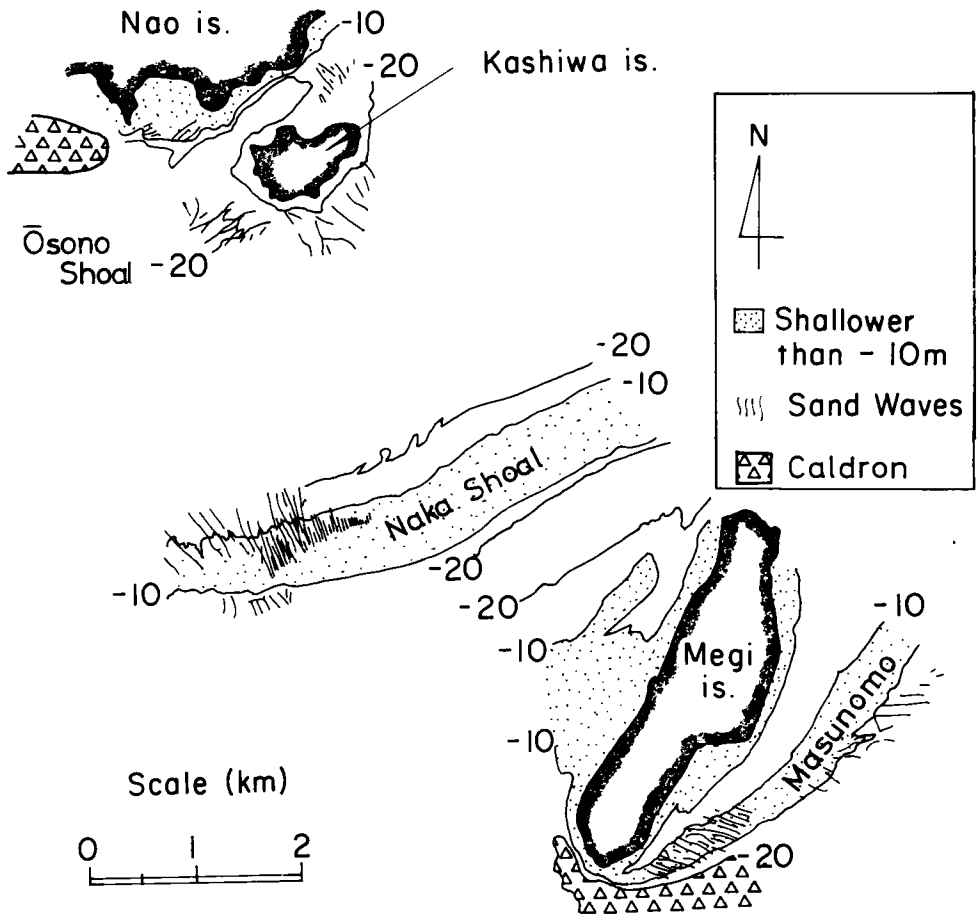

Fig. II -8-4 Submarine topography around Ozuchi Is. and Megi Is.

Anyhow, caldrons — many cobbles are scattered there — seem to mean the existence of strong bottom currents. Mogi and Kato[3] reported that sand waves at the east tip of Osono Shoal (wave length of sand wave λ = 60∼150 m, wave height Δ = 1∼4 m) turn steep slopes to SSE. It is considered that strong currents, which form the caldron, flow aground onto Osono Shoal and sand waves are formed there.

There are sand waves (λ = 20∼130 m, Δ = 0.5∼0.6 m) also on the west of Naka Shoal, and twin caldrons at both east and west sides of the strait between Ogi Is. and Megi Is. (Fig. Ⅱ-8-3-a, east caldron; h_{max} = -55 m, L x B = 2.0 x 0.6 km, west caldron; h_{max} = -55 m, L x B = 0.9 x 0.8 km). Maximum velocity of tidal currents is 4.0 knots at the caldrons between Ogi Is. and Megi Is., and 3.1 knots at the tip of Naka Shoal where many sand waves appear. Likewise, sand waves appear at the places where fast tidal currents flow aground onto the shoal.

A sand bank called Masunomo is formed at the southeastern part of Megi Is. There is a caldron (h_{max} = -40 m, L x B = 1.8 x 0.3 km) at the southern part of Megi Is. from which Masunomo is extended to the northeast. Maximum velocity of tidal currents is 2.4 knots at the center part of Masunomo, and 2.7 knots at the west tip. Most of the sand waves on Masunomo turn steep slopes to the north. When sand waves are formed on an alluvial bed in an experimental channel, the slopes of their downstream sides are steeper than those of their upstream sides. Therefore, the sand waves on Masunomo seem to be formed by mainly eastward ebb current.

8-2-2 Sand waves around Ozuchi Is. and Kozuchi Is. (Fig. Ⅱ-8-5)

At the southern part of Tamano city there is a shoal of gentle slope up to a water depth of -30 m. Water depth is -40∼50 m at the places between the shoal and Ozuchi Is. Velocity of tidal currents is 2.3 knots. There are a lot of sand waves (λ = 10∼150 m, Δ = 0.5∼6.0 m) on the shoal.

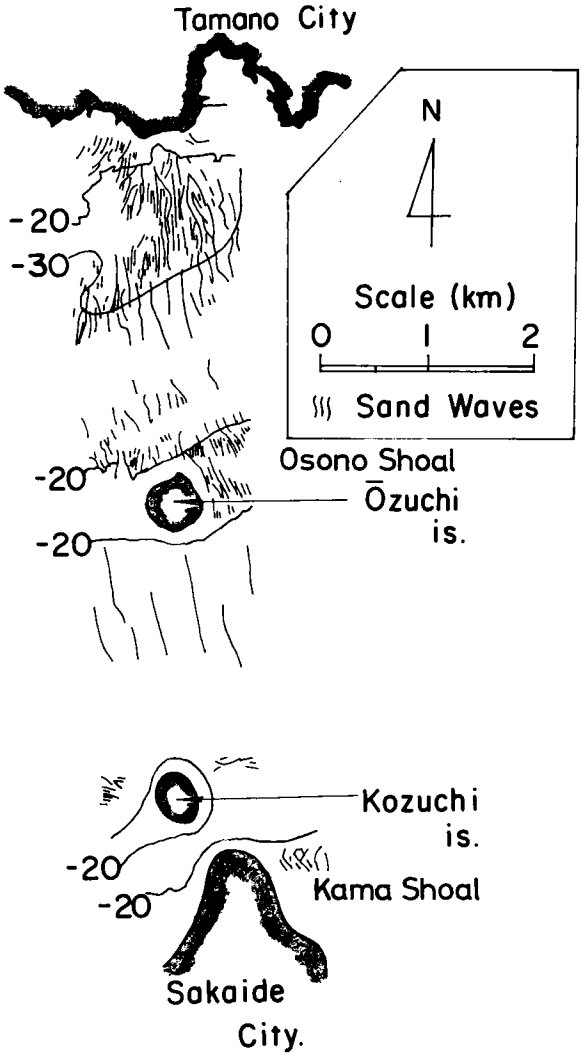

Fig. Ⅱ-8-5 Submarine topography around Ozuchi Is. and Kozuchi Is.

In this region there is not named sand bank. However, if submarine topography is studied in detail, it can be found that there is a shoal and sand waves exist on the shoal.

Northern part of Ozuchi Is. corresponds to west tip of Osono Shoal (Fig. II-8-3-a), and there are sand waves (λ = 10~70 m, Δ = 0.5~4.0 m) on the sand bank. Maximum velocity of tidal currents is 2.0 knots.

Submarine topography is abruptly depressed up to a water depth of -40 m at the southern part of Ozuchi Is., and at the further south place is a comparatively flat place where water depths are -60~70 m. Maximum velocity of tidal currents is 2.2 knots. There are large sand waves (λ = 200 ~ 350 m, Δ = 15~24 m) at a water depth of -40~70 m in this region. Bottom sediments are coarse sand, but clay appears on troughs among sand waves. There is no sand bank or shoal in this area. All sand waves in other areas of the Bisan Strait have relations with sand banks or shoals, but large sand waves in this area without sand bank or shoal are only exception. It seems that Osono, Naka, and Kama Shoals act as if they were side walls of an experimental channel (Fig. II-8-3-a) and macro turbulence which is restrained by both width and depth may occur in this area as seen in channel experiments. Consequently sand waves may be formed corresponding to the phenomenon.

Around Kozuchi Is. sand waves appear on the west tip of Kama Shoal (Fig. II-8-3-a) and on the other shoals. Maximum velocity of tidal currents is 2.5 knots.

8-2-3 Sand waves at the eastern part of Koyo Is. (Fig. II-8-6)

Eastern part of Koyo Is. is a shoal where water depth are -10~20 m, and there are sand waves on the shoal. In this area there are three caldrons; the first exists at the southern part of Murogi Is. (h_{max} = -60 m, L x B = 0.5 x 0.4 km), the second at the southeastern part of Koyo Is.

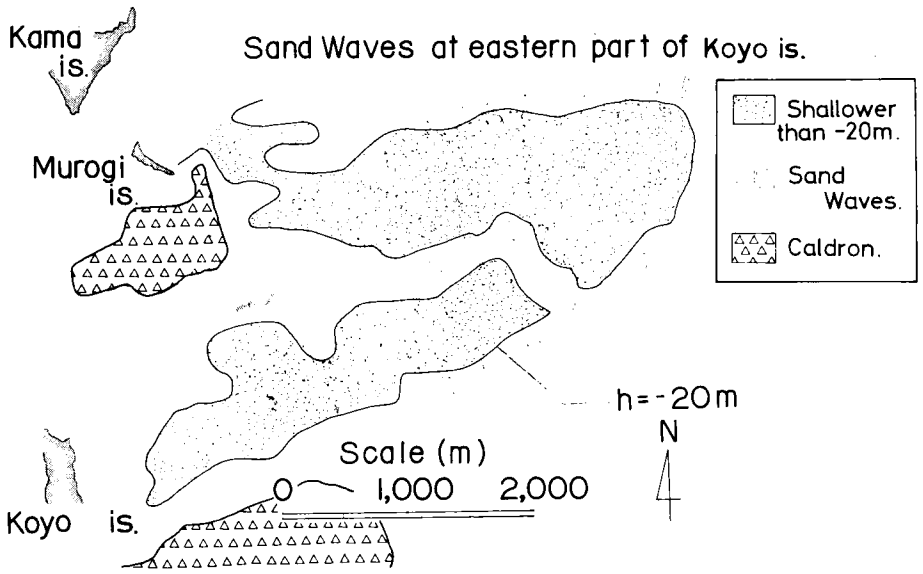

Fig. II -8-6 Submarine topography at the eastern part of Yo Is.

(h_{max} = -96 m, L x B = 2.8 x 0.8 km), and the last at the northern part of Kosei Is. (h_{max} = -90 m, L x B = 1.7 x 0.7 km). The shoal at this area is a saddle part between the caldrons. Maximum velocity of tidal currents is 2.4～2.6 knots.

8-2-4 Sand wave around Kurobana (Fig. Ⅱ-8-7-a and b)

Rare sand wave appears in a line near Kurobana between Hon Is. and Ushi Is. Figs. Ⅱ-8-7-a and b show echo-sounding record and positions of the sand wave's crest respectively. Regarding submarine topography, there are twin caldrons at both east and west sides of the sand wave (Fig. Ⅱ-8-3-b and Ⅱ-8-7-b). At the place where the sand wave appears, sediments consisted of uniform sands with median diameter d_{50} = 1.7 mm and sieve analysis coefficient $S_0=\sqrt{d_{75}/d_{25}}$ = 1.26. There are many cobbles as large as a fist at the places where sand wave does not exist. According to charts of tidal currents, maximum velocity of tidal currents is 2.2 knots.

Formerly the sand wave in this area had been considered as a bedrock. But, the opinion was doubted, because former topography was reformed after dredging of sharp crest. After that, an investigation of sediments and an observation by a diver were practiced, and the projecting topography was proved to be a sand wave. It is supposed that submarine sands gather at a drift pool in this area and a shoal is formed. A sand wave which is as large as the shoal is formed there. How would the topography come out, if the shoal and the whole sand wave were eliminated? It may happen that sands are accumulated at the same place again and similar sand wave is reformed. By the way, apparent upward flow exists in this area. It is colored light brown and can be easily observed through naked eyes as its color differs from one of the surrounding water. The upward flow seems to happen, because the bottom currents are pushed up by the submarine sand wave.

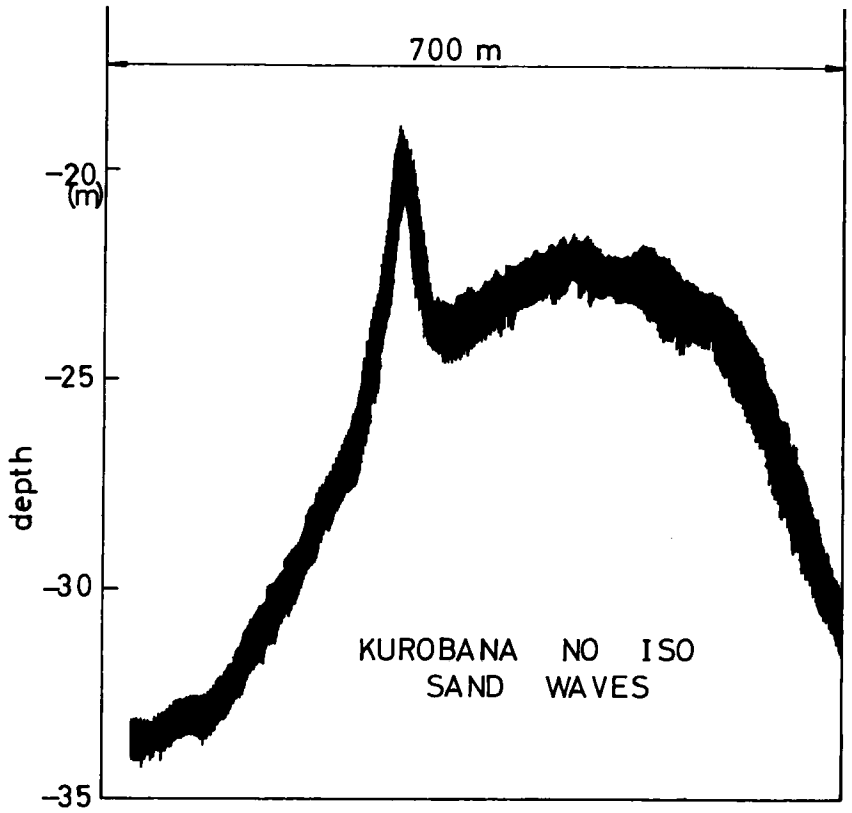

(a)

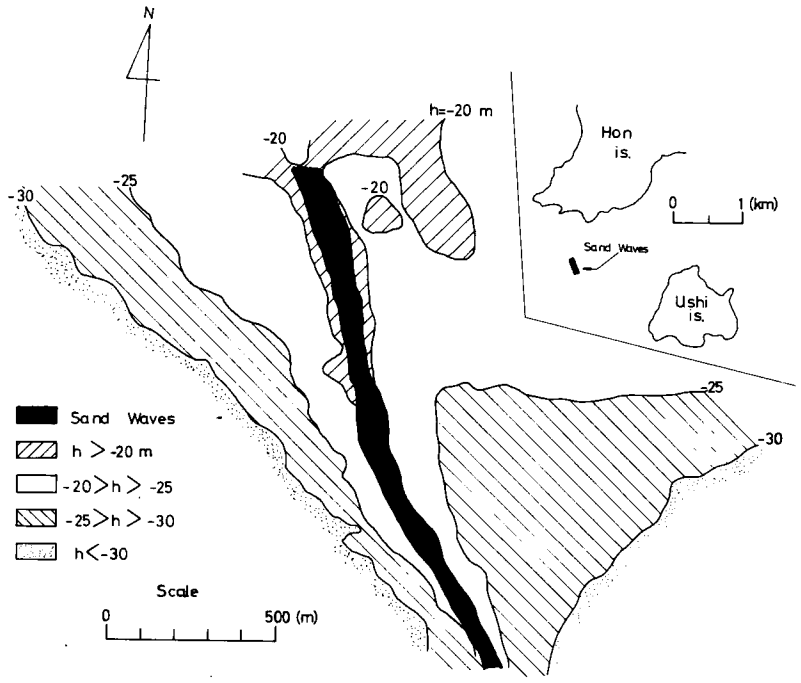

(b)

Fig. II -8-7 Submarine topography around Kurobana

8-3 Field investigation of sand banks and sand waves at Inosakinotsugai

8-3-1 Topographical configurations of sand waves

Figure II-8-8 shows the location of sand waves at Inosakinotsugai. Flood currents flow from east to west and ebb currents flow inversely in this area. According to charts of tidal currents, maximum velocity of tidal currents is 1.9 knots. It is found in Fig. II-8-8 that the crest lines of these parallel sand waves are located perpendicularly to the direction of tidal currents. Sand waves exist in the center of sea way, so it is eagerly demanded to make clear the characteristics and formation mechanism of sand waves in order to make plans of future sea way and maintain them.

Let us consider the submarine topography of this area prior to the consideration of sand waves. Inosakinotsugai is a sand bank which stretches northward from Mitsugo Is. to Hon Is., and its approximate outline is expressed by a submarine contour line of -20 m. There is another unnamed sand bank to the east of Ushi Is. There are twin caldrons between Yo Is. and Mitsugo Is. (scales of the west caldron; h_{max} = -80 m, L x B = 1.7 x 0.8 km). Also, there are twin caldrons between Hon Is. and Ushi Is. (scales of the east caldron; h_{max} = -82 m, L x B = 1.4 x 1.0 km), and the intermediate place between the twin caldrons is Kurobana (Fig. II-8-3-b).

Figs. II-8-9-b ~ h show records of depth surveying along seven lines shown in Fig. II-8-9-a. Line of sounding No. 13 (Fig. II-8-9-b) passes through the central part of Kurobana. Southerly part of the sounding line is at the west end of the caldron located between Hon Is. and Ushi Is. Flat part shown as "Kurobana Sand Wave" is a top of the sand wave described at 8-2-4. Southerly part of line of sounding No. 28 (Fig. II-8-9-c) passes through the deepest part of the caldron between Hon Is. and Ushi Is. and water depth of this deepest part is -85 meters. Southerly part of line of

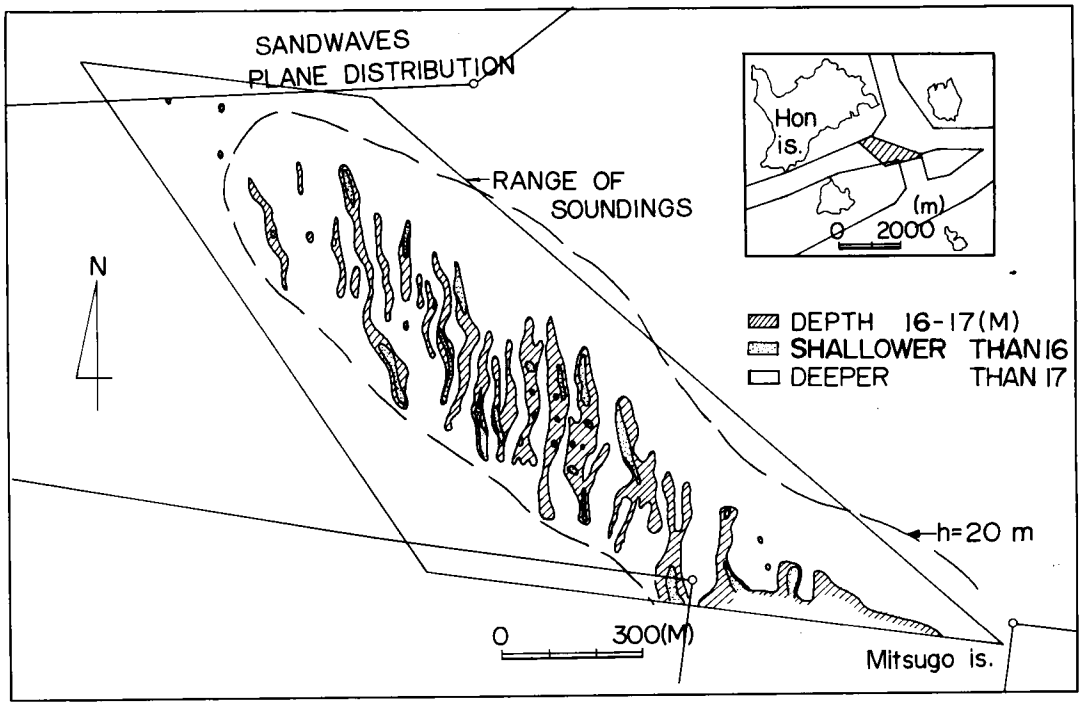

Fig. II -8-8 Plane distribution of submarine sand waves

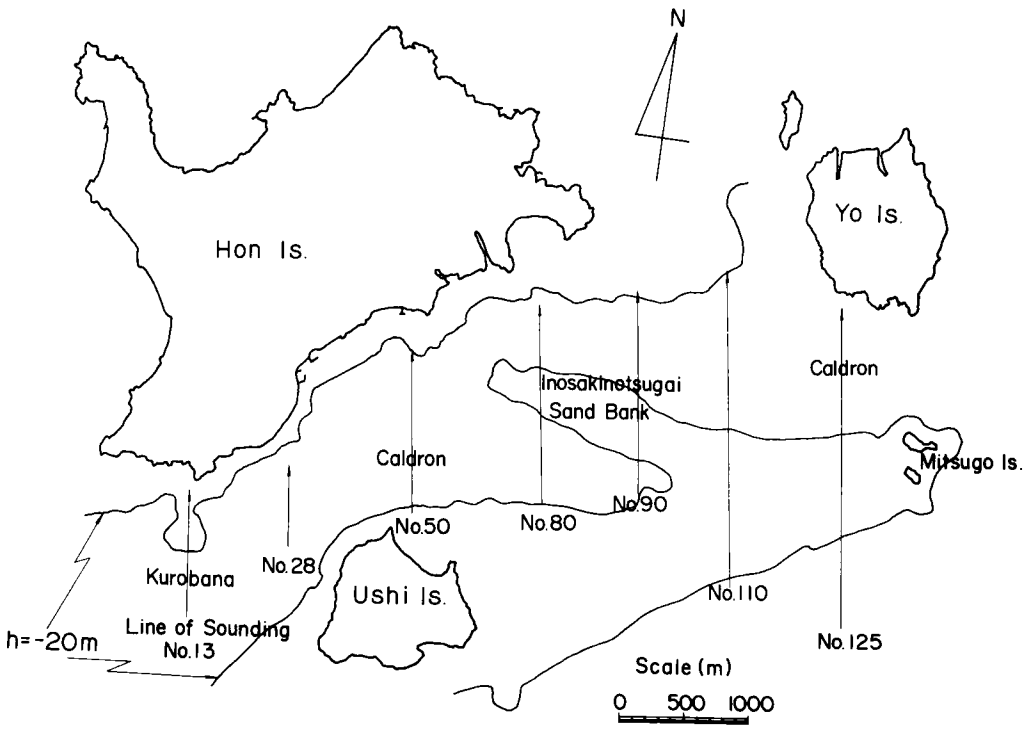

Fig. II -8-9-(a) Depth surveying at Inosakinotsugai area

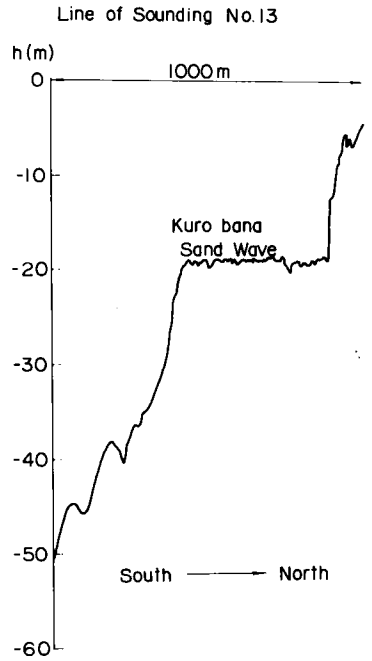

Fig. II -8-9-(b) Depth surveying
(Line No. 13)

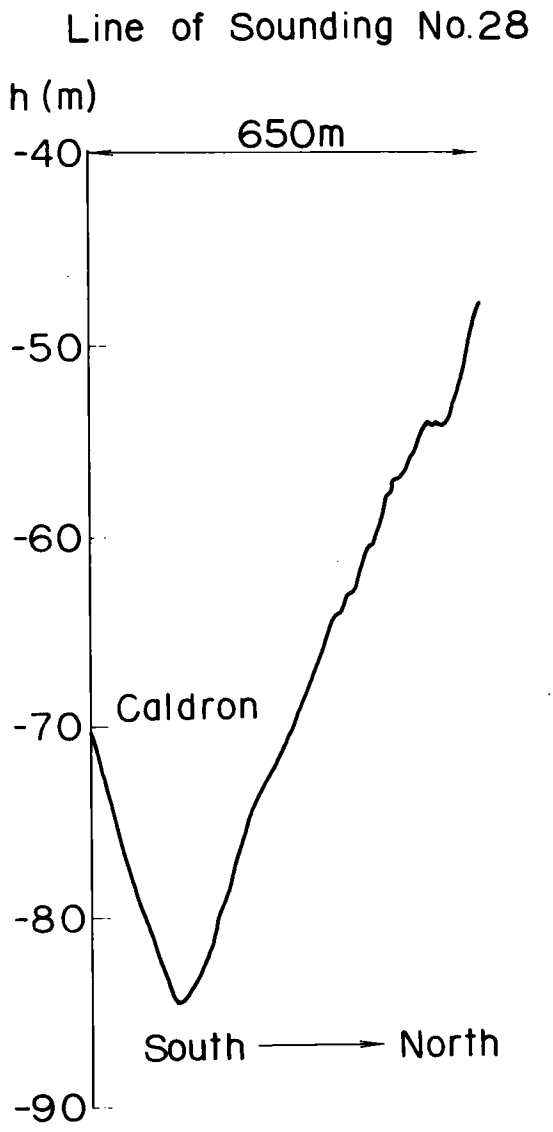

Fig. II -8-9-(c) Depth surveying (Line No. 28)

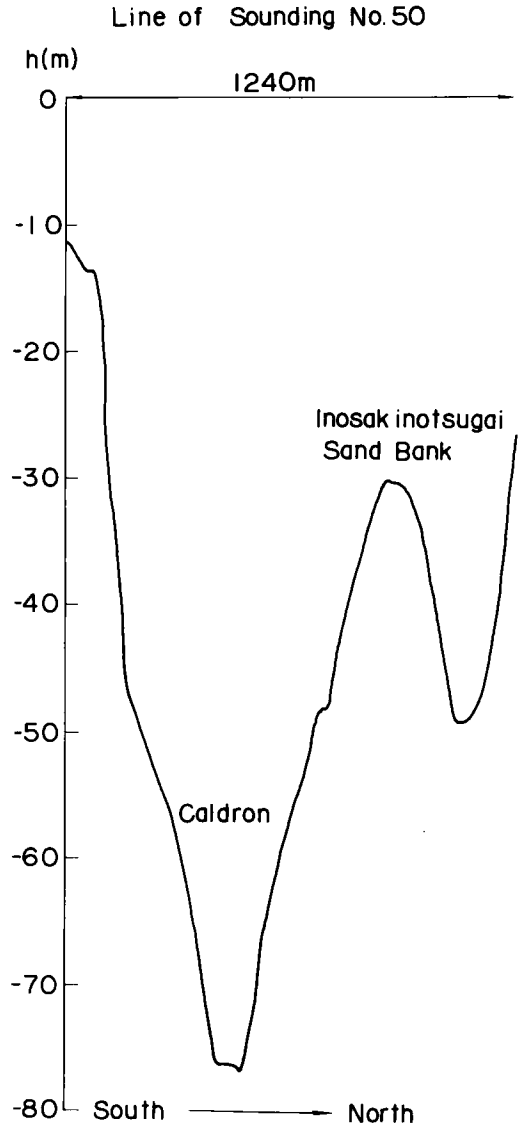

Fig. II -8-9-(d) Detph surveying (Line No. 50)

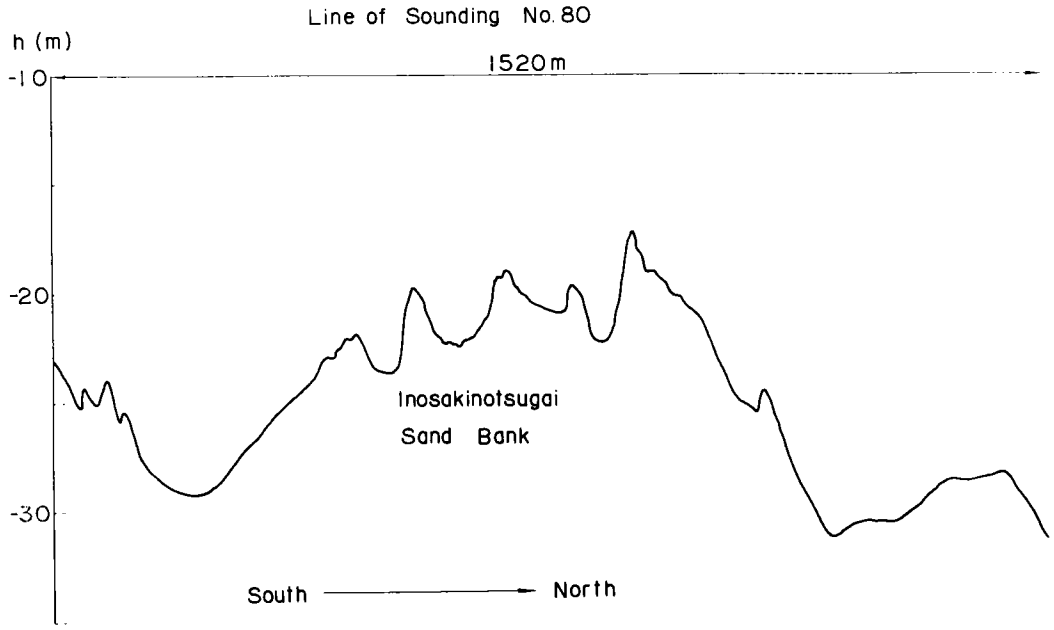

Fig. II -8-9-(e) Depth surveying (Line No. 80)

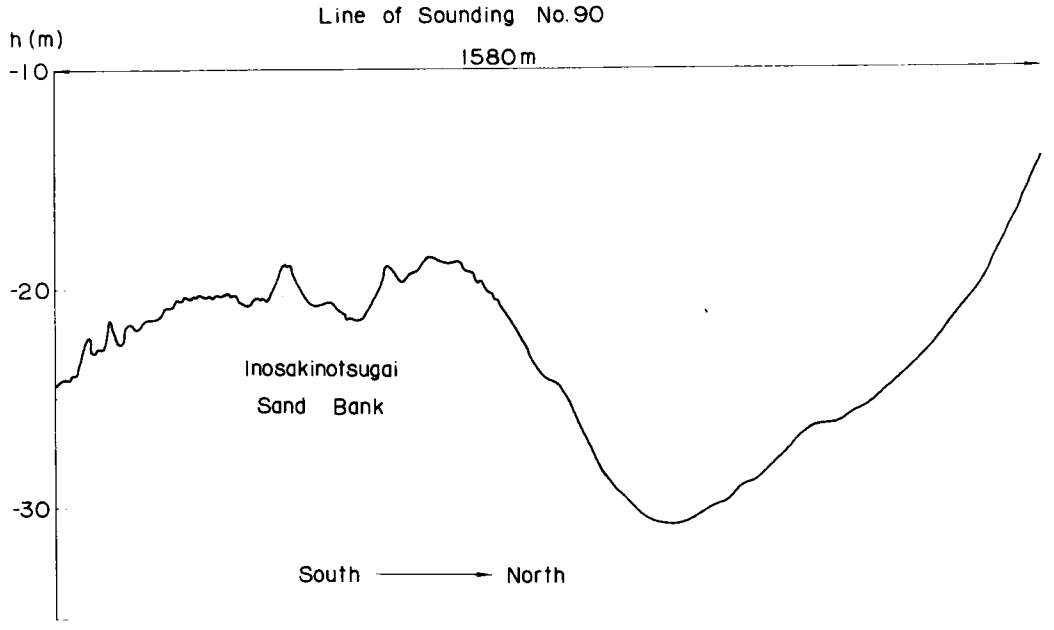

Fig. II -8-9-(f) Depth surveying (Line No. 90)

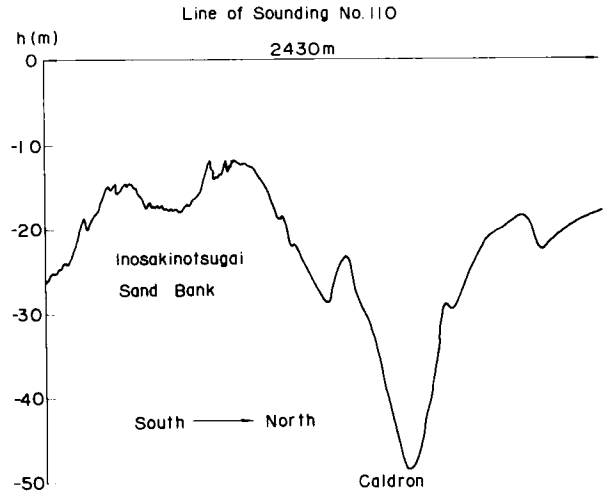

Fig. II -8-9-(g) Depth surveying (Line No. 110)

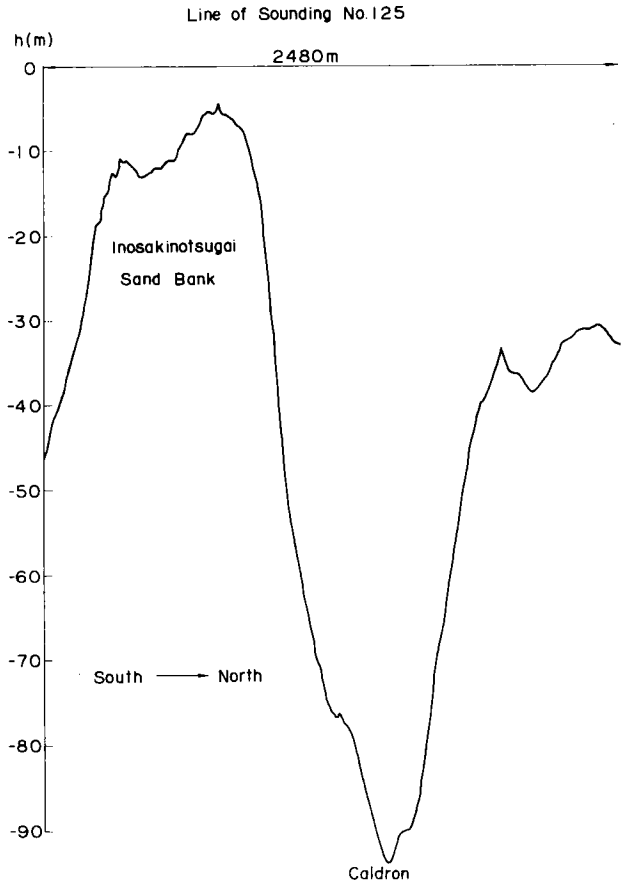

Fig. II -8-9-(h) Depth surveying (Line No. 125)

sounding No. 50 (Fig. Ⅱ-8-9-d) passes through east end of the caldron between Hon Is. and Ushi Is. Northerly part of the line is tip of Inosakinotsugai and the water depth is -30 meters. Central part of line of sounding No. 80 (Fig. Ⅱ-8-9-e) passes through Inosakinotsugai. Undulations on the sand bank are attributed by sand waves. Southerly part of line of sounding No. 90 (Fig. Ⅱ-8-9-f) is between tip of Inosakinotsugai Sand Bank and Mitsugo Is. Line of sounding No. 110 (Fig. Ⅱ-8-9-g) passes through both a sand bank located at the east of Ushi Is. and Inosakinotsugai Sand Bank. Northerly part of the line passes through west tip of the caldron between Yo Is. and Mitsugo Is. Southerly part of line of sounding No. 125 (Fig. Ⅱ-8-9-h) is Inosakinotsugai and northerly part is the deepest area of the caldron (water depth: -95 meters).

Inosakinotsugai is a large sand bank which is formed in the shade of Mitsugo Is. However, water depths around the sand bank are very large, and scale of Mitsugo Is. is much smaller than that of Inosakinotsugai. Why was Inosakinotsugai formed in spite of such circumstances? The author thinks as follows: "Judging from the arrangement of the islands, main part of the westward flood currents perhaps flows toward Kurobana near Hon Is., and main part of the eastward ebb currents flows from Kurobana to Mitsugo Is. through farther southern course. For this supposed mechanism, the specific condition in which submarine sands deposit at Inosakinotsugai happens". Moreover, the author thinks the submarine topography as follows: "Positions of caldrons between Yo Is. and Mitsugo Is. and between Hon Is. and Ushi Is. stand in a line. According to the investigation of Maritime Safety Agency[4], valley lines of these caldrons are connected in a line. Therefore, the valley lines may mean the trace of old rivers. It is inferred that these caldrons and Inosakinotsugai are unreclaimed and reclaimed places respectively". According to Hoshino and Iwabuchi[15], bottom materials at the

inclines of the caldrons between Yo Is. and Mitsugo Is. are deposited as limnetic sediments in a clayey silt, and cobbles are scattered on the rock base and on the inclines of these caldrons. This also means that caldrons are old river valleys which have not been reclaimed and there are strong bottom currents.

8-3-2 Investigation of bottom sediments

Bottom sediments were sampled at 100 points represented by "+" sign in Fig. Ⅱ-8-10. Collection of bottom sediments was practiced with a sand sampler at 200 $\sim$ 400 m meshes in July 1974. Sampling was carried out at any tide level without reference to state of tide, because the author considered that variation of sediment diameters due to difference of sampling time is negligible. Sediment diameters may change depending on locations in a sand wave such as crest, trough, lee, and upstream slope of a sand wave. However, it is difficult to make these locations clear. Sampling mesh is approximately more than ten times of a wave length of a sand wave. In short, the investigation of bottom sediments gives general information only. However, variation of sediments' sizes inside a sand bank and a caldron may be examined.

Total number of collected samples was 100 pieces, and sand was not included in five samples. They were cobbles. Cobble diameter d was defined as $d = \sqrt{a \times b}$ (a: length of the longest side, b: length of shorter side in the two perpendicular sides to the longest side). Sieve analysis tests were carried out for 95 pieces.

Fig. Ⅱ-8-11-(a)$\sim$(c) show distributions of d_{50}, d_{10}, and d_{90} (d_{50}: median diameter, d_{10} and d_{90} are diameters of 10 % and 90 % passing weight percentage.)

The following are considered through Fig. Ⅱ-8-11-a:

1) Sediments at the eastern part of Ushi Is. are fine sand of $d < 0.5$ mm

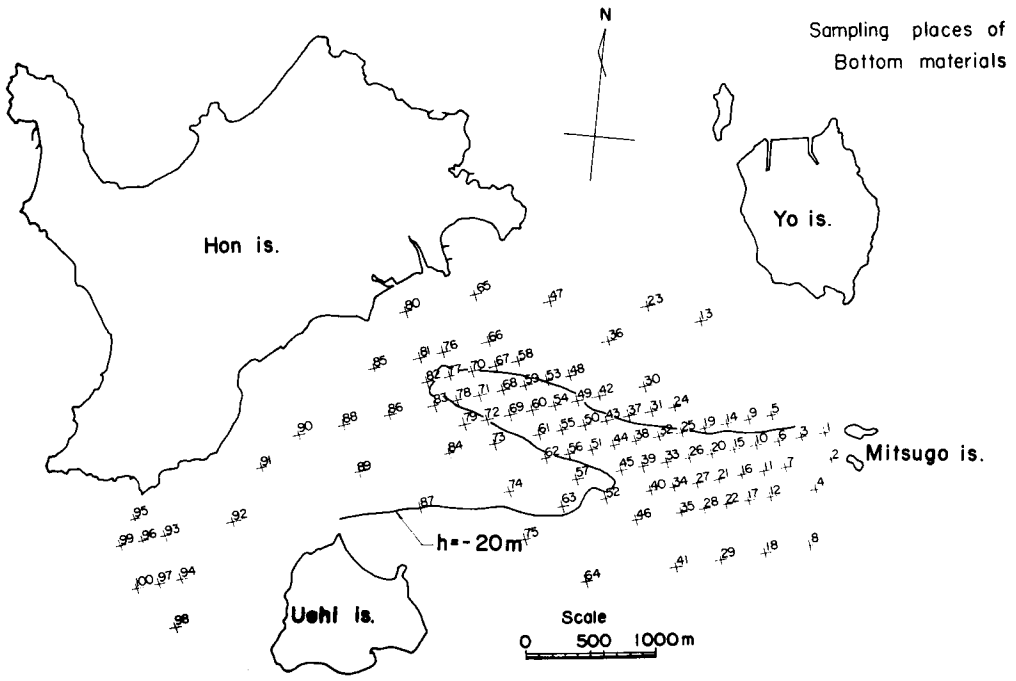

Fig. II -8-10 Sampling places of bottom sediments

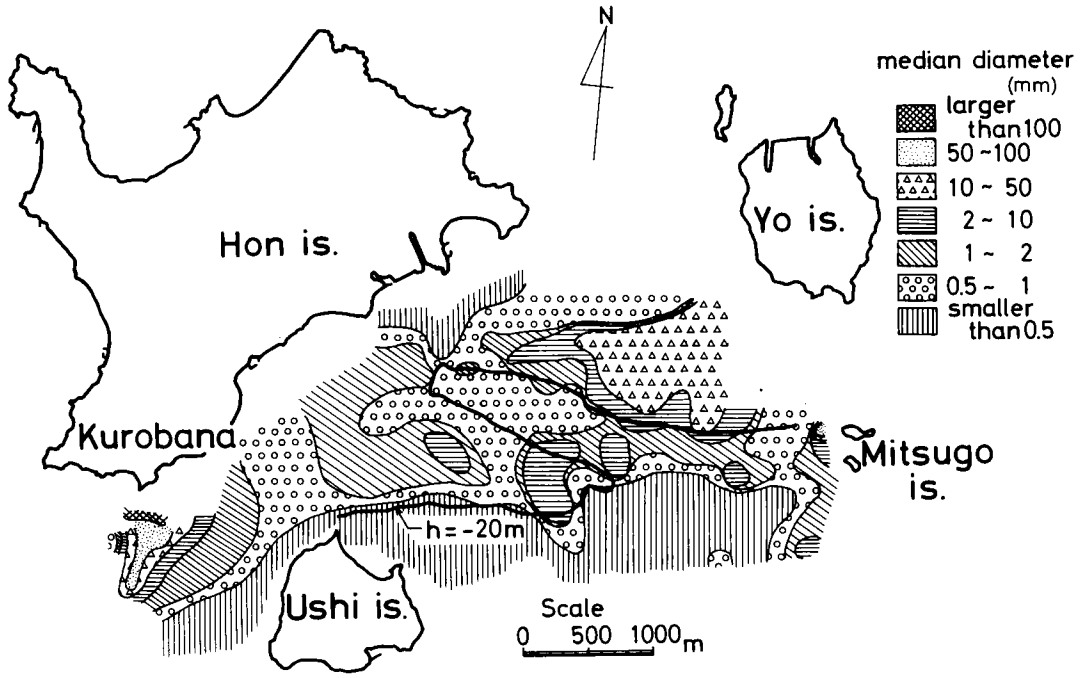

Fig. II -8-11-(a) Plane distribution of median diameter (d_{50}) of bottom sediments

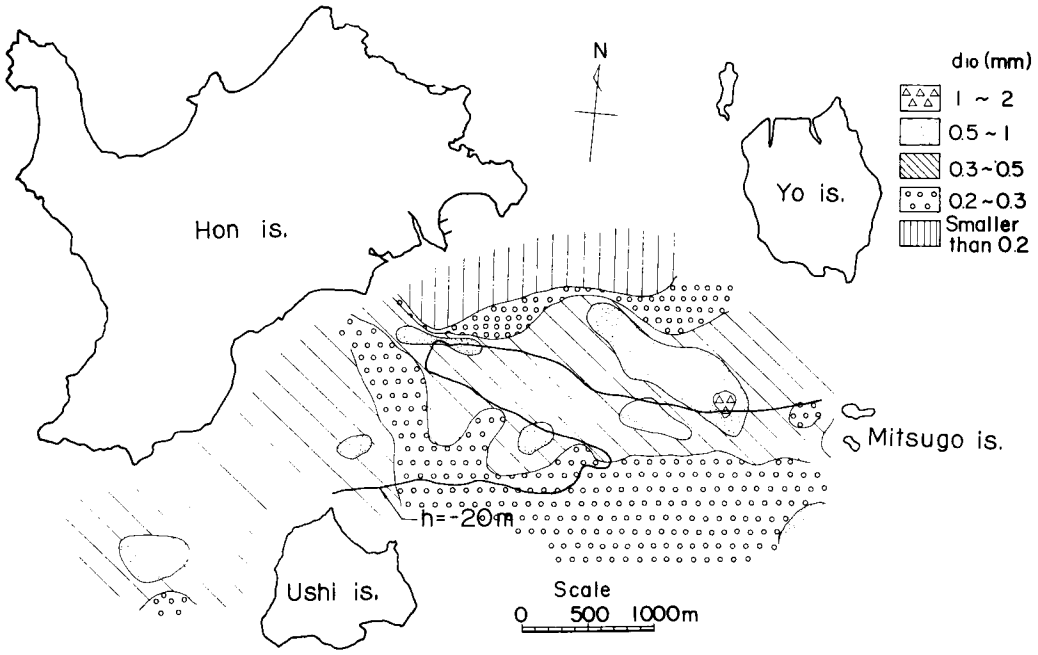

Fig. II -8-11-(b) Plane distribution of d_{10} of bottom sediments

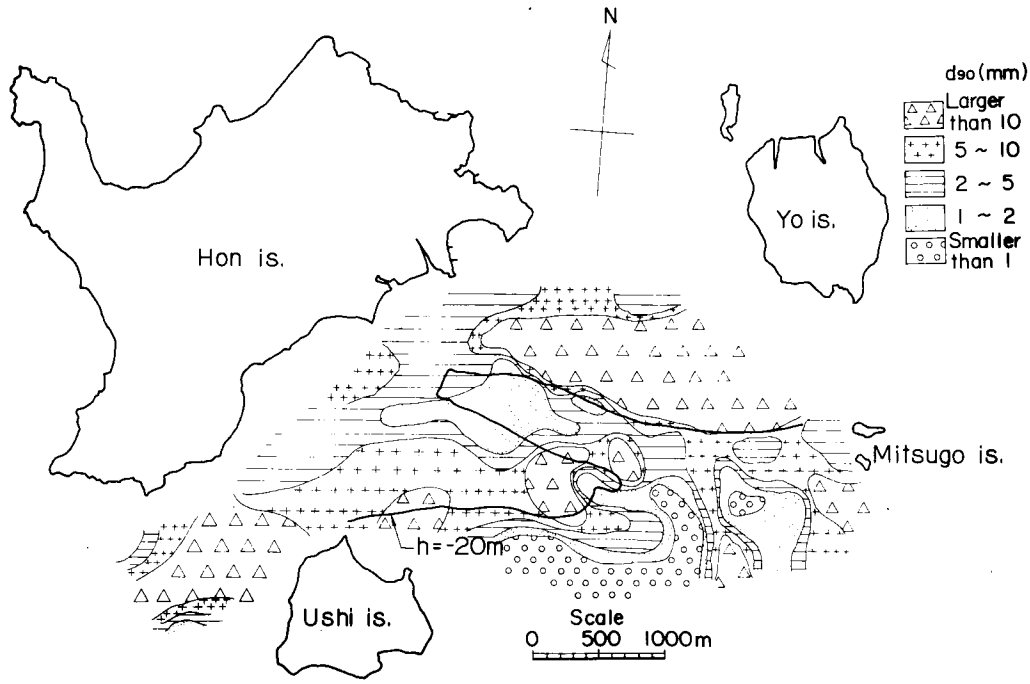

Fig. II -8-11-(c) Plane distribution of d_{90} of bottom sediments

(clay and silt are not almost involved).

2) Diameter of bottom sediments d is 0.5～1 mm at the north tip of Inosakinotsugai, and is 1～10 mm at the intermediate between the north tip of Inosakinotsugai and Mitsugo Is. At the south bottom of Inosakinotsugai (to the west of Mitsugo Is.), d_{50} distributes in a wide range, i.e. between o.5～10 mm. Quartz sampled at Inosakinotsugai is polished and round. This shows sediments are moved vigorously.

3) Sediments in the southern places of east Hon Is. are sand including clay and silt, and the diameter is finer than 0.5 mm.

4) Sediments are large cobbles in the caldrons between Yo Is. and Mitsugo Is. and d_{50} is 2～50 mm. Quartz sampled at this caldron is large and polished poorly. To the east of the caldron between Hon Is. and Ushi Is., d_{50} is 0.5～10 mm, but it becomes coarser rapidly near Kurobana and sampled sediments include stones. However, at the place where a sand wave is existing at Kurobana, d_{50} is 1.7 mm as described at 8-2-4.

Fig. II-8-11-b (plane distribution of d_{10}) shows that

1) To the south of east Hon Is., d_{10} is finer than 0.2 mm, because sediments at this area include silt and clay.

2) To the west of Inosakinotsugai and on the sand bank at the east of Ushi Is., d_{10} is 0.2～0.3 mm. Though sediments are small at these areas, they do not include silt and clay. Sediments existing on the sand bank at the east of Ushi Is. might come from west of Inosakinotsugai, since d_{10} at these areas is almost equivalent.

Fig. II-8-11-c (plane distribution of d_{90}) shows that

1) To the south of Hon Is., d_{90} is 2～5 mm, because sediments at this area contain some cobbles and have wide range distribution of sediment sizes.

2) On the sand bank at the east of Ushi Is., d_{90} is finer than 1 mm.

Sediments are composed of fine sands and coarse sands. They do not include cobbles.

Fig. Ⅱ-8-12-a∼c show percentages of fine sand ($d < 0.25$ mm), coarse sand (0.25 mm$< d <$2 mm), and cobble ($d >$ 2 mm) respectively.

According to Fig. Ⅱ-8-12-a, sediments at the south of east Hon Is. show percentage of larger than 10 %, because they include some silt and clay. However, percentages are less than 10 % at other areas.

Fig. Ⅱ-8-12-b shows that percentage of coarse sand is larger than 60 % at most areas. It is less than 60 % at the south of east Hon Is. (silty sand area) and at the caldron between Yo Is. and Mitsugo Is. (cobble area).

Fig. Ⅱ-8-12-c shows that percentage of cobble is larger than 60 % at the caldron between Yo Is. and Mitsugo Is. and at the east of Kurobana sand wave.

Fig. Ⅱ-8-13 shows plane distribution of sieve analysis coefficient S_0 ($S_0 = \sqrt{d_{75} / d_{25}}$). The followings are considered through this figure:

1) S_0 is between 1 and 2 on the sand bank at the east of Ushi Is., at the north tip of Inosakinotsugai, and at the caldron between Yo Is. and Mitsugo Is. Except at the caldron, S_0 is small, because sorted fine particles have been transported to the above areas.
2) At the south bottom of Inosakinotsugai (to the west of Mitsugo Is.), S_0 is larger than 2. Sediments at this area have a wide distribution of sediment size and some of them might be transported to the tip of Inosakinotsugai and the sand bank at the east of Ushi Is.
3) S_0 is larger than 2 at the south of east Hon Is., because sediments at this area have wide distribution of sediment size, including cobble as well as silt and clay.

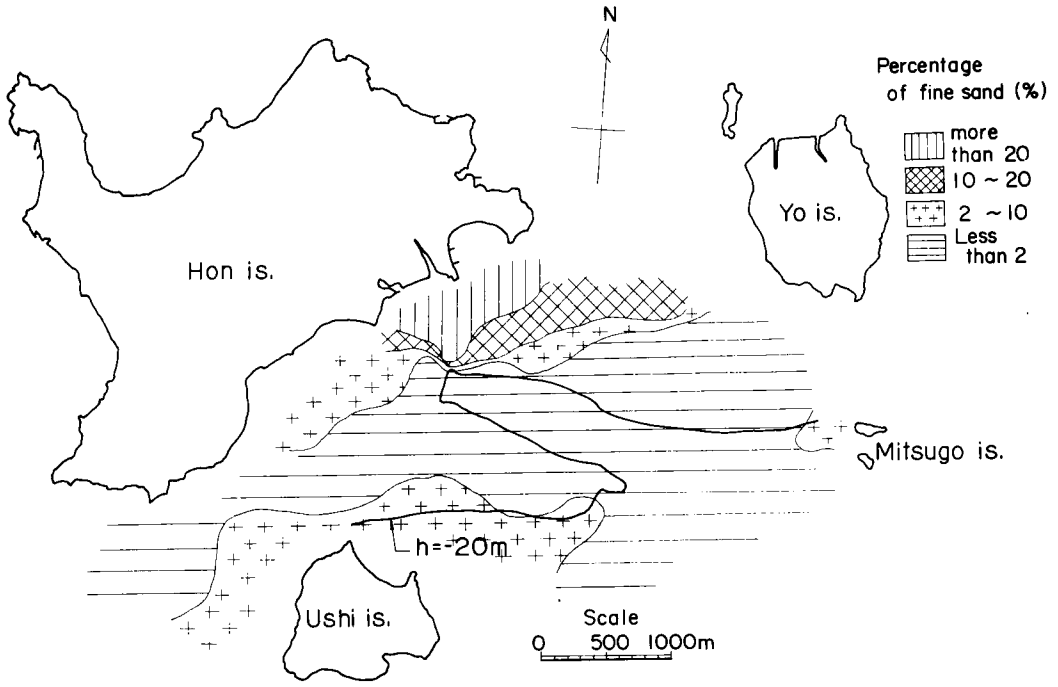

Fig. II -8-12-(a) Plane distribution of percentage of fine sand

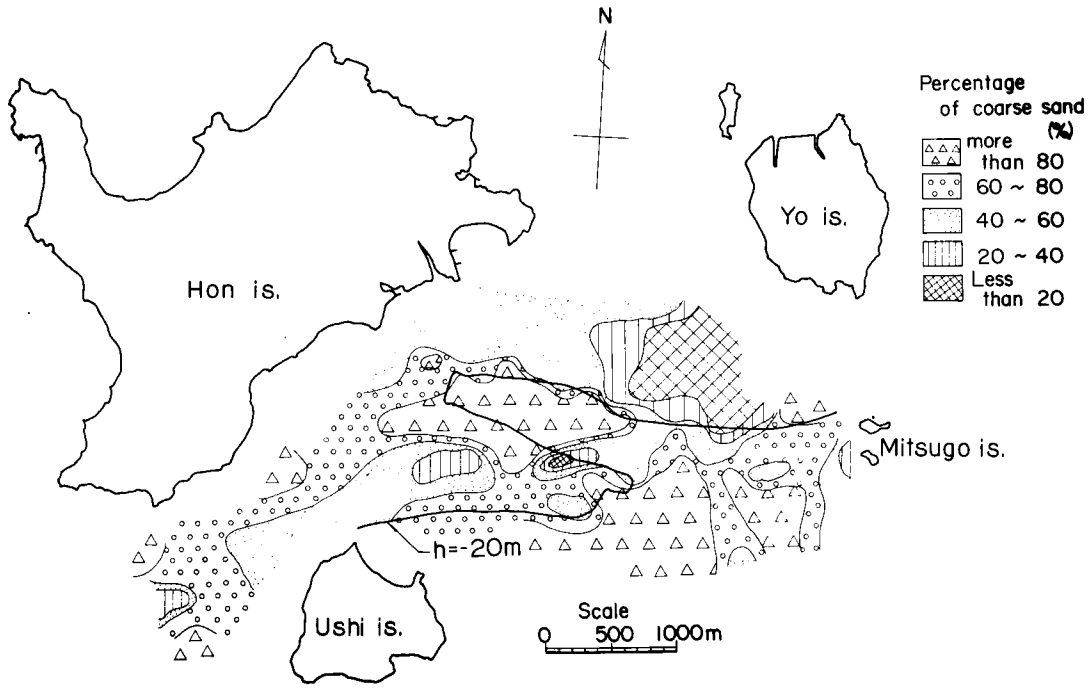

Fig. II -8-12-(b) Plane distribution of percentage of coarse sand

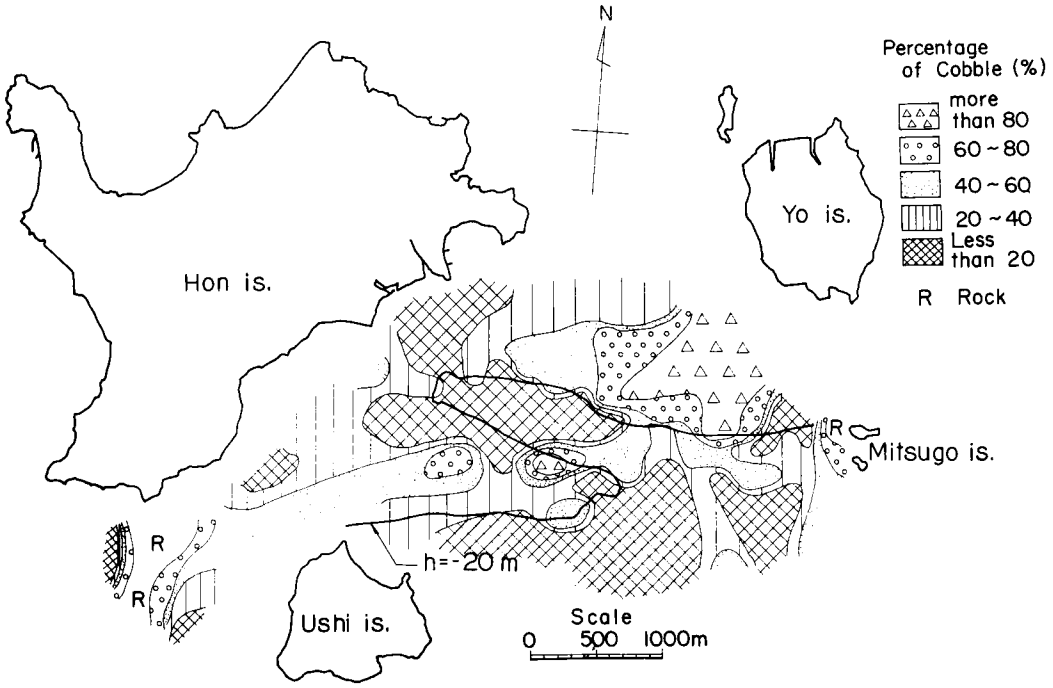

Fig. II -8-12-(c) Plane distribution of percentage of cobble

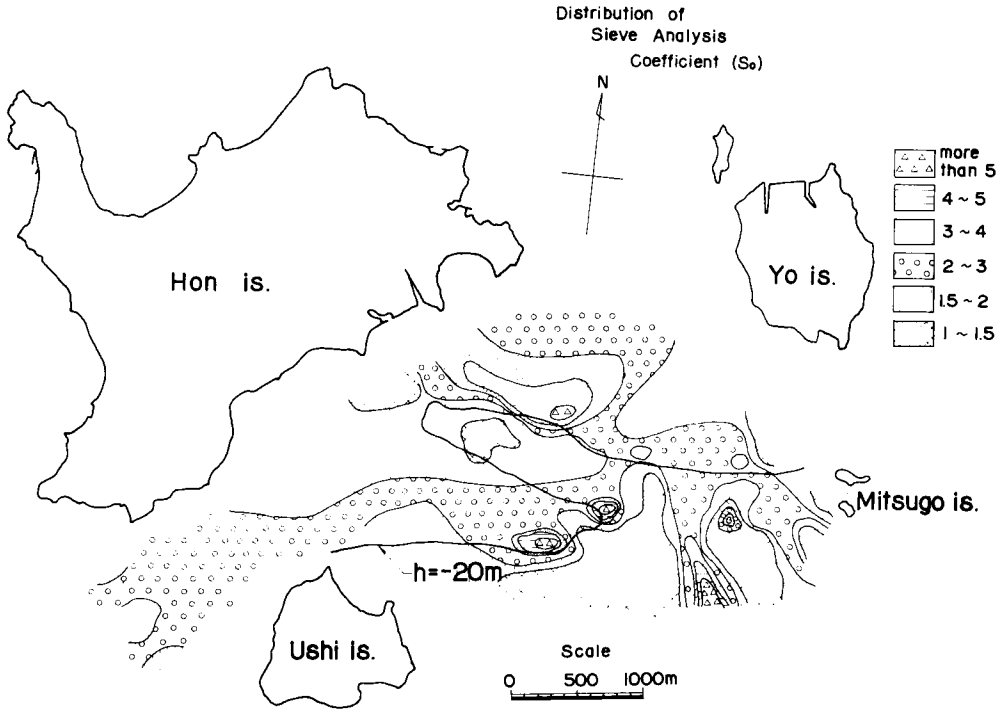

Fig. II -8-13 Plane distribution of sieve analysis coefficient

Let us examine typical grain size distribution curves. Fig. Ⅱ-8-14 shows grain size distribution curves at the sediment sampling points 2, 30, 33, 41, 51, 62, 65 and 77 of Fig. Ⅱ-8-10. No.2 point is at the south bottom of Inosakinotsugai (to the west of Mitsugo Is.). No. 30 point is at the caldron between Yo Is. and Mitsugo Is. No. 33 point is at the meeting place of Inosakinotsugai and the sand bank at the east of Ushi Is. No. 41 is on the sand bank at the east of Ushi Is. No. 51 is at the intermediate between the north tip of Inosakinotsugai and Mitsugo Is. No. 62 is near the center of Inosakinotsugai and at the point where the eastward ebb current flows aground onto Inosakinotsugai. No. 65 is at the south of east Hon Is. where sediments are muddy sand. No. 77 is at the north tip of Inosakinotsugai.

Fig. Ⅱ-8-14 shows that

1) Sediment at No.2 distributes between 0.2～20 mm and d_{50} is approximately in the middle among d_{50} of eight pieces shown at Fig. Ⅱ-8-14.
2) Sediment size distribution curve at No. 51 is almost similar to that at No. 2.
3) Sediments at Nos. 30 and 62 have high portions of large particles.
4) Sediments at Nos. 33, 41, and 77 have many fine particles. Especially, sediment at No. 41 is the finest and dispersed only narrowly.
5) d_{50} of sediment at No. 65 is small and almost same as that at No. 41. This sediment includes 30 % of fine particles smaller than 0.2 mm as well as 30 % of particles larger than 1 mm. The component of fine particles smaller than 0.2 mm might have different origin to other sediments.

Fig. Ⅱ-8-15 shows a geological condition of this area. There are three types of soils. Alluvial soil is composed of sand, cobble, and clay.

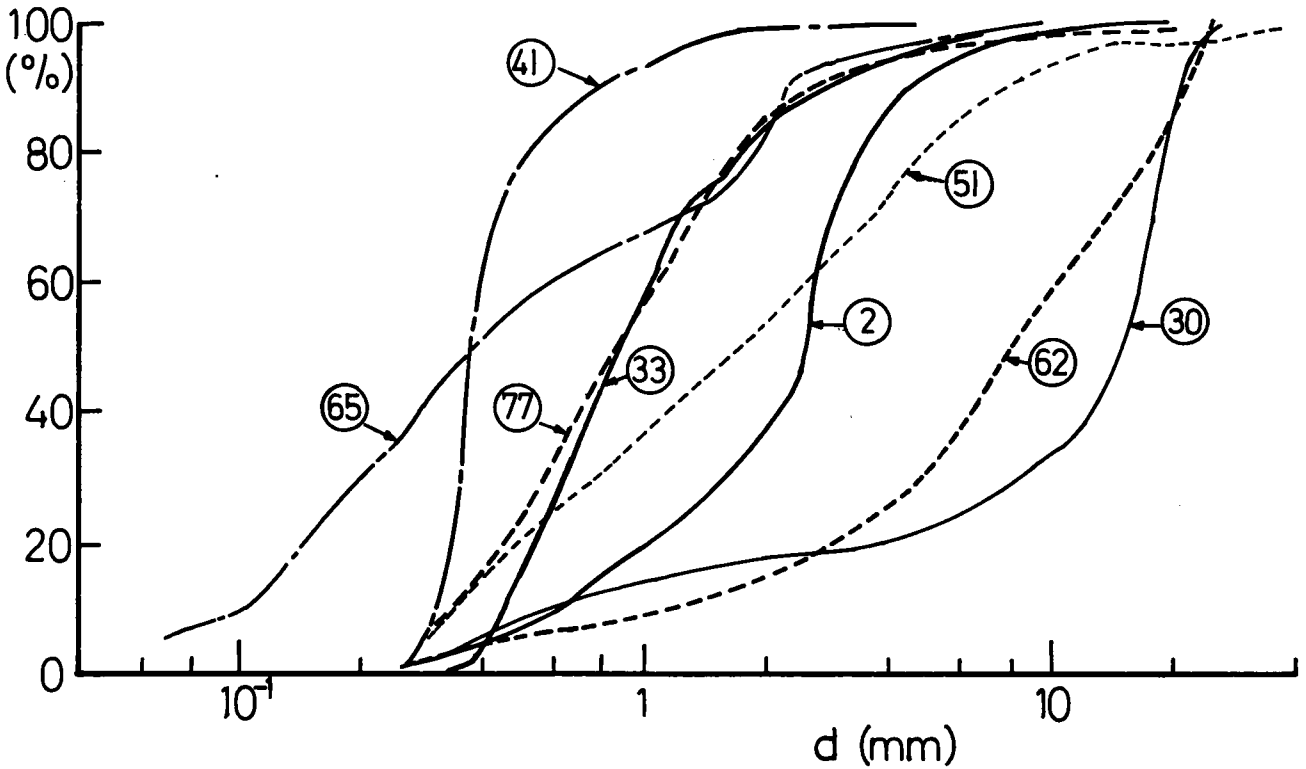

Fig. II -8-14 Typical grain size distribution curves

South - east part of Hon Is. is covered with this alluvial soil. Clay at this area might be washed into the south sea area of east Hon Is. and deposited there.

Fig. Ⅱ-8-16 shows routes of sediment movement which have been assessed using the above - mentioned sedimentation data. Sediments around Mitsugo Is. have a wide range of sediment sizes being composed of fine sand, coarse sand, and cobble. They are carried by a zigzag course to the north tip of Inosakinotsugai. This movement is caused by the tidal currents mechanism that main part of the westward flood currents flows near Hon Is. and main part of the eastward ebb currents flows through father southern course. Sediments which have been transported to the meeting place of Inosakinotsugai and the sand bank at the east of Ushi Is. are sorted by the fast tidal currents. Cobbles will be unmoved or moved only a little bit to the west. Fine and coarse sands are carried to the north tip of Inosakinotsugai. The sand bank at the east of Ushi Is. has possibly been made by fine sands which come from both the north tip of Inosakinotsugai and the vicinity of Mitsugo Is. Some of fine sands which have been deposited on the sand bank at the east of Hon Is. will be transported to the Mitsugo Is. by the ebb current. Sediments which have been drained from Hon Is. have accumulated at the calm place, south of east Hon Is.

Klein[10] indicated after his investigation about Minas Basin at Fundy Bay, Canada that there are both a flood channel (flood current is predominant) and an ebb channel (ebb current is predominant). Smith[16] found the same phenomenon on Middle Ground Sand Bank at Vineyard Sound, U.S.A. This was also proved by the tidal currents observation in Inosakinotsugai described later. It may conclusively be said that this phenomenon of tidal currents is common on sand banks formed behind islands. It is not easy

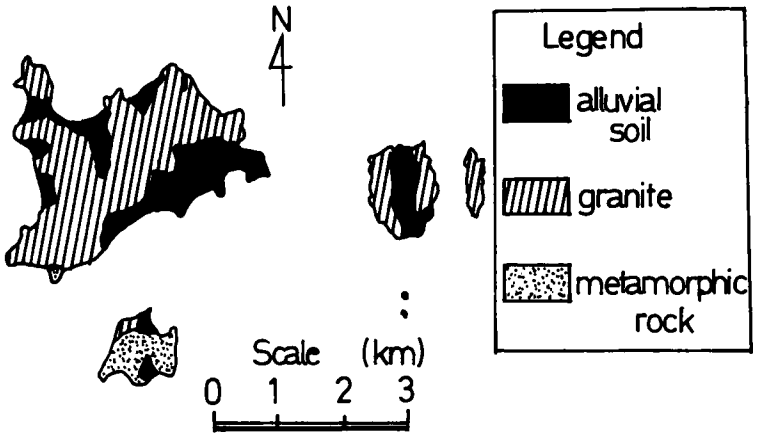

Fig. II -8-15 Geological condition

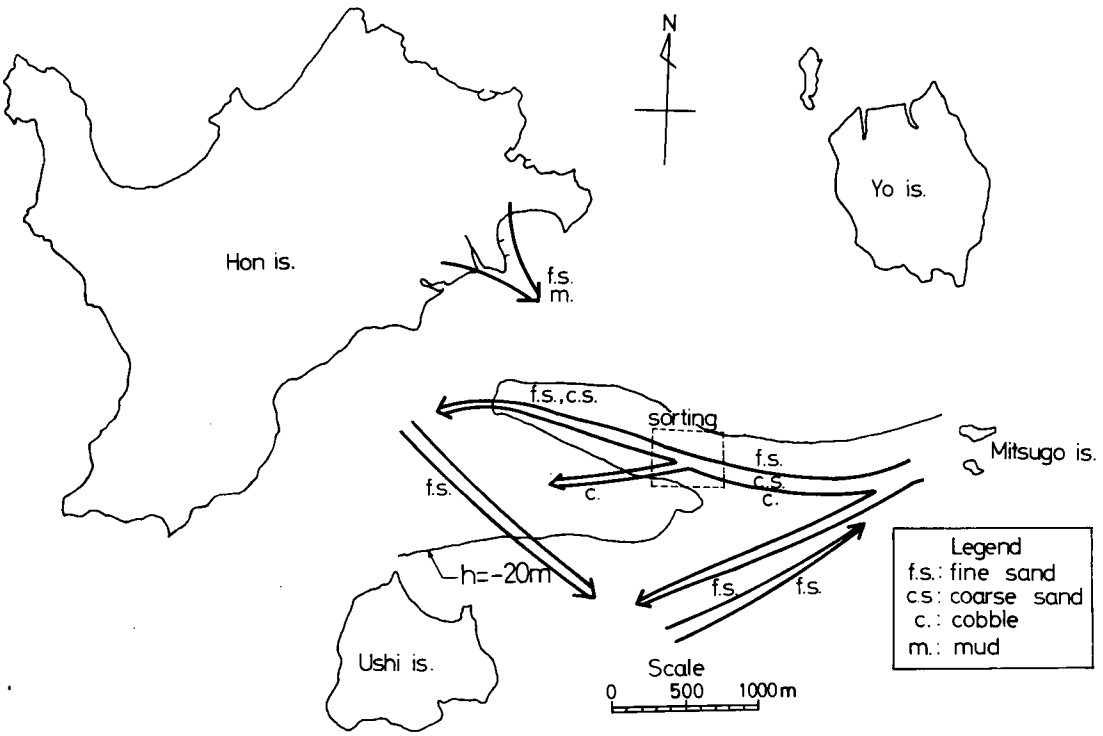

Fig. II -8-16 Routes of sediment movement

to determine whether this pattern of tidal currents is made by a sand bank or tidal currents have formed a sand bank. The author considers that flood and ebb channels are made due to the influence of topographies such as a caldron and an island, then sand banks are formed.

8-3-3 Shapes of sand waves

Let us consider shapes of the sand waves. Periodical soundings on the fixed lines were conducted twelve times during June 1968∼May 1971. Fig. II-8-17 shows these sounding lines and places where tidal currents were observed using a current meter at the bottom layer. Soundings in October 1969 and in May 1971 are shown in Figs. II-8-18-a and b. There are not sand waves on the No. 7 sounding line where bottom sediments are coarse sand (d_{50} is 1∼10 mm) and bottom current velocity is fast. This might mean that sand waves are not formed under such a hydraulic environment as seen on the No. 7 sounding line. When both figures (Figs.II-8-18-a and b) are compared, they show similar pattern of sand waves except small differences. The differences are caused by the difficulties of sounding on the exactly same line. Therefore, it is understood that the shapes of sand waves are comparatively stationary after they have been formed once. Moreover, the followings can be observed through the same figures:

1) Sand waves are formed on Inosakinotsugai sand bank whose scale is about 600 m wide at the south bottom of the bank, and about 400 m wide at its north tip.
2) Large asymmetrical sand waves are formed on the slopes of the sand bank, and comparatively small symmetrical sand waves are formed on its crest. In an experimental channel it is easily observed that dunes and ripples are apt to appear on the midst and top of a slope due to unidirectional flow. Scales of sand waves are also large

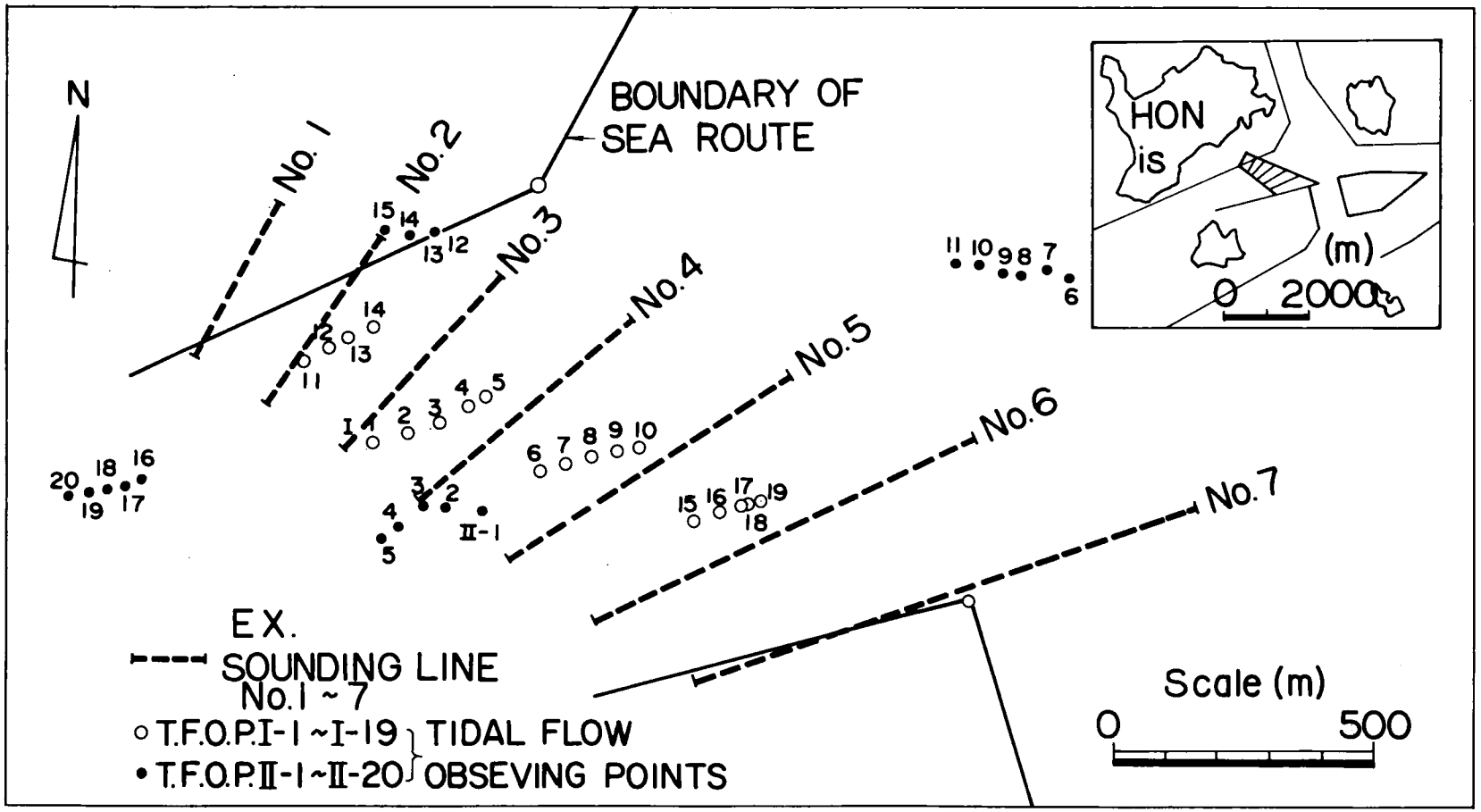

Fig. II -8-17 Locations of soundings and tidal currents observation

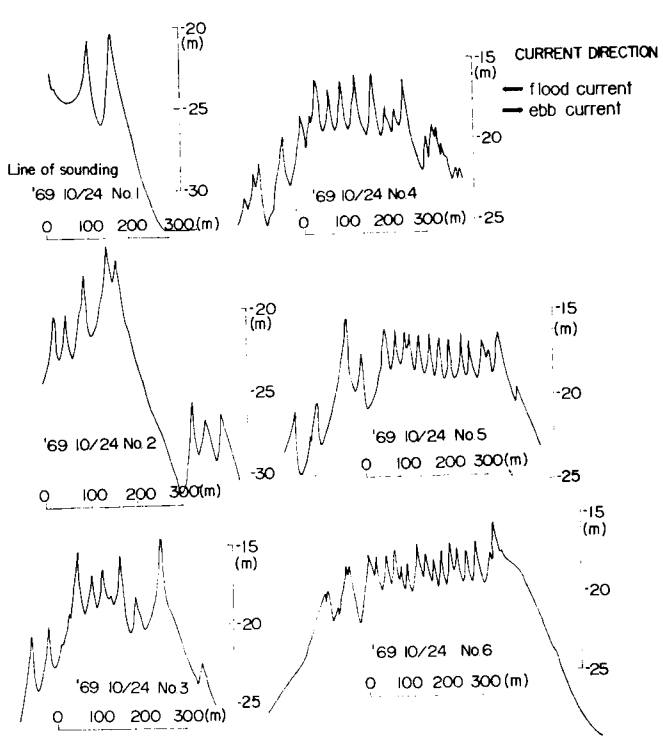

(a)

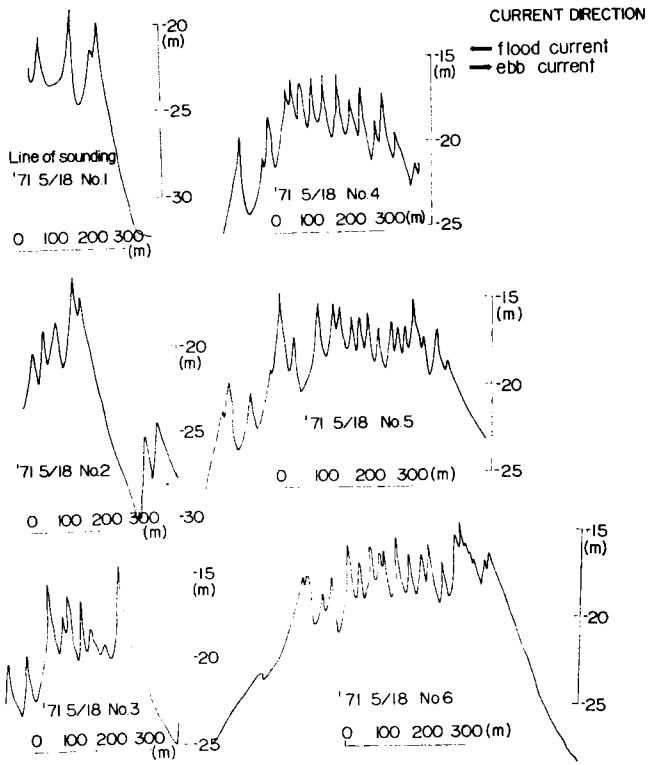

(b)

Fig. II -8-18 Soundings on the fixed lines

on the slope in this case.

According to a diver's observation, it is reported that there are a lot of ripples— wave length is 50～100 cm, wave height is several cm — at the bottom of Inosakinotsugai. Like this, sand waves exist on a sand bank and ripples exist on sand waves. It is very interesting that such a state apparently exists in submarine topography. By the way, topography on the alluvial bed due to unidirectional flow is classified as flat bed, alternating bars, dunes, and ripples in the field of alluvial hydraulics[17]. According to this classification, topography seems to have several stages. Scales of alternating bars are determined by channel widths, scales of dunes are determined by water depths, and scales of ripples are influenced by diameters of sediments. Having never been pointed out formerly, it is guessed that dunes and ripples are apt to be formed at the places where currents flow aground onto alternating bars (the primary topography). According to Yalin[18], wave length λ of ripples formed on alluvial bed due to unidirectional flow is calculated as $\lambda = 1{,}000\,d$ (d is a diameter of sediments). If the diameter of the sediments d in this area is supposed to be d = 0.70 mm according to the results of the investigations, wave length of ripples λ = 70 cm, and this value well agrees with the result of the observations.

By the way, Raudkivi[14] has pointed out that sand wave — water depths of formation places of sand waves are 51～183 m, wave length λ is 900 m wave height Δ is 18 m — are $\Delta/h = 1/5 \sim 1/10$, so they belong to ripples according to the classification in alluvial hydraulics. However, the author thinks that scales of ripples are essentially determined by diameters of bottom sediments and are usually smaller than 1 m, so Raudkivi's comment is suspicious.

Data of water depths h, wave lengths of sand waves λ, and wave heights Δ on each sounding line of Nos. 1$\sim$7 were got by the sounding. An example of those mean and standard deviations are shown in Table II-8-1. Only records, the shapes of which were judged as sand waves with the eye, were adopted, when data of λ and Δ were got. Undulations, the wave lengths of which were several hundred meters, were judged as sand banks, and undulations, the wave lengths of which were 1$\sim$2 m, were judged as small disturbances. So, their undulations were not adopted as the objects on which λ and Δ were got. As Fig. II-8-8 and Fig. II-8-17 are compared, it is noticed that sounding lines and crest lines of sand waves cross obliquely. Therefore, wave lengths λ which were calculated from original sounding papers were larger than actual wave lengths. The measured wave length was corrected to the perpendicular distance between the wave crest lines. The corrected values are shown in Table II-8-1. Decreasing of h, λ, and Δ from No. 1 to No. 7 is appreciated. Moreover, shoaling of sea way was worried on the beginning of sea way capital dredging at Inosakinotsugai, but it was affirmed that both mean and standard deviations of h, λ, and Δ were almost constant during sounding time (June 1968$\sim$May 1971) and notable shoaling has not occurred. According to this fact, the conditions of sediment transportation at Inosakinotsugai are under equilibrium at the time scales of 2$\sim$3 years. (As being mentioned in the latter part of this report, it is judged that sediment transportation at Inosakinotsugai is considerably active. Therefore, the condition of sediment transportaion is under dynamic equilibrium.)

The relation of mean water depth h vs. mean wave length λ, and h vs. mean wave height Δ — each mean value is averaged on each sounding line — are shown in Figs. II-8-19-a and b. According to these figures, it is concluded that the relations of λ = 1.1$\sim$2.6 h and Δ = 0.06$\sim$0.18 h hold.

Table Ⅱ-8-1 An example of water depth, wave length, and wave height

(Unit: m)

Sounding Line	Mean water depth $\bar{h}$	Standard deviation of water depth σ_h	Mean wave length of sand waves $\bar{\lambda}$	Standard deviation of wave length σ_λ	Mean wave height of sand waves $\bar{\Delta}$	Standard deviation of wave height σ_Δ
No.1	24.9	3.7	84.0	6.0	3.8	0.7
2	23.0	3.7	52.3	51.3	3.4	1.4
3	19.8	2.2	35.7	14.7	2.7	2.0
4	19.7	2.1	32.4	9.3	2.6	1.0
5	19.0	2.2	31.6	16.9	2.6	1.7
6	19.8	3.1	32.0	10.7	2.6	1.3
7	19.0	2.4	—	—	—	—

Date of sounding: May 1971

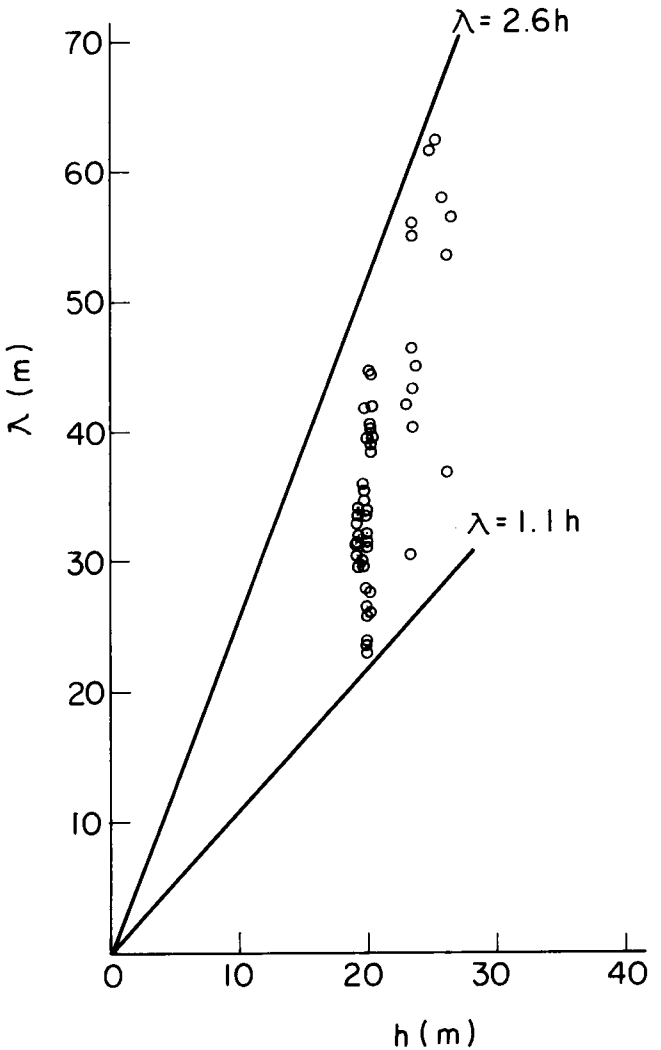

Fig. II -8-19-(a) Water depth vs. wave length

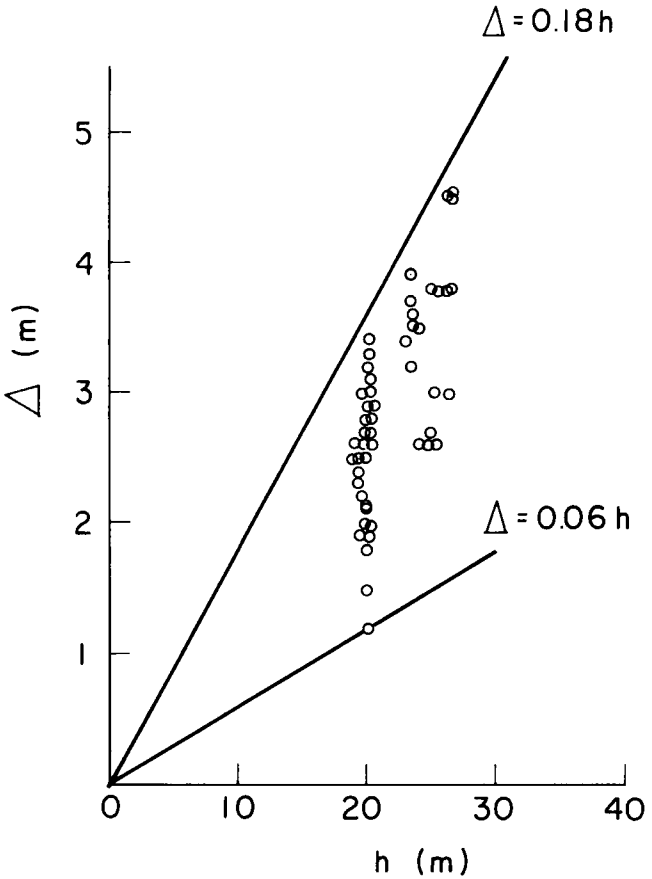

Fig. II -8-19-(b) Water depth vs. wave height

Due to the similar analysis of the data which Honza and Nasu[2] got at the east part of the Bisan Strait, it is concluded that the relation of λ = 1.4 $\sim$4.4 h holds. Moreover, wave steepness Δ/λ of sand waves at Inosakinotsugai is 0.075 and nearly constant.

8-3-4 Brief calculations concerning alluvial hydraulics at Inosakinotsugai

In order to study characteristics of submarine sand waves, let's try brief calculations concerning alluvial hydraulics on the assumption that the sediment transportation due to tidal currents is similar to that due to unidirectional flow like river currents. It must be kept in mind that the former differs from the latter at several points. For example, as tidal wave is a kind of long-period waves, the vertical distribution of velocities of tidal currents is predicted to be a nearly uniform distribution, differing from the logarithmic distribution of unidirectional gravitational flow and these calculations need to be corrected after future investigations concerning sediment transport phenomena due to tidal currents.

The author presumes that Manning roughness n is 0.020 sec/$m^{1/3}$, mean longitudinal velocity $\overline{V}$ is 2 knots = 1.03 m/sec, hydraulic radius R is 20 m, diameter of bottom sediments d is 0.70 mm. Then energy gradient I_e becomes 7.8×10^{-6} —— I_e is calculated by using Manning formula ($\overline{V} = (1/n)R^{2/3}I_e^{1/2}$)——. (According to the measured results of water surface grade at the fastest time of tidal currents in a spring tide, water surface grade I_w of the eastward flow is 9.1×10^{-6} and that of the westward flow is 12.8×10^{-6} in this area. These values are nearly equal to the calculated I_e). Therefore, the following values are calculated: friction velocity $u_* = \sqrt{gRI_e}$ = 3.91 cm/s, nondimensional tractive force $\tau_* = u_*^2/(\sigma/\rho - 1)gd$ = 0.142, and sediment Reynolds number u_*d/ν = 27.4 where ρ , σ , and ν denote specific gravity of water, specific gravity of sand, and kinematic viscosity of water, respectively. Value of τ_* = 0.142 corresponds to the region where the rate

of sediment transportation rapidly increases and ripples and dunes are remarkably developed[17]. Therefore, it is inferred that fairly active sediment transportation occurs at the fastest time of tidal currents at Inosakinotsugai.

Since the water depths at Inosakinotsugai are much larger than those of usual rivers, it is suspicious whether a classification of sand waves which was obtained by observations in rivers and by experiments of unidirectional flow in alluvial channels can be applied to this case. Nevertheless, it has been studied which sand wave in unidirectional flow the sand waves due to tidal currents correspond to. When the classification diagram proposed by Ashida and Michiue[19] is used, the sand waves at Inosakinotsugai belong to lower regime (ripples and dunes region). The sand waves at Inosakinotsugai do not, however, seem to belong to a category of ripples because of the following reasons:

1) It is not imagined that ripples, wave length λ of which is estimated as λ = 1,000 d, grow up to the scales of several scores of meters.
2) According to a diver's observation, it is reported that ripples appear on the submarine sand waves. A category of submarine sand waves seems to quite differ from that of ripples.
3) It is reported on alluvial experiments that ripples appear in $u_*d/\nu < 20$ and dunes appear in $u_*d/\nu > 20$[17]. The sediment Reynolds number at Inosakinotsugai is u_*d/ν = 27.4 (larger than 20).

Therefore, the sand waves at Inosakinotsugai are judged as dunes, scales of which are influenced by water depths.

Since water depths in rivers are not large, scales of ripples are not so different from those of dunes. However, the former is very different from the latter in seas where water depths are large.

Dimensions of submarine sand waves are calculated by using the formula

of dunes proposed by Yalin[18]. Then, $\lambda = 5\ h$ and $\Delta = (h/6)(1 - \tau_c / \tau_0) = 0.13\ h$ are got. (τ_c is a critical tractive force at the bottom. τ_0 is a tractive force at the bottom.) This calculated value of λ is larger than the measured value of λ in Fig. II-8-19-a, but the calculated value of Δ is almost equal to the measured value of Δ in Fig. II-8-19-b.

8-3-5 Statistical analysis of the topography

Hino[20] explained a statistical structure of sand waves due to unidirectional flow on alluvial beds as follows: spectrum density is a function of wave number and an angle of repose of sediments, and is in proportion to -3'th power of wave number.

When power spectrum of the topography was calculated, water depths were measured at intervals of 5 m on the sounding lines by using the recording papers. Intervals of 5 m were changed to actual intervals (sounding lines No. 3: 4.4 m; No. 4: 4.6 m; No.5: 4.9 m), and spectrum densities were calculated. Results at sounding line of Nos. 3, 4, and 6 were shown in Fig. II-8-20 and Figs. II-8-21-a, b, and c. In Fig. II-8-20 the ordinate is $\log\{F(k)\}$ and the abscissa is $\log(k)$ in order to check -3'th power law. In Fig. II-8-21-a, b, and c the ordinate is $k \cdot F(k)$ and the abscissa is $\log(k)$ in order to easily find the wave number at the peaks of spectra. Degree of freedom at spectrum calculation is about 5 and is not so large. In Fig. II-8-20, white circles represent the results of spectrum analysis of original water depths h_i and black circles represent those of h'_i ($h'_i = h_i - \tilde{h}_i$. The latter calculation was performed in order to eliminate the influence of the sand bank, the wave length of which is longer than that of sand wave. $\tilde{h}_i$ is a moving average of thirteen h_i data.) Fig. II-8-20 shows that the formula of -3'th power holds in $k > 0.023\ m^{-1}$. Only results of spectrum analysis of h'_i are shown in Figs. II-8-21-a, b, and c. According

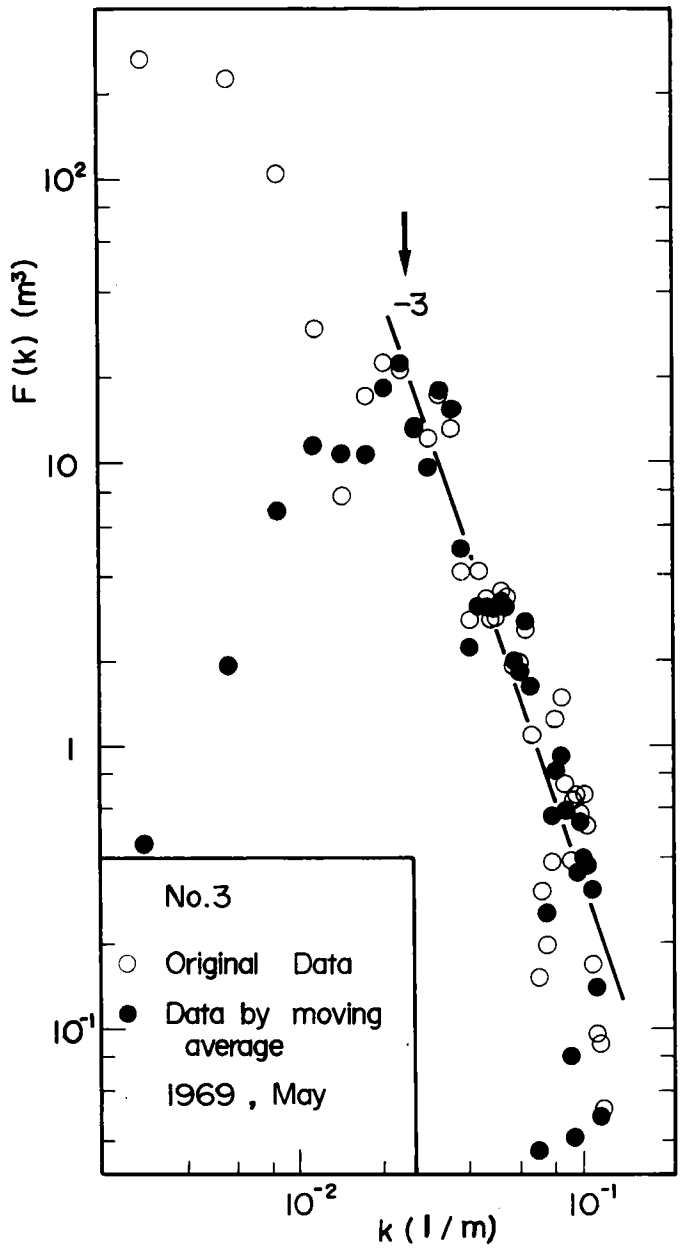

Fig. II -8-20 Spectrum analysis of the topography

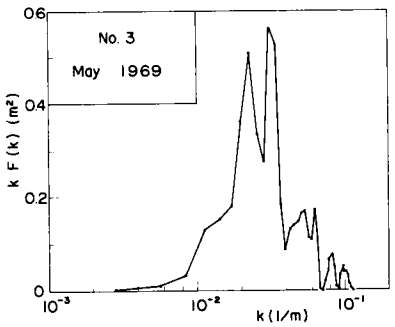

(a)

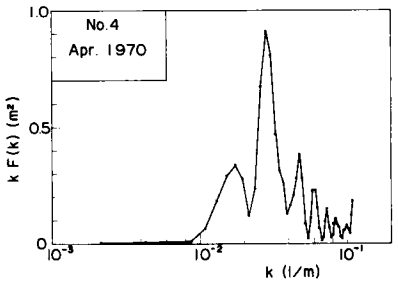

(b)

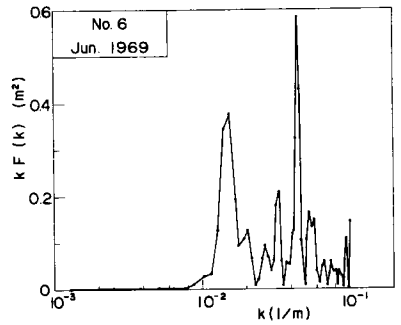

(c)

Fig. II -8-21 Spectrum analysis of the topography

to the figures, the peaks of spectra are as follows: at the sounding line No. 3, k_p = 0.023 m^{-1} (wave length λ_p at the spectrum peak — a reciprocal of k_p — is 43 m) or k_p = 0.031 m^{-1} (λ_p = 32 m). (It is also proper to consider the both peaks as one peak). At the sounding line No. 4, k_p = 0.028 m^{-1} (λ_p = 36 m). At the sounding line No. 6, k_p = 0.015 m^{-1} (λ_p = 76 m) or k_p = 0.045 m^{-1} (λ_p = 22 m). The wave lengths which were calculated by eye measurement by using the sounding records are $\overline{\lambda}$ = 45 m at the sounding line No. 3, $\overline{\lambda}$ = 37 m at No. 4, and $\overline{\lambda}$ = 24 m at No. 6. As the peak of k_p = 0.015 m^{-1} at the sounding line No. 6 is eliminated, the wave lengths which were calculated from the peaks of the spectra are nearly equal to the wave lengths by visual measurement.

8-4 Investigations of tidal currents at Inosakinotsugai

8-4-1 Intension of investigations on tidal currents

Sand waves are formed as a result of interaction between tidal currents as an external force and submarine topography, and they reach the steady state. The author thought that conditions of tidal currents would have to be researched first when the formation mechanism of sand waves was studied. At "8-4" the results of the investigations on tidal currents are discussed.

Sand waves are formed due to variation of sediment transport rate. The variation of sediment transport rate is closely related to the variation of velocity, that is turbulence. Therefore, it is indispensable to investigate turbulence of tidal currents. However, turbulence is established as the condition after mean flow has been made clear. Therefore, the investigations on tidal currents need to be carried forward as follows: (1) the investigation on the mean flow, and (2) the investigation concerning turbulence. The investigation on turbulence also needs to be practiced from the viewpoints that both intensity of turbulence and structure of macro turbulence

are related to the formation of sand waves. After the observation, the structure of turbulence will need to be compared with the configuration of sand waves.

As concrete investigation items, the followings will be considered for example:

1) Measurement on a vertical distribution of velocity and direction of tidal currents.
2) Measurement on velocities and directions of tidal currents at several points of sand waves, for example, at the crests, the troughs, the upstream faces, and the lee of downstream faces of sand waves.

However, in this investigation there was a serious restriction that the observations must be practiced in the sea and besides in the sea way, so it was difficult to set up a fixed tower. Therefore, the following two investigations were performed:

1) In order to obtain a whole phase of tidal currents at Inosakinotsugai a lot of floats set adrift on the water surface were photographed from an airplane, and conditions of tidal currents at water surface were researched from flowing pattern of floats.
2) In order to measure precisely an internal structures of tidal currents, a current meter was set at 50 cm above the sea bottom, and velocities, directions, and turbulence of tidal currents were measured. The former investigation also corresponds to that on currents at the water surface, and the latter corresponds to that on currents at the bottom layer.

8-4-2 Investigation of tidal currents at water surface

8-4-2-1 Method of the investigation

The investigation referred in this section is as follows: a lot of floats set adrift due to tidal currents were photographed in color films

from an airplane, and conditions of tidal currents were researched from the variation of both flowing floats and colors of the water. The investigation was practiced in Oct. 1973. Tidal condition was spring tide, and investigation was performed on the westward flood current.

In this investigation, the floats need not to be moved due to winds etc., but must be moved due to only tidal currents. Therefore, a preliminary test was done before the investigation, and it was checked whether the floats were drifted due to only tidal currents or not. Size of the floats was determined by using this result. Two types of floats — 100 floats of type I and 20 floats of type II — were made. The type I floats, which were boards of 5.5 mm thick and 91 cm square, were drifted due to the currents at the water surface. While the type II floats, which were foamed styrene boards of 50 mm thick and 91 cm square carrying drag plates and concrete blocks under the boards, were drifted due to the currents at the nearly -3.3 m points below the water surface. Since the floats were classified by painting of several colors, the discrimination on the color photographs was easy.

Fixed basic points must be taken in the photographs in order to determine the position of each float. Therefore, the fixed basic points — S1 ~ S8 (fishing boats fixed with anchors), B3~B6 (buoys used as signposts in the sea way), L1 (lighthouse), C1 (breakwater) — were set in the sea at the investigation. The positions of the basic points and distances among them were measured using a Hi-Fix electric positioning equipment.

Co - ordinate of the floats and the fixed basic points were measured on the positive films with a stereocomparater to the unit of 10^{-3}mm. Concerning time intervals of photographing, indications of a digital timer which struck the time with the accuracy of 1/100 sec unit were photographed in the pictures. The time intervals were determined as the differences

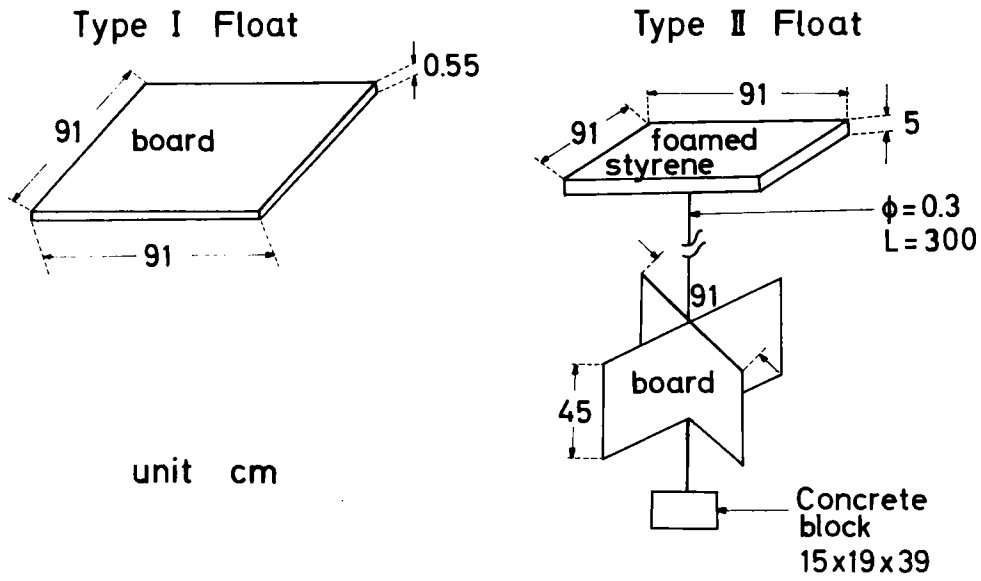

Fig. II -8-22 Floats used for tidal currents observation

between the indications. Distances of the floats were calculated by using their co-ordinates in two pictures. The moving velocities of floats (velocities of tidal currents) were got from the calculation of dividing the moving distances by the time intervals of photographing. Noteworthy points in this analysis are as follows:

1) The calculated tidal velocities are not Euler type velocities which are obtained with a current meter set at one point, but Lagrange type velocities.
2) In this calculation it was assumed that the floats moved on the shortest line between two points, but actually this assumption did not always hold. The calculated velocities are smaller than actual velocities, and are approximate quantities.
3) The calculated velocities are not instantaneous values, but averaged values by the time intervals of photographing.

Moreover, errors of velocities were estimated at 5~20 % on the fact that the fixed basic points did not move actually, but distances of their movements were estimated as if they had moved because of incline of the vertical axis of the camera at the photographing.

8-4-2-2 Results of analysis

Plane distribution concerning velocities and directions of tidal currents which flow from the south part of Inosakinotsugai to the area between Hon Is. and Ushi Is. is shown in Fig. II-8-23-a. This figure was made by comparing two pictures, time intervals of photographing of which were several minutes. To the regret, the velocities at the other parts except the south part in the sea around Inosakinotsugai could not be measured, because few floats drifted near Hon Is. However, followings are observed in this figure:

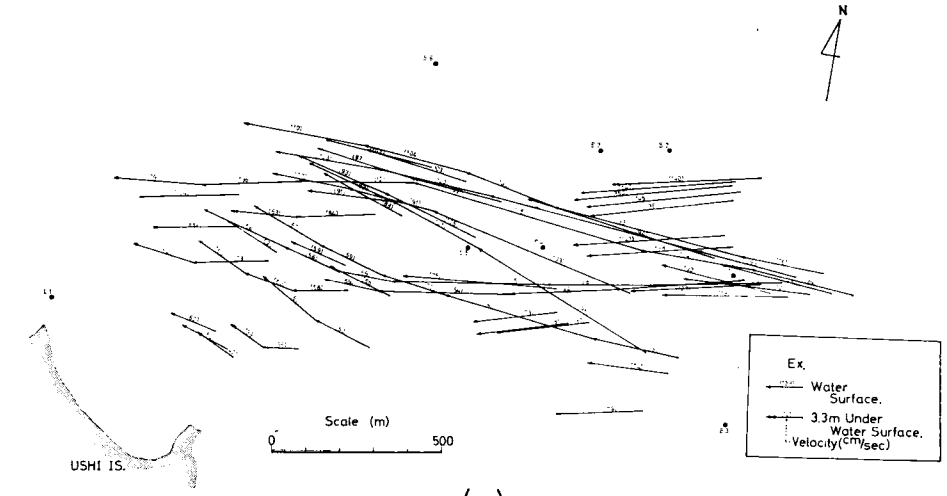

(a)

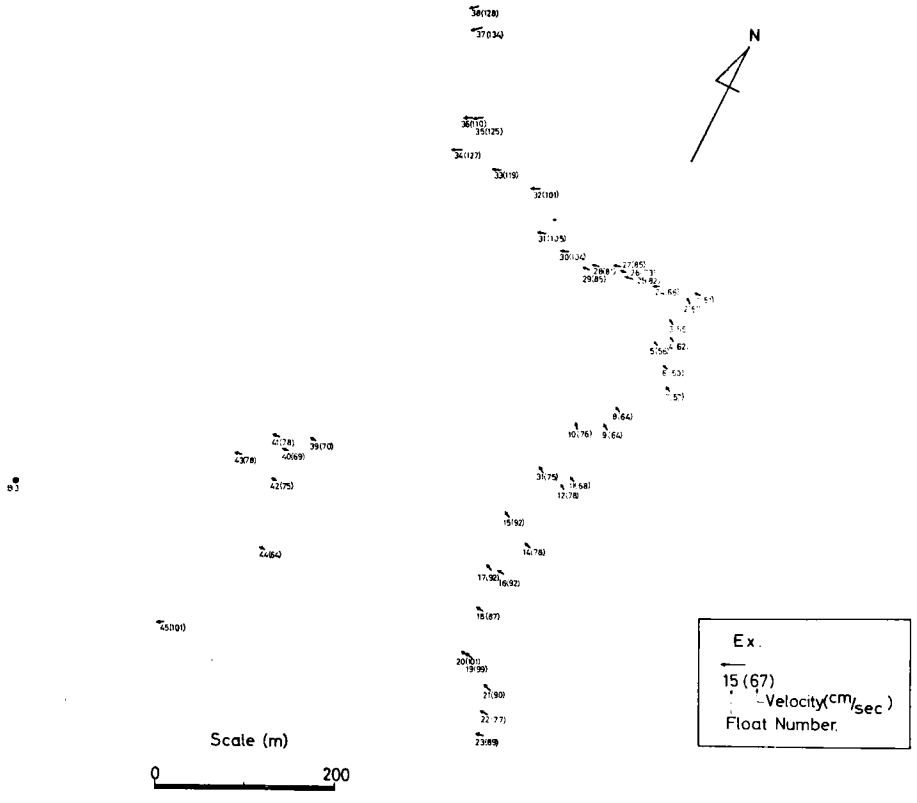

(b)

Fig. II -8-23 Plane distribution of velocities and directions at the water surface

1) Velocities of tidal currents at the north part are faster than that of the south part in this sea, and the former are 150 cm/s near S2 and S3.

2) Differences between directions of type 1 floats and those of type II floats are not almost observed, but velocities of type 1 floats are a little faster than those of type II floats.

Plane distribution concerning velocities and directions of tidal currents is shown in Fig. II-8-23-b, too. This figure was made by comparing two pictures, time interval of photographing of which was 7.85 seconds. Followings are considered in this figure:

1) Floats of NOs. 1～23 are distributed on a circular arc, the diameter of which is about 600 m, and their drifted directions are NW～NNW.

2) Floats of Nos. 24～38 are also distributed on a circular arc, the diameter of which is about 450 m, and their drifted directions are W～WSW.

Similar phenomena are shown on the other figures which were got by using other pictures. It is considered from these facts that macro eddies, diameters of which are several hundred meters, are prominent as to the tidal currents in this sea. The scales of these macro eddies are approximately equal to the cross distance of Inosakinotsugai sand bank. Is the following assumption appropriate? That is, "the topography of sand bank is external cause of disturbance, and the turbulence energy of tidal currents concentrates at the scale which is approximately equal to that of the sand bank. As these results, macro eddies appear". The positions of these eddies generation are summarized in Fig. II-8-24-a. This figure was drawn on the basis of the variations of both directions of floats movement and colors of the sea water. This figure shows that these eddies concentrate at Ino-

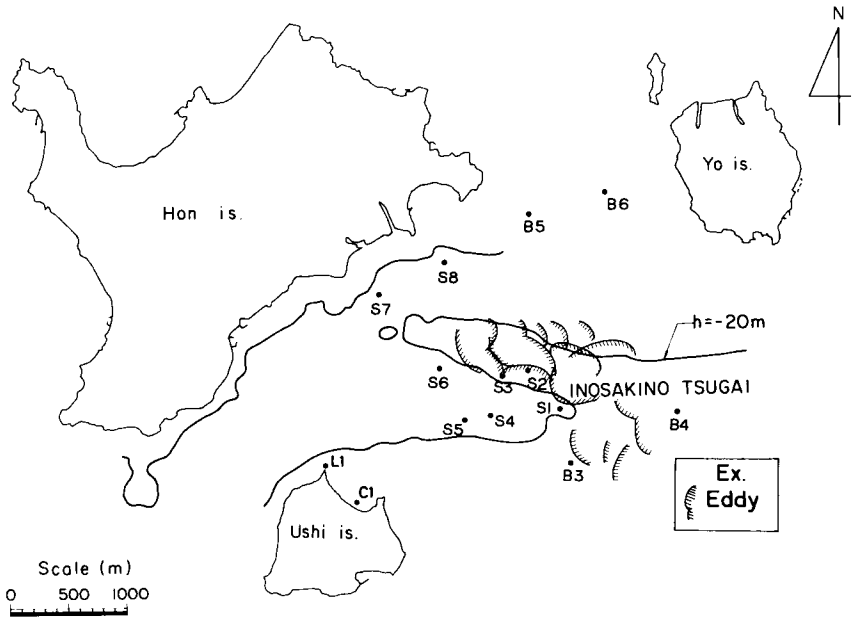

(A) Occurring positions of large eddies

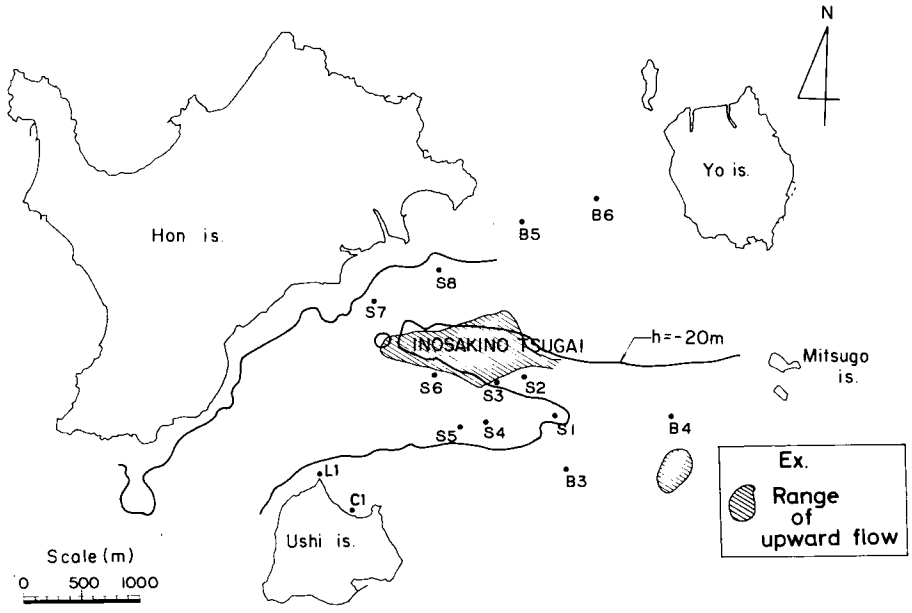

(b) Occurring positions of upward flow

Fig. II -8-24 Positions of large eddies and upward flow

sakinotsugai.

By the way, muddy parts which were light brown and were apparently distinguished from the surrounding water were found in the pictures. Their shapes were nearly circle and their diameters were 30～40 m. They are closely distributed at the several points at Inosakinotsugai and the longitudinal distances between the centers of the neighboring muddy parts were 40～100 m. It must be taken care that the diameters of the muddy parts and the distances between the centers are approximately equal to the wave lengths of the sand waves. According to the opinion of a photograph analysist, many fine sands are apparently included in these muddy parts. The author thinks that strong upward flow occurs due to the sand waves and it winds up fine sands from the bottom. The occurring positions of these upward flows are approximately shown with oblique lines in Fig. Ⅱ-8-24-b. This figure indicates that most upward flows appear at Inosakinotsugai. The upward flows seem to be generated due to the existence of sand waves and inversely act on sand waves as a result of a reaction. The existence of upward flow has not been taken into consideration in the former studies concerning sand wave formation. The upward flows need to be measured in the future research.

Summing up the above considerations, tidal currents which pass through the strait between Yo Is. and Mitsugo Is. come to include two marco turbulences — eddies whose diameters are several hundred meters and upward flows — under the influence of the sand bank and the sand waves at Inosakinotsugai. And passing over Inosakinotsugai, those prominent eddies disappear. These considerations need more detailed investigations, but it is very interesting to study how submarine topography affects tidal currents.

8-4-3 Investigation of bottom currents

8-4-3-1 Method of the investigation

As the description in "8-4-2", two prominent eddies appear at

Inosakinotsugai under the influence of the sand bank and the sand waves. At this section, results of observations concerning tidal currents at the 50 cm points over the sea bottom are explained. These observations were performed with a new current meter of all direction type[21]. The object of these observations is to research conditions of tidal currents in details which are roughly studied in "8-4-2".

The new current meter is a propeller type measuring equipment of velocity and direction of currents, and was developed at the Port and Harbour Research Institute (Photo Ⅱ-8-1). As this equipment is set in currents, the propeller is controled to the main currents by the tail of the equipment and turns in proportion to the velocity. The direction of the tail is detected with a potentiometer. A free compass is attached to this current meter, and the current direction, which is zero degree at the northward flow and is expressed clockwise with accuracy of 1 degree, is detected at intervals of 1 second. The number of rotation of the propeller is detected as electric pulses with no - contact type detector in which magnets and magnet diodes are used. A velocity averaged for a second is detected with accuracy of 0.1 cm/s. A calibration curve, which is indicated with the number of pulse per unit second and the current velocity, is shown in Fig. Ⅱ-8-25-a. Transient response time during which an indication of velocity increases from zero velocity to the constant velocity is shown in Fig. Ⅱ-8-25-b. Moreover, a calibration of response concerning the direction of currents was performed as follows: the tail fixed perpendicularly to the direction of main currents with a stopper is turned toward the main flow after the stopper is taken off. The turning time during which the tail moves 45 degrees is shown in Fig. Ⅱ-8-25-b. Referring to this figure, the velocity for a second was adopted as turbulent velocity data.

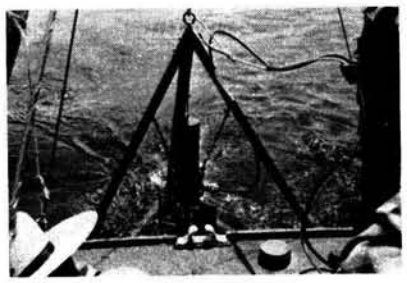

Photo II -8-1
Observations of tidal currents with a new current meter

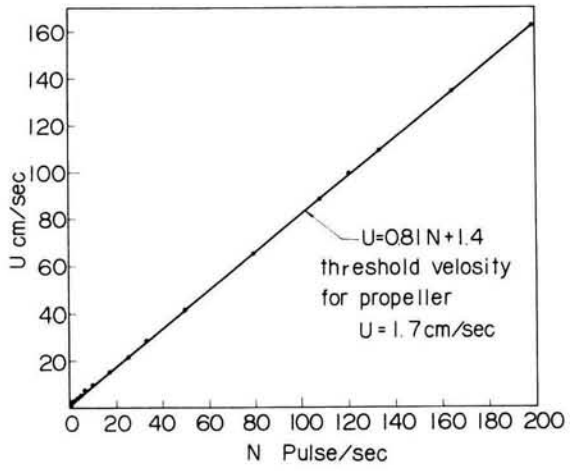

(a) Calibration curve of the propeller

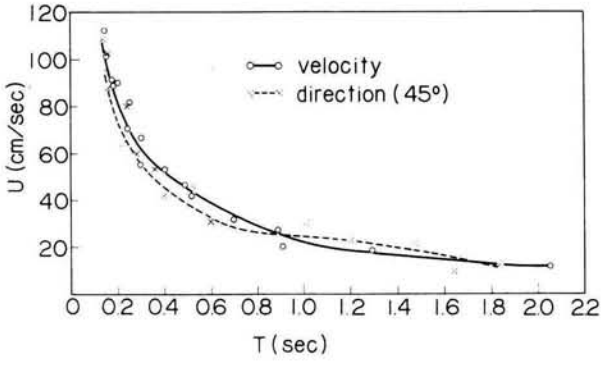

(b) Respondent character of the propeller and the tail

Fig. II -8-25 Characteristics of a new current meter

Observation system of tidal currents is shown in Fig. Ⅱ-8-26. The current meter was installed by chains in the triangular pyramid which was made of 2 m long steel frames. Heavy rails were laid on the bottom sides of the triangular pyramid as a weight, and sharp steel sticks were fixed at the three corners in the bottom of the triangular pyramid. The sticks pierced into the sea bed. An observation ship was fixed with the anchor which was set down from the bow. The triangular pyramid was set down from the stern onto the sea bed. After an observation of tidal currents was over at one observation point (for example T.F.O.P.I-1), the rope joined to the anchor was loosed at about thirty meters and the positions of the ship was changed to the downstream by the tidal currents, and tidal currents observation was done at the next point (for example T.F.O.P.I-2). Soundings were performed both during the observation and after the observation, and moreover the incline of the rope which was joined to the triangular pyramid was measured. Using these records, it was judged where the current meter was set, for example on the crest or on the trough etc. Besides, the scale of the sand wave on which the current meter was set was measured by the soundings.

8-4-3-2 Results of analysis

The observations of tidal currents were performed at 39 places — T.F.O.P.I-1～19 and Ⅱ-1～20 — which are shown in Fig. Ⅱ-8-17. The observations at T.F.O.P.I-1～19 were practiced in May 1973, and then the tidal currents were eastward ebb currents at the spring tide. The observations at T.F.O.P.Ⅱ-1～20 were performed in July 1974, and then the tidal currents were westward flood currents at the neap tide. Concerning submarine topography, noticeable sand waves appeared at I-1～19 and Ⅱ-1～5. Ⅱ-6～11 were on the upstream face of the sand bank and there was no sand wave.

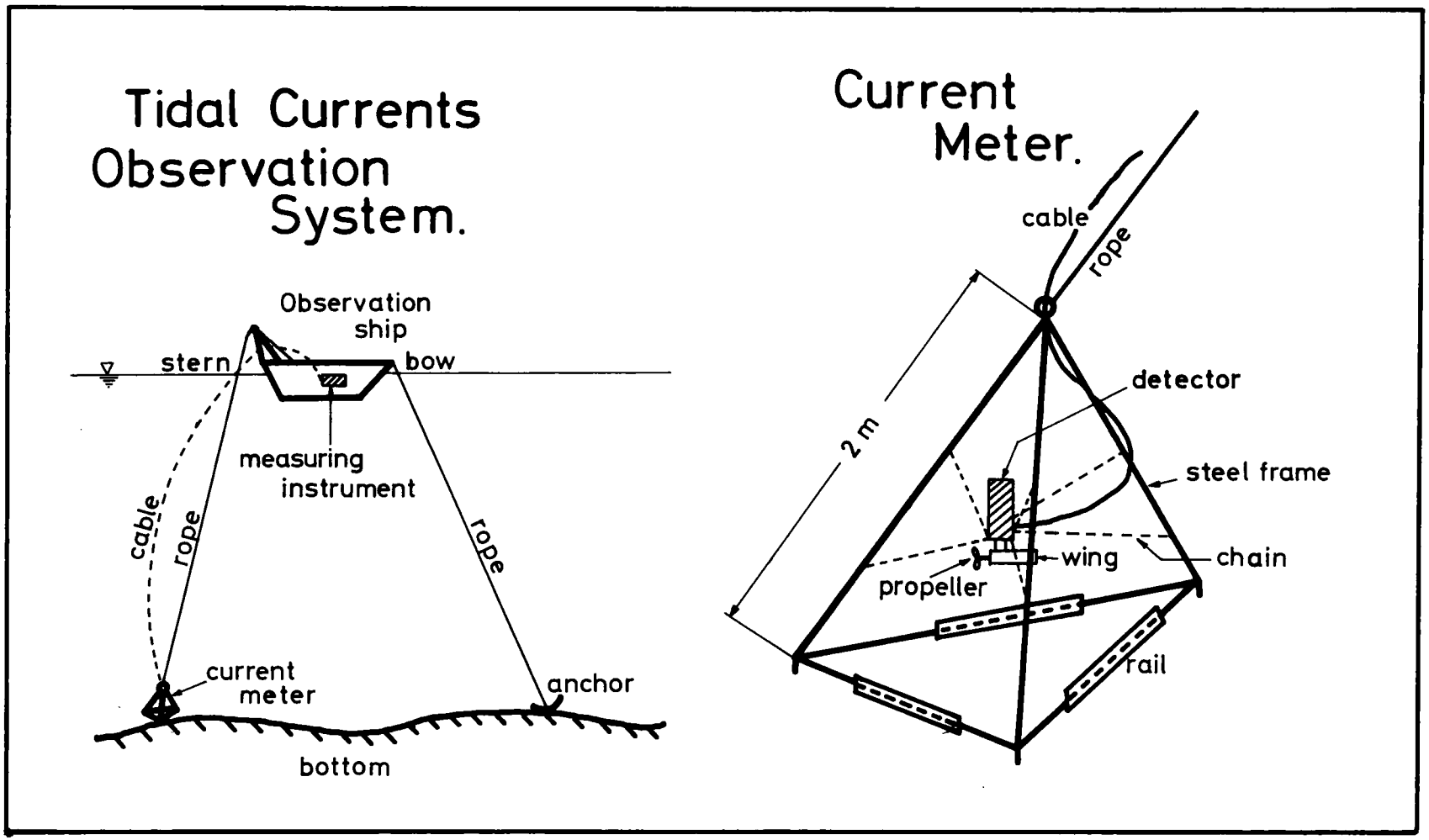

Fig. II -8-26 Observation system of tidal currents

T.F.O.P.Ⅱ-12～15 were at the tip of the sand bank and also there was no sand wave. T.F.O.P.Ⅱ-16～20 were on the downstream face of the sand bank and small sand waves appeared.

The followings are shown in Table Ⅱ-8-2: name of tidal currents observation places, observation time, distinction of flood currents or ebb currents, wave length of sand wave at the observation place λ, wave height at the observation place Δ, water depth at the observation place h, mean of measured velocities $\bar{U}$, root mean square of turbulence $\sqrt{\overline{U'^2}}$, relative intensity of turbulence $\sqrt{\overline{U'^2}}/\bar{U}$, mean of longitudinal velocities concerning main currents direction $\bar{u}(\bar{u}=\overline{U\cos(\phi-\bar{\phi})})$, mean of lateral velocities concerning main currents direction $\bar{v}$ $(\bar{v}=\overline{U\sin(\phi-\bar{\phi})})$, mean of currents direction $\bar{\phi}$, standard deviation of currents direction σ_ϕ. (Some problems exist in the definition of u and v and in the characteristics of the current meter that the measured current velocity is a mean value for a second and the measured current direction is an instantaneous value.) Moreover, "frequency of error concerning current direction (F.E.C.C.D.)" is frequency for the current direction having passed through 0 degree during the observation. This value is shown in Table Ⅱ-8-2, because error concerning calculations of u and v occurs due to passing through 0 degree. In this table "u.s. and l.s." mean that observations of tidal currents have been performed at the upstream face and lee of sand waves, respectively. "u.b., d.b., and t.b." mean that the observations have been performed on the upstream face, the downstream face, and the tip of the sand bank, respectively.

The following points are confirmed in Table Ⅱ-8-2.

1) Mean of $\bar{U}$ at T.F.O.P. I-1～5 is 43.7 cm/s. Similarly, 45.5 cm/s at I-6～10, 43.2 cm/s at I-11～14, 36.2 cm/s at I-15～19, 38.3 cm/s at Ⅱ-1～5, 78.5 cm/s at Ⅱ-6～11, 59.9 cm/s at Ⅱ-12～15, and 30.2 cm/s at Ⅱ-16～20. Considering that the observations at I-1～19 have been

Table II-8-2 Results of the observations of tidal currents

T.F.O.P.	Observation Time	Distinction of flood or ebb currents	Wavelength of sand wave λ (m)	Waveheight of sand wave (m)	Water depth h (m)	Mean of measured velocities $\bar{U}$ (cm/s)	Root mean square of turbulence $\sqrt{\overline{U'^2}}$ (cm/s)	Relative intensity of turbulence $\sqrt{\overline{U'^2}}/\bar{U}$	Longi-tudinal velocity $\bar{u}$ (cm/s)	Lateral velocity $\bar{v}$ (cm/s)	Mean of current directions $\bar{\phi}$ (degree)	Standard deviation of current d rections σ_ϕ (degree)	Frequency of error concerning current direction	Remarks
1 - 2	'73 5/15 11:10~11:30	ebb	36	2.2	24.2	19.7	13.4	0.680	8.1	2.2	200	78	18	l.s.
1 - 3	'73 5/15 11:40~12:05	ebb	24	1.1	23.0	49.6	16.3	0.329	46.4	-0.7	83	25	3	l.s.
1 - 4	'73 5/15 12:20~12:57	ebb	23	2.0	21.5	61.7	13.1	0.212	60.7	0.2	66	10	0	u.s.
1 - 6	'73 5/16 10:20~11:01	ebb	40	3.2	24.5	45.7	10.6	0.232	44.9	0.0	68	10	0	u.s.
1 - 7	'73 5/16 11:10~11:23	ebb	21	1.8	21.8	52.4	11.7	0.223	51.6	0.2	73	10	0	u.s.
1 - 8	'73 5/16 11:32~12:03	ebb	28	2.2	23.4	38.5	15.4	0.400	36.4	-0.6	92	19	0	u.s.
1 - 11	'73 5/17 11:20~11:40	ebb	19	1.4	23.3	37.7	10.7	0.284	35.4	-1.0	70	21	1	u.s.
1 - 12	'73 5/17 11:48~12:25	ebb	34	2.4	22.6	44.0	14.0	0.318	41.4	-0.6	85	21	0	u.s.
1 - 13	'73 5/17 12:36~13:09	ebb	34	2.8	22.8	47.9	14.9	0.311	45.4	0.3	67	19	0	u.s.
11 - 18	'73 5/18	ebb	13	1.9	21.8	36.2	19.5	0.539	33.3	-2.5	111	27	0	u.s.
11 - 1	'74 7/24 10:00~10:20	flood	108	6.8	21.0	29.9	24.0	0.803	21.8	8.2	232	75	14	l.s.
11 - 2	'74 7/24 10:35~10:55	flood	71	6.0	22.0	45.2	20.2	0.447	43.9	0.7	281	16	0	u.s.
11 - 3	'74 7/24 11:00~11:20	flood	28	2.0	24.1	38.3	17.8	0.465	32.5	-1.1	261	34	0	u.s.
11 - 4	'74 7/24 11:30~11:51	flood	53	4.6	25.0	32.0	16.3	0.509	27.4	0.9	278	42	2	l.s.
11 - 5	'74 7/24 12:00~12:25	flood	42	2.8	25.5	46.1	12.4	0.269	44.6	0.2	261	20	0	u.s.
11 - 6	'74 7/25 10:25~10:46	flood	—	—	30.1	88.9	11.3	0.127	76.9	5.1	293	32	0	u.b. no sand wave
11 - 7	'74 7/25 10:53~11:18	flood	—	—	27.6	85.8	21.0	0.245	68.4	11.8	255	39	0	u.b. no sand wave
11 - 8	'74 7/25 11:30~12:00	flood	—	—	25.8	87.2	18.1	0.208	83.2	1.2	280	18	0	u.b. no sand wave
11 - 9	'74 7/25 12:05~12:19	flood	—	—	23.2	62.6	25.4	0.406	57.0	5.3	272	24	0	u.b. no sand wave
11 - 10	'74 7/25 12:25~12:45	flood	—	—	22.0	83.0	12.2	0.147	80.1	0.7	312	16	0	u.b. no sand wave
11 - 11	'74 7/25 12:50~13:02	flood	—	—	22.4	63.3	13.0	0.205	61.7	0.4	273	12	0	u.b. no sand wave
11 - 12	'74 7/26 10:56~11:05	flood	—	—	28.8	52.0	6.7	0.129	51.9	-0.1	263	3	0	t.b. no sand wave
11 - 13	'74 7/26 11:10~11:33	flood	—	—	28.7	56.5	7.2	0.127	56.4	0.0	253	4	0	t.b. no sand wave
11 - 14	'74 7/26 11:40~12:00	flood	—	—	28.4	60.9	8.2	0.135	60.3	0.2	256	8	0	t.b. no sans wave
11 - 15	'74 7/26 12:05~12:26	flood	—	—	29.4	70.1	10.7	0.153	66.7	0.0	271	17	0	t.b. no sand wave
11 - 16	'74 7/27 11:34 ~11:59	flood	41	1.0	34.8	26.3	6.3	0.240	25.5	-0.3	254	14	0	d.b. small sand wave
11 - 17	'74 7/27 12:06~12:29	flood	83	3.0	35.7	28.2	7.5	0.266	27.9	-0.2	267	9	0	d.b. small sand wave
11 - 18	'74 7/27 12:38~13:06	flood	31	1.2	37.2	29.3	7.2	0.246	29.0	0.1	237	8	0	d.b. small sand wave
11 - 19	'74 7/27 13:13 ~13:38	flood	32	1.2	38.2	46.2	7.1	0.154	45.9	-0.2	233	6	0	d.b. small sand wave
11 - 20	'74 7/27 13:45 ~14:10	flood	28	0.7	39.5	20.8	6.5	0.313	20.4	0.3	220	12	0	d.b. small sand wave

l.s. ···· lee of sand wave, u.s. ···· upstream face of sand wave, u.b. ···· upstream face of sand bank, d.b. ···· downstream face of sand bank, t.b. ···· tip of sand bank,

practiced on the conditions of the eastward ebb currents at the spring tide and those at Ⅱ-1∼20 have been performed on the conditions of the westward flood currents at the neap tide, velocities of bottom currents in this area are the fastest at Ⅱ-6∼11, where tidal currents passing through the strait between Yo Is. and Mitsugo Is. flow on the caldron and flow aground onto the sand bank. Secondly, the velocities at Ⅱ-12∼15 which correspond to the tip of the sand bank are fast. This proves the supposition in "8-3-1" that the westward flood current is fast near Hon Is. $\bar{U}$ is nearly 40 cm/s at the places where sand waves appear on the sand bank. The slowest $\bar{U}$ is nearly 30 cm/s at the downstream face of the sand bank. Judging from this fact and previously mentioned phenomenon that tidal currents at the water surface are fast in this area, there is large difference of velocities between upper and bottom layer.

2) $\sqrt{\overline{U'^2}}/\bar{U}$ is larger than 0.1 which is a usual value observed under unidirectional currents in open channels. This is owing to complexity of submarine topography in this area — existence of the sand bank and the sand waves. Mean of $\sqrt{\overline{U'^2}}/\bar{U}$ at the upstream face of the sand bank (T.F.O.P. Ⅱ-6∼11) is 0.223. This value increases due to tidal currents flowing onto the sand bank and the occurrence of sand waves. Mean of $\sqrt{\overline{U'^2}}/\bar{U}$ is 0.336 at the upstream face of sand wave (T.F.O.P.I-3∼18, Ⅱ-2, 3, 5), and 0.580 at the lee of sand wave (I-2, 3, Ⅱ-1, 4). As tidal currents reach the downstream face of the sand bank (Ⅱ-16∼20), this value decreases to 0.224 (nearly equal to the value at the upstream face of the sand bank). As mentioned above, $\sqrt{\overline{U'^2}}/\bar{U}$ increases as tidal currents flow aground onto the sand bank and decreases to the former value after the flow passing over the sand bank. This corresponds to the process mentioned in "8-4-2" that two different eddies appear as tidal currents flow aground onto the sand bank and disappear after the flow

passes over the sand bank. $\sqrt{\overline{U'^2}}/\bar{U} = 0.136$ appears at the tip of the sand bank (II-12∼15), but σ_ϕ and $\sqrt{\overline{U'^2}}$ at this area are nearly equal to the values at the downstream face of the sand bank.

3) σ_ϕ and F.E.C.C.D. at the lee of sand wave are larger than those at the upstream face of sand wave. This shows that there are local strong eddies at the lee of sand wave.

The thick arrows in Fig. II-8-27 indicate $\bar{\phi}$ (measured directions of tidal currents). Also, slender solid lines are drawn perpendicular to the crest lines of sand waves. These slender lines were drawn by considering that directions of tidal currents at the bottom layer are perpendicular to the crest lines of sand waves. To the regret, the comparison of the directions of tidal currents at the water surface (Fig. II-8-23-a) and at the bottom was impossible, because two measuring areas did not overlap. However, judging from the thick arrows in Fig. II-8-27, the westward flood currents seem to flow to the further north places near Hon Is. than the eastward ebb currents. This supports the supposition stated in "8-3-1".

The results of spectrum analysis of U' (turbulence of tidal currents) at T.F.O.P. I-2 and I-6 are shown (length of measuring period of tidal currents at one place was 10∼40 minutes and measured velocities were values averaged for a second) in Figs. II-8-28-a and b. The ordinate is log $\{F(n)\}$ and the abscissa is log(n). Results of spectrum analysis of U' and those of u' approximately coincided. Therefore, only analyzed results of U' are shown. Degree of freedom at the calculation of the spectrum is 20∼50. According to this figure, Kolmogoroff's -5/3'th power formula holds within $n > 0.035$ sec^{-1} in I-2 and within $n > 0.020$ sec^{-1} in I-6. Besides, decreasing of power within $n < 0.035$ sec^{-1} in the spectrum of I-2 is more pronounced than that within $n < 0.020$ sec^{-1} in I-6. This means that small local eddies

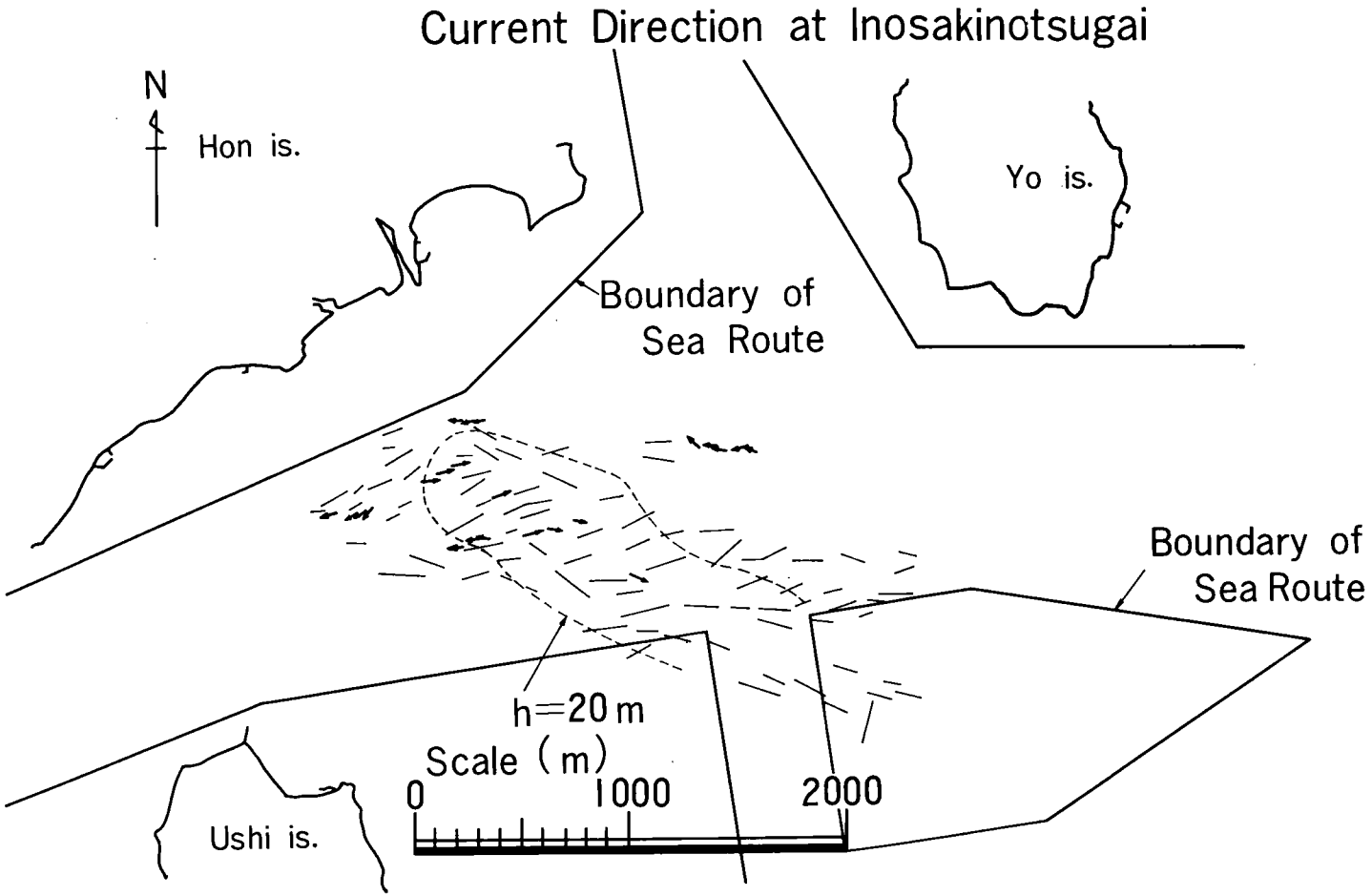

Fig. II -8-27 Plane distribution of current directions at the bottom

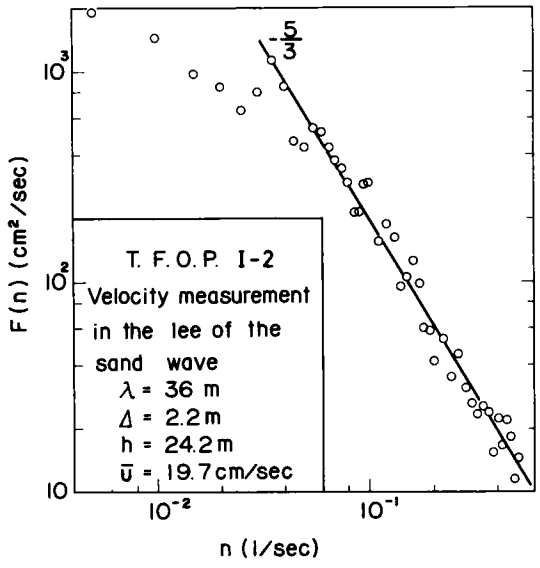

(a)

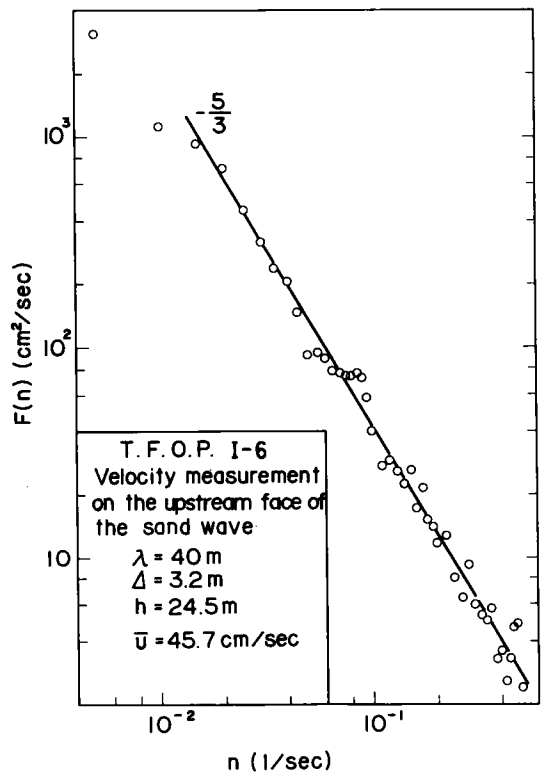

(b)

Fig. II -8-28 Spectrum analysis of velocities

(turbulence of high frequency) are prominent at the lee of sand waves and large eddies (turbulence of low frequency) are not notable there.

Results of spectrum analysis of turbulence at T.F.O.P. I-2, 7 and II-1, 3, 5, 7, 10, 15, 16, 17 are shown in Figs. II-8-29-a$\sim$j. The ordinate is $nF(n)$ and the abscissa is $\log(n)$. The followings are confirmed in these figures:

1) There are two types in the spectra at the upstream face of the sand bank. Powers of Type 1 (Fig. II-8-29-a, II-10) are nearly constant at the whole frequency range and there is not a prominent peak. Type 2 (Fig. II-8-29-b, II-7) has very large power at n = 0.005 sec^{-1}. In any case there is not a prominent peak at the medium frequency.

2) It is supposed that eddies are drifted due to the mean velocity, and $L_p = \bar{U}/100n_p$ (unit m) is defined as a scale of a prominent eddy ($\bar{U}$: mean velocity (cm/s), n_p : the frequency at the peak of a spectrum (sec^{-1})). In the spectrum at the upstream face of sand wave, L_p is nearly equal to 0.2$\sim$2 λ (λ: wave length of sand wave). There is a clear peak at L_p/λ = 34.9/21 = 1.7 in the case of I-7 (Fig. II-8-29-c). Similarly, L_p/λ = 5.9/28$\sim$12.8/28 = 0.2$\sim$0.5 in II-3 (Fig. II-8-29-d). At the upstream face of the sand bank, a large power at L_p/λ = 92.2/42 = 2.2 in II-5 (Fig. II-8-29-e) seems to be a trace of the large power at n= 0.005 sec^{-1}, and there is a small peak at L_p/λ = 15.4/42 = 0.4. The author thinks as follows: the phenomena that at the upstream face of sand wave a clear peak exists at L_p approximately equal to λ apparently corresponds to the occurrence of upward flows mentioned in "8-4-2". Regretfully, the large eddies described in "8-4-2" — those diameters are several hundred meters — could not be observed, because the investigation periods of tidal currents were short.

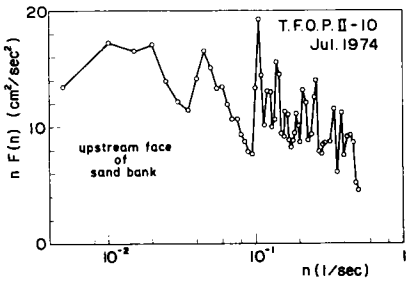

(a)

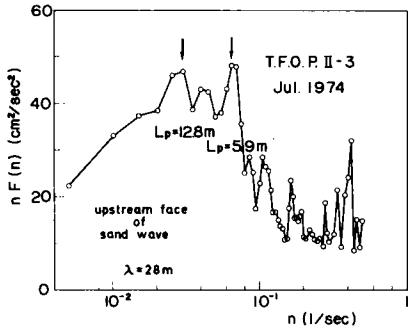

(d)

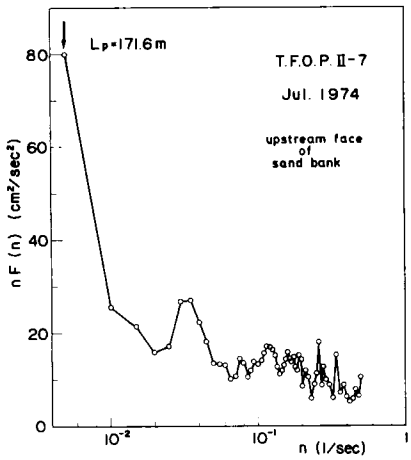

(b)

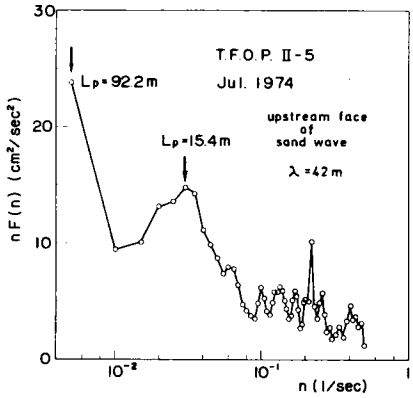

(e)

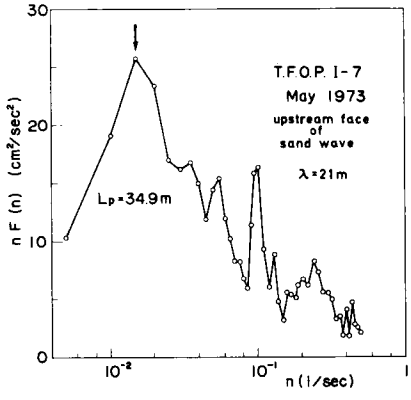

(c)

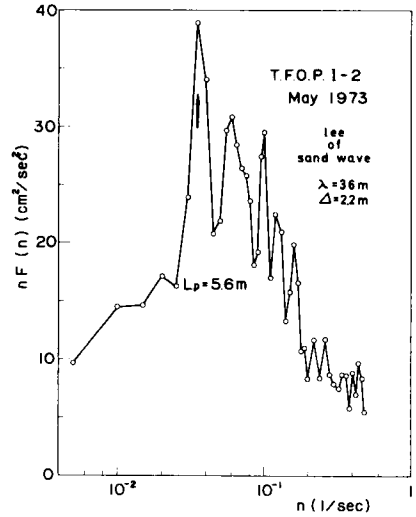

(f)

Fig. II -8-29 Spectrum analysis of velocities

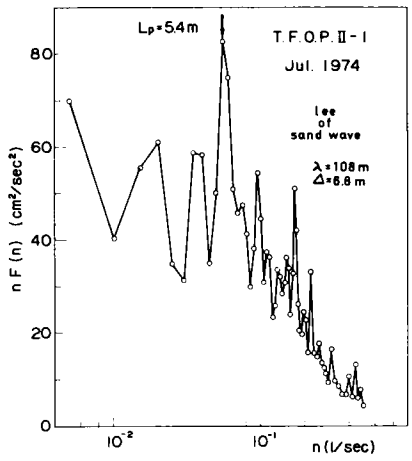

(g)

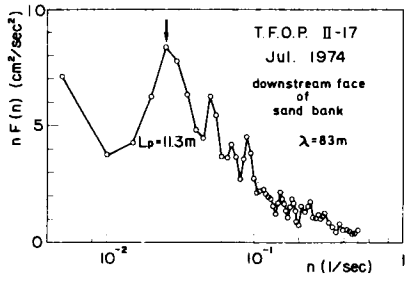

(i)

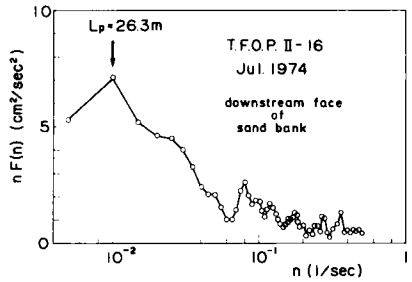

(h)

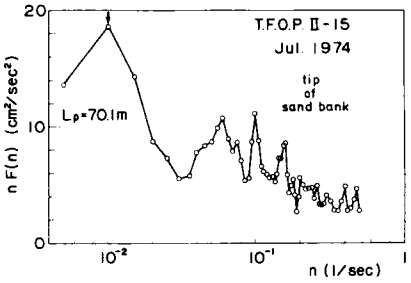

(j)

Fig. II-8-29 (Cont'd) Spectrum analysis of velocities

3) At the lee of sand wave, there is a clear peak at L_p/Δ = 0.5～2.5. There is a peak at L_p/Δ = 5.6/2.2 = 2.5 and are small peaks at higher frequencies in I-2 (Fig. II-8-29-f). There is a peak at L_p/Δ =5.4/6.8 = 0.8 and are low peaks at the both higher and lower frequencies in II-1 (Fig. II-8-29-g).

4) Examples of spectra at the downstream face of the sand bank are shown in Fig. II-8-29-h (II-16) and Fig. II-8-29-i (II-17). There is a peak at n = 0.01 sec^{-1} in II-16 and the shape of the spectrum is similar to the Type 2 at the upstream face of the sand bank. There is a peak at L_p/λ = 11.3/83 = 0.14 in II-17 and this phenomenon seems to be the affection of the existence of small sand waves. Also, a large power at n = 0.005 sec^{-1} seems to mean that this spectrum is the similar shape to Type 2 at the upstream face of the sand bank.

5) At the tip of the sand bank there is a large power at $n \fallingdotseq$ 0.01 sec^{-1} (Fig. II-8-29-j, II-15). This seems to mean that this spectrum is the similar shape to Type 2 at the upstream face of the sand bank.

8-4-4 Inferred formation mechanism of sand waves

Complete theory of explaining formation of sand waves has never been obtained. The mathematical theory that sand waves are formed after growth of small perturbations on alluvial bed will have to be supplemented by physical experiments. It is difficult to imagine that perturbations of such a long wave length have been generated, then grown up, and eventually become sand waves. According to Yokoshi[22], river current includes two types of macro turbulence, the scale of which is in proportion to either river width or water depth. Even though the above mentioned observations were done under the existence of sand waves, two types of macro eddies which might be related to formation of sand waves were found at Inosakino-tsugai.

Inferred formation mechanism of submarine sand waves is shown at Fig. II-8-30. As tidal currents (external force) flow aground onto the sand bank (primary topography), currents become unstable and intensity of turbulence increases, and prominent eddies appear. It is considered that sand waves are formed corresponding to the increase of intensity of turbulence and the occurrence of prominent eddies. Of course, intensity of turbulence increases and prominent eddies also appear due to the existence of sand waves. Sand waves act as roughness against the currents. The above process is cyclic one.

8-5 Application of investigation results to seaway maintenance plan

The following shows investigation results related to making a seaway maintenance plan:

1) Sand waves appear under the hydraulic environment made by a sand bank. Even if the sand waves are dredged, the sand bank still remains. Therefore, sand waves will be formed again. If the whole sand bank is dredged, sand waves might not be formed again. However, this requires enormous capital dredging and is unrealistic.
2) Sediment movement pattern at Inosakinotsugai is a closed system as shown in Fig. II-8-16 and few sediments are carried into the system. Fig. II-8-32 shows historical change of mean water depths of "A" and "B" areas shown in Fig. II-8-31[23]. The mean water depths are changed by dredging, but almost constant after completion of dredging. It will not likely that sediments which are carried into Inosakinotsugai area from outside cause sedimentation of the seaways in future.

Taking the above results into consideration, new dredging water depth was determined as follows so that enough water depth (-19 meters) can be insured all the time[23].

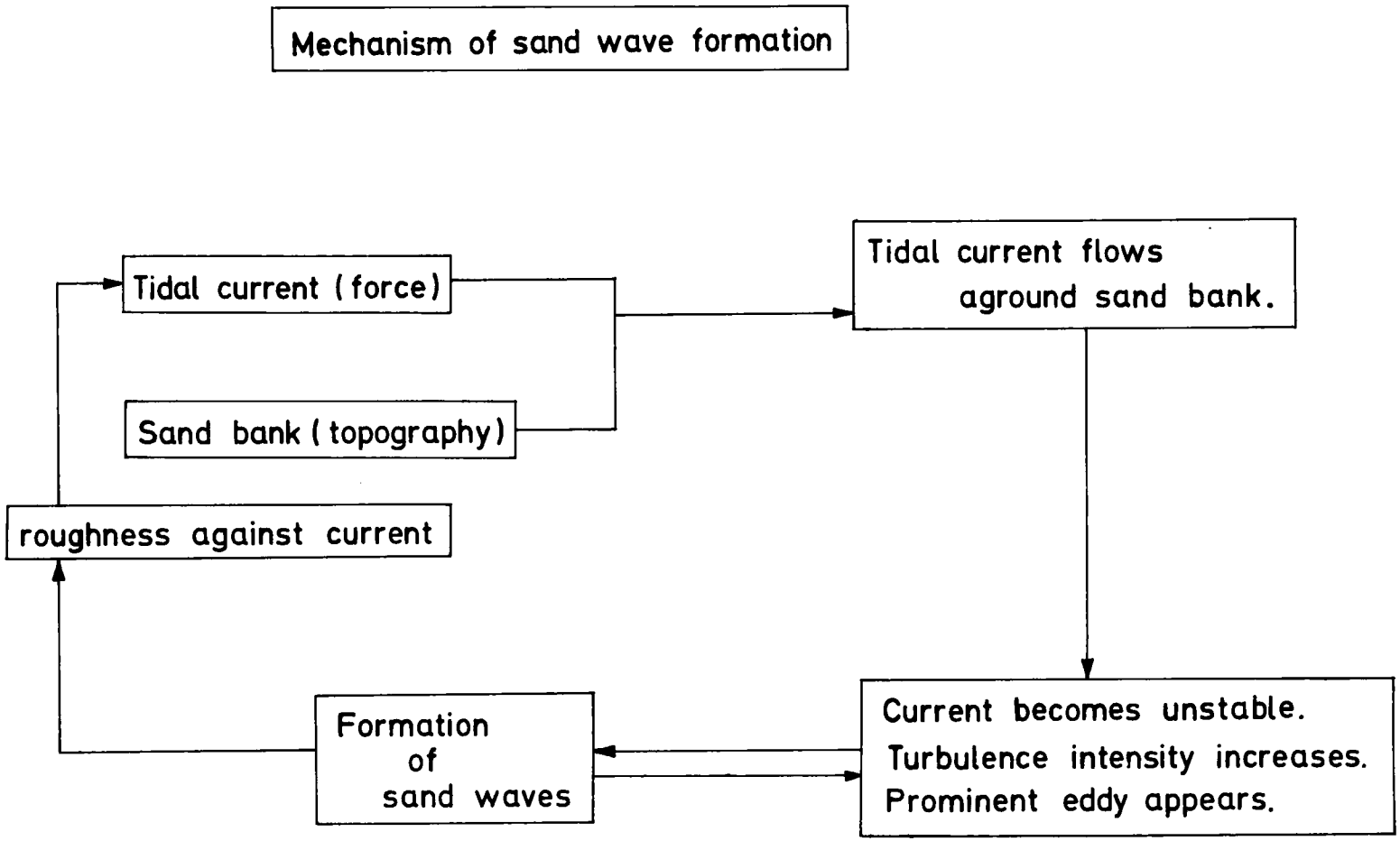

Fig. II -8-30 Block chart of sand wave formation

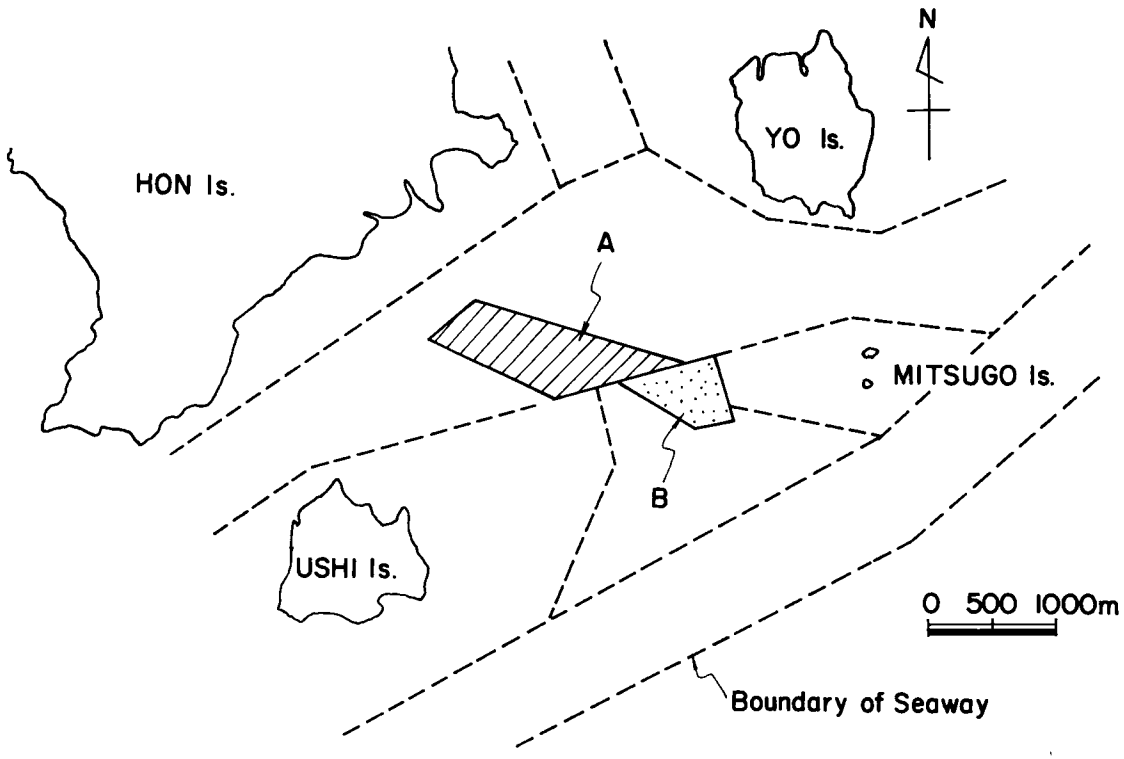

Fig. II -8-31 Dredging area

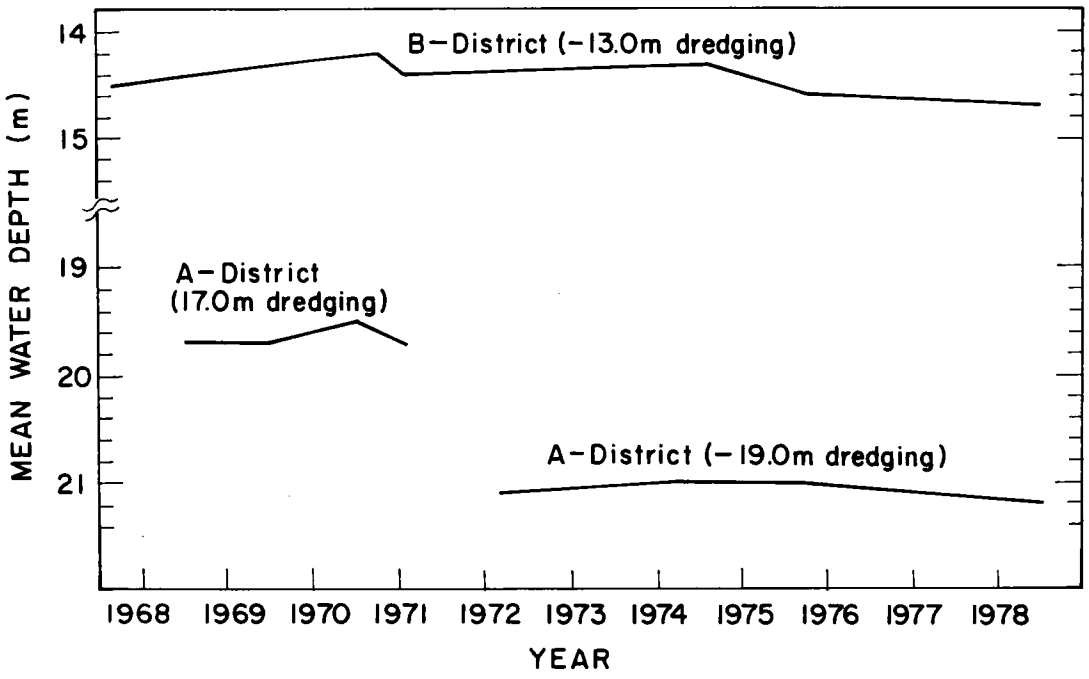

Fig. II -8-32 Changes of the average water depths at the dredging areas

Fig. Ⅱ-8-33 shows sea bottom configurations both just after dredging (solid line) and after reformation of sand waves (dashed line). "h" is a dredging water depth. "A" is an amplitude of bottom undulations just after dredging. "Δ" is wave height of a sand wave. "H" is a design water depth which must be insured after reformation of sand waves. The following equation shows relation among these quantities.

$$h = H + \Delta - A$$

According to Fig. Ⅱ-8-19-b, "Δ" is taken as 0.18 h on the safe side. "A" will be 0.2 m, based on the previous experience of dredging. "H" is 19 m at "A" area in Fig. Ⅱ-8-31. Eventually,

$$h = \frac{1}{0.82}\,(19 - 0.2) = 22.9$$

Similarly, at "B" area, h = 15.6 m. They are dredging water depths for insuring design water depths and actual dredging has been done according to this result at Bisan Seto Seaway.

8-6 Conclusions

There are many mysterious phenomena in the ocean. Submarine sand wave is one of them. The author has just admired dynamic, fine, and mysterious mechanism of the natural phenomena in the process of this investigation, but has been fully convinced that the study concerning submarine sand waves and induced channel sedimentation have been took a step forward.

Major points which have been made clear in this investigation are as follows:

(1) Submarine sand waves appear with sand banks and shoals according to the submarine topography at the Bisan Strait. However, the large submarine sand waves at the southern part of Ozuchi Is. are only one

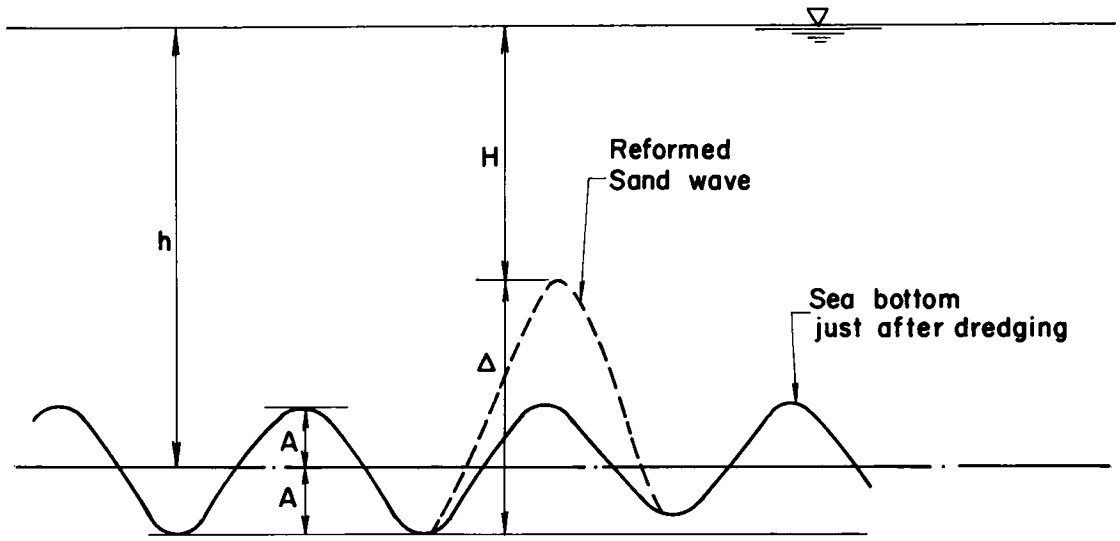

Fig. II -8-33 Sea bottom configurations

exceptional example, the occurrence of which cannot be connected with sand bank.

(2) Due to the arrangement of the islands and caldrons, the westward flood currents are predominant at the north of the sand bank, whilst eastward ebb currents are prevailing at the farther south. Inosakinotsugai has possibly been formed due to this hydraulic conditions. The similar phenomenon has been pointed out by Klein etc. This characteristics of tidal currents is one of the essential conditions for the formation of a sand bank.

(3) Sediment movement routes which have been assessed using sediments data are shown in Fig. II-8-16. Sediment movement pattern is a closed system and few sediments are carried into the system.

(4) Large asymmetrical sand waves are formed on the slopes of a sand bank, and comparatively small symmetrical sand waves are formed on its crest. Shapes of sand waves are stationary after they have been formed once.

(5) It is considered that submarine sand waves are dunes. Those scales are nearly equal to the values which are calculated using Yalin's formula.

(6) According to the spectrum analysis of submarine topography including sand waves, -3'th power formula proposed by Hino holds well. Besides, λ_p which is a reciprocal of wave number k_p at the peak of the spectrum is approximately equal to the wave length of sand waves which is obtained by the visual measurement of echo - sounding records.

(7) As tidal currents flow aground onto the sand bank, two marco turbulences appear. One is a large eddy, the diameter of which is several hundred meters and is nearly equal to the cross length of the sand bank. The other is an upward flow and muddy parts, the diameter of which is scores of meters and is nearly equal to the wave lengths of

sand waves, are observed. After tidal currents pass over the sand bank, these prominent marco turbulences disappear.

(8) According to the results of the investigation concerning tidal currents at the bottom layer performed using the current meter, it has become clear that turbulent phenomenon at the bottom layer is similar to the previously mentioned phenomenon at the water surface. As tidal currents flow aground onto the sand bank and sand waves appear there, intensity of turbulence increases, and the peak, the frequency of which corresponds to the equal scale to the wave length of sand waves, appears in the spectrum at the upstream face of sand wave. After tidal currents pass over the sand bank, the intensity of turbulence decreases and spectrum of turbulence returns to the similar shape to the spectrum at the upstream face of the sand bank.

(9) It is considered that sand waves are formed corresponding to the increase of intensity of turbulence and the occurrence of prominent eddies. Fig. Ⅱ-8-30 shows inferred formation mechanism of sand waves.

(10) Based on the above results, the dredging water depth at Inosakinotsugai was set as -22.9 m which is 3.9 m deeper than the design water depth.

REFERENCES

1) Honza, E. and N. Nasu: Sand wave migration at the Bisan Strait, Seto Inland Sea (Part 1, Monthly observation of sand wave migration), Jour. Marine Geology, Vol. 4, No. 1, 1968. (in Japanese)

2) Honza, E. and N. Nasu: Sand wave migration at the Bisan Strait, Seto Inland Sea (Part 2, Sand wave formation and its relation to sediment and current velocity), Jour. Marine Geology, Vol. 4, No. 2, 1968. (in Japanese)

3) Mogi, A. and T. Kato: On the sand waves in the eastern part of Bisan Seto, Jour. Marine Geology, Vol. 1, No. 1, 1962. (in Japanese)

4) Maritime Safety Agency: Investigations on submarine topography at the Bisan Strait in Seto Inland Sea, Mar., 1974. (in Japanese)

5) Mogi, A.: Geology in shallow water, pp. 200～203, Tokai University Press, 1971. (in Japanese)

6) Van Veen, J.: Sand waves in the North Sea, Hydrographic Review, 12, pp. 21～29, 1935.

7) Jones, N. S., J. M. Kain and A. H. Stride: The movement of sand waves on Warts Bank, Isle of Man, Marine Geology 3, pp. 329～336, 1965.

8) Jordan, G. F.: Large Submarine Sand Waves, Science, Vol. 136, pp. 839～848, Jun., 1962.

9) Ludwick, J. C.: Migration of Tidal Sand Waves in Chesapeake Bay Entrance, Institute of Oceanography, Old Dominion University Technical Report No. 2, Nov., 1971.

10) Klein, G. V.: Depositional and Dispersal dynamics of internal sand bars, Journal of Sedimentary Petrology, Vol. 40, No. 4, pp. 1095～1127, Dec., 1970.

11) Cartwright D. E.: On submarine sand waves and tidal lee-waves, Proc. Roy. Soc. London, Series A 253, pp. 218～241, 1959.

12) Kennedy, J. F.: The mechanics of dunes and antidunes in erodible bed channels, Journal of fluid Mechanics, Vol. 16 Part 4, 1963.

13) Hayashi, T.: Formation of dunes and antidunes in open channels, Proc. ASCE HY2, Feb., 1970.

14) Raudkivi, A. J.: Loose boundary hydraulics pp. 201～208, Pergamon Press, 1967.

15) Hoshino, M. and Y. Iwabuchi: Some problems on the formation of the Seto Inland Sea, Japan, — The case of the Nabeshima Suido — Jour. of Geology, Vol. 69, No. 810, 1963. (in Japanese)

16) Smith J. D.: Geomorphology of a sand ridge, Journal of Geology, Vol. 77, pp. 39～55, 1969.

17) Task Committee on the Bed Configuration and Hydraulic Resistance of Alluvial Streams, Committee on Hydraulics and Hydraulics Engineering: The Bed Configuration and roughness of alluvial streams, Proc. of JSCE, Feb., 1973. (in Japanese)

18) Yalin, M. S.: Geometrical properties of sand waves, Proc. of ASCE HY. 5, Sept., 1964.

19) Ashida, K. and M. Michiue: Study on hydraulic resistance and bed-load transport rate in alluvial streams, Proc. of JSCE, Oct., 1972. (in Japanese)

20) Hino, M.: Equilibrium-range spectra of sand waves formed by flowing water, Jour. of Fluid Mechanics, Vol. 34, 1968.

21) Shibayama, A. and S. Sudo: A new current meters of all direction type (1st Report), Report of the Port and Harbour Research Institute, Vol. 9, No. 1, Mar., 1970. (in Japanese)

22) Yokoshi, S.: Large scale turbulence of the river, Disaster Prevention Research Institute Annuals, No. 10 B, 1967. (in Japanese)

23) Onodera, S.: Improvement of Seaways in the Seto Inland Sea for Large-sized Ships, Proceedings of PIANC Section I - Volume 1 , 1981.

CHAPTER 9. CONCLUSIONS

When construction of Kashima Port, one of the most famous artificially excavated ports in Japan, was planned, it was worried that the channel might be silted up. One of the themes of Niigata Coast Investigation Program in the 1940's and 1950's which impacted progress of coastal engineering in Japan was sedimentation of Niigata Port. Large scale investigations were carried out for these projects and first-class outcomes were obtained.

However, only few studies are recently done for channel sedimentation problems.

The reasons are

first, engineers are apt to consider that the easiest countermeasure of sedimentation of Japanese ports is dredging simply, secondly beach erosion had become a serious problem and attracted scientists' attention.

Hydraulic engineers who go to foreign countries for technical guidance these days often come across channel sedimentation and are asked to solve it. Therefore, it is increasingly stressed that studies of channel sedimentation be encouraged. One of the problems which the author had often come across in the port development studies in developing countries was channel sedimentation.

In this report, channel sedimentation was taken up in Part II, independent of Part I, due to the above mentioned situation.

Main conclusions in Part II are listed as follows.

In Chapter 7, several examples of channel sedimentation were introduced. Taking cases of Irako, Oharai, Fukui, and Sakata-kita Ports, it was shown that channel sedimentation at Japanese ports occur due to the series of sediment transport mechanism which are causing shoreline change.

Cases of Qasim Port, Thames Estuary, and Mersey Estuary were taken up as examples of overseas channel sedimentation. Sediment at Qasim Port approach channel is fine sand whilst sediments at Thames and Mersey Estuaries are mud. These cases are not related to shoreline changes and annual sedimentation volume is several millions cubic meters. Sediments are transported to the Qasim Port approach channel by the action of waves and currents and deposited there. At Thames and Mersey Estuaries, suspended mud is transported to the deposition sites, where suspended solid concentration is high, by the action of density current.

In Chapter 8, investigations about submarine sand waves and channel sedimentation at Bisan Seto Seaway are reported. Many shallow spots appeared in a stripe pattern at Inosakinotsugai sand bank after the completion of dredging in 1972. This sedimentation was caused by sand waves and hydraulic investigations about characteristics of sand waves were carried out in order to find a proper method for maintaining enough water depth.

According to the investigation results, sand waves appear with sand banks and shoals. They are dunes according to the studies from hydraulic point of view.

Formation mechanism of Inosakinotsugai sand bank was also studied. It was formed by the cyclic sediment transport system. This closed system was made by the tidal currents mechanism that flood channel existed at northern part of Inosakinotsugai and ebb channel existed at farther southern area.

Investigations about tidal currents were also carried out. As tidal currents flow aground onto the sand bank, two macro turbulences appear. One is a large eddy, the diameter of which is several hundred meters and is nearly equal to the cross length of the sand bank. The other is an upward flow, and muddy parts, the diameter of which is scores of meters and

is nearly equal to wave lengths of sand waves, are observed. It has also become clear that macro turbulence appears at the bottom layer and the frequency of the peak in the spectrum corresponds to the equal scale to the wave length of sand waves. It was finally described that the dredging water depth at Inosakinotsugai was set newly, based on the above results.

CONCLUDING REMARKS

The main theme of the author's research was sedimentation in rivers when he was a university student. After he entered the Port and Harbour Research Institute, his effort was concentrated onto sedimentation problems in beaches. The main concern was to develop a method for the prediction of changes of a beach topography. Between 1977 and 1979, the author stayed at the Hydraulics Research Station in England and had a chance to study sedimentation in estuaries. After these experiences, the author was convinced that estuaries were objects of applied hydraulic engineering just like rivers and beaches.

Since 1980, at the Overseas Coastal Area Development Institute of Japan, the author has studied sedimentation problems in developing countries and come across many channel sedimentation problems. Based on the above experience, the author splited this report into two parts which have the same weight.

When these parts are compared, it can be noticed that Part I about beach erosion is studied more intensively than Part II about channel sedimentation. This is due to the reason that the author has dealt with more actual beach erosion problems than channel sedimentation problems.

The author expects that Japanese hydraulic engineers have more chances to deal with channel sedimentation in future and more engineers are interested in a new field of hydraulic engineering —— channel sedimentation.

ACKNOWLEDGEMENT

The author would like to express his gratitude to Dr Shoji Sato, Director General of the Port and Harbour Research Institute, and Dr Norio Tanaka, Director of the Marine Hydrodynamics Division of the same Institute, for the various suggestions. He is also indebted to Professor Yuichi Iwagaki, Department of Civil Engineering, Faculty of Engineering, Kyoto University, for the invaluable advice and encouragement.